Characterization of Polysaccharides in Starch using Fluorescence Techniques

by

Lu Li

A thesis

presented to the University of Waterloo

in fulfillment of the

thesis requirement for the degree of

Doctor of Philosophy

in

Chemistry

Waterloo, Ontario, Canada, 2020

Examining Committee Membership

The following served on the Examining Committee for this thesis. The decision of the Examining Committee is by majority vote.

External Examiner	**Dr. John Dutcher** Professor, Department of Physics, University of Guelph, Guelph, Canada
Supervisor	**Dr. Jean Duhamel** Professor, Department of Chemistry, University of Waterloo, Waterloo, Canada
Internal Member	**Dr. Mario Gauthier** Professor, Department of Chemistry, University of Waterloo, Waterloo, Canada
Internal Member	**Dr. Xiaosong Wang** Professor, Department of Chemistry, University of Waterloo, Waterloo, Canada
Internal-external Member	**Dr. Yuning Li** Professor, Department of Chemical Engineering, University of Waterloo, Waterloo, Canada

Author's Declaration

I hereby declare that I am the sole author of this thesis. This is a true copy of the thesis, including any required final revisions, as accepted by my examiners.

I understand that my thesis may be made electronically available to the public.

Abstract

Amylose and amylopectin, which are the two main constituents of starch, were characterized using the pyrene excimer fluorescence (PEF) technique. First, an amylose sample was randomly labeled with the dye pyrene to yield Py-Amylose. Its fluorescence was compared to that of pyrene-labeled poly(methyl acrylate) (Py-PMA) as Py-PMA was expected to experience internal dynamics that were much faster than those of Py-Amylose. Analysis of the PEF signal revealed that Py-Amylose formed excimer as effectively as the more flexible Py-PMA. This result could only be rationalized if Py-Amylose generated a compact environment for the pyrene labels by adopting a helical conformation. Fluorescence blob model (FBM) analysis, where a *blob* is the subvolume inside a macromolecule probed by an excited pyrene, yielded a *blob* size (N_{blob}) of 11 anhydroglucose units (AGUs) for Py-Amylose. The experimental N_{blob} value matched the theoretical N_{blob}^{theo} value obtained by molecular mechanism optimizations (MMOs) only if the pyrene labels were assumed to be covalently attached onto a polysaccharide helix, thus confirming the helical conformation of amylose in DMSO. Second, the FBM analysis was applied to a sample of amylopectin randomly labeled with pyrene (Py-Amylopectin). N_{blob} was found to increase from 11 for Py-Amylose to 20 for Py-Amylopectin in DMSO. MMOs were carried out to establish how N_{blob}^{theo} varied with the interhelical distance (d_{h-h}) between single and double helices of oligosaccharides laid out in a hexagonal array used as a mimic for the arrangement of the side chains of amylopectin. The d_{h-h} value needed for N_{blob}^{theo} to match the experimental N_{blob} of 20 equaled 25 or 29 Å depending on whether the side chain adopted a single or double helical conformation, respectively. This interhelical spacing suggested a density of amylopectin in DMSO which was one order of magnitude larger than the density of amylopectin determined by intrinsic viscosity ($[\eta]$). To resolve this discrepancy, the Solution-Cluster (Sol-CL) model was proposed. In this model, the

interior of amylopectin was depicted as being a network of dense clusters of oligosaccharide helices connected by flexible and linear oligosaccharide segments. Third, nanosized amylopectin fragments (NAFs) prepared from waxy corn starch by high temperature extrusion were characterized by ^{1}H NMR, iodine binding test, viscometry, dynamic light scattering (DLS), and PEF. ^{1}H NMR indicated that the NAFs shared a same chemical composition with amylopectin. The iodine binding test experiments confirmed that the NAFs were essentially amylose-free. [η] measurements suggested that their density increased from 0.04 to 0.12 g/mL in DMSO as their hydrodynamic diameter decreased from 57 nm to 8 nm. Matching the experimental N_{blob} value of Py-NAFs with the N_{blob}^{theo}-*vs*-$d_{h\text{-}h}$ trends yielded $d_{h\text{-}h}$ values that led to densities close to that found for amylopectin. In addition, the density of the NAFs, determined from [η] approached the density values calculated from N_{blob} as their size decreased toward that of a cluster of helices. This result suggested that the linear segments that bridged the clusters of helices and contributed to the excluded volume of the NAFs were cleaved off as the NAFs became smaller. Poly(ethylene glycol)s (PEGs) of different lengths were then added to dilute dispersions of Py-Amylopectin and two Py-NAFs. 10K PEG was unable to penetrate the interior of the macromolecules, thus generating the osmotic pressure that compressed the polysaccharides. Shrinkage of the polysaccharides was monitored by measuring their PEF. Deformation of the polysaccharides was found to only occur in Py-Amylopectin and the larger Py-NAF. The smaller Py-NAF could not be compressed at the same 10K PEG concentration due to the absence of excluded volume. These conclusions provided further supports to the Sol-CL model.

Together the results presented in this thesis suggest that PEF provides reliable structural information on amylose and amylopectin in solution, an information that would be difficult to extract from more traditional characterization methods.

Acknowledgements

First, I would like to express my deepest appreciation to my supervisor, Prof. Jean Duhamel, who has supported and assisted me in numerous ways throughout my PhD study. There are always times during the course of a PhD when one feels like giving up, but it was him who kept reminding me how important this research was for Science and pointed me to the right direction to finalize this work. This thesis would not have been possible without his support, encouragement, and advice. I am very grateful to have had him as my supervisor.

I would also like to thank the members of my committee, Prof. Xiaosong Wang, Prof. Yuning Li, and especially Prof. Mario Gauthier for their helpful suggestions regarding my research.

I wish to gratefully acknowledge the financial support from EcoSynthetix and the Natural Sciences and Engineering Research Council of Canada (NSERC). I also want to thank the many scientists from Ecosynthetix for all their constructive suggestions and advice for my thesis.

I am also thankful for the assistance of two undergraduate students, Chengmeng Sun and Xiaofang Zhai, who provided great help with the experiments presented in the fourth chapter of my thesis.

I would like to acknowledge all the Duhamel and Gauthier lab members who have made my time here at the University of Waterloo fun and memorable.

Foremost, I would like to express my sincere gratefulness to my family. Thanks to my dearest parents for always understanding and supporting me. Without their encouragement, I would never have made it this far. Thanks to my best friend and soulmate, my husband Huayong Jia; you are the best thing that has ever happened to me.

Dedication

To my beloved daughter, Eva Jia

Table of Contents

List of Figures

List of Tables

List of Abbreviations

AGU	Anhydroglucose unit
AOT	Sodium dioctyl sulfosuccinate
CD	Circular dichroism
CL	Chain length
DIC	*N*,*N*′-Diisopropylcarbodiimide
DLS	Dynamic light scattering
DMAP	4-Dimethylaminopyridine
DMF	*N*,*N*-Dimethylformamide
DMSO	Dimethylsulfoxide
DP	Degree of polymerization
ECs	Exterior chains
EEC	End-to-end cyclization
FA	Fluorescence anisotropy
FBM	Fluorescence blob model
FDQ	Fluorescence dynamic quenching
FRET	Fluorescence resonance energy transfer
HM-SNPs	Hydrophobically modified starch nanoparticles
HPAEC	High-performance anion exchange chromatography
HPSEC	High-performance size exclusion chromatography
GPC	Gel permeation chromatography
ICs	Interior chains
LED	Light emitting diode
LRPCD	Long-range polymer chain dynamics
LS	Light scattering
MHS	Mark-Houwink-Sakurada
MMOs	Molecular mechanics optimizations

MWD	Molecular weight distribution
NAFs	Nanosized amylopectin fragments
NMR	Nuclear magnetic resonance
Np-SNPs	Naphthalene labeled starch nanoparticles
NSFs	Nanosized starch fragments
PBA	Pyrenebutyric acid
PC4TMA	Poly(*tert*-butyl methacrylate)
PDI	Polydispersity index
PDMS	Polydimethylsiloxane
PEF	Pyrene excimer fluorescence
PEG	Poly(ethylene glycol)
PGA	Poly(*L*-glutamic acid)
PMA	Poly(methyl acrylate)
PNIPAM	Poly(*N*-isopropylacrylamide)
PS	Polystyrene
Py	Pyrene
Py-Amylopectin	Pyrene-labeled amylopectin
Py-Amylose	Pyrene-labeled amylose
Py/BBA	Pyrene per backbone atom
PyLM	Pyrene-labeled macromolecule
Py-NAF	Pyrene-labeled nanosized amylopectin fragment
SAXS	Small-angle X-ray scattering
SDS	Sodium dodecyl sulfate
SEC	Size exclusion chromatography
SLC	Static light scattering
SNPs	Starch nanoparticles
Sol-CL	Solution cluster
SPC	Single photon counting

SS	Steady-state
TC-SPC	Time-correlated single photon counting
TEM	Transmission electron microscopy
THF	Tetrahydrofuran
TNS	6-(*p*-Toluidino)-2-naphthalenesulfonic acid
UV-Vis	Ultraviolet-visible

List of Symbols

α	Mark-Houwink-Sakurada exponent
ε	Molar extinction coefficient
$\langle\phi\rangle$	Average relaxation time
η	Viscosity
$[\eta]$	Intrinsic viscosity
λ_{em}	Emission wavelength
λ_{ex}	Excitation wavelength
λ_{Py}	Pyrene content
ν	Flory exponent
ρ	R_g/R_h ratio
τ_E	Fluorescence lifetime of pyrene excimer
τ_M	Fluorescence lifetime of excited pyrene monomer
[*blob*]	Blob concentration
D	Diffusion coefficient
d_f	Fractal dimension
D_h	Hydrodynamic diameter
d_{h-h}	Distance separating two helical oligosaccharide side chains in the interior of amylopectin and NAFs
$E0^*$	Well-stacked pyrene dimers
ES^*	Short-lived pyrene excimer species
f_{diff}	Molar fraction of pyrenes forming Py_{k2}^* via diffusion in solution
f_{E0}	Molar fraction of aggregated pyrenes in solution
f_{Ediff}	Molar fraction of pyrene species in an excimer decay which form Py_{k2}^* by diffusion
f_{EE0}	Molar fraction of pyrene species in an excimer decay which are properly stacked and form an excimer $E0^*$ quasi-instantaneously upon direct excitation

f_{EES}	Molar fraction of pyrene species in an excimer decay which are poorly stacked short-lived ground-state aggregates *E*S*
f_{Ek2}	Molar fraction of pyrene species in an excimer decay which form excimer with a rapid rate constant k_2
f_{free}	Molar fraction of isolated pyrenes in solution
f_{k2}	Molar fraction of pyrenes forming excimer via a rapid arrangement
f_{Mdiff}	Molar fraction of pyrene species in a monomer decay which form Py_{k2}* by diffusion
f_{Mfree}	Molar fraction of pyrene species in a monomer decay which do not form excimer
f_{Mk2}	Molar fraction of pyrene species in a monomer decay which form excimer with a rapid rate constant k_2
I_E/I_M	Ratio of excimer to monomer fluorescence intensities
k_1	Rate constant for the diffusive encounter between an excited pyrene and a ground-state pyrene
$<k_1>$	Pseudo-unimolecular rate constant of PEF, $<k_1> = k_1 \times [Py]_{loc}$
k_{-1}	Dissociation rate constant of pyrene excimer
k_2	Rate constant of excimer formation by a fast arrangement
k_{blob}	Rate constant for the formation of Py_{k2}* between one excited and one ground-state pyrene inside a same *blob*
k_{cy}	Cyclization rate constant
k_e	Rate constant of exchange of ground-state pyrenes between *blobs*
k_{nrad}	Non-radiative rate constant
k_{rad}	Radiative rate constant
k_q	Quenching rate constant for an excited dye
M_n	Number-average molecular weight
M_v	Viscosity-average molecular weight
M_w	Weight-average molecular weight
$<n>$	Average number of pyrenes per *blob*
N_{blob}	Number of structural units constituting a *blob*
$P(q)$	Scattering factor

Py_{agg}*	Aggregated pyrenes
Py_{diff}*	Pyrenes forming Py_{k2}* via diffusion
$[Py_{diff}*]_0$	Initial concentration of pyrenes that form an excimer by diffusion
Py_{free}*	Isolated pyrenes
$[Py_{free}*]_0$	Initial concentration of pyrenes in solution that never form an excimer
Py_{k2}*	Pyrenes forming excimer with a rate constant k_2
$[Py]_{loc}$	Local pyrene concentration
q	Scattering vector
R_0	Förster radius
r_{EE}	End-to-end distance
R_g	Radius of gyration
R_h	Hydrodynamic radius
T_g	Glass transition temperature
V_{coil}	Volume of a polymer coil
V_h	Hydrodynamic volume

Chapter 1:
Literature Review

This thesis describes how fluorescence techniques can be applied to provide quantitative information on the internal dynamics and structure of polysaccharides in solution. Therefore, the first part of this introductory chapter reviews the current knowledge, as described in the scientific literature, of the internal structure and dynamics of the polysaccharides studied in this thesis, namely amylose, amylopectin, and starch nanoparticles (SNPs) produced from waxy corn starch. The second part of this chapter presents the fundamentals of fluorescence with their implications for pyrene, the dye that was mainly used in this thesis. It includes some of the interesting features of the fluorescence spectra of pyrene-labeled macromolecules (PyLMs), a description of the different physical concepts that result in specific analytical models used to characterize the kinetics of pyrene excimer formation encountered with PyLMs, and how these concepts are applied to describe the behavior of macromolecules in solution. The third and final section of this chapter introduces the objectives of this thesis and outlines its organization.

1.1 Starch

Starch is the second most abundant biopolymer in nature. It is typically synthesized in plant amyloplasts as discrete granules to store the energy generated by photosynthesis. Besides its well-known role in food, starch and its derivatives have been widely used in the paper coating, pharmaceutical, and cosmetic industries as gelling, thickening, and stabilizing agents.[1] Starch is found in plants as densely packed semi-crystalline granules, with a crystallinity level varying from 17 to 50%.[2-5] The density of the starch granules is typically 1.5 $g.cm^{-3}$.[6] Though the size and morphology of the granules is specific for each plant species, their structure under an optical microscope shows a remarkably similar architecture including growth rings, blocklets, and crystalline and amorphous lamellae as depicted in Figure 1.1.[7]

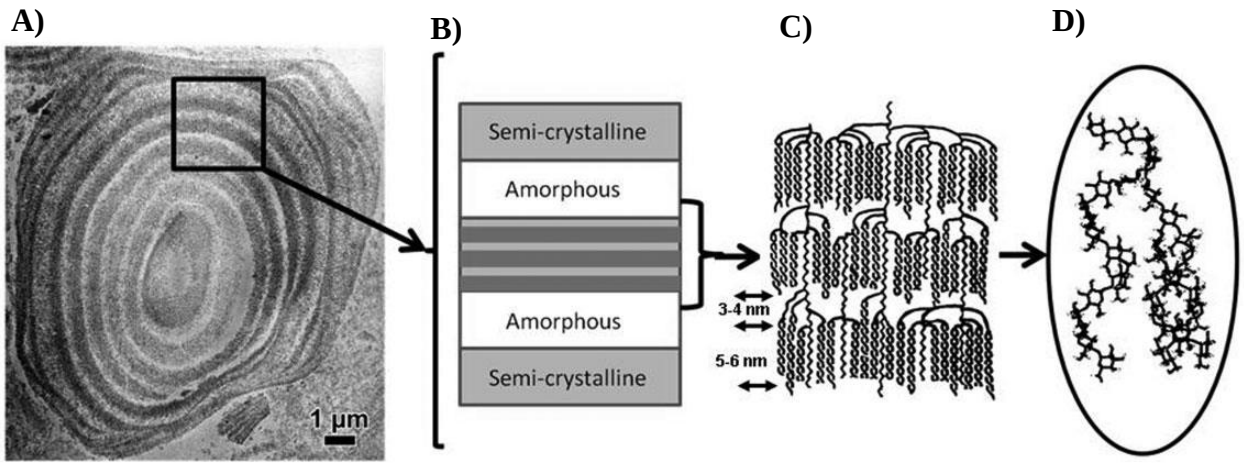

Figure 1.1. Schematic representation of the different length scales found in the ultrastructure of starch. A) Ultrathin section of a waxy maize starch granule after being subjected to H_2SO_4 hydrolysis for 7 days and staining with uranyl acetate and lead citrate. B) Alternation of semi-crystalline and amorphous rings. C) The cluster model proposed for amylopectin. D) Single and double helices generated by the side chains of amylopectin. (adapted from ref. [7] with copyright permission)

The complex architecture of starch shown in Figure 1.1 is the result of the delicate balance between the two chemical "building blocks" of starch, namely, amylose and amylopectin. Amylose has been traditionally considered to be a linear chain of D-glucose residues linked by α-(1,4)-glycosidic bonds (Figure 1.2). However, later studies have suggested that some amylose molecules might be slightly branched.[4,5,8] In contrast, amylopectin is extensively branched with short side chains which are interlinked by α-(1,6)-linkages (Figure 1.2). The method commonly used to assess the apparent amylose content of starch is to determine the iodine affinity of an aqueous solution of defatted starch obtained by treatment with aqueous methanol followed by dioxane.[9,10] Upon formation of an inclusion complex with amylose, iodine in an aqueous starch solution yields a blue colour, because the inclusion complex exhibits a broad absorption peak with its maximum near 600 nm, and this absorption can be quantified to determine the amylose content of starch.[11]

These procedures were instrumental in establishing that for most plants, amylopectin constitutes 70-85% of the starch granules by weight.[4] One exception is waxy corn starch, which consists of nearly 100% amylopectin.[4,9,12] At the other end of the spectrum, Carciofi and coworkers have described a genetically modified variety of barley that produced amylose-only starch granules.[13] The difference in the branching content leads to significantly different physicochemical properties for the two polysaccharides. For example, amylose has a high tendency to retrograde by re-crystallizing after gelatinization, which results in the production of tough gels and strong films, whilst amylopectin is more stable in water and produces soft gels and weak films.[7]

Amylose	Amylopectin
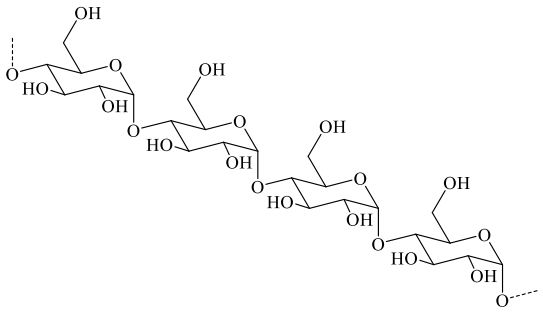	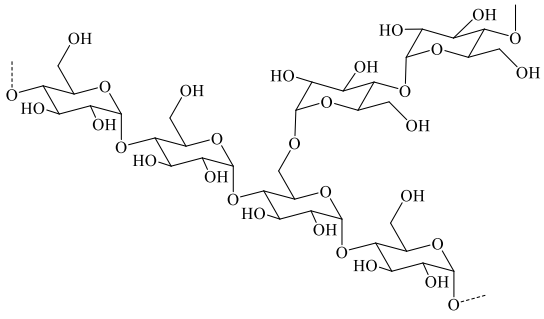

Figure 1.2. Chemical structure of amylose and amylopectin.

1.1.1 Amylose

1.1.1.1 Chemical Structure of Amylose

Amylose is the minor, linear or slightly branched component of starch. Its content is one of the most important factors affecting the cooking and eating quality of starch food products.[14] Generally, amylose-containing starches generate nanocrystals with imperfect symmetry, suggesting that amylose molecules interfere with the crystallization of starch during the formation of starch granules.[5] This observation is taken as evidence that amylose contributes mostly to the

amorphous phase in starch granules. Depending on the plant, amylose molecules may comprise between 200 and 6000 anhydroglucose units (AGUs).[15] The linear nature of amylose was proposed in the early 1940s.[8,16,17] The oldest criterion for linearity consisted in the susceptibility of amylose to be completely hydrolysed by *β*-amylase. This enzyme splits α-(1-4) bonds from the non-reducing end of amylose and releases maltose, a disaccharide constituted of two glucose units joined by an α-(1-4) bond, but it cannot cleave α-(1-6) glycosidic linkages.[8,18] When degraded by *β*-amylase, linear amylose is completely converted into maltose, whereas the degradation of a branched polysaccharide like amylopectin yields *β*-limit dextrin which is the inner core of the polysaccharide remaining after its outer chains have been depolymerized.[18] However, Peat and coworkers reported that *β*-amylase can only convert 70% of amylose into maltose.[19] This end point of molecular weight reduction is defined as the "*β*-amylolysis limit" and reflects the branching level of the polysaccharides. As a comparison, the *β*-amylolysis limit of amylopectin is reported to range between 55% and 61%, indicating that *β*-amylase cannot degrade amylopectin to the same extent as amylose due to the many branching points of amylopectin.[6] It was also confirmed that the *β*-amylase resistance of amylose could not be attributed to retrogradation[20] or oxidation.[21] Support for the view that amylose contains some branches came from the observation that for a given molecular weight, the hydrodynamic radius of amylose is smaller for the samples producing *β*-limit dextrins than for the samples that can be completely hydrolyzed.[20] In addition, a complete hydrolysis of amylose to maltose can be achieved using a mixture of *β*-amylase and pullulanase,[22] the latter enzyme being specifically able to cleave α-(1-6) glycosidic linkages.[8] Further investigation demonstrated that amylose contained two to eight branching points per molecule on average with side chains constituted of 4 to a few hundred AGUs.[23,24] Using fractionated amyloses, the level of branching was shown to increase continuously with increasing molecular weight.[25]

1.1.1.2 Conformation of amylose in dilute solution

The comformation of amylose in solution has been studied by agricultural and physical chemists for decades. However, despite this sustained research, it remains a matter of controversy to this day. Different models have been proposed to describe the conformation of amylose in solution, but their predictions cover the whole conformational range from a helix to a random coil, including a partially coiled chain with some helical segments as depicted in Figure 1.3,[8] which summarizes the main conformations of amylose that have been proposed in the literature. The conclusions for the different conformations proposed for amylose were drawn from the use of different experimental techniques that are discussed in more details hereafter.

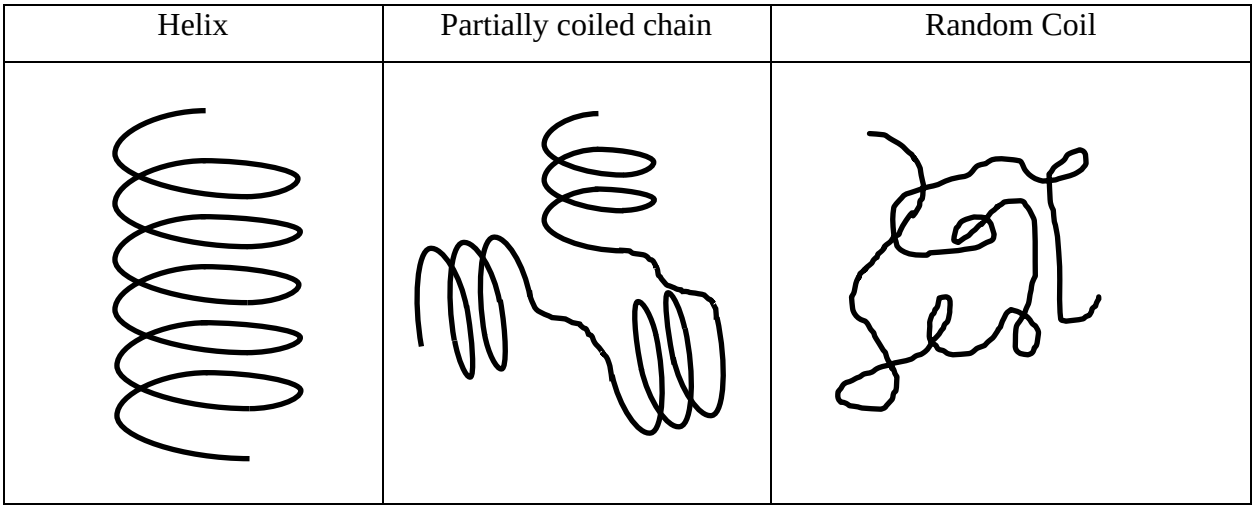

Figure 1.3. Possible conformations of amylose in solution.

Information about polymer conformation in solution can be inferred from the Mark-Houwink-Sakurada exponent (*a*) used to relate the intrinsic viscosity ($[\eta]$) of a polymer to its viscosity-average molecular weight (M_v) as shown in Equation 1.1. For a random coil in a θ– or a good solvent, *a* is expected to equal 0.5 and 0.8, respectively, but it increases to 1.8 if the macromolecule adopts a rod-like conformation.[8]

$$[\eta] = KM_v^a \qquad (1.1)$$

Several studies found that for amylose in a neutral aqueous solution of potassium chloride, a took a value of 0.5 as expected for an unperturbed polymer chain in a θ–solvent.[26-28] Therefore, Banks and Greenwood concluded that amylose in solution behaved like a random coil and, while some helical segments might be present, the helices must be loosely connected.[28] The helical nature of amylose in solution is a consequence of the α-D-(1-4)-linkages rather than intramolecular hydrogen bonding.[28] The values for the a exponent found for amylose in dimethylsulfoxide (DMSO) were more scattered since a was reported to equal 0.64 by Everett and Foster,[26] 0.70 by Banks and Greenwood,[29] 0.82 by Burchard,[30] 0.87 by Cowie,[31] and 0.91 by Fujii et al.[32] The first three values being larger than 0.5 but smaller than 0.8 suggested that DMSO is a good solvent for amylose where it would adopt a random coil conformation, whilst the latter two which are larger than 0.8 implied a semi-flexible and predominantly helical conformation for amylose. The discrepancy between the a exponents for amylose in DMSO was attributed to experimental difficulties in determining the molecular weight of amylose accurately.[33,34]

Indeed, several investigations suggested that the conformation of amylose in solution depended on its molecular weight. Burchard et al. enzymatically synthesized amylose and reported that amylose of molecular weight ranging from 6,500 to 160,000 g/mol could not dissolve in water.[30] Later light scattering and sedimentation equilibrium experiments suggested that amylose within this molecular weight range forms a rigid double helix which can readily retrograde.[35] Moreover, the intrinsic viscosity of amylose in DMSO was found to exhibit an unusually weak dependence with molecular weight when its molecular weight was below 10^4 g/mol.[33] This could be quantitatively explained by the theory developed by Yoshizaki et al.[36] for unperturbed helical wormlike chains when solvation of the polysaccharide chains by DMSO molecules was taken into

account. In this case, no excluded-volume effect needed to be considered, since the data analysis was concerned with low molecular weight amylose samples.[33]

Nevertheless, the results obtained from intrinsic viscosity measurements indicated that amylose, when fully dissolved in water, behaved as a random coil at the macromolecular level. However, studies probing amylose in solution at the micromolecular level led to an opposite conclusion. Theoretical calculations were conducted to build a conformational map of the (1-4) glycosidic bond by computing the conformational energy of amylose as a function of the rotation about the interunit glycosidic bonds. The conformational map showed that the rotations of the glucopyranoyl units were highly restricted.[37] Stronger evidence for the existence of helical segments in amylose dissolved in water was found by Lewis and Johnson. They acquired circular dichroism (CD) spectra of amylose, maltose, and the cyclodextrins.[38] By examining chromophorically equivalent but conformationally different glucans, they demonstrated that CD responded to sugar ring conformation. A comparison of the CD spectra of amylose and cyclodextrins suggested that amylose exhibited a substantial chirality bias. Moreover, the complex formed from the inclusion of butanol with amylose, which was known to have a helical structure, had a CD spectrum similar to that of free amylose in aqueous solution implying that amylose adopted a helical conformation in water.

Along with the direct evidence implying that AGUs constituting the amylose backbone experienced restriction in their orientation and adopted an ordered conformation, several authors reported a possible helix-to-coil transition of amylose when the solution pH was increased to above 11. Erlander et al.[39] and Rao et al.[40] showed that $[\eta]$ of aqueous amylose solutions decreased by approximately 40% at pH 12. Rao and Foster[41] observed a significant decrease in specific rotation for amylose in 1 N KOH solution compared to that in neutral solution. Nuclear magnetic resonance

(NMR) analysis suggested that this transition was due to an increase of rotational freedom about the glycosidic linkages at higher pH. Since changes in [η] or specific rotation could be rationalized by a helix-to-coil transition for amylose under alkaline conditions, these studies led to the conclusion that in aqueous solution, amylose must contain some helical segments that were disrupted at high pH.[39,40]

The contradictory conclusions, reached by studies probing the conformation of amylose in solution at the macro- and micro-molecular level, have led to the proposal that amylose might adopt an interrupted helix conformation resulting in an alternation of coil and helical segments akin to the conformation of a random coil.[37,38,40,42] However, this theory has not yet been fully accepted by academia for the following reasons. First, for a chain to contain both coil and helical portions, the free energy per coiled or helical residue would have to be nearly equal.[34] As a result, a change in environmental conditions should lead to considerable variations in helical content, thereby causing a noticeable change in [η] or radius of gyration. However, although [η] shows a sharp decrease for amylose at high pH,[39,40] it is insensitive to temperature and salt concentration in aqueous solution.[34] Second, it is interesting to note that key evidence supporting the random coil model is mainly obtained from viscosity and light scattering measurements. Since these methods measure the dimensions of entire macromolecules, it can be argued that both the interrupted helix and random coil conformations would experience similar overall excluded volumes even though their conformation would be very different when probed on a shorter length scale. In addition, it was already mentioned that the slightly branched nature of amylose was not well-understood until the 1980s. None of the early viscosity and light scattering studies included discussions on the effect that branching might have on the Mark-Houwink-Sakurada (MHS)

exponent (α) whose value was used to infer the conformation of amylose, and which would be certainly reduced by the presence of branches.

To better understand the behaviour of amylose in solution, Kitamura et al. conducted a series of studies using fluorescence polarization.[43-46] Comparison of the relaxation times of fluorescein-labeled dextran and amylose constructs reflected stronger micro-Brownian motions for dextran than amylose.[45] This result was consistent with previous theoretical predictions[47,48] indicating that a polysaccharide constituted of AGUs linked by α-(1-6) glycosidic bonds was more flexible than a polysaccharide constituted of α-(1-4) linked AGUs. By measuring the fluorescence polarization of the fluorescently labeled polysaccharides as a function of temperature and pH in DMSO,[46] Kitamura et al. observed a transition between pH 11 and 13, similar to that reported in previous studies,[39-41] which suggested a possible helix-to-coil transition. In addition, the polarization study showed a significant upward curvature in the Perrin plots in which the reciprocal of polarization was plotted against the ratio of absolute temperature to viscosity. This behavior was attributed to the accelerated loosening of the structure of amylose with increasing temperature and pH. Since the experimental rotational time of 11 ns found for the fluorescein-labeled amylose was much lower than that of 43 ns expected for a rigid amylose helix, the author concluded that amylose in water took a helical conformation that was not as tight as that of the V-amylose helices found in the solid state. It is worth noting that the intrinsic viscosity and optical rotation of amylose in solution were unaffected by temperature changes.[30,49,50] These results suggest that fluorescence might be more sensitive to change in the local chain conformation compared to viscometry and optical rotatory experiments. In addition, the micro-Brownian motion of the interior and terminal segments of amylose were compared by attaching dyes either randomly along the chain or specifically at the chain ends, respectively.[46] The results suggested that the chain ends were more

flexible than the main chain so that the loosening of the helical structure upon heating had to occur first in the terminal segments. Further study of the relationship between the average relaxation time $<\phi>$ and DP for amylose confirmed that fluorescence polarization reflected only the local segmental motions of the polysaccharides rather than providing information on their overall comformation.[43] Interactions of 6-(*p*-toluidino)-2-naphthalenesulfonic acid (TNS) with amylose in aqueous solution were explored by steady-state fluorescence along with fluorescence polarization.[44] An enhancement in fluorescence intensity upon addition of 0.1 wt% of amylose in a TNS aqueous solution confirmed the formation of amylose-TNS complexes. However, a similar $<\phi>$ value was found for the amylose-TNS complex as for fluorescein-labeled amylose implying that both dyes probed a helical segment of amylose. The result was consistent with a previous CD study of amylose suggesting that amylose underwent a minor conformational change after forming an inclusion complex.[38] Since small linear molecules like TNS are known to induce the section of amylose involved in their complexation to adopt a helical conformation in solution,[51] the lack of variation of the fluorescence signal before and after amylose formed inclusion complexes with TNS implied that amylose must already contain some helical segments prior to the addition of TNS.

As the above discussion made clear, the conformation of amylose in solution, whether it be a random coil or an interrupted or continuous helix remains a matter of debate. Novel techniques, such as fluorescence, can provide new insights to resolve this controversy. Since these conformations would result in very different internal dynamics and local density for amylose in solution, pyrene excimer fluorescence (PEF) which is sensitive to polymer chain dynamics and local density would be ideal to investigate the conformation of amylose in solution.[52-57] To this end, an amylose sample was randomly labeled with different amounts of 1-pyrenebutyric acid and

its fluorescence was analyzed using steady-state and time-resolved fluorescence. It was found that the PEF efficiency was similar for rigid amylose and flexible poly(methyl acrylate) (PMA), an unexpected conclusion considering the rigid polysaccharide backbone. This result could only be rationalized by postulating that amylose adopted a compact helical conformation in DMSO whose large local density was offsetting its slow dynamics for PEF. This study is described in Chapter 2 of this thesis.

1.1.2 Amylopectin

1.1.2.1 Chemical structure of amylopectin

Amylopectin is the highly branched component of starch. It is constituted of short chains, made of AGUs linked together by α-(1-4) bonds, which are connected to each other by α-(1-6) linkages. In amylopectin, 5-6 mol% of AGUs have an α-(1-6) glycosidic bond that acts as a branch point.[5,7] These branch points make the macromolecular structure of amylopectin more complex than that of amylose. It is also a much larger macromolecule with reported M_w values ranging between 2 and 700 × 10^6 g/mol.[7,58] The fine structure of amylopectin has been of particular interest because of its implications for the physicochemical properties of starch, such as crystallinity and viscoelasticity.[59,60] It is also an important parameter for biochemists studying the biosynthetic pathway of amylopectin and its organization inside starch granules.[7,59,61]

Figure 1.4 introduces the different structural elements that have been proposed to describe amylopectin. The exterior chains (ECs) are located between the non-reducing end and the outermost branch points. The interior chains (ICs) represent the parts of a chain spanning two branch points in the interior of the macromolecule. To distinguish the unit chain composition of amylopectin more specifically, Peat and coworkers divided the various chains into three groups according to their substitution level.[62] A-chains are defined as unsubstituted chains that are

connected to the rest of the macromolecule through α-(1-6) linkages. In contrast, B-chains are substituted by one or several A- or B-chains. In addition, each macromolecule contains one single C-chain, which carries the sole reducing terminal end of the macromolecule. The molar ratio of A-chains to B-chains, or the A:B ratio, is also referred to as the degree of multiple branching.

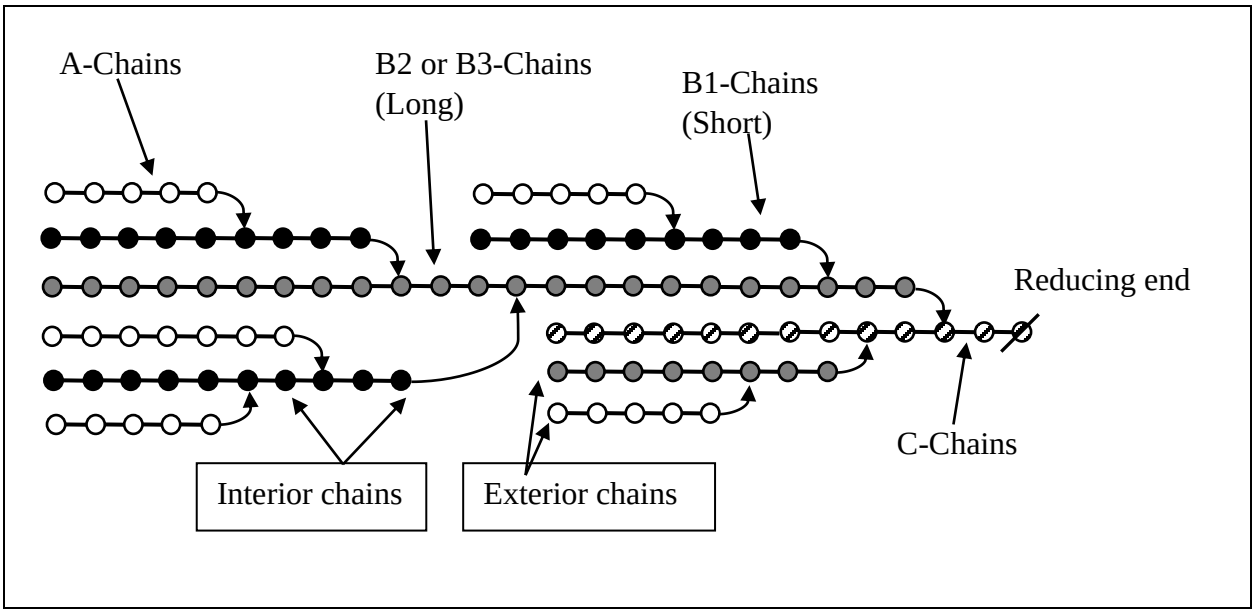

Figure 1.4. Definition of the different types of chains in amylopectin. AGUs are represented by circles. α-(1-4) and α-(1-6) linkages are represented by horizontal lines and bent arrows, respectively. The reducing-end residue is shown at the far right of the figure. (Adapted from ref [7] with copyright permission).

Several models have been proposed based on the side chain distribution of amylopectin to rationalize its physicochemical properties. Early models included the laminated structure suggested by Haworth et al.,[63] the "heringbone" model suggested by Staudinger et al.,[64] and the randomly branched model proposed by Meyer et al.[65] As shown in Figure 1.5, when the molecular weight is large enough, the randomly branched model would give a characteristic A:B ratio equal to 1, while the laminated and herringbone models would have an A:B ratio of 0 and infinity, respectively. Several studies used debranching enzymes to determine the A:B ratio of amylopectin

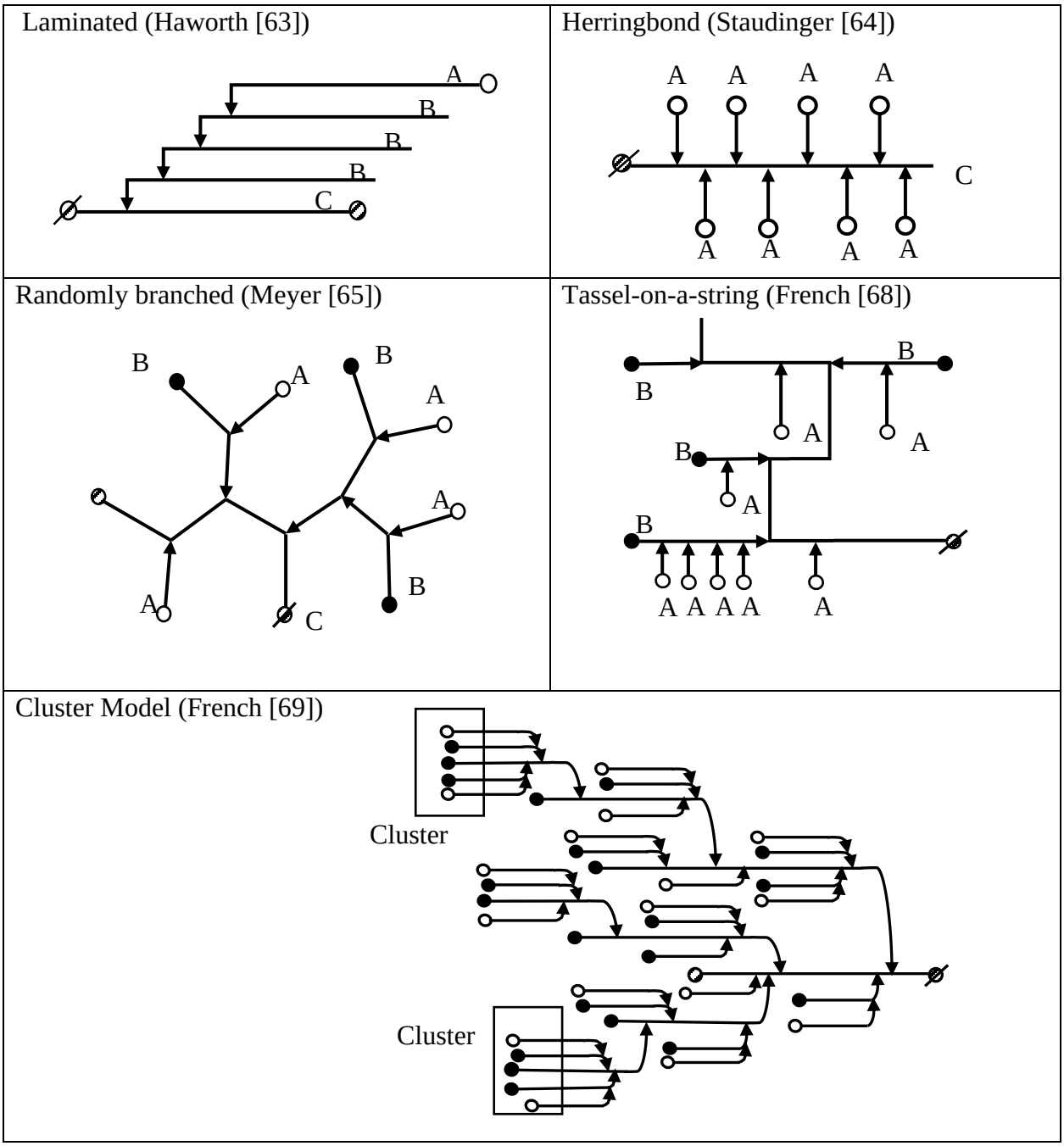

Figure 1.5. Different structural models proposed for amylopectin. The non-reducing end residue of A chains, B chains and C chains are represented by the hollow circles, filled circles and circles crossed by a line, respectively. α-(1-4) and α-(1-6) linkages are represented by horizontal lines and bent arrows, respectively. The reducing-end residue is shown at the far right of the figure. (Figures are adapted from ref [8] and ref [69] with copyright permission)

and found that the A:B ratio was between 1.0-1.5, a result that favored Meyer's randomly branched model.[62,66-68] French reconsidered the randomly branched model and suggested a tassel on a string representation for amylopectin, which became the foundation of the cluster model.[69] Since its inception in 1973, the cluster model has gained increasing support and is now well accepted to describe the fine structure of amylopectin.[70] It suggests that amylopectin is composed of highly ordered clusters of short chains which are linked to each other by much longer chains. A consequence of the cluster model is that the interior of the macromolecule must therefore be heterogenous.

The commercialization of the debranching enzymes pullulanase and isoamylase, which specifically target α-(1-6) linkages in amylopectin, enabled the study of the finer structural details of amylopectin.[7] Following the enzymatic hydrolysis of amylopectin, the size distribution profile of the resulting oligosaccharides was then analyzed by various fractionation techniques, such as size exclusion chromatography (SEC), high-performance SEC (HPSEC), high-performance anion exchange chromatography (HPAEC), and capillary electrophoresis.[7] For instance, Hanashiro and coworkers[59] reported the distribution of C-chains obtained from the hydrolysis of six amylopectin samples (rice, maize, wheat, potato, sweet potato, and yam) after labelling them with a fluorescent dye. The reported C-chain lengths ranged between 10 and 130 AGUs, with a peak in the SEC profile corresponding to a degree of polymerization (DP) of 40 for several amylopectin samples. The distribution of the chains were very similar across different botanical sources suggesting that the biosynthetic process for chains was similar in different plant species. A typical chain distribution profile for A- and B-chains is shown in Figure 1.6. Lee and coworkers debranched waxy maize starch with pullulanase and observed two peaks in the chromatogram corresponding to chains with DP < 20 and DP of about 40.[71]

In later experiments, Akai et al.[72] used isoamylases to cleave the branches of amylopectin. The SEC profiles also showed two characteristic peaks for oligosaccharides with DP values of about 20 and 50. It was interesting to note that the short chains with DP ~ 20 were present in both the amylopectin samples and their corresponding β-limit dextrins suggesting that the short chains were mixtures of A- and B-chains. In other words, the B-chains were composed of at least two distinct populations, shorter chains with DP around 20 and longer chains with DP values of 40-80.

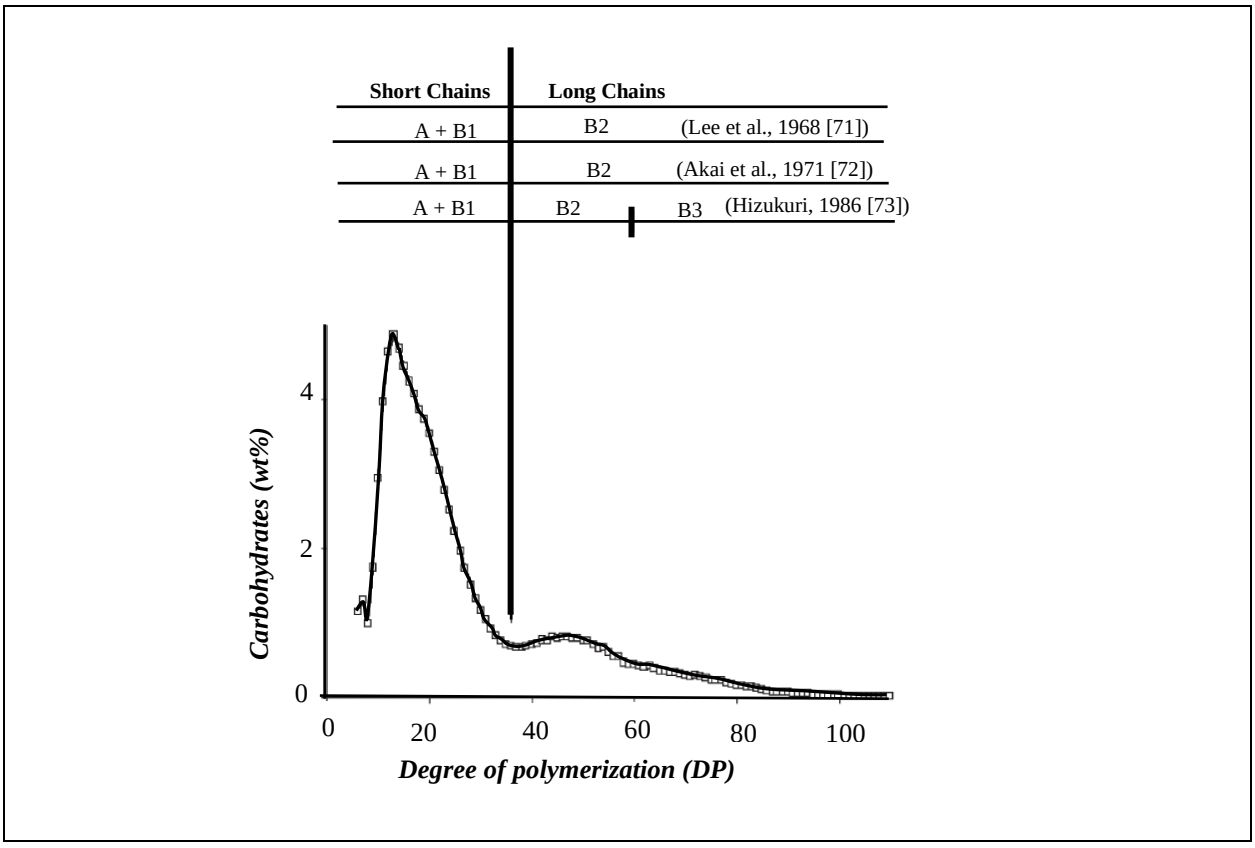

Figure 1.6. Illustration of the polymodal side chain distribution obtained for debranched amylopectin. The division of the side chains into different categories is indicated as suggested by different authors. (Adapted from ref [7] with copyright permission)

Hizukuri[73] reported a polymodal chain distribution profile for amylopectin extracted from tulip, tapioca, and wheat using HPSEC, and subdivided the longer B-chains into B2- and B3-chains. The average DP of the A, B1, B2, and B3-chains was found to be 12-16, 20-24, 42-48, and 69-75, respectively. Based on this polymodal chain distribution, the author proposed a further refinement of the cluster model (Figure 1.7). In the refinement, single clusters were composed of A and B1-chains. The two clusters were then connected by the B2-chains and three clusters were further connected through the B3-chains. The sums of the chains in fraction A and B1 were about 80-90% of the total and constituted a single cluster. The remaining 10-20% of the chains were mainly involved in inter-cluster connections.

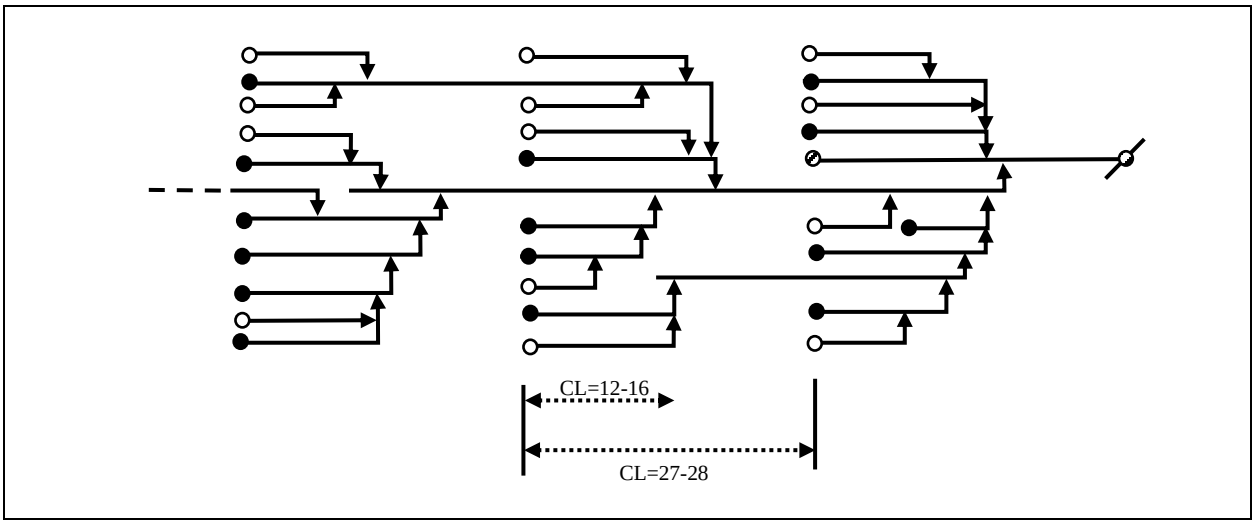

Figure 1.7. Diagram of the refined cluster model proposed by Hizukuri. (Adpated from ref [73] with copyright permission)

The cluster model provides a good explanation for the growth rings structure observed in the starch granules,[74] the relatively higher viscosity of amylopectin samples compared to that of glycogen samples having a higher molecular weight,[70] and the relative resistance of parts of amylopectin when attacked by acids or enzymes.[75] However, it must be emphasized that although the cluster model is generally accepted,[70] rather little is known about the structure of isolated

clusters, particularly in solution. Most discussions, as shown in the above sections, are based on indirect evidence. The basic definitions of a cluster, such as its size and density, are still missing. The organization of the clusters throughout the macromolecule and organization of the chains within the clusters deserve further investigation.

1.1.2.2 Physical properties of amylopectin in dilute solution

Compared to amylose, much less attention has been paid to the behaviour and architecture of amylopectin in solution. The only small-angle X-ray scattering (SAXS) study[76] of amylopectin in dilute solution was conducted on waxy corn starch samples that first had been treated with acid and second were pyrolyzed for different time periods. These were thus degraded amylopectin samples which could be viewed as nanosized amylopectin fragments (NAFs). Even at the lowest concentration studied of 0.5 wt%, interparticle contributions to scattering were observed. The SAXS intensity profiles obtained with the NAFs dissolved in water and DMSO were fitted assuming that the NAFs were impenetrable to the solvent and that they adopted a shape that was either a sphere or a disk. The data analysis required the addition of a Gaussian to account for the polydispersity of the NAFs. Poor fits were obtained by assuming that the NAFs were impenetrable spheres, but the scattering profiles could be fitted satisfactorily by assuming that the NAFs were disks of thickness 27 and 30 Å in water and DMSO, respectively. How this information would relate to non-degraded amylopectin samples remains to be determined.

The majority of the investigations on amylopectin in dilute solution used different laser light scattering techniques to reveal its overall conformation. Dynamic light scattering (DLS) is based on the light scattered by particles diffusing in-and-out of the beam of light as a function of time. Standard DLS instruments yield the hydrodynamic radius (R_h) of particles assuming that they adopt a spherical shape. Static light scattering (SLS) measures the intensity of the light scattered

by macromolecules in solution averaged over a fairly long time (=2 sec)[77] and yields the absolute weight average molecular weight (M_w) and the radius of gyration (R_g) of macromolecules. The R_g/R_h ratio ($\rho = R_g/R_h$) depends primarily on the mass distribution of the macromolecule and is often used as an indication of its overall geometry in solution.[78] The typical ρ-value of a flexible chain in a good solvent is ~1.7 and deceases with increasing branching of the chain. The typical ρ-value of a star polymer with 4 arms is 1.33. Further increasing the number of arms decreases ρ to ~1.079.[79] The fractal dimension, d_f, also obtained from SLS, provides structural information on polymers in solution. This parameter can be retrieved by plotting $log[P(q)]$ as a function of $log[qR_g]$, where $P(q)$ is the scattering factor and q is the scattering vector.[80] Linear polymers in a good solvent, linear polymers in a theta solvent, fully swollen clusters, and non-swollen clusters yield fractal dimensions of 1.67, 2.00, 2.00 and 2.50, respectively.[79] The reported values of M_w, R_g, R_h, ρ, and d_f obtained from different LS studies on amylopectin are summarized in Table 1.1. Despite intensive studies by many authors, the experimental results obtained for amylopectin are very different from each other. The discrepancies between the results are due to the different botanical origins of amylopectin and the different methods applied for the preparation of the amylopectin samples. Some of these results are discussed hereafter to illustrate these differences.

Table 1.1. Summary of light scattering results obtained for amylopectin in dilute solution.

Sample Origin	Preparation method	Solvent and T (℃)	$M_w \times 10^{-6}$ (g/mol)	R_g (nm)	R_h (nm)	R_g/R_h	d_f	Ref
Waxy corn	Amylopectin was dissolved in a 10:90 (v/v) DMSO:water mixture and the solution was heated for 20 min at 100 ℃	10:90 (v/v) DMSO:water at 37 ℃	53.0	242	58	4.17		[77]
Normal corn			13.0	113	59	1.91		
Potato			0.4	15	21	0.71		
Waxy corn	Amylopectin was dissolved in a 0.5 M NaOH solution or a 90:10 (w/w) DMSO:water mixture by stirring for 18 h at 10 ℃	0.5 M NaOH solution at 10 ℃	129	223	172	1.29	2.11	[79]
		0.5 M NaOH solution at 25 ℃	530	276	282	0.98	2.5	
		90:10 (w/w) DMSO:water at 25 ℃	150	238	190	1.25		
Waxy corn	Starch was gently dispersed in a 90:10 (w/w) DMSO:water mixture by stirring at 100 rpm for 1 h at room temperature.	90:10 (w/w) DMSO:water at room temperature	560	342	348	0.98		[81]
Waxy maize	Starch was cooked in a 90:10 (v/v) DMSO:water mixture at 100 ℃ for 1 h, then stirred at room temperature for 24 h before being precipitated with ethanol. The purified amylopectin was dispersed in different DMSO:water mixtures at 100 ℃ for 1 h.	50:50 (v/v) DMSO:water	192.7	182.8	201.2	0.91		[82]
		70:30 (v/v) DMSO:water	54.5	182.3	173.5	1.06		
		90:10 (v/v) DMSO:water	15.3	99.8	107.0	0.93		

Table 1.1. (Continued) Summary of light scattering results of amylopectin in dilute solution.

Sample Origin	Preparation method		Solvent and T (°C)	$M_w \times 10^{-6}$ (g/mol)	R_g (nm)	R_h (nm)	R_g/R_h	d_f	Ref
Waxy corn	Starch samples were dispersed in a sodium azide solution heated at 175 °C for 1 hour for waxy corn starch and for 40 min for potato starch.		0.05% (w/v) sodium azide aqueous solution at room temperature	37.5	121			2.49	[83]
Potato				56.4	199			2.36	
Waxy corn	Starch was cooked in a 90:10 (v/v) DMSO:water mixture at 100 °C for 1 h, then stirred at room temperature for 24 h before being precipitated with ethanol. The purified starch was dispersed in the 90:10 (v/v) DMSO:water mixture at 100 °C for 1h.		90:10 (v/v) DMSO:water mixture	274	255				[84]
Non-waxy corn				208	246				
Corn amylopectin	Starches were purified by dissolving in a 95:5 (v/v) DMSO:water mixture. Solutions were stirred for 3 days at room temperature before being precipitated with ethanol. Purified samples were dissolved in water and heated for 35, 50, 70, and 90 s in a 900 W microwave oven.	35 s	Water at room temperature	270	259	201	1.29	2.20	[85]
		50 s		240	260	221	1.18	2.12	
		70 s		110	190	187	1.02	1.98	
		90 s		78	170	148	1.15	1.80	
Non-waxy corn		35 s		250	267	201	1.33	2.28	
		50 s		160	230	207	1.11	2.10	
		70 s		36	134	135	0.99	1.51	
		90 s		9	131	99	1.32	1.00	

A dispersion of waxy maize starch in a 90:10 DMSO:water mixture kept at 100 ℃ before being stirred for 1 h at room temperature gave M_w and R_g values equal to 560×10^6 g/mol and 349 nm, respectively.[81] In contrast, Yang et al.[79] prepared a waxy maize starch dispersion by mixing amylopectin in 0.5 M NaOH with a magnetic stirrer for 18 h at 10 ℃. The dispersions were characterized by SLS, but the analysis of the scattering data yielded different results depending on the experimental temperature. The M_w, R_g, and R_h values of amylopectin at 10 ℃ were reported to equal 29×10^6 g/mol, 223 nm, and 172 nm, respectively. At 25 ℃, those values for the same amylopectin sample were much larger at 530×10^6 g/mol, 276 nm, and 282 nm, respectively. Apparently, amylopectin formed stable aggregates at 25 ℃ in 0.5 NaOH solution. The value of d_f was found to increase from 2.1 to 2.5 when the temperature was increased from 10 to 25 ℃, suggesting that the amylopectin molecule transitioned from a fully swollen cluster to a non-swollen cluster. Despite lacking a well-established theory describing the architecture of amylopectin in solution, Yang et al. attempted to analyze the internal dynamics of amylopectin. Internal motions are typically observed for scattering angles corresponding to $(qR_g)^2$ values greater than 1 for a flexible polymer chain and 13 for a highly cross-linked microgel.[79,86] In the case of amylopectin, internal motions were detected at $(qR_g)^2$ values larger than 4. This result implied that the branched structure hindered the internal motions of amylopectin to some extent. Lee et al. studied the effect of the water content in DMSO on the conformation of amylopectin obtained from waxy corn.[82] A water content of about 10 wt% appears to represent optimal conditions for the dissolution of amylopectin. Increasing the water content further resulted in aggregation as indicated by larger M_w, R_g, and R_h values. It is noteworthy that in these experiments, the amylopectin dispersion was heated at 100 ℃ for 1 hour before conducting LS measurements, resulting in M_w, R_g, and R_h values of 15.3×10^6 g/mol, 99.8 nm. and 107.0 nm, respectively, that were much smaller than those

obtained in other studies.[79,81,83,84] This result suggested that maintaining the amylopectin dispersion at high temperature for an extended period of time is necessary to prevent aggregation.

The advantage of LS techniques is that they yield parameters which have physical meaning. In turn, the values of these parameters can be compared to those obtained in previous studies with other macromolecules. As the previous discussion made clear, accurate light scattering results are challenging to obtain with amylopectin in solution because the macromolecules aggregate spontaneously, thus generating interferences that significantly affect the overall light scattering signal. Ideally this issue could be resolved by using extremely dilute solutions of amylopectin where no intermolecular interactions could occur. Such experiments would rely on a technique that would have to be sensitive enough to retrieve sufficient signal with amylopectin solutions that would be so dilute as to prevent aggregation. It is, therefore, the purpose of this thesis to apply fluorescence techniques to characterize amylopectin in solution. Fluorescence is a highly sensitive technique that has been widely used to characterize the internal dynamics of linear chains in solution during biophysical processes such as protein folding[87] or a coil-to-helix transition,[88] or to probe chain flexibility of a variety of polymers.[56] As LS techniques do, fluorescence techniques provide quantitative information on the internal dynamics and local concentration of macromolecules in solution, but they do so at concentrations that are orders of magnitude lower than those used for LS. Consequently, the case for applying fluorescence techniques to characterize amylopectin is appealing since they would minimize, not to say completely prevent, aggregation. More information pertaining to the characterization of amylopectin using fluorescence is presented in Chapter 3 of this thesis.

1.1.3 Starch Nanoparticles (SNPs)

Starch nanoparticles (SNPs) can be readily prepared from starch granules. They have been found to present unique physical properties. Recent studies suggest that SNPs constitute one of the most promising biomaterials for applications in foods, cosmetics, medicine as well as fillers to improve the mechanical and barrier properties of biocomposites.[89-91] Acid hydrolysis has been widely used in the preparation of SNPs because the reaction is simple and easy to control. The crystalline regions in starch granules are more resistant to acid hydrolysis than the amorphous regions, thus enabling the isolation of the crystalline domains of starch granules through mild acid hydrolysis with hydrochloric or sulfuric acid.[89] The final products of starch hydrolysis are often referred to as starch nanocrystals since the crystalline parts of the starch remain after the reaction.[89,90] Transmission electron microscopy (TEM) is widely used to characterize the size and morphology of SNPs. Dufresne et al. showed that the crystalline products remaining after prolonged acid hydrolysis consisted of agglomerated individual particles that were a few tens of nanometers in diameter.[92] Putaux et al. observed an edge-on view of the lamellae under the TEM, which were generated by the association of amylopectin side-branches.[93] Subjecting native waxy maize starch to a hydrochloric acid hydrolysis for 2 weeks disrupted the lamellar arrangement to some extent, resulting in the hydrolysis of a number of α-(1-6) bonds located in the amorphous regions between the crystalline lamellae. Because the branching points located in the interlamellar areas were more readily hydrolyzed, the insoluble products could be fairly well identified. These particles could still be observed even after 6 weeks of hydrolysis. The hydrolysis residues were crystalline nanoplatelets approximately 6–8 nm in thickness, 20–40 nm in length, and 15–30 nm in width.[93] SNPs with spherical or polygonal shapes were often found to be microscale aggregates, suggesting that acidic hydrolysis did not generate individual particles.[94-96] Other disadvantages associated

with the preparation of SNPs by hydrolysis included a long preparation time (40 days) that is energy consuming and a relatively low yield (0.5 wt%).[89] Moreover, extra purification processes are often required to remove the salts and hydrolyzed sugars remaining in the reaction medium. Other treatments that were applied to prepare SNPs include microfluidization,[95] ultrasonication,[97] reactive extrusion,[98] precipitation,[99,100] complex formation,[101] and gamma irradiation.[102] SNPs prepared by these methods were found to have a low crystallinity or an amorphous structure.[89]

The most popular commercial SNP-products are Mater-Bi™ from Novamont and Eco-Sphere™ from Ecosynthetix.[90] Mater-Bi is a biopolymer processed by complexing modified starch with variable quantities of complexing agents and mixing that complexed starch with at least one hydrophobic polymer incompatible with starch. The products are commercialized as pellets. The most famous application for Mater-Bi is BioTRED, where Mater-Bi is used to replace some of the lampblack and silica particles that are part of a tire mixture.[90] In contrast, Eco-Sphere is a starch-based biolatex that acts as a substitute for oil-based latexes in paper coating and tissues.[90] These SNPs were produced via reactive extrusion where waxy corn starch is subject to high pressure, heat, and mechanical shear forces.[98] At the high operating temperature of the extruder, starch granules soften and partially melt. The softened and melted starch granules are physically torn apart by the shear force, which allows water into the interior of the starch granules. Similar to other physical treatments, the high shear energy applied during extrusion damages the starch. The SNPs prepared by extrusion have a very low viscosity, compared to the original starch, implying extensive degradation of the starch. They were stable for more than 6 months.[98]

The research-grade particles used in this thesis were derived from waxy corn starch via a reactive extrusion process at high temperature. Since waxy corn starch is amylose-free amylopectin and the amylopectin was degraded during extrusion, these particles are referred to as

nanosized amylopectin fragments (NAFs). Twenty-one research grade NAFs were prepared under different extrusion conditions by EcoSynthetix (Burlington, On). The molecular weight of the NAFs was found to be significantly smaller than that of amylopectin extracted from waxy corn starch, ranging from 0.2×10^6 to 36×10^6 g/mol. The size reduction imparted by the extrusion process increases the solubility of this starch-based material in water, which facilitates the adjustment of its concentration to reach the solution viscosity required in a variety of industry applications. The main application of SNPs has been as binder in the paper industry where it replaces petroleum-based latex emulsions. These new binders have shown unique rheological and optical properties which have been harnessed by the paper coating industry.[103] In addition, hydrophobic groups, such as epoxy alkanes or oleic and stearic acids, can be readily introduced through reaction with the numerous hydroxyl groups of SNPs.[104] The resulting hydrophobically modified SNPs (HM-SNPs) have potential for a broad range of applications, such as drug delivery vehicles and chemical sensors.[105]

The properties of several SNPs and HM-SNPs have been investigated by the Duhamel group. Using a series of pyrene fluorescence techniques including steady-state fluorescence, time-resolved fluorescence, and fluorescence quenching, Kim et al. probed a series of HM-SNPs bearing propionyl and hexanoyl substituents.[104] The results suggested that the hydrophobic domains generated in the particle interior were much less defined compared to the hydrophobic core of surfactant micelles. Information about the local viscosity and polarity of the hydrophobic microdomains was also provided to guide further modifications of those particles to be used as drug delivery carriers. Interactions between HM-SNPs and surfactants in water were studied by Zhang et al. using both pyrene- (Py-SNPs) and naphthalene- (Np-SNPs) labeled-SNPs.[106] Whereas Py-SNPs could be stabilized in water upon addition of linear surfactants such as sodium dodecyl

sulfate (SDS) at extremely low surfactant concentration, branched surfactants such as sodium dioctyl sulfosuccinate (AOT) did not interact with Py-SNPs in water at the same surfactant concentrations. The behavior difference was attributed to the formation of inclusion complexes with the side chains of Py-SNPs and SDS in water. Both investigations showed that the rigid and branched polysaccharide backbone of SNPs had a significant influence on the polymer behavior in solution making HM-SNPs unique in comparison to other amphiphilic materials. The successful application of pyrene fluorescence in these early studies suggested that it could be a powerful tool in the characterization of polysaccharides.

1.2 Characterization of Macromolecules in Solution by Fluorescence

The most popular fluorescence techniques to characterize macromolecules in solution include fluorescence anisotropy (FA), fluorescence resonance energy transfer (FRET), and fluorescence dynamic quenching (FDQ).[107] Fluorescence anisotropy (FA) measures the change in orientation of a molecule in space. When the chromophore is excited by polarized light, the emitted light retains some of that polarization for different lengths of time depending on how quickly the molecule rotates in solution.[108] Therefore, FA is often applied to characterize the segmental motions and conformation of a polymer chain by a chromophore attached to it.[108-112] As discussed in the previous section, Kitamura et al. conducted a series of FA studies to characterize the conformation of amylose in solution.[43-46] The change in rotational times determined by FA indicated that FA is much more sensitive to conformation changes experienced by polymers in solution compared to other techniques. However, FA cannot probe the local density of the interior of macromolecules, and as a result, is not well suited to probe the actual conformation of complex macromolecules like amylopectin, although it can sense a conformational change.[43-46]

Another powerful technique for characterizing polymer chain conformation is FRET.[107] Unlike FA which measures the rotational time of a chromophore attached to a macromolecule, FRET measures the distance between a fluorescent donor and its acceptor. Its most famous application involved the labeling of a series of rigid poly(*L*-proline) type II *trans*-helices with a naphthyl energy donor at one end and a dansyl energy acceptor at the other end to characterize the end-to-end distance of the helices. The excellent correlation found between the end-to-end distance determined by FRET and the known dimension of the helix led to the statement that FRET could be used as a "spectroscopic ruler".[113] In contrast, attachment of a pair of donor and acceptor to the chain ends of a flexible linear chain results in a FRET response that depends on the initial distance distribution between every donor and acceptor pair as well as the diffusion coefficient (*D*) of the chain ends.[114] At the early times, those pairs of dyes separated by a short distance undergo rapid FRET and they are partially replaced by other pairs of dyes separated by longer distances, with a replacement rate that depends on *D*. Quantitative information about the average end-to-end distance and the chain end mobility through *D* can thus be retrieved. However, FRET is not ideal for polysaccharides like amylose or amylopectin, as the large number of hydroxyls decorating the polysaccharide backbone prevents their specific labeling, except perhaps at the single reducing end of the macromolecule. Furthermore, the large size and stiffness of the polysaccharides would forbid the spectroscopic communication between two dyes attached at two specific positions. In theory, these issues could be circumvented by randomly labeling the polysaccharides with donors and acceptors, but the distribution of distances between every pair of donors and acceptors combined with the residual mobility resulting from the internal dynamics of the macromolecule would make the FRET signal too complicated to analyse.[115]

FDQ is used to probe the dynamics of polymer chains by attaching a chromophore and its quencher on a same macromolecule and monitoring how the excited chromophore is being quenched. FDQ differs from FRET because quenching of the dye must occur on contact and not over a distance as for FRET. The most common chromophore used in FDQ studies of macromolecules in solution is pyrene. As stated by Francoise Winnik in her 1993 review, "pyrene is by far the most frequently used dye in fluorescence studies of labeled polymers".[116] Among the reasons provided for this statement were its large molar absorption coefficient, high quantum yield, and extremely long natural lifetime for an organic dye of 200-300 ns. Like many other organic dyes (naphthalene, perylene), pyrene acts as its own quencher through pyrene excimer formation (PEF), thus resulting in a much simpler labeling procedure since the macromolecule needs to be labeled with a single molecule that acts as both dye and quencher.[116] But contrary to these other dyes, the 0-0 transition of pyrene is strongly reduced, thus resulting in a very small molar absorption coefficient for the $S_{0\rightarrow1}$ band.[117] This has two major consequences. First, hardly any overlap exists between the absorption and fluorescence spectra of pyrene, which minimizes energy hopping through FRET when an excited pyrene approaches a ground-state pyrene to form an excimer.[117] Second, since the radiative rate constant (k_{rad}) is proportional to the molar absorption coefficient of the $S_{0\rightarrow1}$ transition which is very small, k_{rad} is very small, which combined with a small non-radiative rate constant (k_{nrad}) explains why pyrene has one of the longest natural lifetime ($\tau_M = (k_{rad}+k_{nrad})^{-1}$) of many organic dyes.[118] Early research using this technique focused mainly on pyrene end-labeled monodisperse linear chains, whereby the PEF rate constant reflected the rate constant of chain end-to-end cyclization (EEC).[119] The application of FDQ was greatly expanded after the development of the fluorescence blob model (FBM) by Duhamel.[57] This novel approach enabled the analysis of PEF for randomly labeled polymers. To date, the FBM has been

applied to probe the chain dynamics of flexible polymers such as poly(methyl acrylate) (PMA),[56] more rigid polymers such as poly(tert-butyl methacrylate) (PC4TMA),[56] and polymers that form rigid helices in solution such as poly(*L*-glutamic acid) (PGA).[120]

The characterization of amylose and amylopectin would benefit tremendously from the application of PEF for the following reasons. First, the labeling procedure is straightforward since it only requires a single chromophore, pyrene, to be randomly attached onto the macromolecule. Second, the FBM works by dividing the macromolecule into a cluster of *blobs* and the analysis focuses on the characterization of a single *blob*. Consequently, the analysis is independent of the molecular weight or polydispersity of the sample since a larger macromolecule will be handled by a larger number of *blobs*.[121] Consequently, experimental complications caused by the large size and polydispersity index (PDI) encountered with polysaccharides are not a problem for FBM-based analysis. Furthermore, since numerous polymers with different chain flexibility and conformation have already been characterized,[56,120,122,123] the internal dynamics of these polymers can now be compared quantitatively with those of these two polysaccharides. The different models that were introduced over the years to study pyrene-labeled polymers are described in the following section.

1.2.1 Pyrene Excimer Formation

When a ground-state pyrene is excited by UV light at around 340 nm, it can either emit a photon as a monomer with its natural lifetime (τ_M), or encounter another ground-state pyrene with a rate constant k_1 to form an excimer that emits with its natural lifetime (τ_E). In a homogeneous solution, this process is described by the Birks scheme as shown in Figure 1.8A.[124] It must be emphasized that due to strong π-π stacking between the two pyrenyl moities, the excimer dissociation rate constant k_{-1} is relatively small compared to $1/\tau_E$ making its contribution negligible below 35 °C.[125]

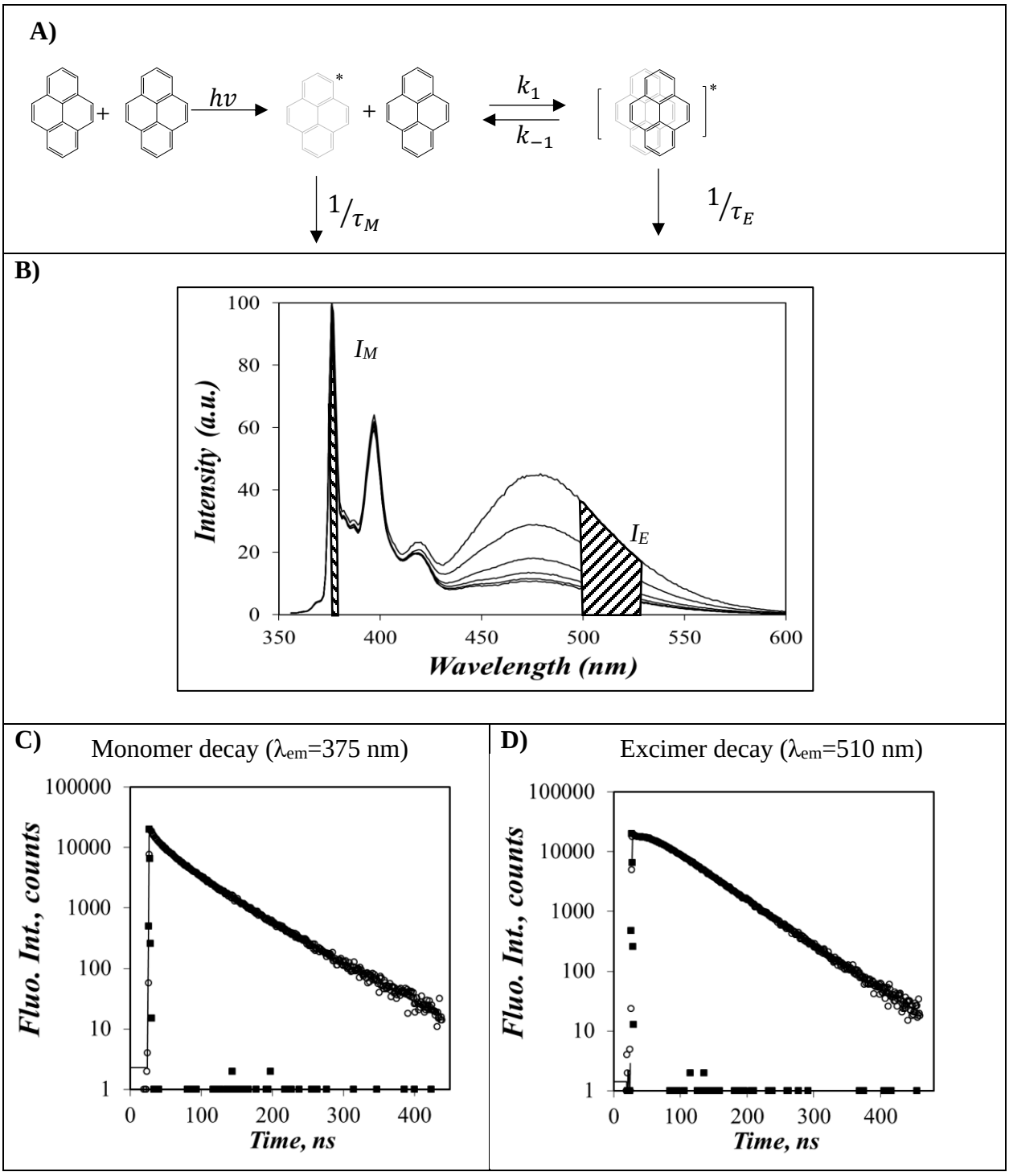

Figure 1.8. A) Birks' scheme for pyrene excimer formation. B) Steady-state fluorescence spectra of a series of pyrene-labeled amylose constructs in DMSO with pyrene content increasing from 5 to 15 mol% from bottom to top. C) Monomer and D) excimer fluorescence decays of amylose labeled with 10 mol% pyrene in DMSO. [Py]=2.5 × 10^{-6} M.

A typical fluorescence spectrum of pyrene is shown in Figure 1.8B. The pyrene monomer emission is characterized by sharp fluorescence bands between 370 and 400 nm, whilst the excimer emits a broad structureless fluorescence in the 400-600 nm range. As shown in Figure 1.8B, increasing the pyrene content increases the number of possible pyrene-pyrene encounters resulting in stronger excimer emission. Qualitative information on the PEF rate constant can be derived from the ratio of the fluorescence intensity of the excimer to that of the monomer in the steady-state fluorescence spectra, namely the I_E/I_M ratio. The value of I_E and I_M can be calculated by integrating the fluorescence intensity of the first monomer peak between 372 and 378 nm and the broad excimer band between 500 and 530 nm, respectively.

The I_E/I_M ratio obtained from the analysis of the steady-state fluorescence spectra of a pyrene-labeled macromolecule represents all pyrene species that contribute to the monomer and excimer fluorescence. These include the pyrene impurities that are free in solution and do not form excimer and the pyrenyl moieties involved into pyrene aggregates that form excimer instantaneously upon excitation. These pyrene species do not provide any information on the dynamic process of excimer formation, and their contribution to the I_E/I_M ratio cannot be isolated by steady-state fluorescence. This problem can be solved through the analysis of the time-resolved fluorescence decays. If the excimer is formed by diffusion between two pyrenyl groups, excimer formation is delayed, and a rise time is observed in the excimer decay. On the other hand, excimer formation by direct excitation of ground-state pyrene aggregates is instantaneous and no rise time is detected in the excimer decay. Examples of monomer and excimer decays of amylose labeled with 10 mol% pyrene are shown in Figures 1.8C and D, respectively. The contribution from each pyrene species contributing to the fluorescence signal can be retrieved quantitatively by global analysis of the pyrene monomer and excimer decays. This procedure enables a more accurate

assignment of the different photophysical processes undergone by the pyrene species and results in greater accuracy when retrieving the kinetic parameters that are used to describe polymer chain dynamics.

The first quantitative analysis of the monomer and excimer fluorescence decays of molecular pyrene in organic solvents was conducted by Birks in 1963.[124] This analysis was then adapted by Winnik to characterize the end-to-end cyclization (EEC) of a series of end-labeled monodisperse polystyrene samples.[119] Since the Birks scheme only applies when excimer formation is described by a single rate constant, EEC is limited to the characterization of linear monodisperse oligomers. This problem was resolved by the development of the FBM by Duhamel et al. in 1993.[126] The FBM handles excimer formation processes involving multiple rate constants and it can be applied to polymers randomly labeled with pyrene.

1.2.2 Analysis of pyrene excimer formation

1.2.2.1 Birks' scheme

The first study where the fluorescence decays of pyrene labeled polymers were used to study polymer chain dynamics was conducted by Winnik in 1980.[119]

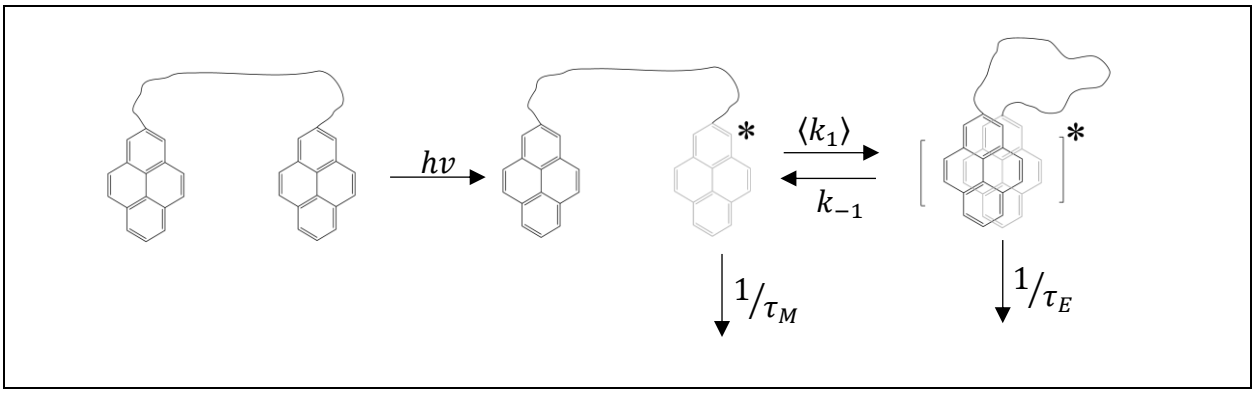

Figure 1.9. Birks' scheme of pyrene excimer formation for a pyrene end-labeled polymer.

In these experiments, a series of monodisperse polystyrenes were end-labeled with pyrene. The kinetics of PEF were analysed according to the Birks scheme as depicted in Figure 1.9 where PEF occurs through diffusive encounters of the chain ends. The rate constant of PEF ($\langle k_1 \rangle$) in Figure 1.9 is a measure of the rate constant of end-to-end cyclization of the polymer chains. The brackets indicate that, although the polymer has a narrow molecular weight distribution (MWD), $\langle k_1 \rangle$ is averaged over all the polymer chain lengths. $\langle k_1 \rangle$ is also a pseudo-unimolecular rate constant whose expression is given in Equation 1.2.

$$\langle k_1 \rangle = k_1 \times [Py]_{loc} \tag{1.2}$$

In Equation 1.2, $[Py]_{loc}$ is the local concentration of ground-state pyrene in the neighborhood of the excited pyrene and k_1 is the bimolecular rate constant for diffusive encounters between two pyrenyl labels and k_{-1} is the excimer dissociation rate constant. The expressions for the time-dependent concentrations of the pyrene monomer ($[Py^*]_{(t)}$) and excimer ($[E^*]_{(t)}$) are given in Equations 1.3 and 1.4, respectively, where $[Py^*_{diff}]_0$ and $[Py^*_{free}]_0$ represent the initial concentration of those pyrenes that form an excimer by diffusion and that never form an excimer, respectively.

$$[Py^*]_{(t)} = [Py^*_{diff}]_{(t)} + [Py^*_{free}]_{(t)}$$

$$= \frac{[Py^*_{diff}]_0}{\sqrt{(X-Y)^2 + 4\langle k_1 \rangle k_{-1}}} \left(\left(X - \tau_2^{-1} \right) \exp\left(-\frac{t}{\tau_1} \right) - \left(X - \tau_1^{-1} \right) \exp\left(-\frac{t}{\tau_2} \right) \right)$$

$$+ [Py^*_{free}]_0 \exp\left(-\frac{t}{\tau_M} \right) \tag{1.3}$$

$$[E^*]_{(t)} = \frac{[Py^*_{diff}]_0}{\sqrt{(X-Y)^2 + 4\langle k_1 \rangle k_{-1}}} \left(\exp\left(-\frac{t}{\tau_1}\right) + \exp\left(-\frac{t}{\tau_2}\right) \right) \tag{1.4}$$

In Equations 1.3 and 1.4, the parameters X and Y equal $\langle k_1 \rangle + 1/\tau_M$ and $k_{-1} + 1/\tau_E$, respectively, and the expression for the decay times τ_1 and τ_2 are given in Equations 1.5 and 1.6, respectively.

$$\tau_1^{-1} = \frac{X + Y + \sqrt{(X-Y)^2 + 4\langle k_1 \rangle k_{-1}}}{2} \tag{1.5}$$

$$\tau_2^{-1} = \frac{X + Y - \sqrt{(X-Y)^2 + 4\langle k_1 \rangle k_{-1}}}{2} \tag{1.6}$$

Winnik's study showed that $\langle k_1 \rangle$ scaled as N^{γ} where N was the number of chain atoms along the polymer backbone and γ was an exponent that depended on the polymer-solvent interactions.[52,127] In the case of polystyrene in cyclohexane, γ was found to equal –1.43. Since $\langle k_1 \rangle$ is proportional to $[Py]_{loc}$ which is itself equal to the inverse of the polymer coil volume ($1/V_{coil}$), since there is a single ground-state pyrene for each doubly labeled chain in which one of the two pyrenyl labels is excited, this result suggested that the radius of the polymer coil scaled as $N^{0.47}$ which is in very good agreement with the Flory exponent 0.50 expected for a polymer in a theta solvent.[52] The strong dependency of $\langle k_1 \rangle$ on polymer chain length suggested that PEF reflected both polymer chain dynamics and local concentration. However, this relationship also resulted in a major limitation for the use of EEC to study polymer chain dynamics. As shown in the Winnik study, end-labeled polystyrenes with M_n equal to 3,100 g/mol (DP=30) and 39,600 g/mol (DP=381) were reported to have $\langle k_1 \rangle$ values in cyclohexane of 22.7×10^6 and 0.3×10^6 s^{-1}, respectively. Since the Birks Scheme retrieves $\langle k_1 \rangle$ from the parameter X in Equations 1.5 and 1.6, which is equal to

$<k_1> + 1/\tau_M$ where τ_M equals 251 ns for the 1-pyrenebutyl label in cyclohexane, the magnitude of $<k_1>$ with respect to $1/\tau_M$ matters since a small $<k_1>$ value compared to $1/\tau_M$ will be retrieved with much larger error bars. As M_n increased from 3,100 to 39,600 g/mol, the contribution of $<k_1>$ to X decreased from ~75% to ~10%. For longer polymers, $<k_1>$ could only be retrieved with little accuracy and for this reason, EEC has been applied solely to the study of linear monodisperse oligomers. Another implication of the strong dependency of $<k_1>$ on the polymer chain length is that polydisperse polymers yield a distribution of $<k_1>$ values that cannot be handled by the Birks Scheme since it deals with a single PEF rate constant.[56] Consequently, EEC experiments are typically carried out with monodisperse oligomers. Another limitation of EEC experiments is that polymers adopting a helical conformation would be too rigid to undergo EEC over the fluorescence time scale and could not be studied.

1.2.2.2. Fluorescence Blob Model (FBM)

The derivation of the FBM, whose basic principles were first proposed in 1993, was implemented incrementally.[126] The exchange of ground-state pyrenes between *blobs* was introduced in 1999 to better describe PEF in randomly labeled polymers.[121] Since the polymer was randomly labeled, PEF would take place according to a distribution of rate constants reflecting the contour length separating every pair of two pyrenyl labels. The complexity of working with a distribution of rate constants was dealt with by noting that while it remains excited, an excited pyrene monomer can only probe a finite volume inside the polymer coil, referred to as a *blob* in the framework of the FBM. The polymer coil can then be divided into *blobs* where the pyrene pendants distribute themselves randomly according to a Poisson distribution. Inside a *blob*, the structural units onto which the excited and ground-state pyrenes are attached diffuse slowly toward each other with a rate constant k_{blob} until the two pyrenyl pendants are within a short distance where they undergo a

rapid rearrangement with a large rate constant k_2 to form an excimer. The determination of k_2 could only be achieved with a faster time-resolved fluorometer that could probe the faster phenomena observed at the early times of the fluorescence decays and the first study that included a k_2 component in the FBM analysis was carried out with randomly labeled polystyrene.[128]

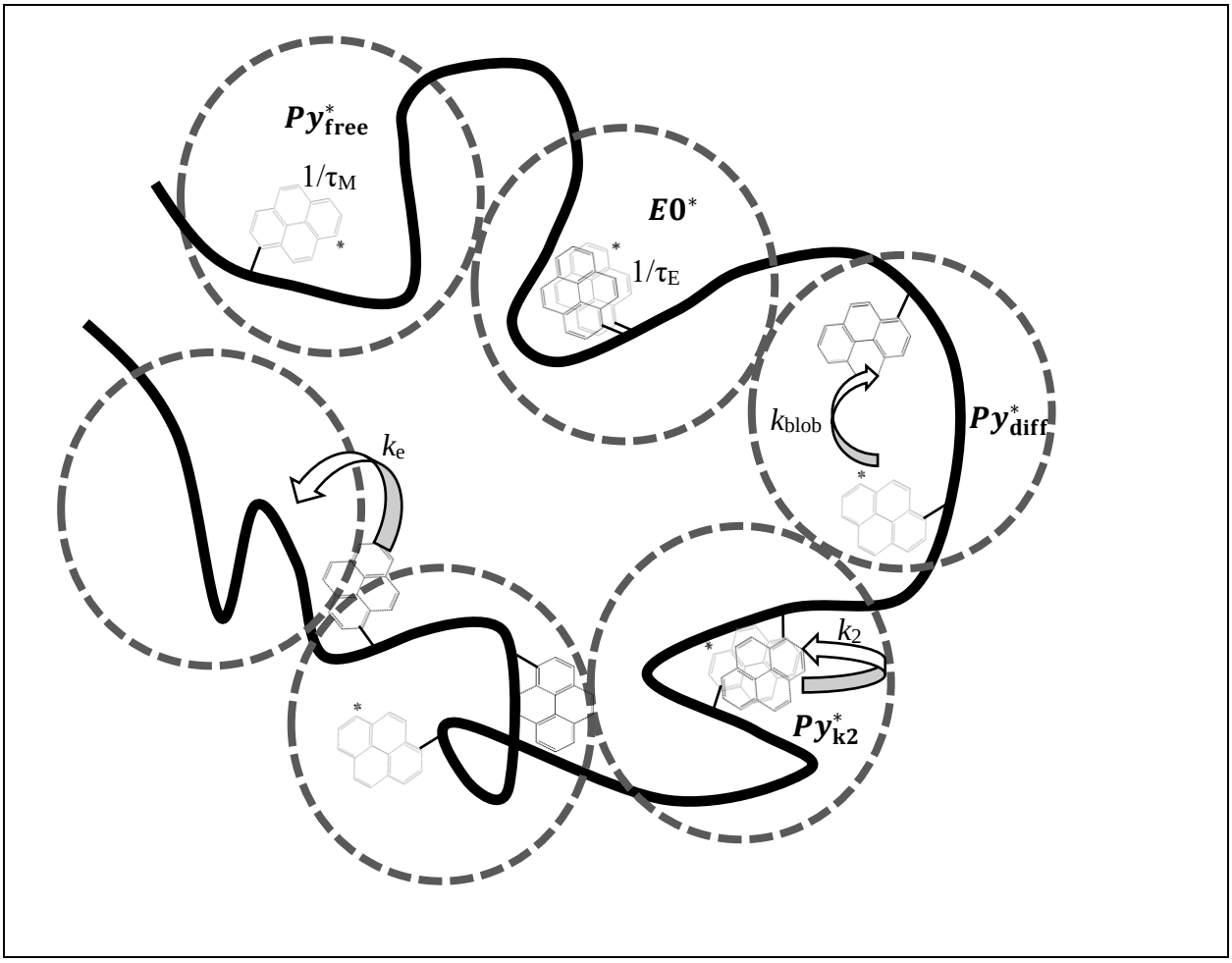

Figure 1.10. Illustration of how different pyrene species distributed among different *blobs* participate in PEF.

Figure 1.10 introduces four pyrene species involved in PEF. The species Py_{free}* represent the pyrenes that are isolated, cannot form excimer, and emit with their natural lifetime (τ_M). The species *E*0* represents the pre-stacked pyrenes attached next to each other and form a ground-state

pyrene aggregate, that can be excited directly to form an excimer instantaneously. The species Py_{diff}* accounts for the pyrenes attached onto structural units that undergo slow diffusive motions in solution before an encounter between these structural units brings the two pyrenyl labels in close proximity, whereby they transform into the species Py_{k2}*. By its nature, the pyrene species Py_{k2}* always has a ground-state pyrene nearby which results in a rapid rearrangement with a rate constant k_2 to form an excimer. For some pyrene-labeled polymers, especially for polymers whose rigid backbone yields little PEF, a short decay time of 2 to 4 ns is often observed. The short decay time has been attributed to light scattering or emission from poorly stacked short-lived ground-state pyrene aggregates (*ES**). Their contribution is included in the global analysis of the fluorescence decays but ignored in the calculation of the molar fraction of the Py_{free}*, Py_{diff}*, Py_{k2}*, and *E*0* species. The equations used to fit the monomer and excimer fluorescence decays according to the FBM are given in Equations 1.6 and 1.7, respectively.

$$[Py^*]_{(t)} = [Py^*_{diff}]_{(t)} + [Py^*_{k2}]_{(t)} + [Py^*_{free}]_{(t)}$$

$$= [Py^*_{diff}]_0 \exp\left(-\left(A_2 + \frac{1}{\tau_M} \right) t - A_3 \left(1 - \exp\left(-A_4 t \right) \right) \right)$$

$$+ \left([Py^*_{k2}]_o + [Py^*_{diff}]_o e^{-A_3} \sum_{i=0}^{\infty} \frac{A_3^i}{i!} \frac{A_2 + iA_4}{A_2 + iA_4 - k_2} \right) \exp\left(-\left(k_2 + \frac{1}{\tau_M} \right) t \right)$$

$$- [Py^*_{diff}]_o e^{-A_3} \sum_{i=0}^{\infty} \frac{A_3^i}{i!} \frac{A_2 + iA_4}{A_2 + iA_4 - k_2} \exp\left(-\left(A_2 + iA_4 + \frac{1}{\tau_M} \right) t \right) + [Py^*_{free}]_o \exp(-t / \tau_M) \quad (1.6)$$

$$[E^*]_{(t)} = [E0^*]_{(t)} + [ES^*]_{(t)}$$

$$= k_2 \left([Py^*_{k2}]_o + [Py^*_{diff}]_o e^{-A_3} \sum_{i=0}^{\infty} \frac{A_3^i}{i!} \frac{A_2 + iA_4}{A_2 + iA_4 - k_2} \right) \times \frac{\exp\left(-\frac{t}{\tau_{E0}} \right) - \exp\left(-\left(k_2 + \frac{1}{\tau_M} \right) t \right)}{k_2 + \frac{1}{\tau_M} - \frac{1}{\tau_{E0}}}$$

$$+ [Py^*_{diff}]_o e^{-A_3} \sum_{i=0}^{\infty} \frac{A_3^i}{i!} \frac{A_2 + iA_4}{A_2 + iA_4 - k_2} \frac{\exp\left(-\left(A_2 + iA_4 + \frac{1}{\tau_M} \right) t \right) - \exp\left(-\frac{t}{\tau_{E0}} \right)}{A_2 + iA_4 + \frac{1}{\tau_M} - \frac{1}{\tau_{E0}}}$$

$$+ [E0^*]_o \exp\left(-\frac{t}{\tau_{E0}} \right) + [ES^*]_o \exp\left(-\frac{t}{\tau_{ES}} \right) \qquad (1.7)$$

The parameters A_2, A_3, and A_4 used in Equations 1.6 and 1.7 are given in Equation 1.8.

$$A_2 = \langle n \rangle \frac{k_{blob} k_e [blob]}{k_{blob} + k_e [blob]} \qquad (1.8A)$$

$$A_3 = \langle n \rangle \left(\frac{k_{blob}}{k_{blob} + k_e [blob]} \right)^2 \qquad (1.8B)$$

$$A_4 = k_{blob} + k_e [blob] \qquad (1.8C)$$

Among other parameters, the analysis yields the number of structural units making up a *blob* (N_{blob}), the rate constant (k_{blob}) describing the slow diffusive motions of two structural units located inside a *blob* and bearing an excited and a ground-state pyrene, and the product $k_e \times [blob]$ of the rate constant (k_e) describing the exchange of ground-state pyrenes between *blobs* and the local *blob* concentration [*blob*].

Numerous studies have established the validity of the parameters retrieved from FBM analysis of the fluorescence decays of pyrene-labeled macromolecules. They were found to faithfully describe the internal dynamics of polymer chains.[56,57] It is currently the only analytical tool that can probe the internal dynamics of long polydisperse chains in solution.[129] More recent developments have shown that N_{blob} which represents the number of structural units inside a *blob* can also be used as a structural parameter to infer the conformation of a macromolecule in dilute solution.[115,117,118] Its application to the study of amylose and amylopectin in dilute solution is expected to provide new insights into the conformation and internal dynamics of these polysaccharides.

1.3 Thesis Objectives

The main objective of this thesis is to use the FBM analysis to study the chain dynamics and internal conformation of the two main components of starch, namely, amylose and amylopectin, in dilute solution. In this respect, this thesis reports two major accomplishments. The first one is an attempt to resolve the long-standing debate in the literature about whether amylose forms a helix in DMSO. Random labeling of amylose with pyrene yielded a series of Py-Amylose constructs whose fluorescence decays could be analyzed according to the FBM to yield N_{blob}. In turn N_{blob} could be used as a structural parameter to determine the conformation of amylose in DMSO. This study published in *Macromolecules* was a second example, after helical poly(*L*-glutamic acid),[120,122] of the use of the FBM to study the helical conformation of macromolecules in solution.[130] Applying this method to characterize the conformation and structure of macromolecules in dilute solution has now became an exciting field of research.[120,122,123,131]

The second accomplishment of this thesis was to provide a deeper understanding of the internal conformation of amylopectin in solution. Despite a significant volume of work to

characterize amylopectin by SEC and LS, the arrangement and dynamics of the side chains in the amylopectin interior is still poorly understood in dilute solution. Answering this question is challenging due to the gigantic size and high polydispersity of amylopectin. This thesis took advantage of the ability of the FBM to probe the density of a macromolecule locally, thus circumventing the detrimental effects of polymer size and polydispersity which plague many other techniques. A series of amylopectin constructs randomly labeled with pyrene (Py-Amylopectin) were prepared and their fluorescence decays were analyzed according to the FBM. The N_{blob} value was used to assess the distance (d_{h-h}) separating two helical oligosaccharide side chains in the interior of amylopectin. The surprisingly small d_{h-h} values retrieved from this analysis suggested that the internal density of amylopectin in dilute solution was impossibly large. This result implied that the oligosaccharide side chains did not distribute themselves homogeneously inside amylopectin, but rather formed clusters resulting in an inhomogeneous interior for amylopectin. Further investigations conducted using SNPs as a comparison supported the conclusion that the interior of amylopectin is made of dense clusters of helical oligosaccharide side chains loosely connected to each other via linear expanded segments. This molecular arrangement could be depicted by the Solution-Cluster model which rationalizes many of the fascinating properties of amylopectin in solution.

1.4 Thesis Outline

This thesis is composed of five chapters. Chapter 1 is a literature review describing the polysaccharides that were used in the thesis, including amylose, amylopectin, and starch nanoparticles, as well as the application of the fluorescence techniques used in this thesis to study these macromolecules. Chapter 2 focuses on the characterization of the conformation of a series of pyrene-labeled amylose constructs in DMSO. Chapter 3 is a study of the conformation of the

interior of amylopectin through the FBM analysis of the fluorescence decays acquired with a series of amylopectin constructs that were randomly labeled with pyrene. The experimental results led to the formulation of the Solution Cluster model to describe the conformation of the amylopectin interior. Chapter 4 presents an investigation that is similar to that done with amylopectin in Chapter 3, but focuses on nanosized amylopectin fragments (NAFs) prepared through extrusion of waxy corn starch under different conditions. The experiments conducted with the NAFs randomly labeled with pyrene confirmed that amylopectin contains excluded volumes whose contribution to the amylopectin interior decreases with decreasing NAF size. The results obtained with the NAFs supported the validity of the Solution-Cluster model that was introduced in Chapter 3. Chapter 5 summarizes the many conclusions that were reached in this thesis and provides suggestions for future work.

Chapter 2:
Conformation of Pyrene-Labeled Amylose in DMSO Studied with the Fluorescence Blob Model

2.1 Abstract

Amylose and poly(methyl acrylate) (PMA) were randomly labeled with pyrene to yield a series of Py-Amylose and Py-PMA constructs and their ability to form excimer in dimethylsulfoxide (DMSO) was characterized quantitatively by steady-state and time-resolved fluorescence. First, the ratio of the fluorescence intensity of the excimer over that of the monomer, namely the I_E/I_M ratio, was obtained from the fluorescence spectra. Second, the product $<k_{blob} \times N_{blob}>$, where N_{blob} is the number of monomers found in the volume probed by an excited pyrene and referred to as a *blob* and k_{blob} is the rate constant of excimer formation inside a *blob*, was obtained from the fluorescence blob model (FBM) analysis of the fluorescence decays. Both I_E/I_M and $<k_{blob} \times N_{blob}>$ yielded similar values in terms of moles of pyrene per backbone atom (Py/BBA) for Py-Amylose and Py-PMA. Since I_E/I_M and $<k_{blob} \times N_{blob}>$ reflect the efficiency of pyrene excimer formation, the similar behaviour observed for both parameters obtained for rigid amylose and flexible PMA could only be rationalized by postulating that amylose adopted a compact helical conformation in DMSO. To confirm whether this was possible, molecular mechanics optimizations (MMOs) were conducted with the HyperChem program on Py-Amylose assuming that amylose adopted a helical conformation in DMSO. By determining the extent of overlap between two pyrene labels attached onto helical amylose, it was found that two pyrene labels would overlap properly, and thus form excimer efficiently, if they were separated by no more than 5 anhydroglucose units up and down the amylose helix corresponding to a total of 5 + 5 + 1 = 11 units in perfect agreement with our findings that $<N_{blob}>$ obtained from the FBM analysis of the fluorescence decays which equaled 11 ± 2. This study provides a new example of how pyrene excimer fluorescence in combination with MMOs can be applied to provide structural information on macromolecules that adopt a helical conformation in solution.

2.2 Introduction

The conformations of macromolecules in solution can be broadly divided into two major categories, whether they are flexible (random coil) or rigid (helical). In turn, the conformation of a macromolecule in solution will have a major impact on its solution properties. For instance, the viscoelasticity or osmotic pressure of the solution of a macromolecule will be more strongly affected if the macromolecule adopts a more flexible conformation, as it will result in more pronounced conformational changes upon application of an external shear[1] or addition of a chemical like an acid/base[2] or a ligand,[3] respectively, an outcome that might be desired or unwanted depending on the applications at hand. Consequently, the determination of the conformation of macromolecules in solution has always been of tremendous importance to rationalize their solution properties.

One such macromolecule is amylose which is one of the two main constituents of starch, the other constituent being amylopectin. Amylose is a linear polysaccharide where the anhydroglucose units are connected via α–(1–4) linkages. Water, dimethylsulfoxide (DMSO), and water-DMSO mixtures have been shown to effectively solubilize amylose. In aqueous solutions, optical rotation, intrinsic viscosity, light scattering, and sedimentation measurements have demonstrated that amylose adopts a random coil conformation.[4-6] However, despite much experimental work done on dilute solutions of amylose, its conformation in DMSO is still a matter of controversy. Early work trying to establish a scaling relationship between intrinsic viscosity [η] and weight-average molecular weight (M_w) led to different conclusions. The Flory exponent ν obtained by intrinsic viscosity experiments in DMSO has been reported to equal 0.64,[7] 0.70,[4] 0.87,[8] and 0.91.[9] The first two results indicated that the chain is a random coil, while the last two results suggested a semirigid and predominantly helical conformation. Some of the above studies have

also reported the persistence length which is a measure of the stiffness of this biopolymer. Interestingly, reported values of this parameter vary from 2 nm,[10] which is comparable to that of flexible poly(methyl methacrylate) (PMMA) to 9 nm,[9] which oppositely suggests a stiff biopolymer. The origin of these differences in interpretation are probably rooted in the experimental difficulties associated with the accurate determination of the molecular weight of polysaccharides as well as the weak dependence of the intrinsic viscosity with molecular weight for shorter polysacharides.[10]

On the other hand, a conformational transition from a coil to an helix induced by changing the solvent conditions has been observed by NMR,[11,12] specific optical rotation,[13] and intrinsic viscosity.[7] The ^{1}H NMR spectra of amylose in DMSO-d_6 at elevated temperature showed an upfield shift of the hydroxyl proton signals. This observation was taken as evidence that the intramolecular hydrogen bonds necessary for amylose to form a helical structure were severed at high temperature.[12] Another study based on specific optical rotation showed that the addition of tetramethylurea decreased the specific optical rotation of amylose in DMSO. This result suggested that amylose was capable of forming the numerous intramolecular hydrogen bonds necessary to maintain a helical conformation and that these H-bonds were disrupted by the addition of urea.[11] While informative about a possible change in amylose conformation, the above studies were aimed to detect the conformational transitions induced by a change in solvent conditions rather than characterize the actual conformation of amylose in DMSO. More recently, molecular simulations on amylose segments 55 anhydroglucose units long have shown that the amylose helix is not stable and rapidly denatures into a random coil in DMSO.[14]

As the above discussion made clear, the conformation of amylose in DMSO, being either a random coil or a helix, remains to be determined. Since the two conformations would be expected

to exhibit very different internal dynamics, pyrene excimer formation was applied to characterize the internal dynamics of amylose in DMSO. To this end, amylose was randomly labeled with pyrene and fluorescence measurements were conducted. Over the past few decades, pyrene labeled polymers have become a means to study how internal chain dynamics in solution are affected by solvent quality,[15-20] polymer concentration,[21-23] solution temperature,[24-26] and side chain length.[27,28] Many studies aiming to probe the internal dynamics of macromolecules in solution obtained this information by measuring the rate constant (k_q) for the quenching of an excited dye by a quencher which were both covalently attached to a same macromolecule. Since a quenching event demonstrates an encounter between dye and quencher, and consequently between two segments of the macromolecule, k_q is thus a measure of the macromolecular internal dynamics. Early studies required the challenging preparation of monodisperse linear chains labeled at each end with a single pyrenyl moiety to measure the rate constant of end-to-end cyclization (EEC) but this approach was limited by the poor efficiency of pyrene excimer formation for long chains and stiff polymeric backbones.[24] The recent advent of the fluorescence blob model (FBM) has overcome these drawbacks. Work from this laboratory over the past 15 years has established that the FBM can be used to faithfully retrieve quantitative information about the chain dynamics of polymers randomly labeled with pyrene.[28-30] The FBM assumes that during its lifetime the motions of an excited pyrene label covalently attached onto a polymer are limited to a small volume which is referred to as a *blob*. The polymer coil is then divided into a cluster of *blobs* where the pyrene groups distribute themselves randomly according to a Poisson distribution. FBM analysis of the fluorescence decays yields N_{blob}, the number of monomers encompassed inside a *blob*, and k_{blob}, the rate constant of excimer formation between an excited and a ground-state pyrene both located inside a same *blob*.[29,30] In particular, the product $<k_{blob} \times N_{blob}>$ was reported to be a universal

parameter that measures internal chain dynamics in solution in a manner similar to T_g for polymers in the bulk.[28]

Excimer formation between pyrene labels covalently and randomly attached onto an α-helical polymer, namely poly(*L*-glutamic acid) or PGA, has also been studied in dimethylformamide (DMF). In this case, pyrene excimer formation did not reflect the long-range polymer chain dynamics (LRPCD) but rather the rearrangement of the PGA side chains. Application of the FBM analysis to the fluorescence decays of the Py-PGA constructs yielded N_{blob} which was the number of glutamic acids representing a patch on the side of the PGA α-helix where excimer formation could occur between two pyrene labels. In fact, N_{blob} was found to reflect perfectly the maximum number of glutamic acids separating two pyrene labels covalently attached to a PGA α-helix while still being able to encounter and form an excimer. These conclusions were reached through comparison of the N_{blob} value determined through FBM analysis and the distances between two pyrene labels along the PGA helix measured by conducting molecular mechanics optimizations.[31,32] In the present study, amylose was randomly labeled with different amounts of pyrene to yield Py-Amylose. A pyrene labeled flexible polymer, poly(methyl acrylate) (Py-PMA), was also studied in DMSO for comparison. PMA is a well-known flexible polymer with a T_g equal to 12 ˚C. However, the product $<k_{blob} \times N_{blob}>$ retrieved from FBM analysis of the Py-PMA decays yielded similar values for rigid amylose and flexible PMA suggesting that pyrene excimer formation was highly efficient for the Py-Amylose constructs. This unexpectedly large excimer formation rate constant could only be possible if amylose formed a compact structure in DMSO to reduce the average distance between pyrenyl moieties. FBM analysis of the fluorescence decays yielded an N_{blob} value of 11 ± 2, which is in good agreement with the value obtained via molecular mechanics optimization if amylose adopts a helical conformation. To the best of our knowledge,

this study is the first attempt in the literature to apply pyrene excimer fluorescence to investigate the conformation of amylose in DMSO.

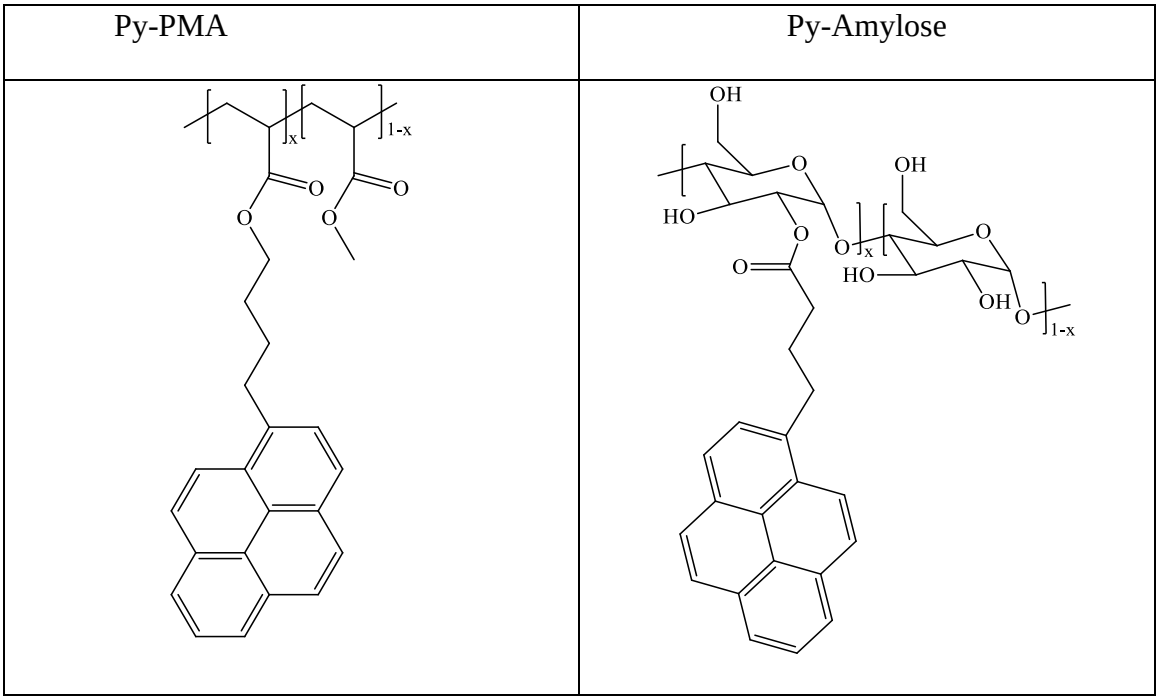

Figure 2.1. Chemical structures of the pyrene-labeled polymers. Left: poly(methyl methacrylate), right: amylose.

2.3 Experimental Section

Materials: Chemicals were purchased from Sigma-Aldrich (Milwaukee, WI) and used as received unless otherwise stated.

Synthesis of pyrene-labeled PMA (Py-PMA): The synthesis, purification, and characterization of the pyrene-labeled PMA samples has been described elsewhere.[28]

Synthesis of pyrene-labeled amylose (Py-Amylose): All Py-Amylose constructs were prepared in a similar manner. The synthesis of Py-Amylose with 7 mol% pyrene is described in more detail hereafter. Amylose (0.5 g, 3 mmol in terms of glucose units) was dissolved in 20 mL of a 3:1 DMSO:DMF mixture at 60 ˚C until the solution was clear. DMF was added to DMSO to prevent

the reaction mixture from freezing at 0 ˚C and since DMF is a poor solvent for amylose, the amount of DMF added was low enough to ensure that amylose was fully dissolved in this solvent mixture. Pyrenebutyric acid (PBA) (0.5 g, 1.7 mmol) and 4-dimethylaminopyridine (DMAP, 0.05 g, 0.4 mmol) were dissolved into the DMSO/DMF mixture. The reaction mixture was then cooled in an ice bath followed by the addition of *N,N'*-diisopropylcarbodiimide (DIC) (0.4 mL, 2.7 mmol) dropwise under a nitrogen atmosphere. The reaction mixture was kept at 0 ˚C for 5 min and then left stirring in the dark for 48 hours at room temperature under nitrogen. The molar amount of amylose was kept constant for all reactions. The amounts of PBA, DMAP, and DIC could be adjusted to obtain the desired pyrene content. The Py-Amylose product was precipitated in cold methanol. The recovered product was redissolved in DMSO and reprecipitated in methanol. The precipitation cycle was repeated 3-5 times to remove any unreacted PBA. The final product was dried in a vacuum oven at room temperature overnight.

Pyrene content determination: The pyrene content, λ_{Py} expressed in mole of pyrene per gram of polymer, was determined using Equation 2.1. A mass, m, of dried Py-Amylose was carefully weighed before being dissolved in a known volume, V, of DMSO. The pyrene concentration [Py] was determined by UV-Vis absorption measurements by applying Beer-Lambert's law to the pyrene absorption at 346 nm with an extinction coefficient of 41,400 $M^{-1}.cm^{-1}$. The molar fraction, x, of pyrene-labeled anhydroglucose units in Py-Amylose was determined by applying Equation 2.2 where M_{Glu} and M_{Py} represented the molar mass of the unlabeled and pyrene-labeled anhydroglucose units, equal to 162 and 432 $g.mol^{-1}$, respectively.

$$\lambda_{Py} = \frac{[Py]}{m/V} \tag{2.1}$$

$$x = \frac{M_{Glu}}{M_{Glu} - M_{Py} + 1/\lambda_{Py}} \tag{2.2}$$

Steady-State Fluorescence Measurements: Steady-state fluorescence spectra were acquired on a Photon Technology International LS-100 steady-state fluorometer with an Ushio UXL-75 Xenon lamp and a PTI 814 photomultiplier detection system. The spectra were obtained using the usual right-angle geometry with a 346 nm excitation wavelength. The samples were dissolved in DMSO with a pyrene concentration below 2.5×10^{-6} M to avoid intermolecular excimer formation. The fluorescence spectra were acquired with either aerated or degassed Py-Amylose solutions. The Py-Amylose solutions in DMSO were degassed for 40 minutes by bubbling a gentle flow of nitrogen to remove oxygen. The solutions were degassed to test the effect of monomer lifetime on the rate of excimer formation. The monomer (I_M) and excimer (I_E) intensities were obtained by integrating the fluorescence spectra between 373 – 379 nm and 500 – 530 nm, respectively.

Time-resolved fluorescence measurements: The monomer and excimer fluorescence decays were acquired with an IBH Ltd. time-resolved fluorometer using an IBH 340 nm NanoLED as the excitation source. Samples were prepared in the same manner as for the steady-state fluorescence experiments. Samples were excited at a wavelength of 346 nm and the monomer and excimer emissions were collected at 375 nm and 510 nm, respectively. A cut off filter at 370 nm for the monomer and 500 nm for the excimer were used to reduce contamination of the fluorescence signal by light scattering. The fluorescence decays were acquired over 1,024 channels using a time-per-channel of 1.02 or 2.04 ns/ch with up to 20,000 counts at the peak maximum for the instrument response function and decay curves.

Analysis of the fluorescence decays using the FBM: Five pyrene species are being considered within the FBM framework. The pyrene species Py_{diff}* represents the pyrenyl labels covalently

attached onto a structural unit that undergoes slow diffusive motions inside the polymer coil. These diffusive motions are described by the three FBM parameters which are $<n>$, the average number of ground-state pyrenes per *blob*, k_{blob}, the rate constant of excimer formation inside a *blob* which contains only one excited pyrene and a single ground-state pyrene, and the product $k_e \times [blob]$ where k_e describes the exchange of ground-state pyrenes between *blobs* and [*blob*] is the local *blob* concentration inside the polymer. The second pyrene species, Py_{k2}*, is formed by the rapid rearrangement of Py_{diff}* with a nearby ground-state pyrene after the two pyrene labels have been brought in close proximity through the internal dynamics of the macromolecule. An excimer *E*0* is then formed with a rate constant k_2 and emits with a lifetime τ_{E0}. The random labeling of the polymer results in a small population of pyrenes that are isolated from each other along the backbone and cannot form excimer. This pyrene species emits as free pyrene in solution with the natural lifetime τ_M of a pyrene monomer and is referred to as Py_{free}*. After labeling, a short-lived pyrene species, *ES**, was observed in the excimer decays of Py-Amylose only and it emitted with a short lifetime τ_S of 3.5 ns. The *ES** species is usually observed in pyrene-labeled macromolecules that form little excimer.[33] Equations 2.3 and 2.4 have been shown to fit satisfactorily the fluorescence decays of the pyrene monomer and excimer for a number of polymers randomly labeled with pyrene.[24,26,27]

$$
\begin{aligned}
&[Py^*]_{(t)} = [Py^*_{diff}]_{(t)} + [Py^*_{k2}]_{(t)} + [Py^*_{free}]_{(t)} \\
&= [Py^*_{diff}]_0 \exp\left(-\left(A_2 + \frac{1}{\tau_M} \right) t - A_3 \left(1 - \exp\left(-A_4 t \right) \right) \right) \\
&+ \left([Py^*_{k2}]_0 + [Py^*_{diff}]_0 e^{-A_3} \sum_{i=0}^{\infty} \frac{A_3^i}{i!} \frac{A_2 + iA_4}{A_2 + iA_4 - k_2} \right) \exp\left(-\left(k_2 + \frac{1}{\tau_M} \right) t \right) \\
&- [Py^*_{diff}]_0 e^{-A_3} \sum_{i=0}^{\infty} \frac{A_3^i}{i!} \frac{A_2 + iA_4}{A_2 + iA_4 - k_2} \exp\left(-\left(A_2 + iA_4 + \frac{1}{\tau_M} \right) t \right) \\
&+ [Py^*_{free}]_0 \exp\left(-\frac{t}{\tau_M} \right)
\end{aligned}
\tag{2.3}
$$

$$
\begin{aligned}
&[E^*]_{(t)} = [E0^*]_{(t)} + [ES^*]_{(t)} \\
&= k_2 \left([Py^*_{k2}]_0 + [Py^*_{diff}]_0 e^{-A_3} \sum_{i=0}^{\infty} \frac{A_3^i}{i!} \frac{A_2 + iA_4}{A_2 + iA_4 - k_2} \right) \\
&\times \frac{\exp\left(-\frac{t}{\tau_{E0}} \right) - \exp\left(-\left(k_2 + \frac{1}{\tau_M} \right) t \right)}{k_2 + \frac{1}{\tau_M} - \frac{1}{\tau_{E0}}} \\
&+ [Py^*_{diff}]_0 e^{-A_3} \sum_{i=0}^{\infty} \frac{A_3^i}{i!} \frac{A_2 + iA_4}{A_2 + iA_4 - k_2} \frac{\exp\left(-\left(A_2 + iA_4 + \frac{1}{\tau_M} \right) t \right) - \exp\left(-\frac{t}{\tau_{E0}} \right)}{A_2 + iA_4 + \frac{1}{\tau_M} - \frac{1}{\tau_{E0}}} \\
&+ [ES^*]_0 \exp\left(-\frac{t}{\tau_{ES}} \right)
\end{aligned}
\tag{2.4}
$$

The expression of the constants A_2, A_3, and A_4 used in Equations 2.3 and 2.4 are given in Equation 2.5 as a function of the parameters $\langle n \rangle$, k_{blob} and $k_e \times [blob]$ which have been defined earlier.

$$A_2 = \langle n \rangle \frac{k_{blob} k_e [blob]}{k_{blob} + k_e [blob]}$$
$$A_3 = \langle n \rangle \left(\frac{k_{blob}}{k_{blob} + k_e [blob]} \right)^2 \qquad (2.5)$$
$$A_4 = k_{blob} + k_e [blob]$$

The fluorescence decays of the pyrene monomer and excimer were fitted globally with Equations 2.3 and 2.4, respectively. The parameters used in these equations were optimized with the Marquardt-Levenberg algorithm.[34] The unquenched lifetime of the pyrene monomer, τ_M, was determined from the monomer decay of a polymer sparingly labeled with pyrene where more than 80% of the total pre-exponential weight could be attributed to isolated pyrene monomers that did not form excimer and emitted with a lifetime τ_M. In DMSO, τ_M was found to equal 86 ns for Py-PMA and 89.5 ns and 135 ns for Py-Amylose before and after degassing, respectively. The fit yielded the parameters $<n>$, k_{blob}, and $k_e[blob]$. The monomer decay analysis yielded the molar fractions, f_{Ediff}, f_{Ek2}, f_{EE0} and f_{EES} which represent the contribution of the pyrene species Py_{diff}*, Py_{k2}*, and Py_{free}* to the monomer decays, respectively. In a similar manner, the excimer decay analysis with Equation 2.4 yielded f_{Ediff}, f_{Ek2}, f_{EE0}, and f_{EES} which are the molar fractions of the pyrene species Py_{diff}*, Py^*_{k2}, $E0^*$, and ES^* that contribute to the excimer decays, respectively. The fractions f_{Mdiff}, f_{Mk2}, f_{Mfree}, f_{Ediff}, f_{Ek2}, f_{EE0}, and f_{EES} were then combined to determine the overall molar fractions of each pyrene species present in solution which are f_{diff}, f_{k2}, f_{free}, f_{E0} and f_{ES}. The molar fraction f_{Mfree} together with $<n>$ and the pyrene content λ_{Py} could be used to determine N_{blob}, the average number of structural units per *blob* whose expression is given in Equation 2.6 where x is the molar fraction of AGUs labeled with pyrene.

$$N_{blob} = \frac{1 - f_{M_{free}}}{x} < n > \qquad (2.6)$$

The fits of the monomer and excimer fluorescence decays were considered good if the χ^2 was smaller than 1.2 and the residuals and the autocorrelation function of the residuals were randomly distributed around zero. A sample of the fit of the pyrene monomer and excimer fluorescence decays is given Figure S2.1 in the Appendix.

2.4 Results and Discussion

All fluorescence spectra and decays were acquired for samples with a corresponding pyrene concentration in DMSO of 2.5×10^{-6} M. To confirm that this concentration was dilute enough to prevent intermolecular excimer formation between Py-Amylose samples, a concentration study was conducted. Py-Amylose samples with pyrene contents of 5.1, 7.5, and 14.9 mol% were dissolved in DMSO and their final concentrations were adjusted to approximately 3, 6, and 9 mg/L. These concentrations matched the lowest and highest mass concentrations of pyrene-labeled polymers used in this study. The steady-state fluorescence spectra of the solutions were acquired. The I_E/I_M ratio of the solutions was determined and plotted as a function of Py-Amylose concentration in Figure 2.2. Within experimental error, the I_E/I_M ratios remained constant as a function of Py-Amylose concentration. This behavior indicated that within the range of polymer mass concentration used in this study, pyrene excimer formation of Py-Amylose only occurred intramolecularly.

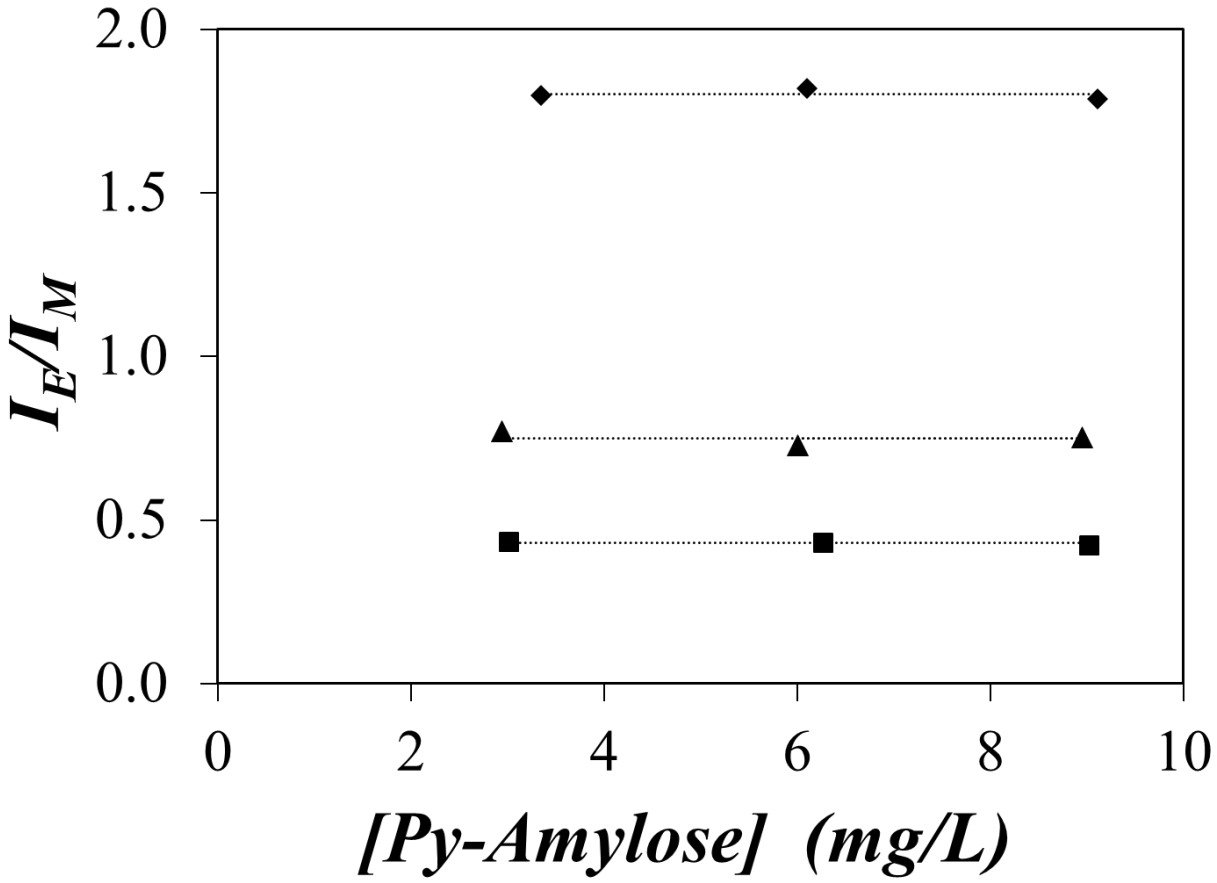

Figure 2.2. Plot of I_E/I_M as a function of Py-Amylose concentration in DMSO. (■) 5.05 mol%, (▲) 7.5 mol% and (◆) 14.9 mol%.

The steady-state fluorescence spectra acquired for both Py-PMA and Py-Amylose in DMSO are shown in Figure 2.3A and B, respectively. The fluorescence intensity was normalized at 376 nm and set to an arbitrary value of 100. More pyrene excimer was formed with increasing pyrene content due to the increased probability of encounter between the pyrene labels.

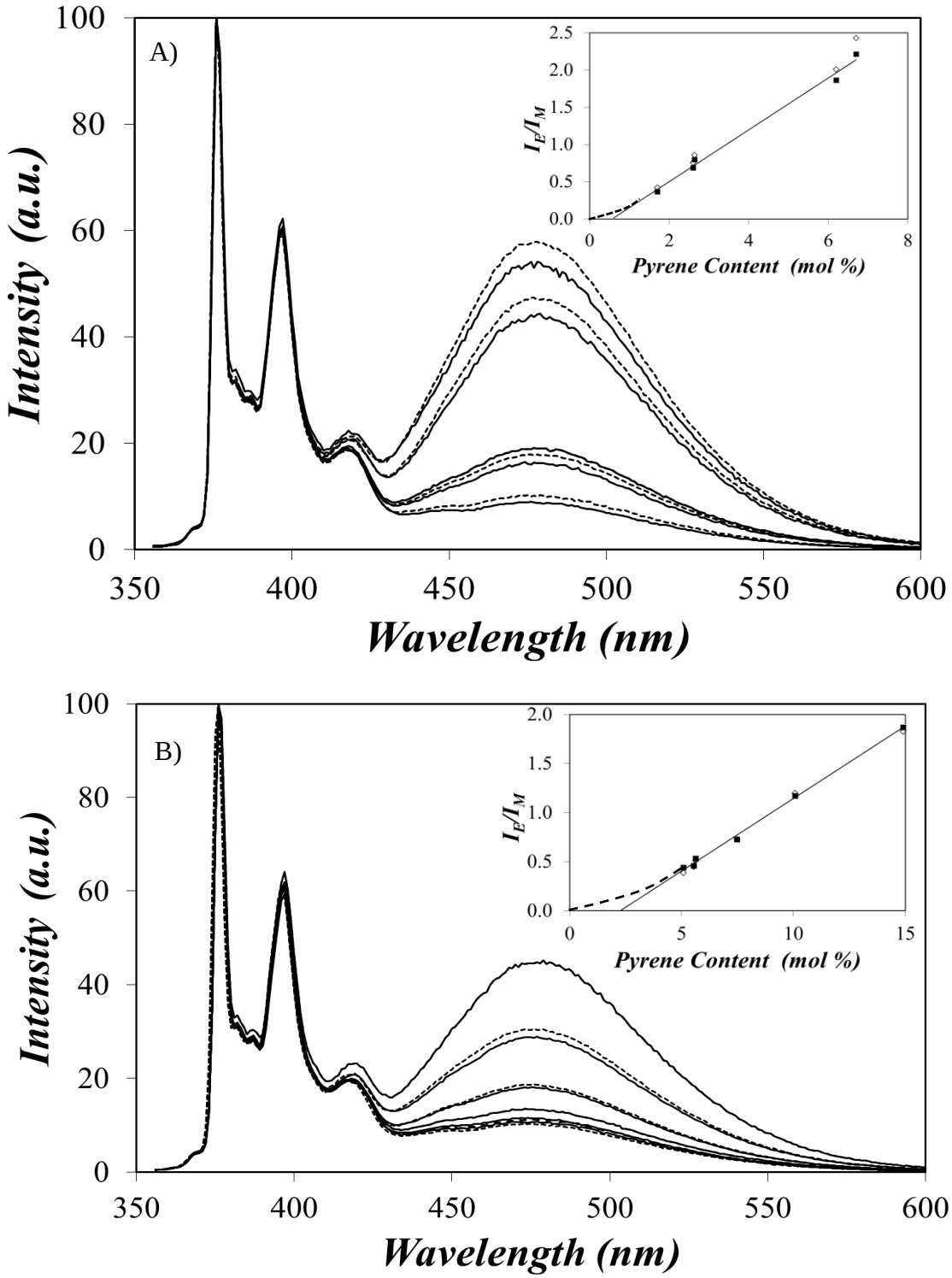

Figure 2.3. Steady-state fluorescence spectra of degassed (⋯) and undegassed (—) (A) Py-PMA in DMSO and (B) Py-Amylose in DMSO (■) before degassing and (□) after degassing. [Py] = 2.5×10^{-6} M, λ_{ex} = 346 nm.

When studying pyrene labeled polymers, the I_E/I_M ratios are typically used as a qualitative measure for the rate constant of excimer formation.[35] It was noticeable that none of the lines representing the I_E/I_M ratios passed through the origin. This observation is a result of excimer formation being a local phenomenon that occurs between an excited and a ground-state pyrene labels that are separated by a few tens of monomers, as will be found later using the FBM analysis. Consequently, enough pyrene needs to be covalently attached to the polymer to bring the pyrene labels within striking range from each other to form an excimer. According to the inset of Figure 2.3, no pyrene excimer could be formed until a threshold pyrene content of ~0.6 mol% for Py-PMA and ~2.2 mol% for Py-Amylose was reached. The slope of the lines, $m(I_E/I_M)$, equaled 0.35 for Py-PMA which was significantly larger than that of 0.15 found for Py-Amylose. At first glance, this result would suggest that excimer formation is less efficient for Py-Amylose as would be expected based on its more rigid backbone. However, this conclusion is somewhat misleading because each anhydroglucose unit (AGU) contributes 5 backbone atoms to the chain contour length for Py-Amylose compared to 2 backbone atoms contributed by each methyl acrylate monomer for Py-PMA (see Figure 2.1). In fact, on a "per backbone atom" basis, $m(I_E/I_M)$ of Py-Amylose would be 5 times larger, yielding an $m(I_E/I_M)$ slope value of 0.75 comparable to the value of 0.70 obtained by multiplying $m(I_E/I_M)$ for Py-PMA by 2. We will come back to these considerations at a later stage in the discussion.

It is important to note at this point that the I_E/I_M ratio obtained from the analysis of the steady-state fluorescence spectra is a parameter that represents all pyrene species that contribute to the monomer and excimer fluorescence. These include the species Py_{free}* that does not form excimer and $E0^*$ that forms excimer instantaneously upon excitation and does not provide any information on the dynamic process of excimer formation. In fact, beside the contribution of

Py_{diff}*, all other pyrene species contributing to the fluorescence signal can be viewed as fluorescent impurities that contaminate the dynamic information pertaining to excimer formation in the pyrene-labeled macromolecule. To isolate the contribution of each pyrene species and most importantly that of Py_{diff}* reporting on the internal dynamics of the pyrene-labeled macromolecule, analysis of the time-resolved fluorescence decays needs to be conducted.

Global analysis of the monomer and excimer decays using Equations 2.3 and 2.4 was conducted first by letting all parameters beside the monomer lifetime τ_M vary. The rate constant k_2 obtained for a given polymer series was then averaged and this average value was fixed in the decay analysis which was then repeated. This procedure has been found to yield a much tighter set of values for the parameters $<n>$, k_{blob}, and $k_e[blob]$ which represent the kinetics of pyrene excimer formation.[28] The values of $<n>$ and f_{Mfree} obtained from the decay analysis were then introduced in Equation 2.5 to calculate N_{blob} which was plotted as a function of pyrene content in Figure 2.4. Within experimental error, N_{blob} was found to remain constant with pyrene content. Increasing the monomer lifetime from 89.5 ns to 135 ns by degassing the solution did not lead to a larger blob size. The averaged N_{blob} value, $<N_{blob}>$, was found to equal 10 ± 1 AGUs for amylose before degassing and 12 ± 2 glucose units after degassing resulting in an overall average $<N_{blob}>$ value of 11 ± 2. On the other hand, $<N_{blob}>$ was found to equal 43 ± 2 monomer units for PMA before degassing and 46 ± 4 units after degassing which makes the overall average to be 45 ± 4 units. A previous study of PMA in tetrahydrofuran (THF) reported an $<N_{blob}>$ value of 59 ± 5.[28] The smaller blob size obtained in DMSO can be rationalized by the viscosity difference between THF

and DMSO. The higher viscosity of DMSO reduces the mobility of a pyrene label of Py-PMA resulting in a smaller volume probed by pyrene during its lifetime.

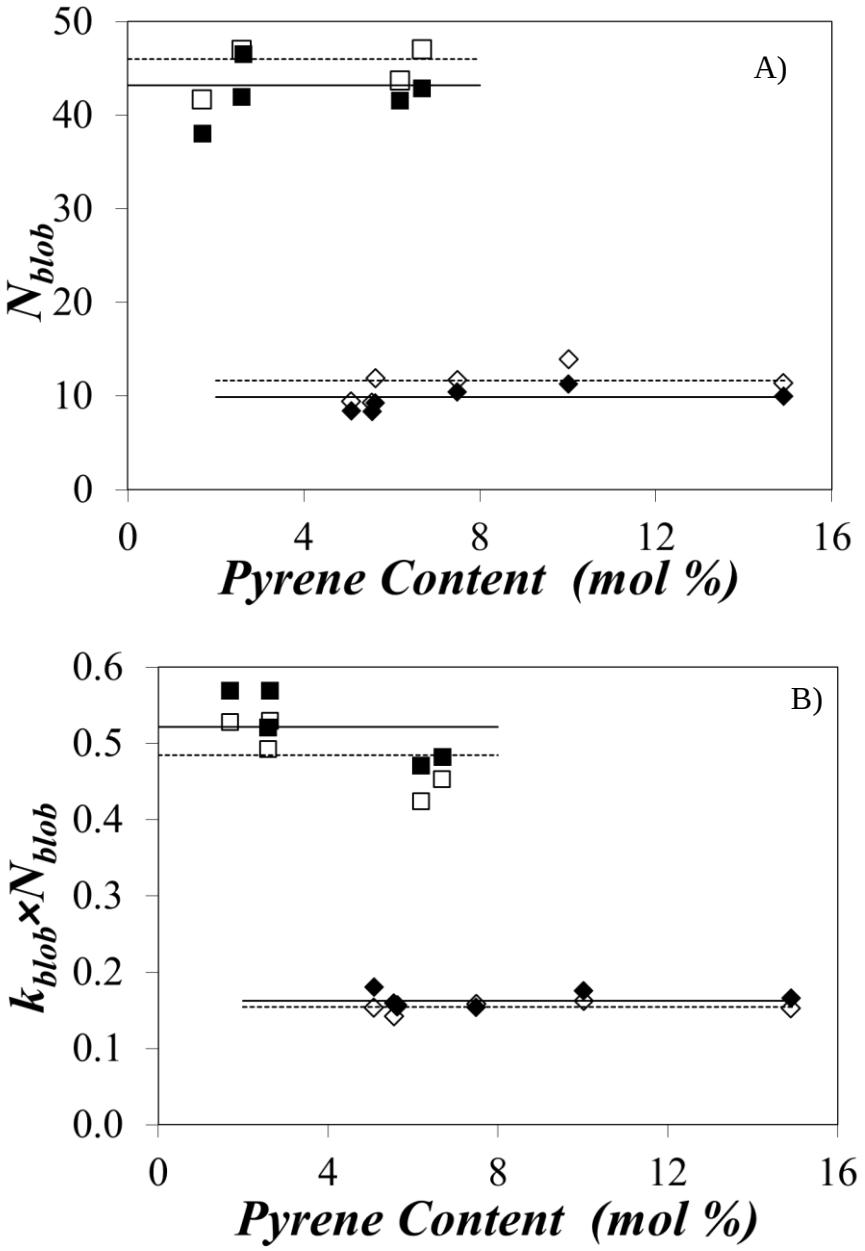

Figure 2.4. Plot of A) N_{blob} and B) $\langle k_{blob} \times N_{blob} \rangle$ as a function of pyrene content. (□) PMA before degassing, (■) PMA after degassing, (◇) amylose before degassing, and (◆) amylose after degassing.

When plotted against pyrene content in Figure 2.4, $k_{blob}\times N_{blob}$ was also found to remain more or less constant with pyrene content. The averaged value of the product $k_{blob}\times N_{blob}$, $\langle k_{blob}\times N_{blob}\rangle$ for amylose, was found to equal 0.16 ± 0.01 ns^{-1} and 0.15 ± 0.01 ns^{-1} before and after degassing, respectively. By comparison, $\langle k_{blob}\times N_{blob}\rangle$ was found to equal 0.52 ± 0.05 ns^{-1} and 0.48 ± 0.05 ns^{-1} for PMA before and after degassing, respectively. However, direct comparison of the $\langle N_{blob}\rangle$ and $\langle k_{blob}\times N_{blob}\rangle$ values between amylose and PMA is biased since both parameters are calculated in terms of the number of monomers constituting a *blob* which contribute differently, in terms of backbone atoms, to the chain length of the polymers. This difference can be corrected by reporting $\langle N_{blob}\rangle$ and $\langle k_{blob}\times N_{blob}\rangle$ normalized per backbone atom instead of monomer units. With only two chain atoms per monomer, PMA would have $\langle N_{blob}\rangle$ and $\langle k_{blob}\times N_{blob}\rangle$ equal to 90 ± 4 atoms and 1.0 ± 0.1 ns^{-1} per backbone atom, respectively. Similarly, amylose with its five backbone atoms per structural unit, would have $\langle N_{blob}\rangle$ and $\langle k_{blob}\times N_{blob}\rangle$ values of 55 ± 10 atoms and 0.78 ± 0.05 ns^{-1} per chain atom, respectively. Interestingly, the product $\langle k_{blob}\times N_{blob}\rangle$ in terms of chain atoms of amylose and PMA becomes comparable after this correction. Since $\langle k_{blob}\times N_{blob}\rangle$ is a measure of the rate of excimer formation, the fact that similar $\langle k_{blob}\times N_{blob}\rangle$ values were obtained for Py-PMA and Py-Amylose suggests that both macromolecular constructs form excimer with a similar efficiency. For polymers having a similar conformation, such as poly(alkyl methacrylate)s with different side chain lengths, the product $\langle k_{blob}\times N_{blob}\rangle$ faithfully reflects the chain mobility of different polymer backbones in solution.[28] However the amylose backbone is certainly more rigid as compared to that of PMA. Thus, the unexpectedly large value of $\langle k_{blob}\times N_{blob}\rangle$ cannot be explained by the higher mobility of the amylose backbone. Another factor that can increase the rate of excimer formation is the local pyrene concentration. For a similar level of labelling, a more compact conformation of the polymer

backbone would bring the pyrene groups closer to each other, leading to a higher local pyrene concentration which would increase the rate of pyrene excimer formation. A random coil conformation of amylose would be very unlikely to provide this compactness. In turn, this unexpectedly large $<k_{blob} \times N_{blob}>$ value could be a result of amylose adopting a helical conformation in DMSO.

In fact, the formation of a compact helix in solution has also been reported earlier for a rigid polycarbonate backbone following the finding that pyrene excimer formation occurred as quickly as for a much more flexible polydimethylsiloxane (PDMS) backbone.[36] In addition, even though $<N_{blob}>$ for amylose is smaller than for PMA, a *blob* consisting of 11 AGUs represents a significantly large volume to probe for a pyrene pendant attached to the backbone via a short butyl linker. In this context, a study of the physical dimensions of the space probed by an excited pyrene bound to amylose adopting an extended random coil or a compact α-helical conformation would be quite informative to assess which conformation of amylose in DMSO is best represented by the $<N_{blob}>$ value obtained by fluorescence.

To this end, the Hyperchem software (version 7.04) was used to create amylose constructs having helical and random coil conformations. Even though the crystal structure of amylose has been well characterized by X-ray, no structural information could be found in the literature regarding a helix conformation of amylose in DMSO. Therefore, two possible helical structures were considered in this study to test the effect of geometry on the *blob* size. The first helix was optimized from the default conformation built by Hyperchem for an amylose construct made of 40 AGUs. The optimized structure was a symmetrical 9-fold helix which is shown in Figure 2.5A. The number of AGUs per turn in the helix is slightly larger than the reported literature values obtained from the analysis of the crystal structure of amylose. For comparison purposes, a second

helix structure was imported into HyperChem based on an X-ray crystallography study by Nishiyama et al.[39] The optimized structure is a 7-fold helix which is shown in Figure 2.5B. The random coil conformation of amylose was optimized by extending an amylose chain made of 20 AGUs and letting it relax into the conformation shown in Figure 2.5C.

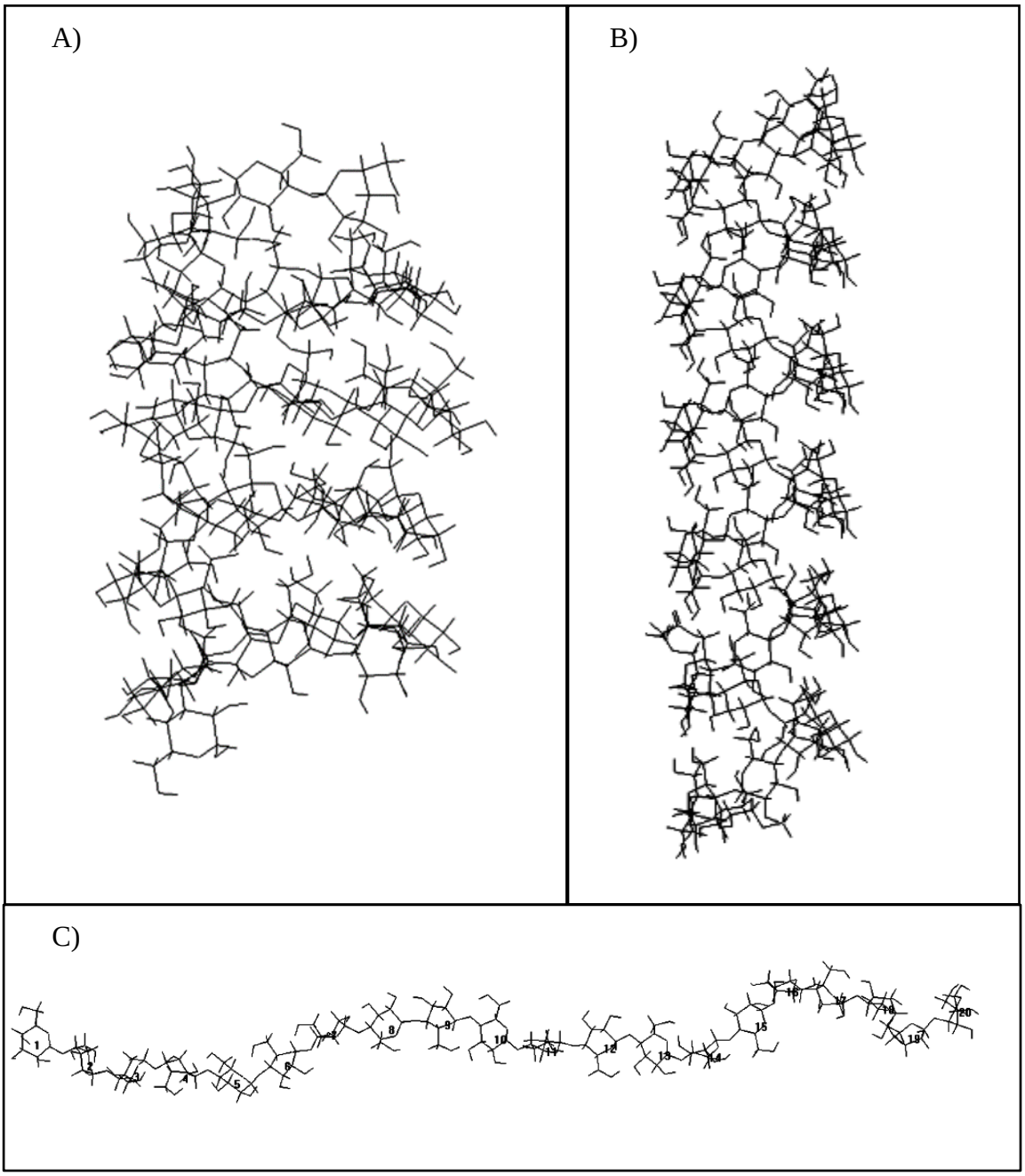

Figure 2.5. Two possible helical structures for amylose: A) 9-fold helix, B) 7-fold helix, and C) relaxed random coil conformation of amylose.

FBM analysis of the decays found that an amylose *blob* was made of 11 ± 2 AGUs. Since two pyrenes located inside a same *blob* form an excimer with the rate constant k_{blob}, the FBM implies that two pyrenes can overlap and form an excimer when they are located within a section of the α-helix made of 11 AGUs. The symmetry of the α-helix imposes that if a reference pyrenyl label is located at the center of the *blob*, an excimer will be formed if a second pyrenyl label is located within 5 AGUs from the reference pyrene on either side. A first structure was created where one pyrenebutyric acid pendant was attached onto the 3rd residue along the helix and a second pyrenebutyric acid was attached on the 4th residue. For both α-helical conformations, the hydroxyl group of C6 was little accessible as it pointed towards the inside of the helix. Therefore, the pyrene labels were attached to the C2 hydroxyl instead of the C6 hydroxyl which appeared to be less accessible. A molecular mechanics optimization (MMO) using the Fletcher-Reeves algorithm was performed during which the following constraints were imposed. The distance separating the carbons C2 or C7 of a pyrene label from the carbons C2 or C7 of the other pyrene label was set to equal 3.4 Å by the end of the MMO.[30] Whether the C2 or C7 carbons were selected depended on which orientation of the pyrene would result in the best overlap. None of the backbone atoms of the helices were included in the MMOs so that the polysaccharide backbone was not altered during the MMOs. Only pyrene and the atoms connecting pyrene to the AGU where allowed to be displaced during the MMO. At the end of the MMO, the extent of overlap between the two pyrenes was estimated by calculating the number of carbon atoms of the first pyrene molecule which overlapped the frame of the second pyrene molecule. This procedure was repeated by keeping the first pyrene on the 3rd residue and moving the second pyrene moiety from the 4th to the 33rd residue one residue at a time. An illustration of the extent of overlap is shown in

Figure 2.6 using the 7-fold amylose helix. When attached on two adjacent AGUs, the two pyrene labels can be arranged to achieve a good overlap involving 9 overlapping carbons.

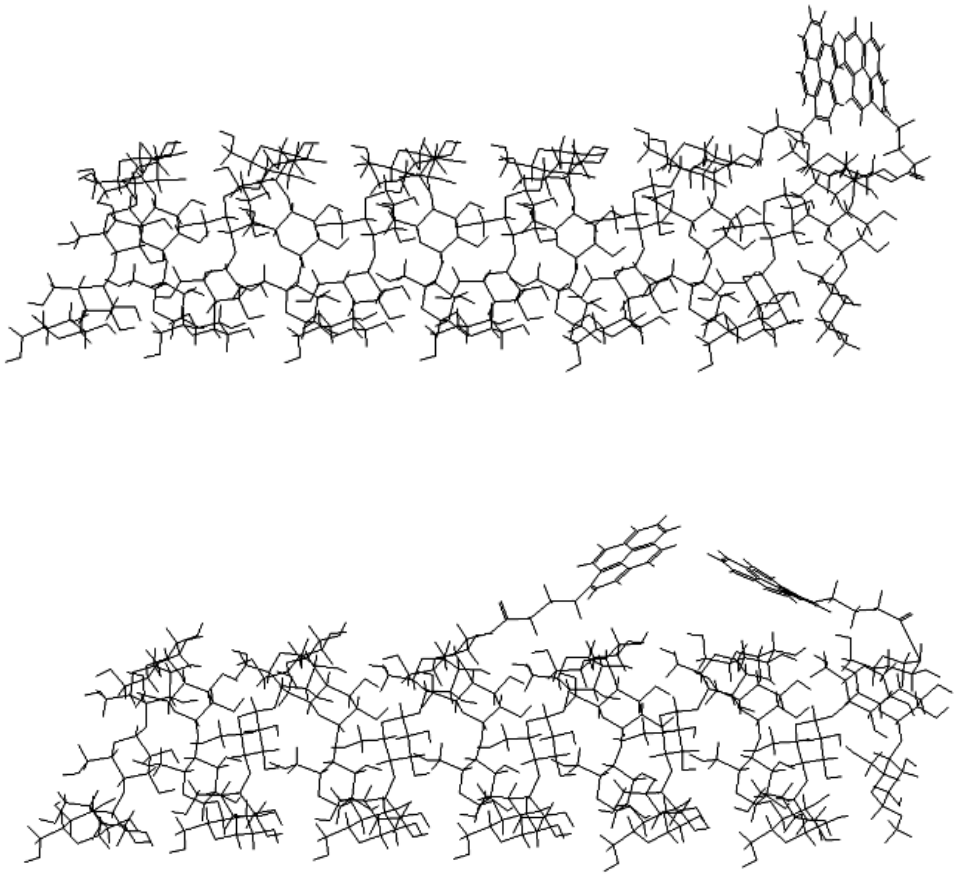

Figure 2.6. An illustration of the ability of two pyrene groups to overlap when separated by 7 AGUs (top: good overlap) and 21 AGUs (bottom: no overlap).

However, when separated by 21 AGUs, the two pyrene pendants could not overlap even though the butyl linkers were fully extended. Geometry optimization of the pyrene labels attached to amylose adopting a random coil conformation was conducted in a similar manner except for the following two differences. First, since the three hydroxyls were fully accessible in the random coil conformation, the pyrene moiety was attached on the C6 hydroxyl which gave it the longest reach for excimer formation. Second, it was also observed that the orientation of an individual glucose

unit changed along the chain. Consequently, a series of MMOs was carried out with one pyrene attached on the first AGU as reference while the second pyrene was moved from the 2nd to the 8th AGU, one AGU at a time. In each case, the extent of overlap between the two pyrenes was recorded. A second series of MMOs was then conducted with the reference pyrene attached onto the 2nd AGU and the second pyrene attached to the residues 3 to 9 in one residue increments. The extent of overlap was recorded. In total, 8 series of MMOs were carried out and the final result for the number of overlapping carbons was averaged. For all simulations, a good overlap between two pyrenes was characterized by one pyrene having at least 7 C-atoms covered by the area of the second pyrene as had been done earlier.[27]

The results obtained from the MMOs based on two helix conformations, one with a 7-fold and the other with a 9-fold periodicity, are shown in Figure 2.7. The similar trends obtained for the 7-fold and 9-fold helices indicated that the extent of overlap depends strongly on the position of the pyrene pendants along the helix. The overlap was nonexistent when two pyrene moieties were three AGUs apart since they pointed to opposite directions away from the helix. The overlap was restored when the two pyrene moieties were located on two AGUs separated by one helical turn. The trends obtained by optimization of the 7-fold and 9-fold helices were essentially the same. Both trends demonstrated that two pyrenes showed a good overlap if the AGUs, onto which the pyrenes are attached, were separated by 1, 2, 7, 8, and 9 AGUs or 1, 2, 8, 9, and 10 AGUs for the 7-fold and 9-fold helices, respectively, both helices yielding a set of five residues ($N_o = 5$) enabling good overlay between two pyrene labels. Since these MMOs considered the number of AGUs (N_o) allowing good pyrene-pyrene overlap on one side of the reference pyrene along the polymer backbone, a theoretical N_{blob}^{theo} can be obtained by multiplying N_o by a factor of 2 to account for the other side of the reference pyrene along the polymer backbone and adding 1 to account for the

reference pyrene. Consequently, the MMO results of the amylose helices point to a *blob* made of 2×5+1 = 11 AGUs, in excellent agreement with the $<N_{blob}>$ value of 11 ± 2 obtained by FBM analysis of the Py-Amylose constructs. The MMO results for an extended amylose conformation more representative of a random coil were plotted in Figure 2.8. The trends show that the extent of overlap decreases rapidly with separation distance if amylose forms a random coil in solution.

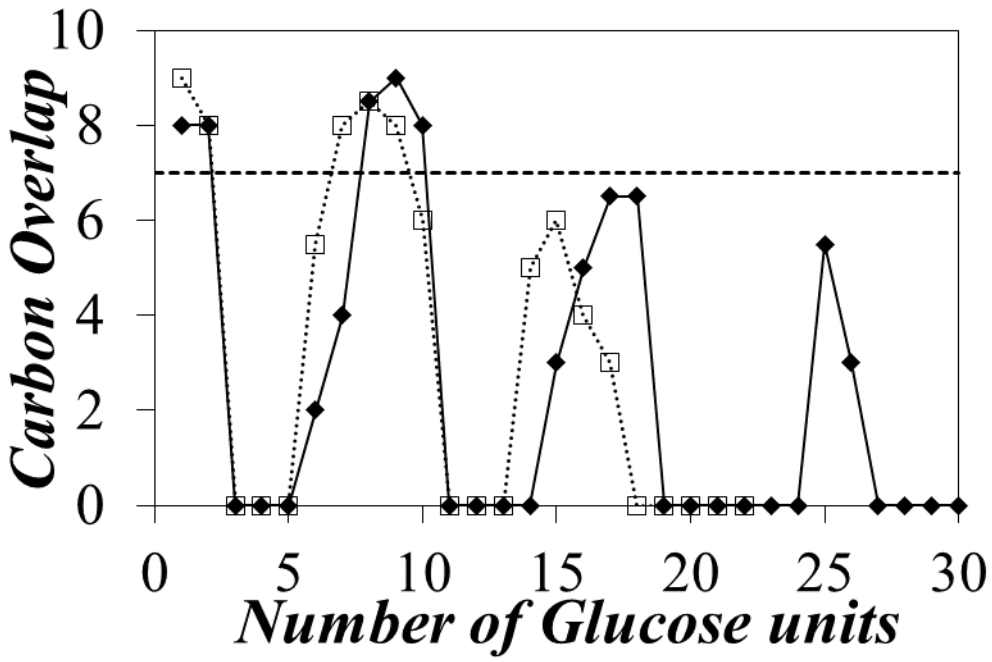

Figure 2.7. Pyrene carbon-overlap as a function of the number of AGUs between pyrene groups obtained via MMO of an amylose helix. (□) 7 fold helix, (◆) 9 fold helix

Based on the results shown in Figure 2.8, poor overlap was obtained when two pyrene pendants were four AGUs apart. In other words, if Py-amylose adopted a random coil conformation, the *blob* size would be less than 3×2+1=7 AGUs which is much smaller than the $<N_{blob}>$ value of 11 obtained by the FBM analysis of the fluorescence decays and thus rules out the possibility of amylose adopting a coiled conformation in DMSO. Consequently, the results

obtained by FBM analysis of the fluorescence decays and MMOs strongly suggest that the conformation of amylose in DMSO is that of a rigid helix.

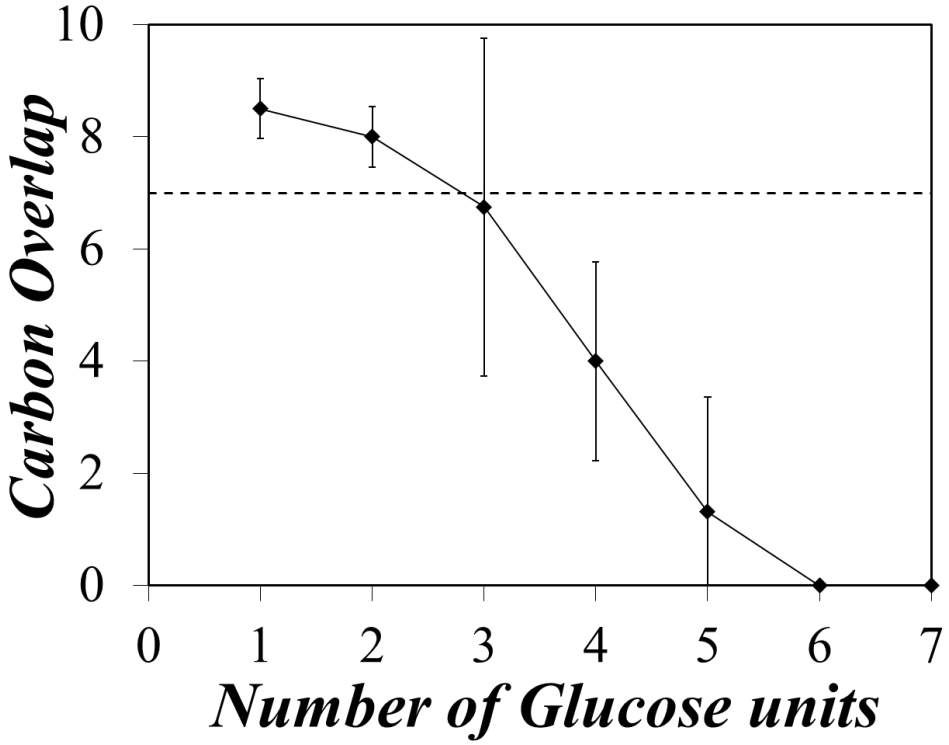

Figure 2.8. Pyrene carbon-overlap as a function of the number of AGUs between pyrene groups obtained via MMOs of an amylose random coil.

Further indication that amylose adopts a compact conformation in DMSO was obtained by plotting f_{E0} versus pyrene content for Py-PMA and Py-Amylose. The molar fraction f_{E0} represents the pyrene labels involved in pre-stacked pyrene dimers before excitation. Due to the random labeling of the polymers, higher pyrene contents lead to a smaller distance between the pyrene groups resulting in higher f_{E0} values. As shown in Figure 2.9, f_{E0} increases with pyrene content for both Py-PMA and Py-Amylose. Interestingly, f_{E0} for Py-Amylose is much higher than that for a same pyrene content of the Py-PMA series. This trend is unexpected considering that one glucose unit introduces 5/2 = 2.5 times more backbone atoms into the polymer than one methyl acrylate

monomer. Consequently, the pyrene labels should be much more spread out along the Py-Amylose samples for a same pyrene content compared to Py-PMA and thus generate much less pyrene aggregation. That this is not the case indicates that the pyrene pendants attached on the backbone of amylose are located in a very compact environment, which can only be explained if amylose forms a helical structure in DMSO.

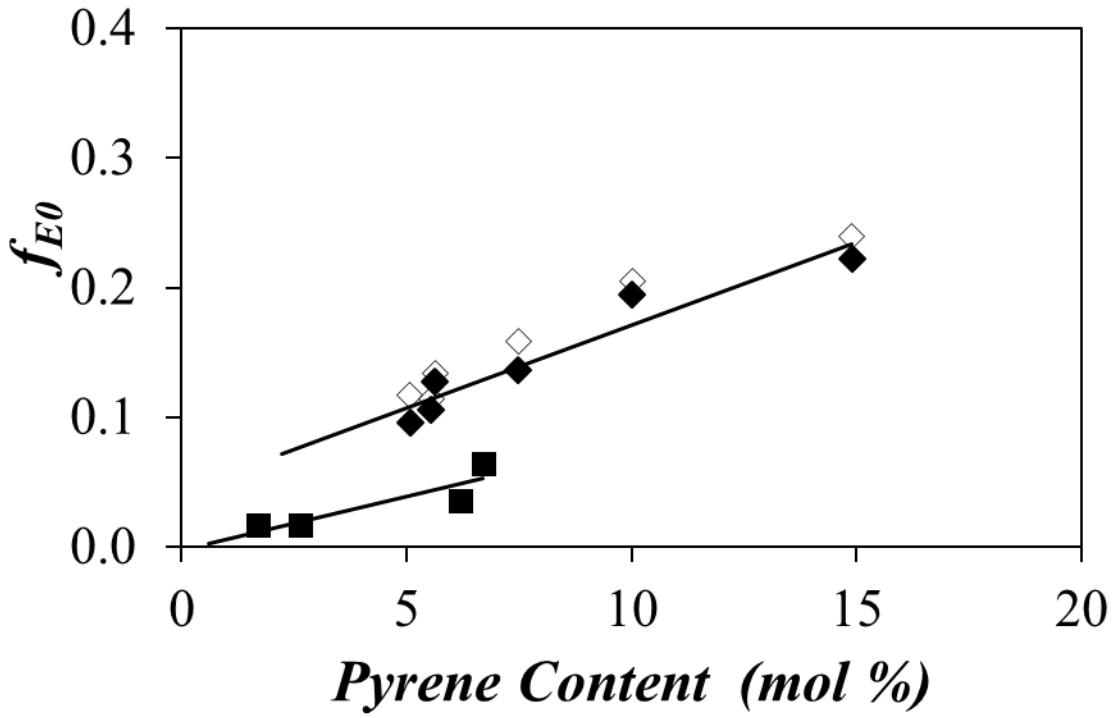

Figure 2.9. Plot of f_{E0} as a function of pyrene content. Solutions in DMSO of (■) Py-PMA and Py-Amylose (◆) before degassing and (◇) after degassing.

2.5 Conclusions

A series of Py-Amylose constructs were synthesized, and their chain dynamics were characterized in DMSO by steady-state and time-resolved fluorescence. As a comparison, a flexible polymer, Py-PMA, was studied under the same conditions. Analysis of the steady-state fluorescence spectra to determine $m(I_E/I_M)$ based on the plots presented in Figure 2.3 showed that amylose formed excimer less efficiently compared to PMA if the pyrene content was expressed in molar percentage

of pyrene-labeled structural units. However, $m(I_E/I_M)$ became similar for Py-Amylose and Py-PMA if the pyrene content was expressed in mole of pyrene per backbone atom, indicating that both polymers formed excimer as effectively. Since the steady-state fluorescence spectra account for the contributions of all the pyrene species present in solution, quantitative information on polymer chain dynamics was obtained by applying the FBM analysis to the fluorescence decays. One strength of the FBM analysis is to identify the different pyrene species that contribute to the monomer and excimer decays. The FBM analysis revealed that amylose had a significantly larger level of pyrene aggregation compared to the PMA samples with a similar labeling level. This result was a consequence of the more compact conformation adopted by amylose in DMSO compared to that of the more flexible PMA backbone. More importantly, FBM analysis yielded $<N_{blob}>$ and $<k_{blob} \times N_{blob}>$ which reflected the polymer chain dynamics of the samples. Interestingly, the $<k_{blob} \times N_{blob}>$ values obtained for the Py-Amylose and Py-PMA samples were comparable when reduced in terms of the number of chain atoms. This unexpected large value of $<k_{blob} \times N_{blob}>$ for amylose could not be rationalized by enhanced mobility of the amylose backbone. Rather this result indicated that the pyrene pendants attached onto the amylose backbone were probing a compact environment which was compatible with amylose adopting a helical conformation in DMSO.

To further confirm that this was indeed the case, MMOs were conducted to examine how far two pyrene labels could encounter along the amylose backbone when amylose adopted different conformations. The MMO results obtained based on a random coil conformation of amylose gave a *blob* size smaller than seven AGUs which disagreed with the N_{blob} value of 11 ± 2 AGUs obtained by FBM analysis. In contrast, when amylose adopted a helical structure, the more compact geometry of amylose resulted in a *blob* size of eleven AGUs based on MMOs. This result was in

excellent agreement with the results obtained by the FBM analysis. In view of the above, the fluorescence measurements conducted on the Py-Amylose constructs in combination with the MMOs carried out with Hyperchem demonstrated that amylose formed a rigid helix in DMSO. As it turns out, this study represents the second example in the literature where pyrene excimer fluorescence is applied to determine the helical conformation of a macromolecule in solution, the first example being for PGA.[31,32] It suggests that pyrene excimer fluorescence constitutes a robust analytical means to probe the compact conformation of condensed macromolecules by taking advantage of the restricted spatial range of pyrene encounters that lead to excimer formation upon contact.

Chapter 3:
Interior of Amylopectin Dissolved in DMSO Characterized by Pyrene Excimer Fluorescence and Molecular Mechanics Optimizations

3.1 Abstract

Amylopectin was labeled with 1-pyrenebutyric acid (PBA) to yield a series of Py-Amylopectin constructs and the fluorescence spectra and decays of their dispersions in DMSO were acquired. The analysis of the fluorescence data indicated that pyrene excimer formation was highly efficient, much more efficient than expected for pyrene labels covalently attached onto a rigid polysaccharide backbone. These results suggested that excimer formation occurred in a pyrene-rich environment indicative of a dense interior for amylopectin. Molecular mechanics optimisations (MMOs) were conducted with the program HyperChem to determine the extent of overlap between two pyrene labels attached at different positions of a single or double polysaccharide helix as a function of the number of anhydroglucose units separating the two fluorescent labels. These MMOs established that isolated polysaccharide helices labeled with pyrene could not justify the efficient pyrene excimer formation found for the Py-Amylopectin constructs. MMOs were then employed to determine the distance between polysaccharide helices arranged in a hexagonal array that would be necessary for pyrene excimer formation to occur as efficiently as found by fluorescence. Regardless of whether the polysaccharide helices were single or double helices, they were found to be separated by 2.7 (±0.3) nm, thus implying that the density of the amylopectin interior experienced by the pyrene labels equaled 0.29 (±0.01) g/mL, a value that was one-to-two orders of magnitude larger than what would be expected based on intrinsic viscosity measurements. This discrepancy was rationalized by introducing the Solution-Cluster (Sol-CL) model whereby clusters of polysaccharide helices are being held together by flexible polysaccharide segments. The Sol-CL model was found to satisfyingly account for the many scientific observations that have been reported about amylopectin in DMSO.

3.2 Introduction

Starch is an abundant biopolymer whose two main components are amylose and amylopectin. Whereas amylose is a linear chain constituted of anhydroglucose units (AGUs) connected via (1-4) linkages with degrees of polymerization (DP) between a few hundreds and a few thousands, amylopectin is a much larger, highly branched polysaccharide with DP ranging between 10^5 and 10^6 depending on the plant of origin.[1-3] Amylopectin is comprised of short side chains and long chains of AGUs connected via (1-4) linkages, the side chains being covalently attached onto the long chains via (1-6) linkages. The DP of the side chains ranges between 6 and 30.[1,2,4,5] The arrangement of the side chains of amylopectin in the solid state has been described by several cluster-type models.[6-8] According to these models, the side chains pack in 9 nm-thick crystalline lamellae[1,3,9] composed of single and mostly double helices.[10] The crystalline lamellae alternate with amorphous domains encompassing the branching points. Both amylose and the side chains of amylopectin form helices in the solid state with X-ray structures indicating that the C6 hydroxyl groups are confined to the walls lining up the central cavity of the helices.[2] Consequently, these crystallographic structures suggest that the primary C6 hydroxyl of the AGU, despite being less sterically hindered than the secondary C2 and C3 hydroxyls in an isolated AGU, is actually much less accessible to chemical modification than the two latter hydroxyls if the side chains of amylopectin adopt a single or double helical conformation. This information matters to food and material scientists who aim at modifying starch chemically to improve its savory[2,3] or mechanical properties.[11,12]

In particular, small scale hydrophobic modifications are often conducted in DMSO,[13,14] an organic solvent that solubilizes both starch and the desired hydrophobic derivatives. However, no structural information can be found in the literature regarding the structural state of the side chains

of amylopectin in DMSO. A helical conformation of the side chains of amylopectin in DMSO would result in the C6 hydroxyls being oriented toward the helical wall as in a crystal, and thus being inaccessible. The absence of structural information on the interior of an amylopectin macromolecule dissolved in DMSO is hardly surprising since after gelatinization at 60 ^{o}C, amylopectin in DMSO exhibits no crystalline microdomains, preventing the use of X-ray diffraction for structure determination, and can be viewed as an ill-defined *mega*-molecule (DP around 10^6 makes amylopectin much larger than any typical macromolecule), which complicates its characterization by gel permeation chromatography as it has been found to undergo shear-induced degradation.[15-17] In fact, little structural information at the molecular level is presently available for amylopectin and its "averaged" properties are usually characterized such as its weight average molecular weight (M_w) and radius of gyration (R_g) by static light scattering or intrinsic viscosity [η].[5] A priori, fluorescence techniques, and particularly fluorescence resonance energy transfer (FRET) which is often used as a spectroscopic ruler,[18] could provide structural information on the conformation of the side chains of amylopectin.[19] In practice however, most examples found in the literature indicate that quantitative FRET analysis on fluorescently labeled macromolecules is mainly applied to short monodisperse linear chains where the ends can be specifically modified, one end with an energy donor and the other with an energy acceptor.[20] Unfortunately, this nicely laid out protocol is somewhat irrelevant when dealing with the question at hand where the macromolecule under study is ill- instead of well-defined, exhibits an extremely large number of labeling points in the form of hydroxyl groups distributed throughout the entire macromolecule instead of the two and only two required for specific labeling, and has physical dimensions that are so large (several hundreds of nm) that any meaningful photophysical communication would be

prevented by the large separation distance between fluorescent labels covalently attached at two specific positions of amylopectin.

It is in situations like this that the fluorescence blob model (FBM) analysis conducted on the fluorescence decays of macromolecules randomly labeled with pyrene becomes most appealing.[21,22] In these experiments, the macromolecule is randomly labeled with pyrene and the kinetics for pyrene excimer fluorescence (PEF) are characterized. Contrary to FRET that depends strongly on the distance between the energy donor and acceptor, PEF occurs only on contact between an excited and a ground-state pyrene, a requirement that makes the interpretation of the fluorescence signal much simpler to interpret as described in a recent review.[23] In recent PEF experiments carried out on dilute solutions of Py-Amylose constructs in DMSO, the fluorescence decays of the pyrene monomer and excimer were analyzed globally with the FBM.[24] FBM analysis led to the conclusion that an excited pyrene attached to amylose formed an excimer with a ground-state pyrene that was attached to one of 10 AGUs surrounding the excited pyrene label used as reference. In turn, MMOs indicated that excimer formation would occur under these conditions only if amylose adopted a helical conformation.[21] This study supported the conclusion that amylose adopts a helical conformation in DMSO, a result that is still being debated in the scientific literature.

Following this early success in probing the conformation of amylose in DMSO, the present study describes how PEF experiments were also conducted on amylopectin randomly labeled with pyrene (Py-Amylopectin) in combination with MMOs to investigate whether PEF could provide some structural information about the conformation of the side chains of amylopectin in DMSO. Amylopectin was randomly labeled with 1-pyrenebutyric acid to generate several Py-Amylopectin constructs and their solutions in DMSO were characterized by steady-state and time-resolved

fluorescence. Excimer formation for relatively rigid Py-Amylose was found to be surprisingly efficient in DMSO, leading to the conclusion that amylose must be adopting a compact helical conformation that brought the pyrene labels closer to each other, thus favoring pyrene-pyrene encounters and excimer formation.[21] But when the efficiency of pyrene excimer formation was compared between the Py-Amylose and Py-Amylopectin constructs, excimer formation was found to occur 50% more efficiently in Py-Amylopectin, a probable consequence of the highly branched nature of amylopectin. MMOs demonstrated that the increased efficiency for excimer formation in Py-Amylopectin compared to Py-Amylose was compatible with the proposal that the side chains of amylopectin adopt a single or double helical conformation and are held within 25-29 Å from each other, thus allowing for intra- and inter-helix excimer formation. In turn, the existence of clusters of polysaccharide helices in amylopectin led to the formulation of the Solution-Cluster (Sol-CL) model that proposes that the interior of amylopectin is composed of dense clusters of helices held together by flexible polysaccharide segments. The Sol-CL model acknowledges that the interior of amylopectin has a morphology presenting dense and diffuse domains which rationalizes most, if not all, experimental observations reported on amylopectin in the scientific literature.

3.3 Experimental Section

The same procedures, chemicals, and instruments were used as described in detail in earlier publications.[24,25] In brief, Py-Amylopectin was prepared by reacting 1-pyrenebutyric acid with the hydroxyl groups of amylopectin (Aldrich) in the presence of diisopropylcarbodiimide (DIC) and dimethylaminopyridine (DMAP) in a 1:3 mixture of *N*,*N*-dimethyl formamide (DMF) and dimethylsulfoxide (DMSO) at 0 ^{o}C. The solution was kept at 0 ^{o}C for 5 minutes, left to equilibrate to room temperature, and stirred in the dark for 48 hours. After the reaction, the Py-Amylopectin

product was precipitated 3-5 times to remove unreacted 1-pyrenebutyric acid and the pyrene content of the Py-Amylopectin constructs was determined by UV-Vis absorption with a Varian Cary 100 Bio spectrophotometer. Fluorescence spectra and decays of Py-Amylopectin dispersions in DMSO having a pyrene concentration of 2.5×10^{-6} M were acquired with the right-angle geometry on a Photon Technology International LS-100 steady-state fluorometer and an IBH Ltd. time-resolved fluorometer, respectively. The excitation wavelength was set at 346 nm in all fluorescence experiments. A 340 nm nanoLED with an excitation wavelength of 340 nm with the excitation monochromator set at 346 nm provided the excitation photons for the fluorescence decay acquisition for which a 370 and 495 nm cut-off filters were employed for, respectively, the pyrene monomer and excimer to prevent stray scattered light from reaching the detector. The monomer and excimer fluorescence decays were fitted globally according to the FBM which is based on the assumption that while a pyrene label remains excited, it can only probe a subvolume in the polymer coil that is referred to as a *blob*.[18,19] The FBM assumes the existence of four distinct pyrene species in the Py-Amylopectin constructs. Some pyrene labels were attached in pyrene-poor domains of amylopectin where they were isolated, could not encounter a ground-state pyrene to form an excimer, and thus emitted as if they were free in solution with a natural lifetime (τ_M) found to equal 92 ns. Pyrene labels undergoing diffusive motions, induced by the displacement of the structural units bearing the pyrene labels or the linker connecting pyrene to amylopectin, were referred to as Py_{diff}* and they probed the volume of a *blob* with a rate constant k_{blob}. As the Py_{diff}* species came next to a ground-state pyrene, they turned into the species Py_{k2}* that underwent a rapid rearrangement with a large rate constant k_2 to form an excimer. Some pyrenes located on neighboring structural units formed excimer quasi-instantaneously upon excitation and were referred to as the *E*0* species. Finally, the excimer decays exhibited a short-lived fluorescent

species *ES** that emitted at early times in the excimer decay and which is often encountered with pyrene-labeled macromolecules that form little excimer. The species *ES** was accounted for by adding an exponential with a lifetime of 3.5 ns that was fixed in the decay analysis. The molar fractions of the pyrene species Py_{diff}*, Py_{free}*, Py_{k2}*, *E*0*, and *ES** were referred to as f_{diff}, f_{free}, f_{k2}, f_{E0}, and f_{ES}, respectively. The abbreviation Py_{agg}* was used to represent the species *E*0*, as it describes the aggregated pyrenes. More explanations on the FBM analysis can be found in earlier reviews and publications therein.[26,27]

3.4 Results and Discussion

The fluorescence spectra of Py-Amylopectin in DMSO were acquired. They were normalized at the 0-0 transition of pyrene (375 nm) and compared to those acquired earlier for Py-Amylose[21] in Figure 3.1. The fluorescence spectra showed two sharp bands at 375 and 410 nm typical for the pyrene monomer, as well as the broad structureless emission of the pyrene excimer centered at 480 nm. A higher pyrene content for amylose or amylopectin led to an increased number of pyrene-pyrene encounters, which resulted in increased excimer fluorescence. The fluorescence spectra were further analyzed by integrating the fluorescence signal corresponding to the pyrene monomer (I_M) and excimer (I_E) to yield the I_E/I_M ratio which was plotted as a function of pyrene content in Figure 3.1C. The Py-Amylopectin constructs showed a steeper increase in excimer formation than the Py-Amylose constructs. The slopes ($m(I_E/I_M)$) of the I_E/I_M plots shown in Figure 3.1C were found to equal 0.22 ± 0.01 and 0.15 ± 0.01 for amylopectin and amylose, respectively. The slope $m(I_E/I_M)$ is being viewed as a measure of the efficiency of pyrene excimer formation.[28,29] The surprisingly large $m(I_E/I_M)$ value found for Py-Amylose, considering the expected rigidity of the polysaccharide backbone, led to the suggestion that efficient pyrene excimer formation takes place in Py-Amylose because amylose adopts a compact helical conformation in DMSO that brings the

pyrene labels closer to each other. The additional 50% increase in $m(I_E/I_M)$ found for amylopectin compared to amylose was attributed to the branched nature of amylopectin that brought several side chains in close proximity, thus enhancing pyrene-pyrene encounters and pyrene excimer formation. As often observed for macromolecules randomly labeled with pyrene, the I_E/I_M plots did not go through the origin in Figure 3.1C (see for instance refs. 24 and 25). This behavior is a consequence of the inherent sequestration of the pyrene labels within pyrene-poor domains along the macromolecule. At low pyrene contents, the pyrene labels are isolated and cannot form excimer. A threshold must be reached in terms of pyrene content above which a sufficiently large fraction of pyrene labels are within reach of each other to form excimer. Above that threshold, an increase in pyrene content leads to an increase in the I_E/I_M ratio as observed in Figure 3.1C.

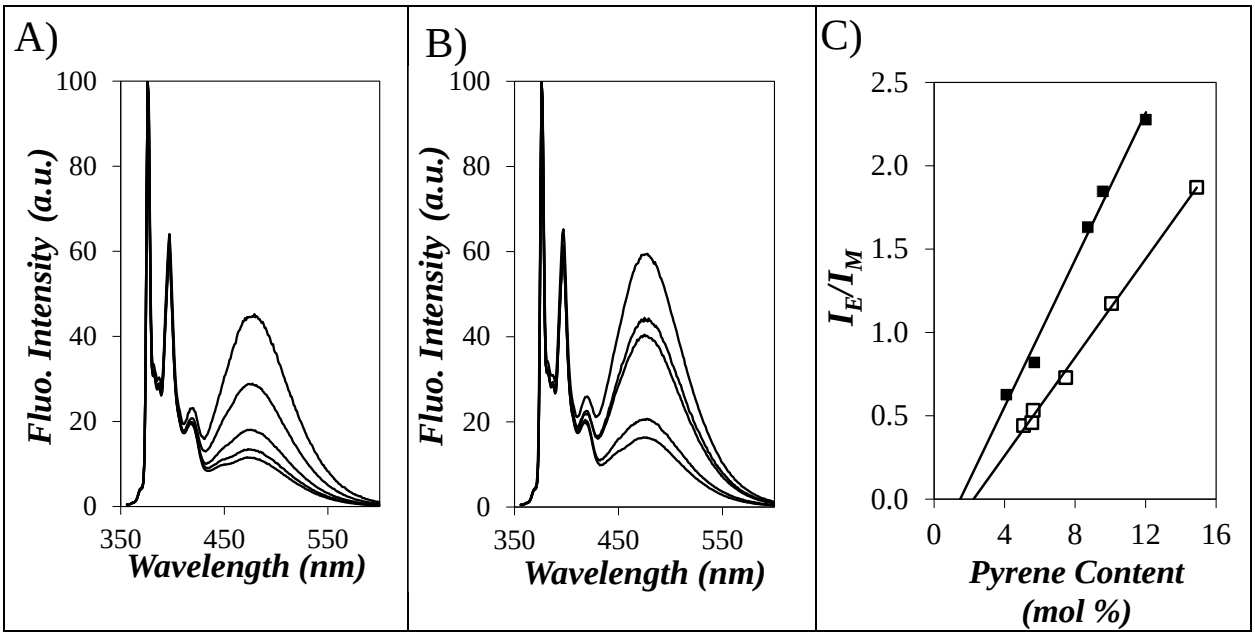

Figure 3.1. Fluorescence spectra of constructs of A) Py-Amylose and B) Py-Amylopectin in DMSO. From bottom to top, the pyrene content equals A) 5.1, 5.6, 5.6, 7.5, 10.0, and 14.9 mol% and B) 4.1, 5.7, 8.7, 9.6, and 12.0 mol%. C) Plot of I_E/I_M as a function of pyrene content for (■) Py-Amylopectin and (□) Py-Amylose. λ_{ex} = 346 nm.

Since the purpose of this study was to obtain structural information on amylopectin in DMSO, it was important to confirm that the excimer formation of Py-Amylopectin only occurred intramolecularly in DMSO. To confirm this, Py-Amylopectin constructs with low, intermediate, and high pyrene contents of respectively 4.1, 8.7, and 12.0 mol% were dissolved in DMSO, and the concentration of these Py-Amylopectin solutions was adjusted to 4, 8, and 12 mg/L. Steady-state fluorescence spectra of the solutions were then acquired. The I_E/I_M ratio was determined and plotted as a function of Py-Amylopectin concentration in Figure 3.2. Within experimental error, the I_E/I_M ratio remained constant for the range of Py-Amylopectin concentrations used in this study. Figure 3.2 demonstrated that in this concentration range, pyrene excimer was formed intramolecularly.

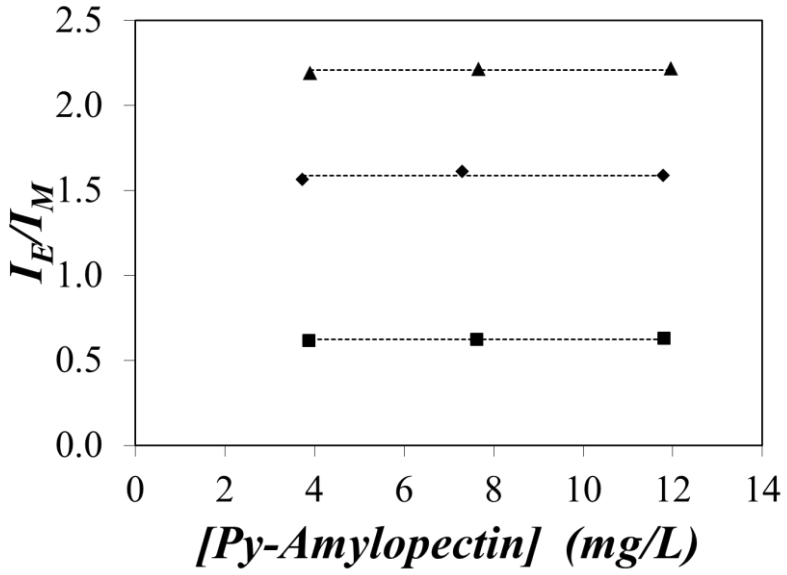

Figure 3.2. Plot of I_E/I_M as a function of Py-Amylopectin concentration in DMSO: (■) 4.1 mol%, (◆) 8.7 mol%, and (▲) 12.0 mol%.

Since the fluorescence spectra report on all the pyrene species present in solution and not only on those referred to as Py_{diff}* that reflect the internal dynamics of the macromolecule of interest, the conclusions drawn on the internal dynamics of Py-Amylose and Py-Amylopectin from the analysis of the fluorescence spectra in Figure 3.1 could be affected by the contribution of the other pyrene species. These include the pyrene species that do not form excimer and emit as if they were free in solution (Py_{free}*) and those that form excimer quasi-instantaneously upon excitation as they are located on neighboring AGUs and behave as if they were aggregated (Py_{agg}*).[22,23] As the pyrene content of a pyrene-labeled construct increases, the concentration of Py_{free}* and Py_{agg}* decreases and increases, respectively, which complicates the analysis of the fluorescence spectra. Fortunately, careful analysis of the pyrene monomer and excimer fluorescence decays can identify the contribution of each pyrene species, thus providing a means to solely characterize those pyrene labels Py_{diff}* that form excimer by diffusive encounters.[22,23] Consequently, the monomer and excimer time-resolved fluorescence decays of Py-Amylopectin and Py-Amylose were acquired and analyzed according to the FBM. Since the global FBM analysis of the monomer and excimer decays can distinguish between the different pyrene species, it provided dynamic information specific to the Py_{diff}* species in the Py-Amylopectin constructs.[22,23] An example of the fit of the pyrene monomer and excimer fluorescence decays of Py-Amylopectin is presented in Figure 3.3. In all cases, the fits were good with reduced χ^2 values of 1.15 or less and residuals and autocorrelation of the residuals being randomly distributed around zero. All parameters retrieved from the global FBM analysis of the monomer and excimer decays have been listed in Tables S3.1-3.2 in the Appendix.

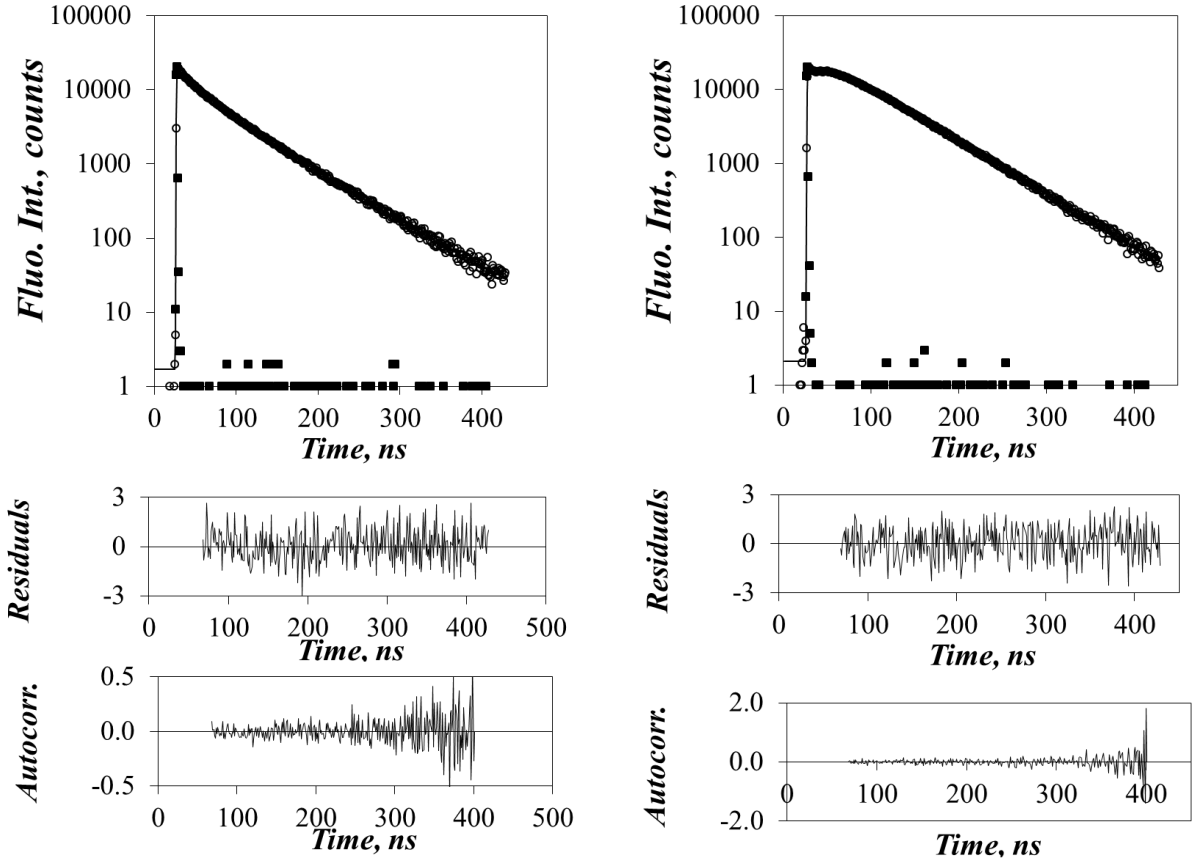

Figure 3.3. Global FBM analysis of the pyrene A) monomer (λ_{em} = 375 nm) and B) excimer (λ_{em} = 510 nm) fluorescence decays acquired with Py-Amylopectin labeled with 5.8 mol% of 1-pyrenebutyric acid. (λ_{ex} = 346 nm).

The natural lifetime (τ_M) of the 1-pyrenebutyrate derivative used to label amylose and amylopectin was found to equal 89.5 and 92.0 ns in aerated DMSO, respectively. It was determined from the analysis of the monomer fluorescence decay of a Py-Amylose and Py-Amylopectin construct having a very low pyrene content of 1.4 and 1.3 mol%, respectively, so low that it ensured minimal excimer formation and that the monomer emission was dominated by the Py_{free}* species. As a result, the pyrene monomer decay could be fitted with a sum of two exponentials where one of the exponentials accounted for 80% of the pre-exponential contribution and whose lifetime was thus attributed to τ_M. The pyrene excimer generated by Py-Amylopectin and Py-

Amylose in DSMO had a similar lifetime equal to 45 ± 1 and 48 ± 3 ns, respectively. These lifetimes are typical for pyrene excimer in an organic solvent. As described in the Experimental section, excimer formation occurs in a sequential manner with the pyrene labels moving toward each other via a slow diffusive process described by the rate constant k_{blob} followed by a rapid rearrangement of the pyrene labels to form excimer with a rate constant k_2. For Py-Amylopectin, k_{blob} and k_2 equalled 1.4 (±0.2)×10^7 s^{-1} and 2.7 (±0.1)×10^8 s^{-1}, respectively, whereas k_{blob} and k_2 equalled 1.8 (±0.2)×10^7 s^{-1} and 2.0 (±0.5)×10^8 s^{-1} for Py-Amylose, respectively. For both constructs, k_2 was one order of magnitude larger than k_{blob}, as would be expected for rapid rearrangement of the pyrene labels.

The parameter N_{blob} was also retrieved from the FBM analysis of the fluorescence decays. N_{blob} and the product $k_{blob}\times N_{blob}$ were plotted in Figure 3.4 as a function of pyrene content and compared with the values obtained earlier with Py-Amylose. Both N_{blob} and $k_{blob}\times N_{blob}$ remained constant with the pyrene content, yielding the averaged $<N_{blob}>$ and $<k_{blob}\times N_{blob}>$ values of 20 ± 3 and 0.27 (±0.02)×10^9 s^{-1}, respectively. These values were larger than the $<N_{blob}>$ and $<k_{blob}\times N_{blob}>$ values obtained with non-degassed Py-Amylose solutions and found earlier to equal 10 ± 1 and 0.17 (±0.01)×10^9 s^{-1},[21] respectively. Since $<k_{blob}\times N_{blob}>$ reflects the frequency of pyrene-pyrene encounters within the volume defined by the macromolecule in solution, the 50% increase in $<k_{blob}\times N_{blob}>$ observed for Py-Amylopectin with respect to Py-Amylose agreed with the 50% increase found for the slope $m(I_E/I_M)$ of the I_E/I_M plot in Figure 3.1C for Py-Amylopectin with respect to that of Py-Amylose. Together, these findings reflect the higher local pyrene concentration $[Py]_{loc}$ experienced by an excited pyrene in the highly branched amylopectin. The twice larger N_{blob} value found for Py-Amylopectin also supported the increased density of

amylopectin with respect to amylose, since more AGUs could be found inside a same *blob* for Py-Amylopectin.

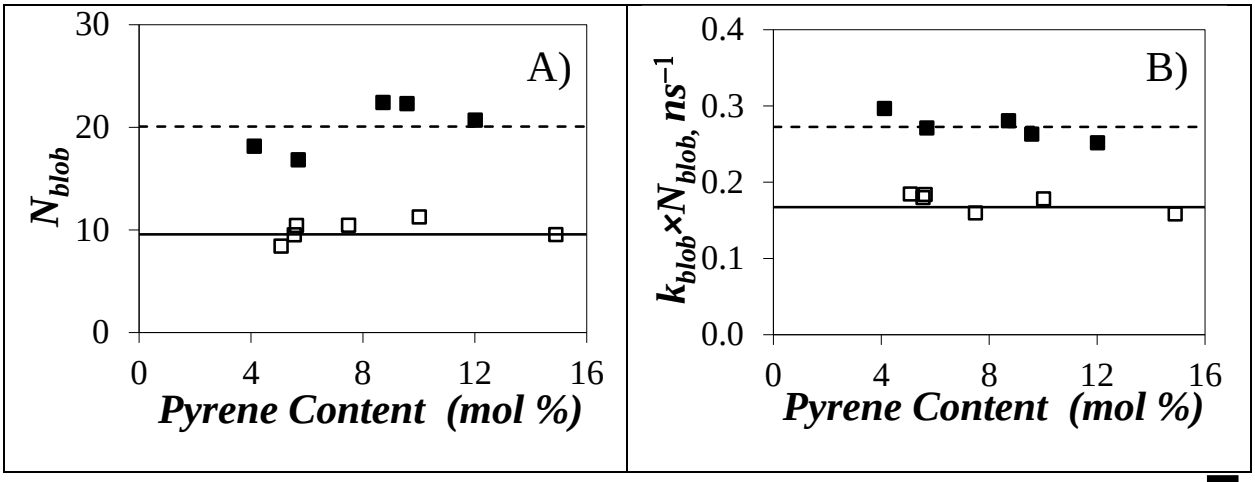

Figure 3.4. Plot of A) N_{blob} and B) the product $k_{blob} \times N_{blob}$ as a function of pyrene content for (■) Py-Amylopectin and (□) Py-Amylose.

What the results retrieved from the FBM analysis did not provide so far, was an indication that the pyrene labels were covalently attached onto the side chains of amylopectin in a helical or random coil conformation. Certainly, the substantially enhanced ability of Py-Amylopectin to form excimer compared to Py-Amylose, whose surprisingly efficient capacity at forming excimer in DMSO was rationalized by the high local pyrene concentration resulting from its helical conformation, suggested that the side chains of Py-Amylopectin adopt a helical conformation themselves. This proposition was further supported by considering the molar fraction (f_{E0}) of pyrene labels that were pre-associated in the ground-state and formed excimer quasi-instantaneously upon direct excitation. Because f_{E0} reports on those pyrene labels that are pre-associated, f_{E0} reflects the level of clustering of the pyrene labels along the polymer backbone and is not affected by the time-dependent process of excimer formation by diffusive encounters between the pyrene labels Py_{diff}*. Unusually large f_{E0} values have been reported each time a pyrene-labeled polymer was adopting a helical conformation such as a series of pyrene-labeled

poly(*L*-glutamic acid) in DMF[30,31] or amylose in DMSO.[21] The high f_{E0} values are due to the increased local concentration of the pyrene labels that is generated upon helix formation, bringing the pyrene labels closer to each other. Tellingly, Figure 3.5 indicates that the Py-Amylopectin samples yielded f_{E0} values that matched closely those obtained for helical Py-Amylose. This result strongly suggested that like amylose, the side chains of amylopectin adopted a helical conformation in DMSO.

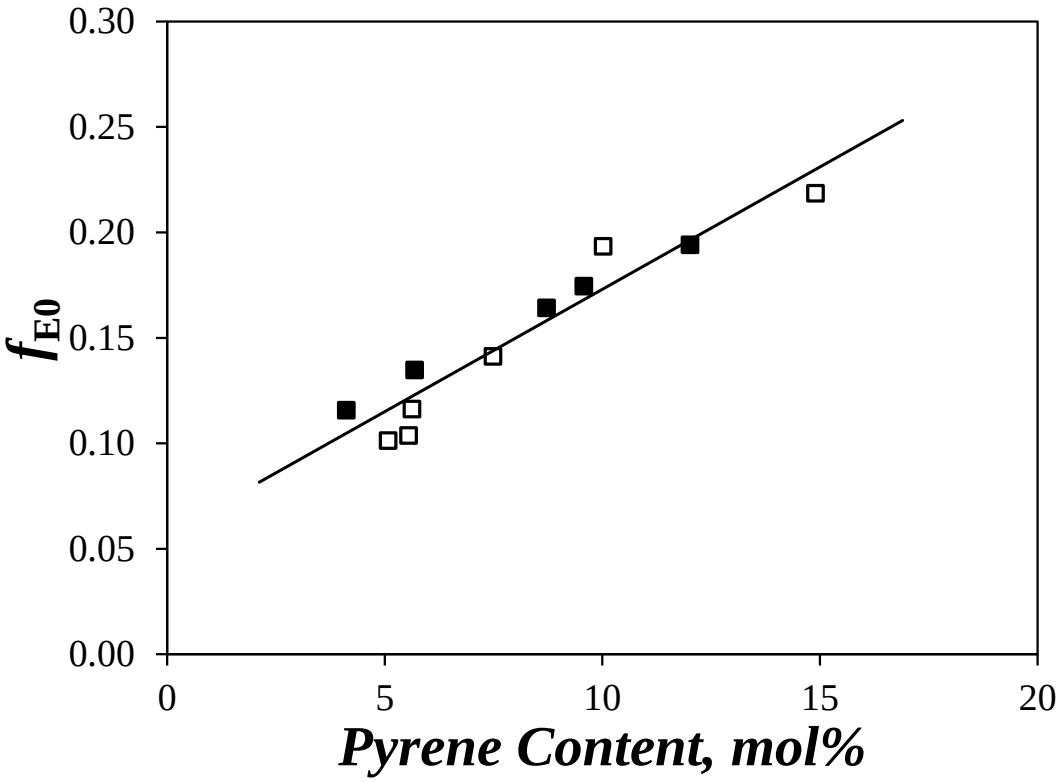

Figure 3.5. Plot of the molar fraction of pyrene labels involved in pyrene dimers (*E*0) as a function of pyrene content in mol% (■) Py-Amylopectin and (□) Py-Amylose.

If the side chains of amylopectin formed isolated helices in the same manner as amylose does in DMSO, the large N_{blob} value of 20 AGUs found for Py-Amylopectin compared to an N_{blob} value of 10 for helical Py-Amylose[24] indicates that other factors must be at play. One such factor could be the double helical conformation adopted by the side chains of amylopectin in the solid

state.[1-4,32] To investigate whether a double helix conformation could lead to a larger N_{blob} value, MMOs were conducted with HyperChem. To this end, the structure of the optimized double helix generated with 36 anhydroglucose residues was imported into HyperChem[33] and it was used to build a double helix constituted of 18 AGUs for each strand. To this double helix, one 1-pyrenebutyrate label was attached to the C2-hydroxyl of an AGU located toward the center of the double helix and referred to as residue #1 and a second 1-pyrenebutyrate label was attached to the C2-hydroxyl of residue #2 as shown in Figure 3.6A. We note that the C6-hydroxyl was not selected for pyrene attachment because it was oriented toward the center of the helix as is well-established in the literature.[2] A constraint was imposed in HyperChem that the carbons C2 or C7 of the two pyrene moieties be brought within 3.4 Å from each other by applying the Fletcher-Reeves algorithm while leaving all atoms of the helix fixed during the optimization. Good overlap between the two pyrene labels was judged by aligning the frame of the pyrene labels until they appeared almost as two vertical parallel lines on the computer screen. Then the two pyrene labels were rotated by 90^{o} and the extent of overlap between the two pyrenyl frames was estimated by counting the number of carbon atoms of one pyrene unit that overlapped the frame of the other pyrene label. The number of carbon atoms was recorded and the 1-pyrenebutyrate label that was connected to the C2-hydroxyl of residue #2 was moved to the C2-hydroxyl of residue #3 and its extent of overlap with the pyrene label remaining on residue #1 used as reference was determined. This exercise was continued by displacing the second pyrene label one AGU at a time for each strand of the double helix and recording the number of overlapping carbon atoms between the two pyrenyl frames as a function of residue position along the double helix using residue #1 as reference.

Two conformations of a double helix where two pyrene labels are separated by 1 and 6 AGUs on the same strand of the double helix were presented in Figure 3.6A and B. Residues

located on the same strand as the reference residue are referred to as residues #1, 2, 3… whereas the residues on the other strand of the double helix are referred to as residues #D1, D2, … Earlier studies have found that N_{blob} represented the number of structural units that could be labeled with pyrene and would allow good overlap between the pyrene labels where a good overlap corresponds to a minimum of 7 carbon atoms.[24,31] Based on this constraint, a good overlap between the pyrene labels was observed when two pyrene labels were separated by 2, 3, 4, and 5 AGUs on the other strand and by one AGU on the same strand. Larger numbers of AGUs held the pyrene labels too far apart and prevented any overlap between them. Consequently, the reference pyrene attached on residue #1 could overlap with another pyrene situated up to a total of 5 AGUs away along the double helix above and below the reference pyrene. These considerations would result in an N_{blob} value equal to 2 + 8 + 1 = 11 AGUs, a value much smaller than the N_{blob} value of 20 found experimentally for Py-Amylopectin. Consequently, this analysis led to the conclusion that the origin of the large N_{blob} value found for Py-Amylopectin was not due to the single or double helical conformations that might be adopted by the side chains of amylopectin in DMSO since both conformations would result in an N_{blob} value of 11 AGUs based on MMOs.

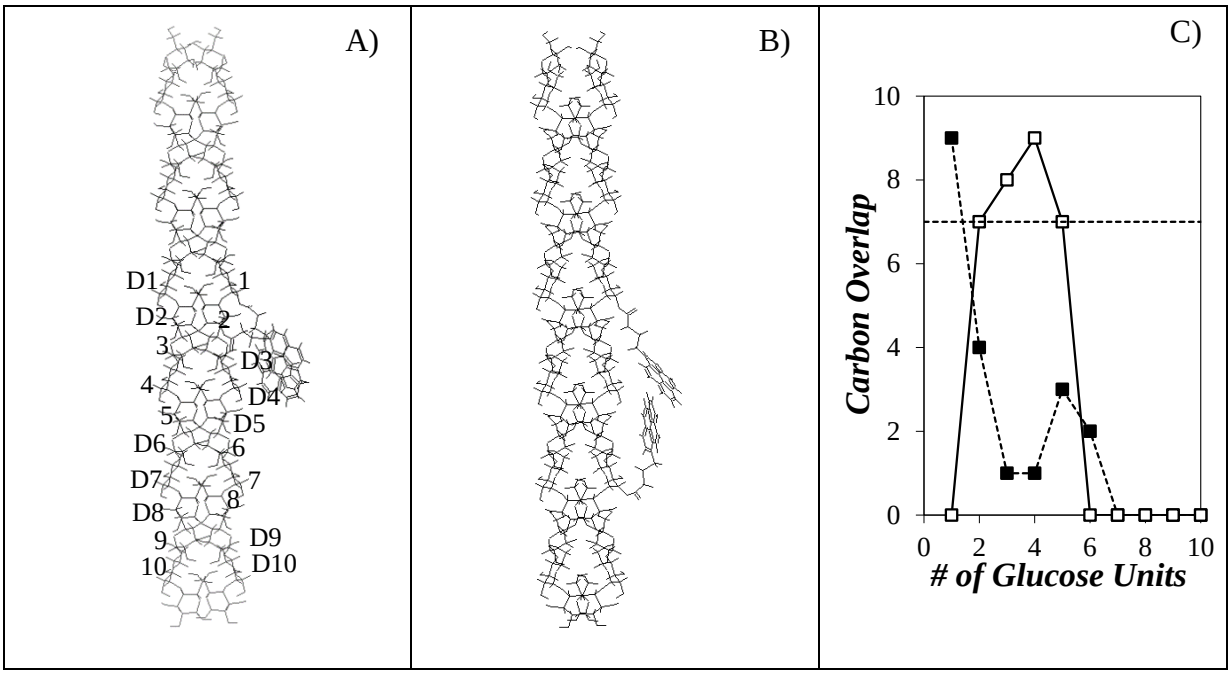

Figure 3.6. Effect of separation distance between pyrene-labels attached at positions A) 1 and 2 and B) 1 and 7 on a same strand of the double helix. C) Extent of overlap as a function of separation distance for two pyrenes attached on the (■) same and (□) other strand of the double helix. In A), residues located on the same or the other strand of the double helix compared to the reference pyrene attached at the C2 hydroxyl of residue #1 are labeled as residues # 2, 3… or residues #D1, D2, respectively.

Another possibility that might lead to a larger *blob* size for amylopectin in DMSO was that its side chains were packed close enough to allow pyrene excimer formation between adjacent helixes. To investigate this possibility, an amylopectin cluster consisting of seven polysaccharide helices placed in a hexagonal arrangement was created using HyperChem as shown in Figure 3.7. The cluster was built by duplicating Helix #0 located at the center of the cluster to create Helix #1 and translating the axis of Helix #1 along the x-axis by an interhelix distance d_{h-h} corresponding to the separation between the helix axes. Helix #2 was created by duplicating Helix #0, rotating the duplicated helix by 60 °, and translating it by the same d_{h-h} distance along a line making a 60°

angle with the x-axis. The other helices were created in the same manner by duplicating Helix #0, rotating the duplicated helix by a multiple of 60 °, and translating Helix #2 – 6 along a line making an angle with the x-axis corresponding to the angle used to rotate the helix. The MMO results obtained with a cluster of seven double helices are discussed first.

The longest d_{h-h} value was set at 38 Å since two pyrene labels attached on any residue of two adjacent helices held at this distance were too far apart to overlap and form an excimer as shown in Figure 3.7C for a shorter d_{h-h} value of 30 Å. d_{h-h} was then reduced 2 Å at a time from 38 Å down to 16 Å. Considering that the diameter of a starch double helix is 10 Å[3,32] and the frame of a pyrene molecule is about 3.4 Å thick, a d_{h-h} of 16 Å represents the limit where two pyrene molecules can stack between the two double helix envelops separated by 6 Å. At each distance d_{h-h} between 16 and 38 Å, several MMOs were conducted as follows. One 1-pyrenebutyrate label was attached to the C2-hydroxyl of residue #1 on Helix #0 and it was considered to be the reference point for the MMOs. A second 1-pyrenebutyrate label was attached to the anhydroglucose units of Helix #1 starting from residue #D1 in Helix #1. In the helix cluster shown in Figure 3.7A, residue #1 in Helix #0 faces residue #D1 in Helix #1. The two pyrene labels were induced to come within 3.4 Å from each other and the number of carbon atoms in the frame of one pyrene found to overlap the frame of the other pyrene label was recorded. The 1-pyrenebutyrate label on residue #D1 of Helix #1 was then attached to the C2 hydroxyl of residue #D2, induced to come within 3.4 Å of the reference pyrene on residue #1 of Helix #0, and the number of carbon atoms in the frame of one pyrene overlapping the frame of the other pyrene was recorded. This operation was repeated for residues #D1, D2, … along one strand, and then for residues #1, #2, #3, … along the other strand until any overlap between the two pyrenes would become impossible. Examples of good and poor overlap between two pyrene labels can be viewed in Figure 3.7B and C, respectively.

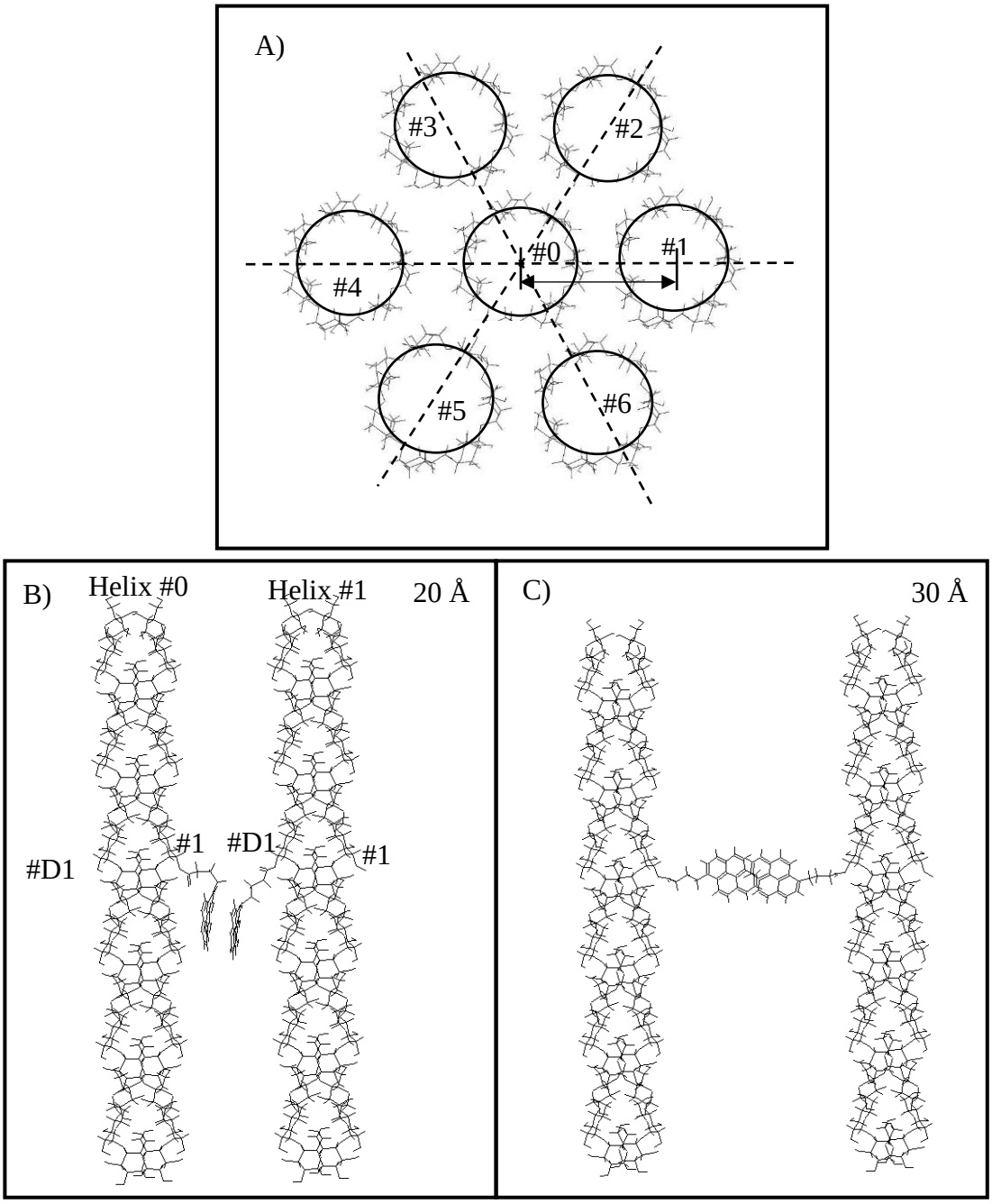

Figure 3.7. A) Illustration of the amylopectin cluster consisting of an array of seven double helices placed in a hexagonal arrangement. Illustration of the ability of the pyrene group attached on the reference residue #1 of Helix #0 to reach the pyrene label on residue #D1 on Helix #1 when d_{h-h} equals B) 20 Å and C) 30 Å showing good and poor overlap, respectively.

This analysis led to the plots shown in Figure 3.8A and B representing the number of overlapping carbons in the frames of the reference pyrene attached to residue #1 of Helix #0 and the other pyrene being attached to residues #1 – 10 of the same strand and residues #D1 – D10 of the other strand of Helix #1 for d_{h-h} values equal to 22 and 30 Å, respectively. In Figure 3.8A, a good overlap between two pyrenyls corresponding to 7 or higher carbon atoms was obtained for residues #D1, D2, and 3 when d_{h-h} equals 22 Å. When the helix axes were separated by d_{h-h} equal to 30 Å, no good overlap with more than 7 C-atoms was possible in Figure 3.8B regardless of the AGU where 1-pyrenebutyrate was attached.

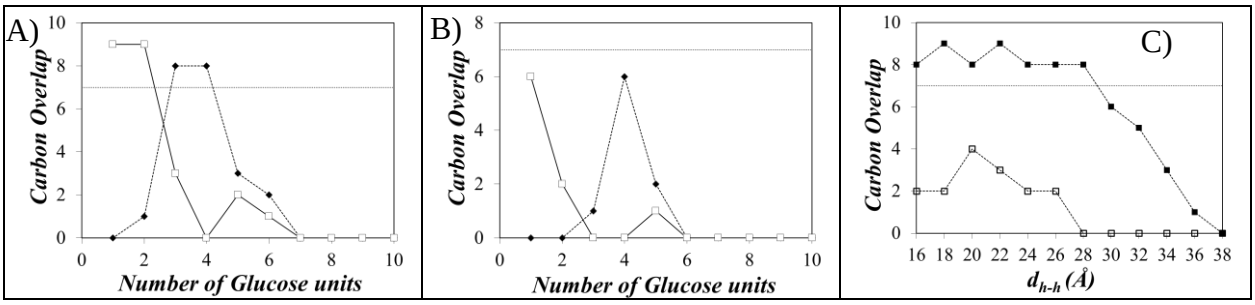

Figure 3.8. Extent of overlap as a function of the position of the AGU on Helix #1 when the interhelical distance equals A) 22 Å and B) 30 Å and the reference pyrenyl is attached on residue #1 of Helix #0. C) Extent of overlap between the reference pyrene on residue #1 of Helix #0 and two pyrenes attached on, respectively, (■) residue #D1 or residue #D3 (□) on Helix #1 as a function of d_{h-h}.

This analysis could also be employed to follow the extent of overlap between the reference pyrene attached on residue #1 of Helix #0 and the other pyrene label attached to any other residue of Helix #1 such as residues #D1 or D3 as shown in Figure 3.8C. Since residue #D1 on Helix #1 is facing residue #1 on Helix #0 (see Figure 3.7B), a good overlap between the pyrenyl pendants is obtained even as the interhelix distance is increased up to 28 Å, above which the pyrenyl groups

are too far apart resulting in poor overlap (number of overlapping C-atoms is less than 7). The situation is different for residue #D3 which is located on the face of the double helix that is diametrically opposite to residue #D1 (see Figure 3.7B to appreciate the position of residue #D1 relative to that of residue #D3). Consequently, two pyrenyl labels attached on residue #1 of Helix #0 and residue #D3 of adjacent Helix #1 cannot overlap as found in Figure 3.8C.

This exercise was repeated with residues #D1 – D10 and residues #1 – 10 on Helix #1 and at each d_{h-h} distance, the number of C-atoms resulting from the overlap of a pyrenyl label on Helix #1 with the reference pyrene on residue #1 of Helix #0 was determined. As done in earlier studies,[24,29,30,34] a number of overlapping C-atoms larger than 7 was deemed to reflect good overlap between the pyrene labels and the AGUs allowing a good overlap were recorded. Residue #D1 in Helix #1 was always among those residues as it was facing residue #1 on Helix #0. To determine the number of residues that needed to be added to the N_{blob} value of 11 found for an isolated double helix, residue #D1 was counted once but the other residues that enabled good overlap between the reference pyrene on Helix #0 and the secondary pyrene on Helix #1 were counted twice to account for their mirror image above residue #D1 in Helix #1. For example, since residues #D1, D2, and 3 were found to result in a good overlap in Figure 3.9A, the contribution of additional residues from Helix #1 would equal 1 (for Res. #D1) + 2×2 (for Res. #D2 and 3) = 5. The contribution of additional residues from Helix #1 to the calculation of N_{blob} (ΔN_{blob}) was plotted in Figure 3.9A as a function of d_{h-h}. At distances greater than 30 Å, no overlap between pyrenyl labels attached onto adjacent Helix #0 and #1 was possible, but as d_{h-h} was decreased from 30 to 24 Å, the number of residues on Helix #1 that provided good overlap increased up to 7 and that number remained the same for shorter d_{h-h} values.

MMOs were then conducted in the same manner for Helix #2. The distance $d_{h\text{-}h}$ was increased in 2 Å increments from 16 to 38 Å and the number of residues between residues #1 – 10 and #D1 – D10 on Helix #2 that allowed two pyrenes to overlap was recorded as a function of $d_{h–h}$. The result of this series of MMOs is shown in Figure 3.9B. Whereas Helix #0 and #1 had to be within 28 Å before two pyrenyl labels could overlap properly, a minimum $d_{h\text{-}h}$ of 26 Å was required to allow two residues on Helix #2 to overlap properly with the reference pyrene on Helix #0. The number of residues allowing good overlap between the reference pyrenyl on Helix #0 and a pyrenyl label on Helix #2 increased with decreasing $d_{h\text{-}h}$ until a $d_{h\text{-}h}$ value of 22 Å was reached below which a constant number of 5 residues on Helix #2 allowed good overlap with the reference pyrene on residue 1 of Helix #0. The calculation of the number of residues that would lead to a good pyrene-pyrene overlap followed the same procedure as the one applied for Helix #1 where the contribution from residues D1 and 1 was counted once while the contributions from the other residues located on the other side of residues 1 and D1 were counted twice to account for their mirror image resulting from the symmetry of the double helix. The final contributions resulting from the overlap with Helix #2 are presented in Figure 3.9B.

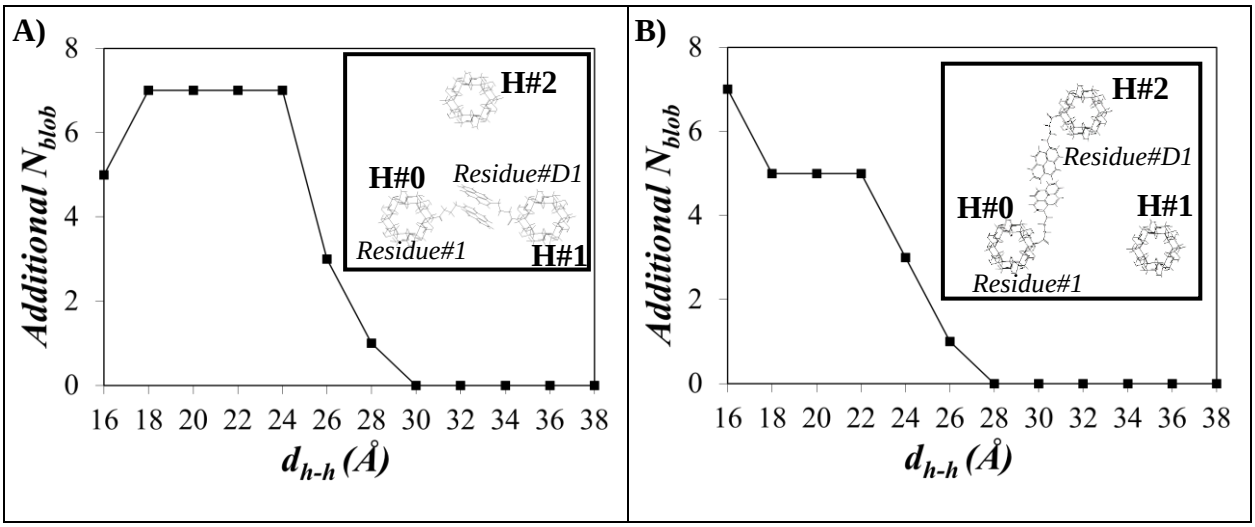

Figure 3.9. Additional contributions to N_{blob} (ΔN_{blob}) caused by inter-helix excimer formation when the second pyrene was situated on A) Helix #1 and B) Helix #2 as a function of inter-helix distance.

Since no overlap was observed between the reference pyrene on residue 1 of Helix #0 and a pyrenyl label attached on any residue of Helix #3 – 5, the additional contribution from Helix #1 (ΔN_{blob}(H#1)) in Figure 3.9A and from Helix #2 (ΔN_{blob}(H#2)) in Figure 3.9B were counted, respectively, once and twice to obtain a theoretical N_{blob} value ($N_{\text{blob}}^{\text{theo}}$) according to Equation 3.1.

$$N_{blob}^{theo} = N_{blob}(\text{H\#0}) + \Delta N_{blob}(\text{H\#1}) + 2 \times \Delta N_{blob}(\text{H\#2}) \qquad (3.1)$$

N_{blob}(H#0) in Equation 3.1 corresponds to the N_{blob} value found to equal 11 for an isolated single or double helix determined in an earlier publication[21] and in Figure 3.6, respectively. The resulting $N_{\text{blob}}^{\text{theo}}$ values obtained with the ΔN_{blob}(H#1) and ΔN_{blob}(H#2) values, such as the ones shown in Figures 3.9 for a hexagonal array of double helices, were plotted as a function of $d_{\text{h–h}}$ in Figure 3.10. The same procedure was then repeated for a hexagonal array of 7 single oligosaccharide helices and the $N_{\text{blob}}^{\text{theo}}$ values obtained from these MMOs were also included in Figure 3.10.

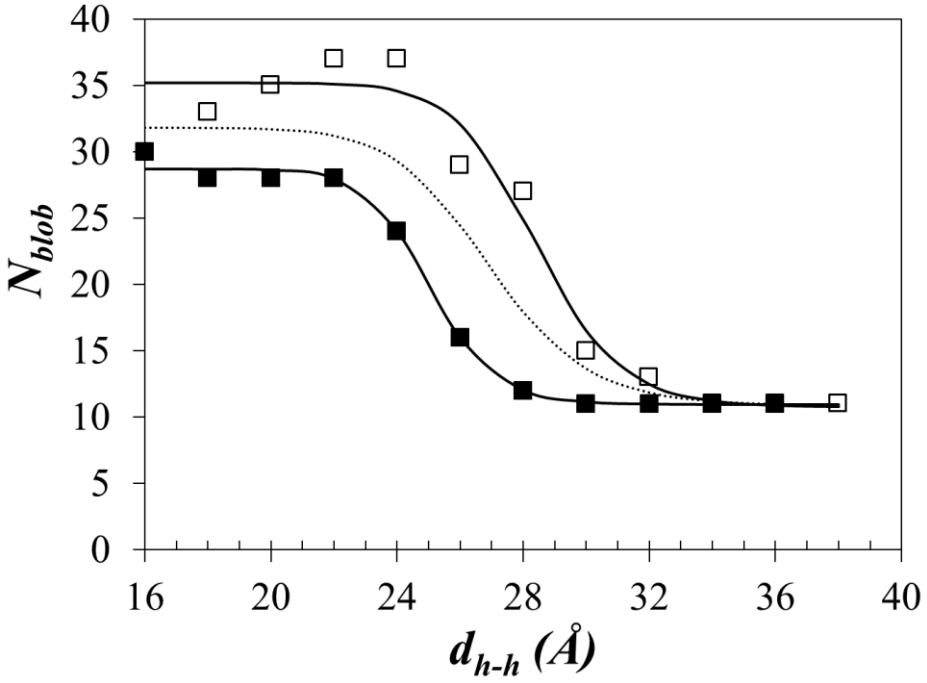

Figure 3.10. N_{blob} as a function of intra-helix distance $d_{h\text{-}h}$ if the side chains of amylopectin adopt a (■) double helix conformation or a (□) single helix conformation in a hexagonal cluster.

The trends shown in Figure 3.10 indicate that N_{blob}^{theo} increases sharply from 11 for an isolated single or double helix to 28 or 32 when $d_{h\text{-}h}$ decreases over a narrow range of interhelical distances from 32 to 22 Å for, respectively, a cluster of double or single helices. The N_{blob}^{theo}-*vs*-d_{h-h} trend could be satisfyingly fitted with an empirical logistic function of the type shown in Equation 3.2 where the parameters A_1, A_2, x_o, and p were listed in Tables S3.6A-C along with their respective errors.

$$N_{blob}^{theo} = A_2 + \frac{A_1 - A_2}{1 + (x / x_o)^p} \tag{3.2}$$

The number of overlapping carbons found from the MMOs conducted with HyperChem have been listed in Tables S3.4 and S3.5. Based on the fits, N_{blob}^{theo} would equal the experimental

N_{blob} of 20 for d_{h-h} equal to 2.50 and 2.90 nm for a double and single helix, respectively. The interhelical distance d_{h-h} was used in Equation 3.3 to determine the density ρ_{fluo} of the oligosaccharide environment experienced by the pyrenyl labels inside a cluster of hexagonally packed oligosaccharide helices separated by an interhelical distance d_{h-h}. In Equation 3.3, M_o is the molar mass of an AGU (162 g/mol) and N_A is the Avogadro number (6.02×10^{23}). The parameter n_{AGU} is the number of AGUs per helix pitch (h) and n_{AGU} and h were deduced from the X-ray structures reported for single[35] and double[33] helices. For a single or double oligosaccharide helix, n_{AGU} equals 7 or 12 and h equals 8.8 or 21.5 Å, respectively.

$$\rho_{fluo} = \frac{n_{AGU} \times M_o}{\sin(60^o) \times h \times N_A} \times \left(\frac{1}{d_{h-h}} \right)^2 \qquad (3.3)$$

The ρ_{fluo} values of Py-Amylopectin were calculated to equal 0.29 and 0.28 g/mL for single and double helices, respectively, or 0.29 ± 0.01 g/mL on average. On the other hand, the density of dispersed amylopectin can be determined by multiplying the inverse of its intrinsic viscosity value by 2.5 (2.5/[η]). As reported by Damin Kim, a graduate student in the laboratory of Prof. Jean Duhamel, the intrinsic viscosity of amylopectin from maize was 122.5 mL/g in DMSO. The density of dispersed amylopectin in DMSO can be calculated as 2.5/(122.5 mL/g) = 0.0204 g/mL. The discrepancy between the dense amylopectin interior reflected by the excimer fluorescence resulting from the diffusive encounters between two pyrenes randomly attached to the macromolecule and the low density expected from intrinsic viscosity measurements suggested that amylopectin in DMSO exhibits a heterogeneous interior. Densely packed domains must exist in amylopectin, probably taking the form of clusters of helices as depicted in Figure 3.7A, where PEF occurs in Py-Amylopectin between nearby pyrenyl labels, but these clusters of helices must be

spread out in the amylopectin interior, resulting in the overall low density obtained from intrinsic viscosity measurements. A representation of the amylopectin interior in DMSO showing clusters of helices connected to each other by linear oligosaccharide segments is shown in Figure 3.11.

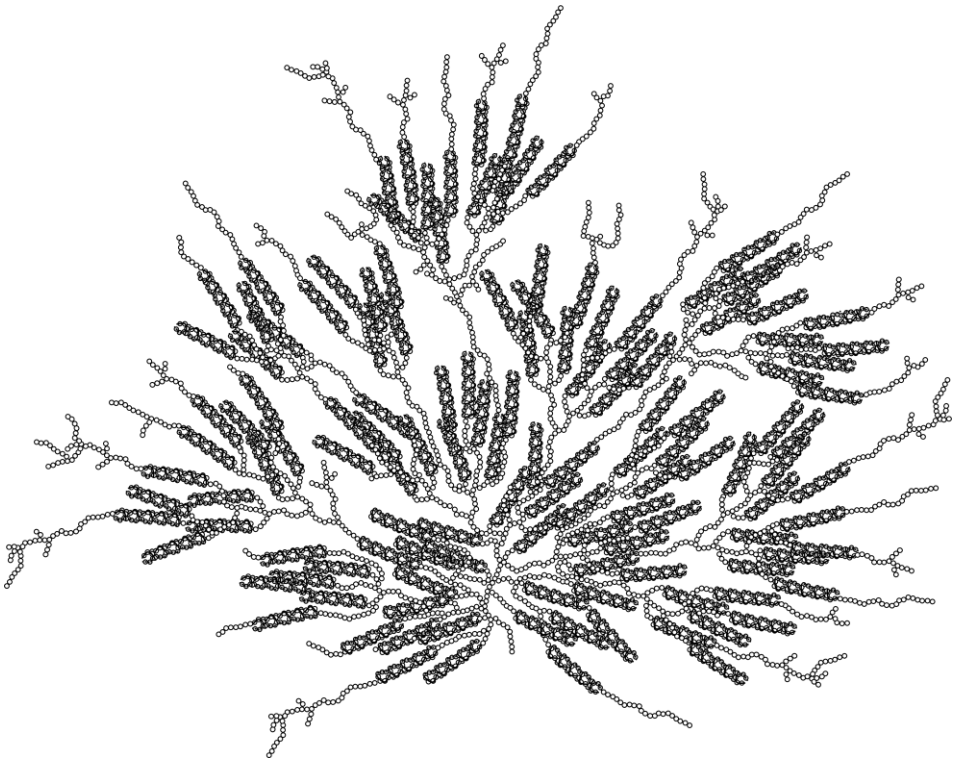

Figure 3.11. Depiction of the Solution-Cluster (Sol-CL) model where dense clusters of double helices are connected to each other by flexible polysaccharide segments.

Figure 3.11 provides the basis for the formulation of the solution-cluster (Sol-CL) model which is a consequence of the cluster model that is firmly established to represent the macromolecular arrangement of amylopectin in starch granules,[6-8] but whose main features are expected to be retained for amylopectin dispersed in DMSO. The Sol-CL model would follow the nomenclature employed for the cluster model which considers A and B chains to rationalize the arrangement of the side chains of amylopectin in the solid state. A chains would form dense clusters of single or double helices connected to each other by longer B chains.[36] Pyrene labeling

would target the denser clusters of helices where PEF would occur effectively. Pyrenyl labels attached onto the B chains bridging the different clusters would form excimer less efficiently, but they would also contribute less to the overall fluorescence signal as they would have a sparser presence in the low-density regions of the amylopectin interior.

As it turns out, the Sol-CL model depicted in Figure 3.11 agrees with some of the conformational features expected from amylopectin in DMSO and might improve our understanding of some of the surprising behavior observed with amylopectin dispersions. First, the PEF measurements indicate that amylopectin in DMSO forms compact domains made of clusters of helices. This agrees with the small Mark-Houwink-Sakurada (MHS) exponents of 0.3 and 0.4 recovered for the relationship $[\eta] = K \times M_w^{\alpha}$ that indicates a compact conformation for amylopectin dispersed in DMSO.[37,38] Second, the Sol-CL model accounts for the non-zero exponent in the MHS equation which implies that amylopectin in DMSO becomes less dense with increasing molecular weight as expected for linear chains due to excluded volume effects. In the case of amylopectin, the flexible polysaccharide segments joining the clusters of helices would be subject to excluded volume effects that would result in a decrease in density of the macromolecular interior with increasing molecular weight. However, this decrease would not be as pronounced as for linear polymers due to the compact clusters of helices distributed inside the amylopectin interior. Third, the Sol-CL model does not contradict the oblate ellipsoid shape that amylopectin has been found to adopt from pulsed-field gradient nuclear magnetic resonance,[37,38] small angle X-ray scattering,[39] and a combination of rheology and field flow fractionation experiments as the PEF results do not provide information about the arrangement of the clusters of helices with respect to each other.[40] Fourth, the proposal that amylopectin in DMSO would be constituted of dense clusters of helices loosely linked to each other by flexible polysaccharide segments suggests that,

under flow, the clusters would be sufficiently mobile to allow their alignment along the shear direction, resulting in the shear-thinning behaviour that is usually observed experimentally.[41-46] However, if the helix clusters were small enough or/and sufficient shear was applied to the amylopectin solution, the loose oligosaccharide chains linking the clusters could entangle, resulting in the shear-thickening that has also been reported.[40,41] Furthermore, one would expect these entanglements to be somewhat permanent as disentangling the chains would require the cooperative displacement of several clusters of helices that might prove impossible to achieve. This would rationalize the hysteresis that has been observed for amylopectin solutions in DMSO under shear.[40,41] In summary, the Sol-CL model depicted in Figure 3.11 seems to account for many of the observations that have been reported in the literature for amylopectin in DMSO, including those obtained in this study of Py-Amylopectin based on PEF.

3.5 Conclusions

This study has established that PEF in Py-Amylopectin constructs is so efficient that the pyrene labels must be highly concentrated in the Py-Amylopectin interior. This conclusion led to the proposal that PEF must be taking place between pyrene labels covalently attached onto clusters of single or double helices held within 2.65 (±0.26) nm from each other. In turn, such a spacing between oligosaccharide helices would result in an internal density of 0.29 (±0.01) g/mL for amylopectin in DMSO. This value was one order of magnitude larger than the density of amylopectin calculated by multiplying the inverse of its intrinsic viscosity by 2.5. At first glance, such a clear contradiction was surprising considering that the exponent retrieved for the MHS relationship based on the reported amylopectin samples[47,48] was smaller than the value of 0.5 or 0.8 expected for linear polymers in θ– and good solvents,[49] which suggested that amylopectin adopted a dense conformation in DMSO. However, the high density expected for the interior of

amylopectin in DMSO begged the question as to why its density determined by intrinsic viscosity measurements would be so much lower than that obtained by the PEF experiments. This contradiction was resolved by invoking the Sol-CL model shown in Figure 3.11.

Although the MHS exponent was lower than that expected for linear chains, it was not equal to zero, implying that amylopectin is also subject to excluded volume effects, albeit to a lesser extent than linear chains. These considerations led to the suggestion that the interior of amylopectin in DMSO is constituted of clusters of single or double helices that are connected by flexible polysaccharide segments as shown in Figure 3.11. The linear chains are subject to excluded volume effects, as normal linear polymers are, which leads to a non-zero MHS exponent, but the cluster of helices are much denser and expand in DMSO to a much smaller extent than the linear polysaccharide segments, thus resulting in a small MHS exponent of 0.3-0.4 which reflects a dense interior.[47,48] The proposal for this arrangement of the interior of amylopectin was described as the Sol-CL model since it is a direct consequence of the well-established cluster model describing the arrangement of the interior of amylopectin in the solid state.[6-8] The Sol-CL model was found to satisfyingly describe many of the scientific observations that have been already published about amylopectin in DMSO. Whether the Sol-CL model will also apply to describe the properties of amylopectin in aqueous solutions remains to be determined.

Chapter 4:
Characterization of Starch Nanoparticles by Pyrene Fluorescence

4.1 Abstract

Nanosized Amylopectin Fragments (NAFs), prepared by extrusion of waxy corn starch which is >99% amylopectin, were characterized using ^{1}H NMR, iodine binding test, viscometry, and dynamic light scattering (DLS). These experiments showed that the NAFs were amylose-free and had a chemical composition similar to that of amylopectin, and that their internal density increased from 0.041 to 0.125 g/mL in dimethylsulfoxide (DMSO) as their number average hydrodynamic diameter decreased from 57 to 8 nm. While these experiments yielded parameters that described the properties of amylopectin averaged over the entire macromolecule, pyrene excimer formation (PEF) was applied to probe the interior of NAFs at the molecular level. To this end, NAF8.3 and NAF57, where the number represents the NAF hydrodynamic diameter expressed in nanometers, were randomly labeled with pyrene and their fluorescence decays were analyzed with the fluorescence blob model (FBM) to determine N_{blob} which is the maximum number of anhydroglucose units (AGUs) that could separate two pyrene-labeled AGUs and still yield good overlap between the pyrenyl labels and thus result in efficient PEF. Comparison of the experimental N_{blob} with the theoretical N_{blob}^{theo} value obtained from Molecular Mechanics Optimizations for oligosaccharide constructs labeled with pyrene yielded a density of 0.26 g/mL for the polysaccharide domains probed by PEF. Since the density determined by PEF was much larger than that of amylopectin and NAFs determined from intrinsic viscosity, it suggested the existence of excluded volumes in NAFs and amylopectin. The existence of these excluded volumes was demonstrated by using PEF to probe changes in the osmotic pressure experienced by the NAFs upon addition of poly(ethylene glycol)s of different lengths. Small particles like Py-NAF8.3, with less excluded volume, were less deformable as compared to the large Py-NAF57, with more excluded volume under the same osmotic pressure. These observations were well-explained by the Solution-Cluster model which was developed originally for amylopectin.

4.2 Introduction

Starch nanoparticles (SNPs) can be employed as substitutes of petroleum-based latex used in the paper coating industry, and their potential as food additives or drug carriers is being actively researched.[1] A number of different SNPs can be generated by chemical, biochemical, or mechanical processes. Examples of such processes include acid or enzymatic hydrolysis, high pressure homogenization, ultrasonication, or reactive extrusion.[1] One of the goals of these processes is to reduce the size of starch to increase the dispersibility of the particles in solution and enable the adjustment of their size to meet the requirements for different industry applications.[2] Unfortunately, the properties of starch and SNPs are somewhat limited and they do not meet the vast majority of applications relevant to the polymer industry. To expand the applicability of SNPs, the chemical modification of SNPs is currently the object of intense research. Most chemical modifications have aimed so far at imparting some hydrophobicity to otherwise hydrophilic SNPs by grafting octenyl succinic anhydride,[3,4] oleic and stearic acids,[5] polystyrene,[6] and more recently, propionic and hexanoic anhydride.[7] But to be most effective, these chemical modifications require the characterization of SNPs not only from a viewpoint pertaining to synthetic polymer particles, based on their hydrodynamic diameter (D_h) and internal density from, respectively, dynamic light scattering (DLS) and intrinsic viscosity ([η]) measurements, but perhaps more importantly, as biopolymer particles, open entities whose interior must be understood at the molecular level in solution. Such studies are particularly relevant for non crystalline SNPs such as those produced through extrusion, whereby the crystalline microdomains of the starch granules are fully melted at the high temperatures experienced in the extruder. Upon dispersion in a suitable solvent like dimethylsulfoxide (DMSO) or water, such SNPs are swollen and their interior, which is exposed to the solvent, can readily react with the chemicals desired for a given chemical modification. A recent study has shown that SNPs produced through extrusion behave differently from typical

synthetic polymer particles and that the term particle might be inadequate to describe SNPs.[8] Recently it has been suggested that SNPs could be described as nanosized starch fragments (NSFs). The nature of NSFs is still poorly understood and their interior would be worthy of more detailed investigation

The present study uses pyrene excimer fluorescence/formation (PEF) to probe at the molecular level the interior of 21 research grade NSFs prepared by extrusion of waxy corn starch. Since this type of starch is 99% amylopectin, these particles were identified in this thesis as nanosized amylopectin fragments or NAFs. Experiments typically conducted on synthetic polymer particles were also performed on the NAFs such as ^{1}H NMR to probe the chemical composition, DLS to characterized D_h, and intrinsic viscosity to assess their internal density. While informative, these techniques only provide information about the properties of NAFs averaged over length scales of tens of nanometers representing the overall size of the NAFs. In contrast, labeling the NAFs with 1-pyrenebutyric acid to generate Py-NAFs allowed probing of the interior of NAFs over distances of 5.0 nm and shorter, thus providing valuable information about the spatial arrangement of the oligosaccharide side chains in the NAFs interior.

This was achieved through a combination of PEF, fluorescence blob model (FBM), and molecular mechanics optimization (MMOs) as explained hereafter. An excited pyrene label bound to a macromolecule, such as in the case of the Py-NAFs, can only probe a finite volume within the macromolecular volume referred to as a *blob* where it can encounter a ground-state pyrene and form an excimer. The FBM takes advantage of this feature to divide the macromolecule into *blobs* among which the randomly attached pyrenes distribute themselves randomly according to a Poisson distribution. Based on this assumption, the FBM analysis of the fluorescence decays acquired with Py-NAFs retrieves the average number $\langle n \rangle$ of pyrenyl labels per *blob*, which is used

to determine N_{blob}, the number of anhydroglucose units (AGUs) found inside a *blob*. N_{blob} represents the maximum number of AGUs included inside a *blob* that allows PEF between one excited and one ground-state pyrene to occur. In turn, MMOs can be conducted on pyrene-labeled oligosaccharide constructs to assess the maximum distance that can separate two pyrenyl groups while still affording a good stacking conducive of PEF. By combining N_{blob} obtained by fluorescence and the length scale determined by MMOs over which PEF occurs, the density of the macromolecular environment experienced by the pyrenyl labels can be quantified and compared to $2.5 \times N_A/[\eta]$, which is the average density of the macromolecule. The one-order of magnitude difference uncovered between the two quantities for the Py-NAFs investigated herein suggests that like amylopectin, NAFs generate clusters of dense helical side chains that are separated by excluded volume.

The existence of excluded volume in the Py-NAFs was further examined by probing the deformability of Py-NAFs in dilute dispersions when the osmotic pressure experienced by the Py-NAFs was increased by adding poly(ethylene glycol)s (PEGs) with molecular weights of 0.2, 0.4, 2.0, 5.0, and 10 K to the dispersion. On the one hand, the smaller PEGs diffused throughout the Py-NAF interior, and as the solution viscosity increased with increasing PEG concentration, diffusive encounters between pyrenyl labels were reduced and PEF decreased. The larger PEGs, on the other hand, were unable to penetrate the Py-NAFs interior, which increased the osmotic pressure experienced by the Py-NAFs as the PEG concentration was increased. Compression of the Py-NAFs raised the local pyrene concentration, which favored PEF. The deformability of the Py-NAFs under increased osmotic pressure was taken as evidence for the existence of excluded volume in the NAF interior.

Consequently, this study on Py-NAFs confirmed the existence of oligosaccharide-rich clusters inside NAFs separated by the excluded volume generated by linear oligosaccharide segments bridging the clusters of helices. It represents another example of the use of PEF in the characterization of polysaccharides in solution.

4.3 Experimental Section

Instrumentation: Instruments used in this chapter include an Innova 4000 incubator shaker to prepare the polysaccharide dispersions, a Freezone 6 Labconco freeze-dryer for lyophilization, a Photon Technology International LS-100 steady-state fluorometer to acquire the fluorescence emission spectra, an IBH Ltd. time-resolved fluorometer equipped with an IBH 340 nm NanoLED to acquire the fluorescence decays, a Bruker 300 MHz NMR spectrometer for the ^{1}H NMR spectra, a Malvern Zetasizer NanoZS for dynamic light scattering (DLS) measurements, a Varian Cary 100 Bio spectrophotometer to acquire UV-Vis absorbance spectra, and a Cannon D449-200 Dilution Ubbelohde viscometer for intrinsic viscosity measurements.

Chemicals: 1-Pyrenebutyric acid (PyBA, 97%), 4-dimethylaminopyridine (DMAP, 99%), *N,N'*-diisopropylcarbodiimide (DIC, 99%), DMSO (ACS reagent, ≥ 99.9%), deuterated DMSO (99.9% atom), *N,N'*-dimethylformamide (DMF, ACS reagent, ≥ 99.8%), ethanol (HPLC grade), acetone (HPLC, ≥ 99.9%), PEG (M_n = 0.2, 0.4, 2, 5, and 10 kg/mol), trifluoroacetic acid (TFA, Reagent Plus, 99%), nitric acid (≥ 65%), sodium hydroxide (ACS Reagent, ≥ 97%), iodine (ACS Reagent, ≥ 99.9%), and potassium iodide (BioUltra, 99.5%) were purchased from Sigma-Aldrich. Twenty-one research grade NAFs were supplied by EcoSynthetix (Burlington, ON) with a number average particle diameter ranging from 8.3 to 57 nm as measured by DLS. As a precaution to remove possible additives leftover during the production of NAFs, all NAFs were purified by dialysis or precipitation.

Amylose-free amylopectin hydrate from waxy corn and amylose from potato purchased from, respectively, TCI America (Portland, OR) and Sigma-Aldrich (Milwaukee, WI) were used without further purification as, respectively, amylopectin and amylose standards for the iodine binding experiments as done in an earlier publication.[9] The iodine binding experiments were conducted to assess the amylose content of the NAFs.

Amylopectin from maize was purchased from Sigma-Aldrich (Milwaukee, WI). Its chemical composition was analyzed by ^{1}H NMR. The iodine binding test showed that this sample was essentially amylose-free and it was used to conduct the PEF experiments.

Doubly distilled Milli-Q water was obtained from a Millipore Milli-RO 10 Plus or Milli-Q UFPlus (Bedford, MA) system. Dialysis tubing with a 1 kDa molecular weight cutoff (MWCO) was purchased from Spectrum Laboratories Inc.

Purification of the NAFs by dialysis: Aqueous dispersions of NAF8.3 (2 wt%) were prepared by adding dry NAF8.3 to Milli-Q water and by leaving the mixtures overnight in a shaker set at 250 rpm and 60 °C. The homogeneous dispersions were allowed to cool to room temperature before being transferred to a dialysis bag. The bags were immersed in Milli-Q water and dialyzed for 5 days with stirring against 2 L of deionized water. The Milli-Q water was replaced every day. After 5 days of dialysis, the NAF dispersion remaining in the membrane was transferred to a vial and lyophilized for 3 days. White puffy powders were obtained and stored in clear vials.

Purification of the NAFs by precipitation: NAFs (5 wt %) were dispersed in DMSO through vigorous stirring overnight in a shaker set at 250 rpm and 60 °C. The dispersion was cooled to room temperature and precipitated dropwise into ethanol. The precipitated samples were collected through suction filtration before being rinsed 4 times with acetone to remove any trace of leftover

DMSO. The product was then collected and dried in a vacuum oven overnight at 40 °C. The NAF8.3 sample was purified by dialysis and precipitation. Since NAF8.3 purified by either method yielded products having similar physical properties in terms of [η] and D_h values, precipitation was chosen as the standard purification method for all other NAFs since dialysis was more time-consuming.

Pregelatinization of amylopectin: Amylopectin from maize (3 wt%) was cooked in a 90:10 (w/w) DMSO:water mixture by heating the solution at 90 °C for 1 hour. The solution was stirred at room temperature overnight and then precipitated dropwise in ethanol. Precipitated samples were collected through suction filtration before being rinsed 4 times with acetone. Amylopectin was then collected as a white powder which was dried in a vacuum oven overnight at 40 °C. The pregelatinized amylopectin was then ready to be employed for pyrene labeling.

Dynamic light scattering (DLS): NAFs were dispersed at a concentration of 1 g/L in DMSO by leaving the mixtures overnight in a shaker set at 250 rpm and 60 °C. All DLS measurements were conducted at 25 ℃ by acquiring the autocorrelation function of the light scattering signal over 5 minutes in order to obtain a stable baseline. Measurements were repeated 4 times to obtain an average of the number average D_h determined by DLS for each sample.

Viscometry: The NAF dispersions were prepared with concentrations ranging from 1 to 8 g/L. Homogenous dispersions were obtained by keeping the samples in a shaker set at 250 rpm and 60 °C overnight. Intrinsic viscosity measurements were performed with an Ubbelohde viscometer in DMSO (η = 1.99 mPa•s at 25 °C). A circulating water bath kept the temperature of the viscometer steady at 25 ℃ during the measurements.

Proton nuclear magnetic resonance (^{1}H NMR) spectroscopy: To minimize their water content, the polysaccharides were all lyophilized before acquiring their ^{1}H NMR spectrum. Amylopectin from maize and NAF57, which had been precipitated, were dispersed in water at 1 g/L before being lyophilized. NAF8.3, which had been purified by dialysis, had already been lyophilized and was ready for use. Samples were dissolved in deuterated DMSO with a polysaccharide concentration of 3 and 10 g/L for, respectively, amylopectin and the NAFs, to ensure a sufficient signal-to-noise ratio. ^{1}H NMR spectra were first acquired under neutral conditions. Then three drops of TFA were added to the solutions to shift the hydroxyl protons of starch and water down field.

Degradation of NAF57 by nitric acid: NAF57 was dispersed in water at a concentration of 10 wt% at 60 ℃. The degradation was initiated by adjusting the solution pH to 1 with nitric acid. After the desired samples were obtained, the degradation was quenched by adjusting the pH to 6 with a 0.1 M sodium hydroxide aqueous solution. The sodium chloride salt was eliminated by dialysis. The degraded NAFs were recovered by lyophilization.

Determination of amylose content: The method used to assess the amylose content of a polysaccharide sample was based on the earlier observation that the difference between the absorbances at 620 and 510 nm obtained from the absorption spectrum of an iodine aqueous solution of an amylose/amylopectin mixture is proportional to its amylose content.[10] First, amylose, amylopectin, NAF57, and NAF8.3 were dried in a vacuum oven at 40 °C overnight to remove moisture. Each starch sample (50 mg) was dispersed in 10 g of 90:10 (w/w) DMSO:water mixture in a water bath at 95 ℃ for 1 hour and the dispersions were vortexed for 30 s every 10 min. After the starch was dispersed, the samples were cooled to room temperature to yield 0.5 wt% polysaccharide dispersions in a 90:10 (w/w) DMSO:water mixture. These 0.5 wt% dispersions of each polysaccharide were then used to prepare 0.5 wt% dispersions of polysaccharide mixtures of

known amylose:amylopectin ratio. For example, a dispersion containing 10 wt% of amylose was prepared by mixing 0.20 g of the 0.5 wt% amylose solution with 1.8 g of the 0.5 wt% amylopectin dispersion. A small mass (0.08 g) from each dispersion was weighed into a 25 mL glass vial followed by the addition of 19.6 g of Milli-Q water. To this dispersion, 0.4 g of a 0.2 wt% iodine solution, prepared by mixing 0.4 g of potassium iodide and 0.04 g of iodine in 19.6 g of Milli-Q water, was added. This final aqueous dispersion with a starch concentration of 20 mg/L was vortexed for 1 min and allowed to sit for 30 min to fully develop its colour. The absorption of samples with amylose contents of 30 wt% and above were measured with UV-Vis cells having a 1 cm-pathlength. Samples with a lower amylose content, and thus a lower absorbance at 620 nm, were measured with a UV-Vis cell having a 10 cm-pathlength. The absorbance of samples measured with the 10 cm-long UV-Vis cell was therefore divided by 10 to compare its value with the absorbances obtained with a 1 cm-long UV-Vis cell. Plotting the difference between the absorbance at 620 and 510 nm (ΔABS = Abs(620nm)-Abs(510 nm)) as a function of amylose content yielded a straight line with and R^2 value of 0.998, a y-intercept y_o, and a slope m. This straight line was used as a calibration curve to determine the amylose content of a given polysaccharide dispersion. The calibration curve was repeated three times to obtain the average value and standard deviation for the slope and intercept. The amylose content of NAF8.3, NAF57, and amylopectin was calculated as $(\Delta ABS - y_o)/m$.

Synthesis of pyrene-labeled NAFs (Py-NAFs): All pyrene-labeled constructs used in this chapter were prepared in a similar manner. As a specific example, the synthesis of Py-NAF8.3 with 10 mol% pyrene is described hereafter. NAF8.3 (0.5 g, 3 mmol in terms of AGUs) was dissolved in 20 mL of a 1:3 DMF:DMSO mixture at 60 ^oC until a transparent solution was obtained. PyBA (0.4 g, 1.4 mmol) was then reacted with the starch hydroxyls in the presence of DIC (0.4 mL, 2.7

mmol) as a coupling agent and DMAP (0.05 g, 0.4 mmol) as a catalyst. The solution was kept at 0 ^{o}C for 5 minutes before being allowed to equilibrate to room temperature and left stirring in the dark for 48 hours. After the reaction, the pyrene-labeled product was precipitated 3-5 times to remove unreacted PyBA and the pyrene content of the product was determined by UV-Vis absorption. Fluorescence spectra and decays of dispersions in DMSO having a pyrene concentration of 2.5×10^{-6} M were acquired with steady-state and time-resolved fluorometers, respectively. The monomer and excimer fluorescence decays were fitted globally according to the FBM. Detailed information about the FBM analysis can be found in the previous chapters and earlier publications.[11-13]

Deformability of the polysaccharides: Py(4.8)-NAF57, Py(5.8)-NAF8.3, and Py(4.1)-Amylopectin where the polysaccharide substrate was labeled with 4.8, 5.8, and 4.1 mol% pyrene were dispersed in DMSO to prepare the stock solutions. All dispersions were prepared such that the pyrene concentration in all experiments equaled 2.5×10^{-6} M. This pyrene concentration is equivalent to polysaccharide concentrations of 9.2, 7.8, and 6.3 mg/L for Py(4.1)-Amylopectin, P(4.8)y-NAF57, and Py(5.8)-NAF8.3, respectively. PEGs with a molecular weight of 0.2, 0.4, 2.0, 5.0, and 10K were added into the stock dispersions to yield dispersions with PEG concentrations ranging from 0 to 600 g/L. The dispersions were heated to 60 ℃ for 30 minutes to fully dissolve the PEGs. Steady-state fluorescence spectra of the dispersions were acquired as soon as they had equilibrated to room temperature with minimum disturbance to avoid the eventual crystallization of PEGs at high concentration.

4.4 Results and Discussion

The characterization of NAFs was conducted with a combination of techniques to probe the polysaccharides over different length scales. The results obtained from these studies are described hereafter.

Chemical composition of NAFs: ^{1}H NMR measurements of amylopectin, NAF57, and NAF8.3 were conducted in deuterated DMSO. The ^{1}H NMR spectra are shown in Figure 4.1. No significant difference was observed between the samples, suggesting that the NAFs retained the chemical composition of amylopectin despite possible degradation during the extrusion. The different hydroxyl groups of the polysaccharides complicate the interpretation of their ^{1}H NMR spectra.[14] The labile hydroxyl protons can exchange with the solvent and generally exhibit broad signals that can hide peaks of interest. Moreover, a signal for residual water is found at 3.14 ppm, despite using a freshly opened bottle of d_6-DMSO and lyophilizing the samples over 3 days prior to analysis. The water signal is present because of the hygroscopic nature of both DMSO and starch, and is difficult to avoid.[14] The broad peaks generated by the starch and water hydroxyl protons are detrimental to a rigorous ^{1}H NMR analysis, as they might hide the signal of starch impurities resulting from the eventual degradation of extruded starch. To eliminate this possibility, ^{1}H NMR spectra were acquired after three drops of TFA were added to the polysaccharide solutions.

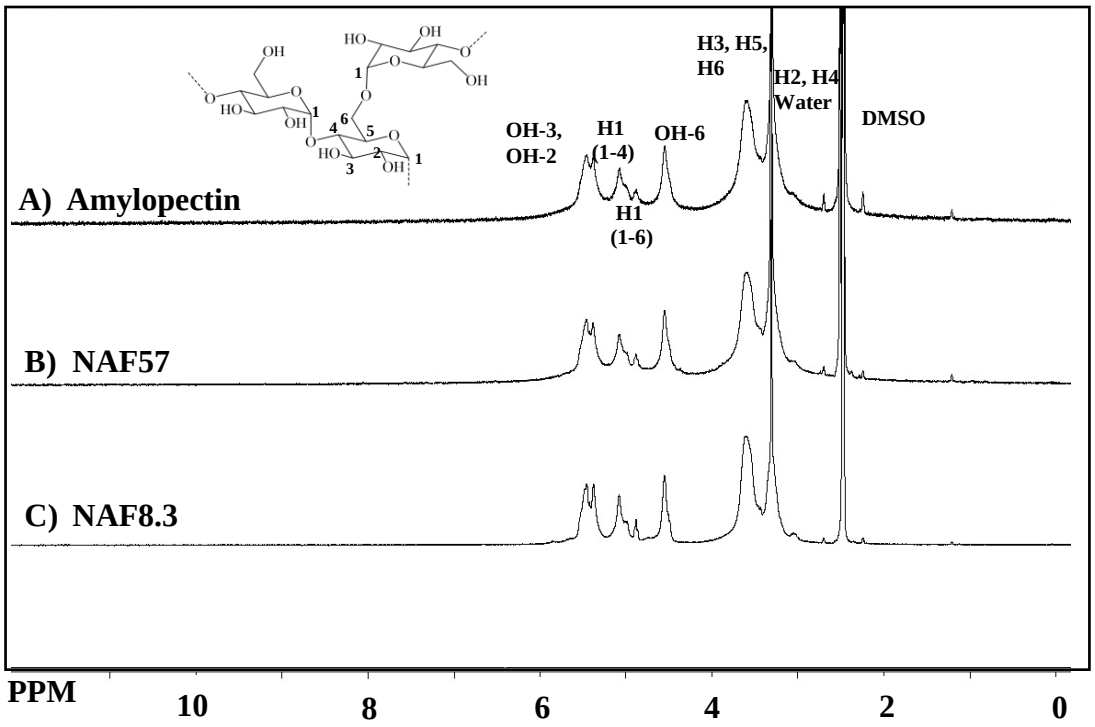

Figure 4.1. ^{1}H NMR spectra of A) amylopectin, B) NAF57, and C) NAF8.3 in neutral d_6-DMSO.

The labile TFA proton can exchange quickly with the starch hydroxyl protons, resulting in a shift in their signal above 9 ppm.[14] Figure 4.2 presents the ^{1}H NMR spectra of amylopectin, NAF57, and NAF8.3 after addition of TFA to the NMR tube. The protons belonging to water, the starch hydroxyls, and TFA underwent rapid exchange, giving rise to a single broad signal. The chemical shift of the final signal of the exchangeable protons was sensitive to the amount of TFA added, as also observed in previous studies.[14,15] The addition of TFA resulted in well-defined ^{1}H NMR spectra and no additional peaks could be detected for NAF8.3 and NAF57 as compared to amylopectin, indicating that these three samples shared a similar chemical structure.

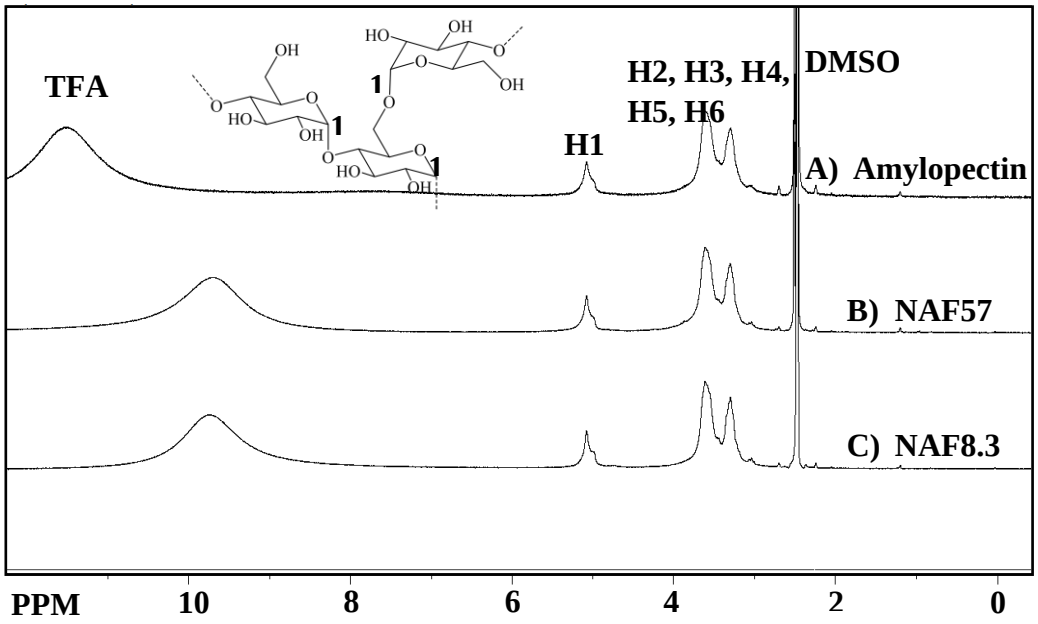

Figure 4.2. [1]H NMR spectra for A) amylopectin, B) NAF57, and C) NAF8.3 in d_6-DMSO mixed with three drops of TFA.

Amylose content of NAFs: The [1]H NMR results led to the conclusion that the NAFs were chemically similar to waxy starch (corn amylopectin) from which they were prepared. One common contaminant of amylopectin samples is amylose. The presence of a small amount of amylose has been found to affect the overall properties of starch. Furthermore, the extrusion process used to generate the NAFs could also create some linear oligosaccharides that might behave like amylose and thus affect the experimental results. As shown in Chapters 2 and 3, amylose and amylopectin respond differently to PEF. To address this concern, iodine binding experiments were conducted to assess the amount of linear polysaccharide segments present in NAFs. The dual wavelength iodine binding procedure was applied since it was reported as being a more precise method.[10] The absorption spectra acquired for iodine dissolved in an aqueous dispersion prepared with different amylose-to-amylopectin ratios are shown in Figure 4.3. The

maximum of the broad absorbance band and the adjacent valley for the samples with high amylose contents were located at approximately 620 nm and 510 nm, respectively. A calibration curve was then generated in the inset of Figure 4.3 by plotting the difference in absorbance (ΔAbs) between the absorbances at 620 and 510 nm as a function of the amylose content of the amylose:amylopectin mixtures. This calibration curve was repeated three times and the average values of the slope and intercept of the calibration curves were equal to 0.40 ± 0.01 and −0.063 ± 0.001, respectively, which were close to the values found by Zhu et al. for starch from cereals (ΔAbs = Amylose content × 0.3995 – 0.0542).[10] Based on this calibration curve, the amylose content of NAF57, NAF8.3, and amylopectin from maize were calculated to equal 0.6% ± 0.5%, −1.5% ± 0.4%, and 0.3% ± 0.4%, respectively.

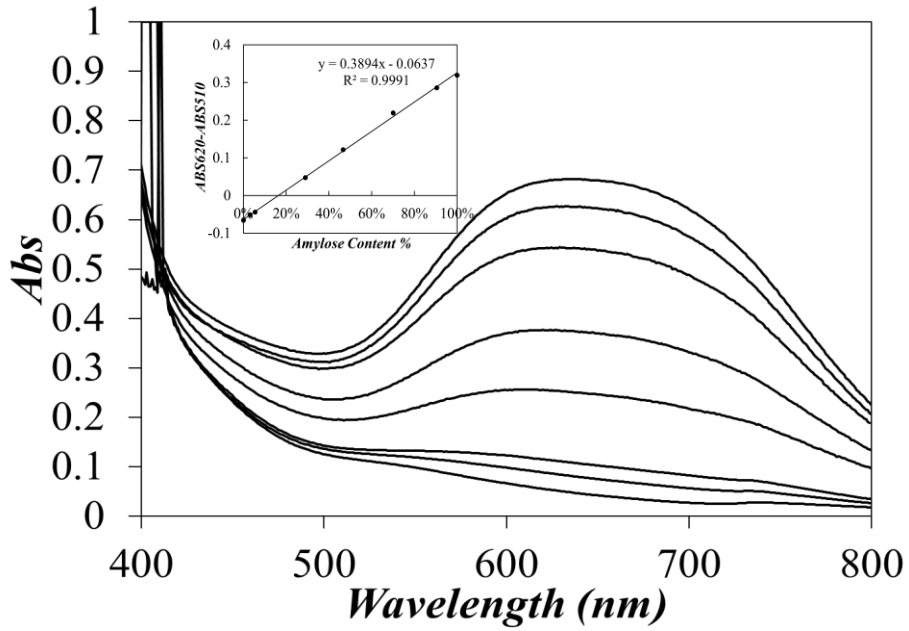

Figure 4.3. Absorption spectra of iodine in a 20 mg/L aqueous dispersion of amylose and amylopectin. Amylose content from bottom to top: 0, 5, 10, 30, 50, 70, and 90 wt%. The absorbance of the samples with amylose contents of 0, 5, and 10 wt% was divided by 10 to account for the 10 cm pathlength of the UV-Vis cell used to acquire their absorption spectra. Insert: Plot of ΔAbs as a function of amylose content.

Consequently, the iodine binding experiments and ^{1}H NMR measurements demonstrated that NAFs were amylose-free and had the same chemical composition as the amylopectin from which they were prepared. Their characterization on several length scales is now described.

Characterization of the size and density of NAFs in DMSO: To ensure that the NAFs were not affected by the purification process used to remove small molecules that might have been employed during their preparation, the D_h of the NAFs was measured by DLS before and after purification. A long acquisition time of 5 min was selected to acquire the autocorrelation functions with a good signal-to-noise ratio. Dispersions were prepared with a concentration of 1 g/L in DMSO, to ensure that a sufficient number of scattered photons could be collected while minimizing sample aggregation. In fact, these conditions were indispensable to obtain reproducible DLS measurements since the samples were polydisperse in nature. As shown in Figure 4.4, the DLS measurements were reproducible based on their analysis by intensity and number percentages. Both results showed that the purification process applied to the NAFs did not affect their particle size. As the D_h value obtained by the light scattering intensity was much more sensitive to the presence of a minuscule number of particle aggregates, only D_h values obtained in terms of number percentage are reported and discussed hereafter.

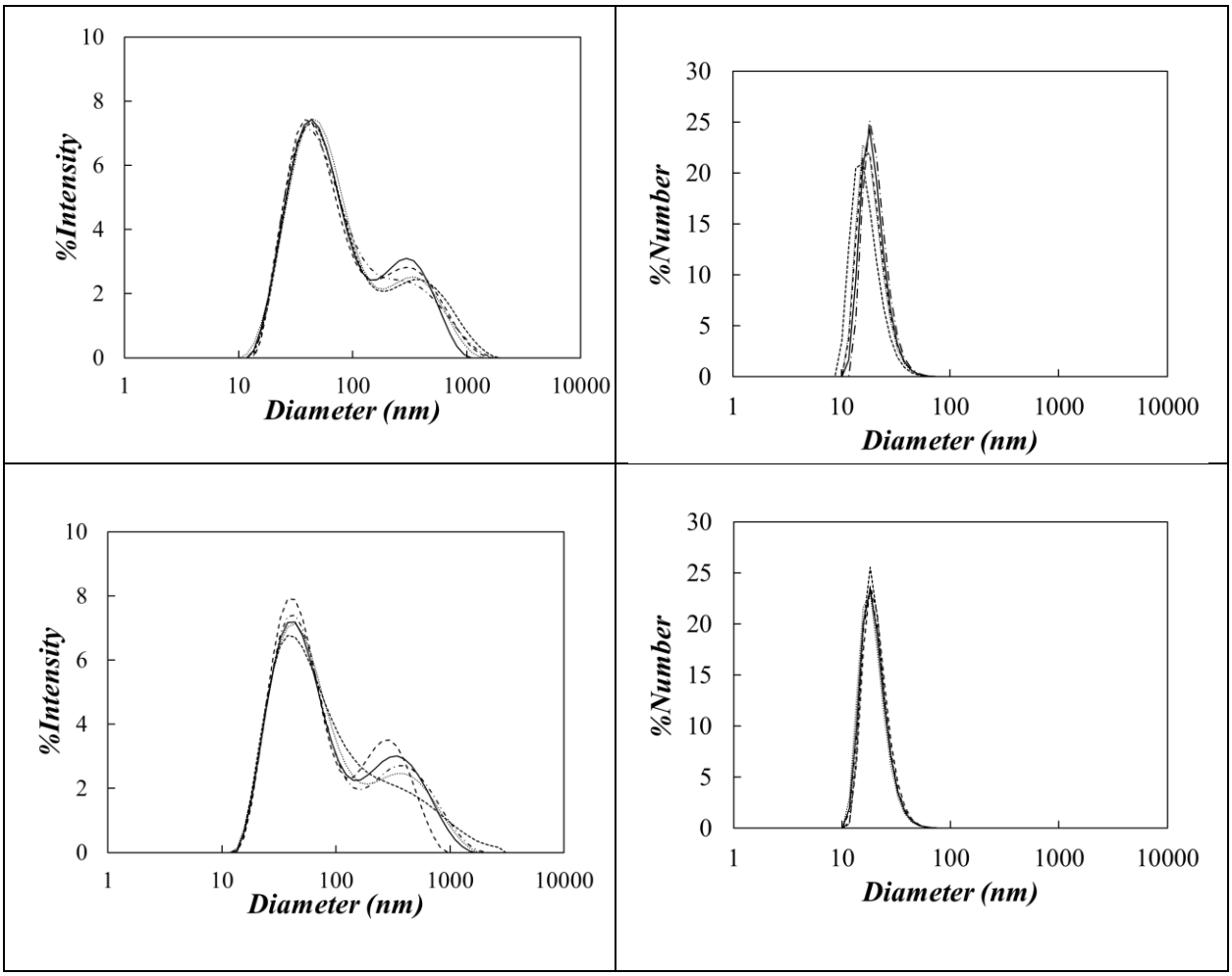

Figure 4.4. Hydrodynamic diameter distribution of the (top) unpurified and (bottom) purified NAF18 sample in terms of (left) intensity (%) and (right) number (%).

Intrinsic viscosity measurements were then conducted in DMSO using the purified NAFs since the leftover additives used during their extrusion might affect the calculation of the concentration of the unpurified NAFs. The [η] values obtained for the NAFs were plotted as a function of D_h in Figure 4.5. More detailed information on DLS and viscosity measurements can be found in the Appendix. A substantial increase in [η] from ~20 to ~60 mL/g was observed as D_h of the NAFs increased from 8 to 57 nm. These [η] values were much smaller than for amylopectin which has been reported to have [η] values ranging from 80 to 200 mL/g.[18] The lower [η] values of the NAFs prepared through extrusion of waxy starch (corn amylopectin) in Figure 4.5 implied

that the NAFs were denser than the waxy starch (corn amylopectin) from which they were made. The fact that all $[\eta]$ and D_h values clustered around a same master line in Figure 4.5 suggested that not only did the NAFs shared a similar chemical composition with amylopectin, but that they might also share a similar internal architecture resulting in an internal density given by $M/V_h = 2.5 \times N_A/[\eta]$ that would decrease with increasing D_h. Such a trend would be indicative of excluded volume. To assess the validity of this proposal, NAF57 was degraded using nitric acid to yield three degraded NAFs. NAF57 was selected in this experiment since it was the largest NAF based on its D_h value. As shown in Figure 4.5, the degraded NAF57 products also clustered on the same line as the other NAFs. Consequently, the variation in particle density with size shown in Figure 4.5 was attributed to the highly branched nature of amylopectin from which all these NAFs were created. A better experimental design would have used amylopectin as the starting material for degradation. However, the amylopectin sample used in the study had a broad size distribution making its characterization by DLS difficult, and thus the determination of its D_h challenging. Its degradation with nitric acid generated highly polydisperse products which further complicated the analysis of the DLS results.

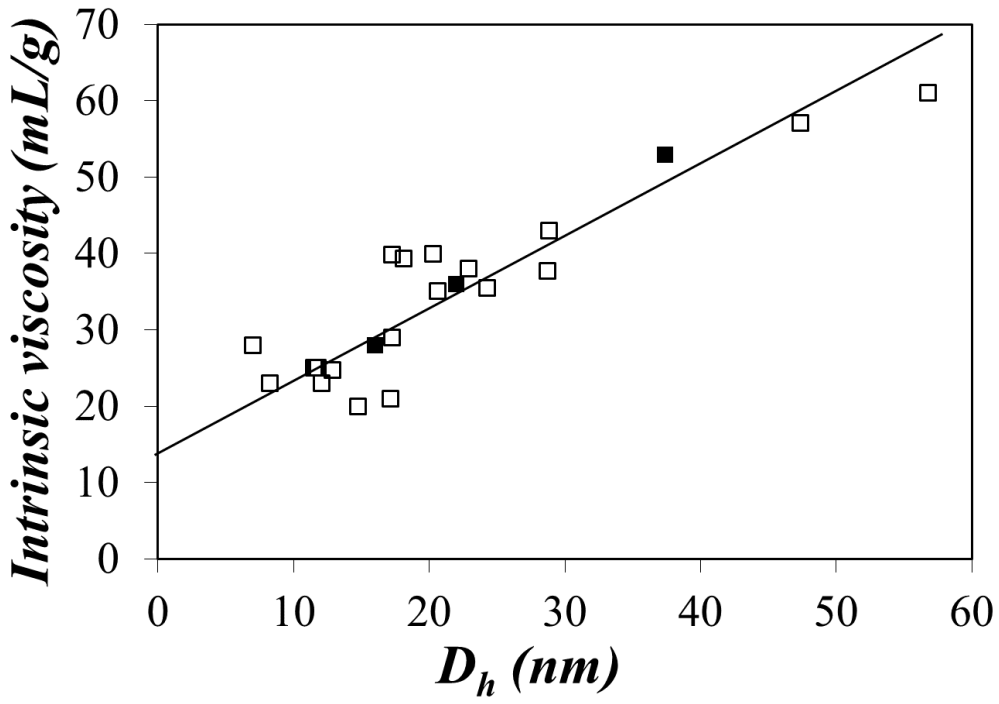

Figure 4.5. Plot of intrinsic viscosity as a function of D_h for (□) NAFs and (■) degraded NAF57 in DMSO.

As shown in Equation 4.2 which is a re-arrangement of the classic relationship between [η], the viscosity average molecular weight (M_v), and the hydrodynamic volume (V_h) given in Equation 4.1, the internal density (ρ) of NAFs in DMSO can be calculated from the ratio 2.5/[η]. ρ was plotted as a function of D_h in Figure 4.6 and it was compared to the ρ and D_h values obtained by applying Equation 4.2 to the published [η] and $M_w \sim M_v$ values obtained for different amylopectin samples in a 90:10 DMSO:water mixture.[18] The difference in solvent from pure DMSO to a 90:10 DMSO:water mixture was not expected to affect the intrinsic viscosity, as similar [η] values were obtained in both solvents for NAF 8.3 and NAF57. All ρ data obtained for the NAFs, the nitric acid degraded NAF57 samples, and the amylopectin samples clustered around a same master curve when plotted against their respective D_h value, with the scaling law given in Equation 4.3.

$$[\eta] = \frac{2.5 N_A V_h}{M_v} \tag{4.1}$$

$$\rho = \frac{M_v}{N_A V_h} = \frac{2.5}{[\eta]} \tag{4.2}$$

$$2.5/[\eta] = 0.36 \times D_h^{-0.53} \tag{4.3}$$

Together with the ^{1}H NMR study, the master curve shown in Figure 4.6 indicates that the NAFs prepared from extruded waxy corn starch have comparable composition and intrinsic viscosity behavior as the small fragments of amylopectin. The decrease in density with increasing D_h confirms the existence of excluded volumes in both the NAFs and the amylopectin samples. While $[\eta]$ and DLS measurements provide information that is averaged over the entire macromolecule covering length scales ranging from 8 to 200 nm for the NAF and amylopectin samples described in Figure 4.6, pyrene excimer fluorescence (PEF) experiments probe macromolecules over length scales that are 5 nm and lower. Thus, PEF experiments were carried out to complement the information retrieved for the polysaccharides on much longer length scales by $[\eta]$ and DLS measurements.

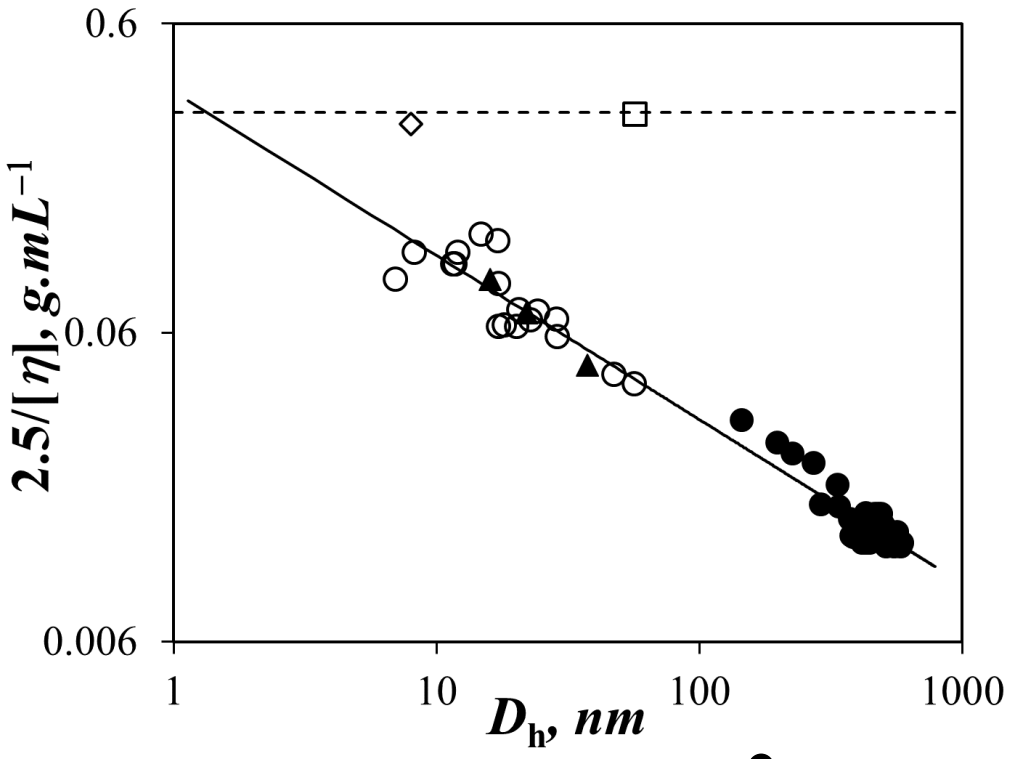

Figure 4.6. Plot of density of polysaccharides versus D_h for the (●) amylopectin samples in a 90:10 DMSO:water mixture, (○) NAFs in DMSO, and (▲) degraded NAF57 samples in DMSO. Density of (dashed line) Py-amylopectin, (□) Py-NAF57, and (◇) Py-NAF8.3 determined by a combination of fluorescence and MMOs.

Fluorescence study of the pyrene-labeled NAFs and amylopectin: Amylopectin, NAF57, and NAF8.3 were labeled with different amounts of 1-pyrenebutyric acid to yield Py-Amylopectin, Py-NAF57, and Py-NAF8.3, respectively. The steady-state fluorescence spectra were acquired for all samples in DMSO and those of the Py-NAF57 and Py-NAF8.3 samples are shown in Figure 4.7A and B, respectively. The fluorescence intensity was normalized at 376 nm, which corresponds to the 0-0 transition of the pyrenyl derivative and set to an arbitrary value of 100. The fluorescence spectra were acquired for samples with a pyrene concentration of 2.5×10^{-6} M, which was dilute enough to avoid aggregation that would otherwise lead to intermolecular excimer formation. The

fluorescence spectra show the sharp peaks of the pyrene monomer between 376 nm and 410 nm as well as the broad emission of the pyrene excimer centered at 480 nm. More pyrene excimer was formed with increasing pyrene content due to the increased probability of encounters between the pyrene pendants covalently attached to the polysaccharide backbone. The fluorescence spectra were further analyzed by integrating the fluorescence signal corresponding to the pyrene monomer (I_M) and excimer (I_E) to yield the I_E/I_M ratio which was plotted as a function of pyrene content in Figure 4.7C.

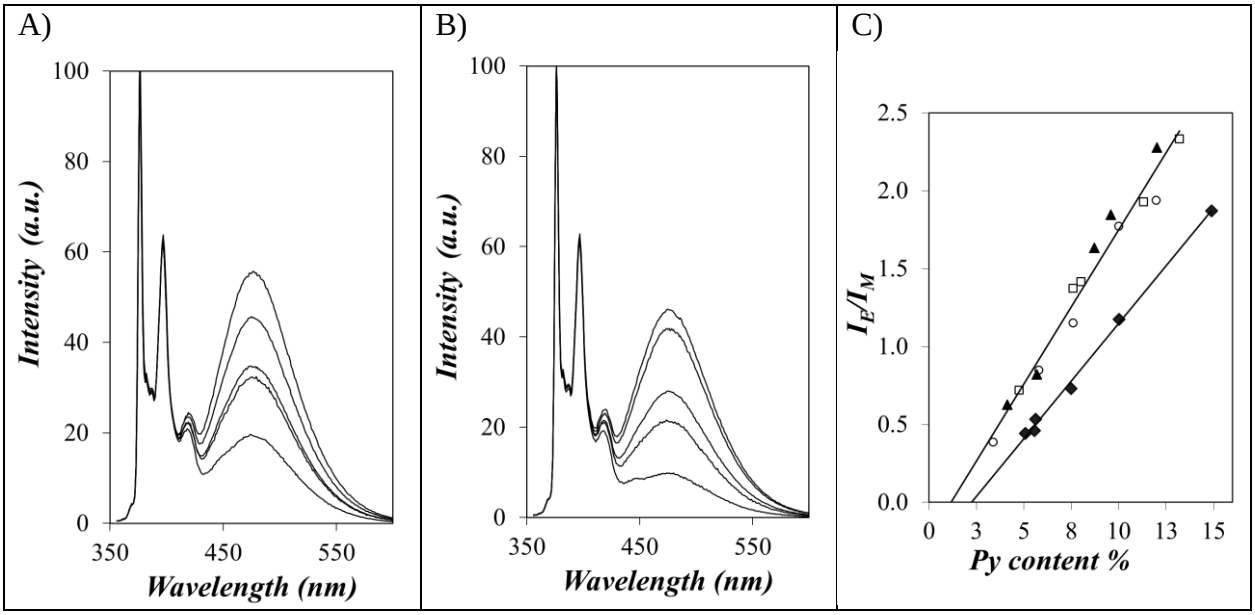

Figure 4.7. Fluorescence spectra of A) Py-NAF57 and B) Py-NAF8.3 in DMSO. From bottom to top, the pyrene content equals A) 4.8, 7.6, 8.0, 11.3, and 13.2 mol% and B) 3.4, 5.8, 7.6,10.0, and 12.0 mol%. C) Plot of I_E/I_M as a function of pyrene content for (▲) Py-Amylopectin (from Chapter 3), (□) Py-NAF57, (○) Py-NAF8.3, and (◆) Py-Amylose (from Chapter 2).

When studying pyrene-labeled polymers, the I_E/I_M ratio is typically viewed as a measure of the rate constant of pyrene excimer formation. All I_E/I_M ratios obtained for the Py-Amylopectin, Py-NAF57, and Py-NAF8.3 samples clustered along a master line when plotted as a function of pyrene content, indicating similar PEF efficiencies for these three samples. This observation

implied that the environment probed by an excited pyrene was the same inside these three polysaccharides, further strengthening the conclusions drawn from ^{1}H NMR, DLS, and [η] measurements that the NAFs displayed the same structural features as amylopectin over length scales that were less than 1 nm (^{1}H NMR), less than 5 nm (PEF), and larger than 5 nm (DLS and [η]). All I_E/I_M ratios obtained for the Py-Amylopectin, Py-NAF57, and Py-NAF8.3 samples were also consistently larger than the I_E/I_M ratios obtained for Py-Amylose in Chapter 2. This result most certainly was due to the branched nature of amylopectin which brought the pyrene labels closer to each other than linear amylose. This represents an important observation, as it suggests that PEF responds to the architecture of a specific polysaccharide and might be used to differentiate between the origins of two unknown polysaccharides.

While the trends obtained with the I_E/I_M ratios in Figure 4.7 indicate that Py-NAF8.3, Py-NAF57, and Py-Amylopectin have a similar interior over a length scale of less than 5.0 nm, the I_E/I_M ratio does not provide information about the density of the interior of these polysaccharides as the [η] measurements do. The I_E/I_M ratio, being proportional to the product $k_{diff}\times[Py]_{loc}$, where k_{diff} is the rate constant for PEF and $[Py]_{loc}$ is the local pyrene concentration, combines information about the dynamics of the polysaccharides and their density through k_{diff} and $[Py]_{loc}$, respectively. To separate the information pertaining to dynamics and density, the fluorescence blob model (FBM) is applied. The FBM acknowledges that an excited pyrene can only probe a finite subvolume of the macromolecular volume when it is covalently attached to a macromolecule. By defining this finite subvolume as a *blob*, the macromolecule can be divided into a cluster of *blobs* among which the randomly attached pyrenyl labels distribute themselves randomly according to a Poisson distribution. Excimer formation is then modelled as taking place between an excited pyrene and a number *n* of ground-state pyrenes located inside a *blob* with a rate constant k_{blob}. k_{blob}

represents the rate constant for the formation of an excimer between one excited pyrene and one ground-state pyrene located inside a same *blob*. Fitting the fluorescence decays acquired with a pyrene-labeled macromolecule with the FBM yields k_{blob} and the average number $<n>$ of pyrenes per *blob*, in effect separating the dynamics from the density of the macromolecule being considered. In turn, $<n>$ can be used with Equation 4.4 to determine N_{blob} which, in the case of pyrene-labeled polysaccharides, is the number of AGUs encompassed inside a *blob* where two pyrenyl labels attached onto AGUs can form excimer. In Equation 4.4, x is the molar fraction of pyrene-labeled AGUs in the pyrene-labeled polysaccharide and f_{Mfree} is the molar fraction of pyrenyl labels that are isolated and do not form excimer as probed in the fluorescence decay of the pyrene monomer.

$$N_{blob} = \frac{< n >}{x}(1 - f_{Mfree}) \tag{4.4}$$

Time-resolved fluorescence decays were acquired for dilute dispersions of Py-NAF57 and Py-NAF8.3 in DMSO. Global analysis of the monomer and excimer decays with the FBM yielded the parameters $<n>$ and f_{Mfree} used in Equation 4.4 to determine N_{blob}, which was plotted as a function of pyrene content in Figure 4.8.

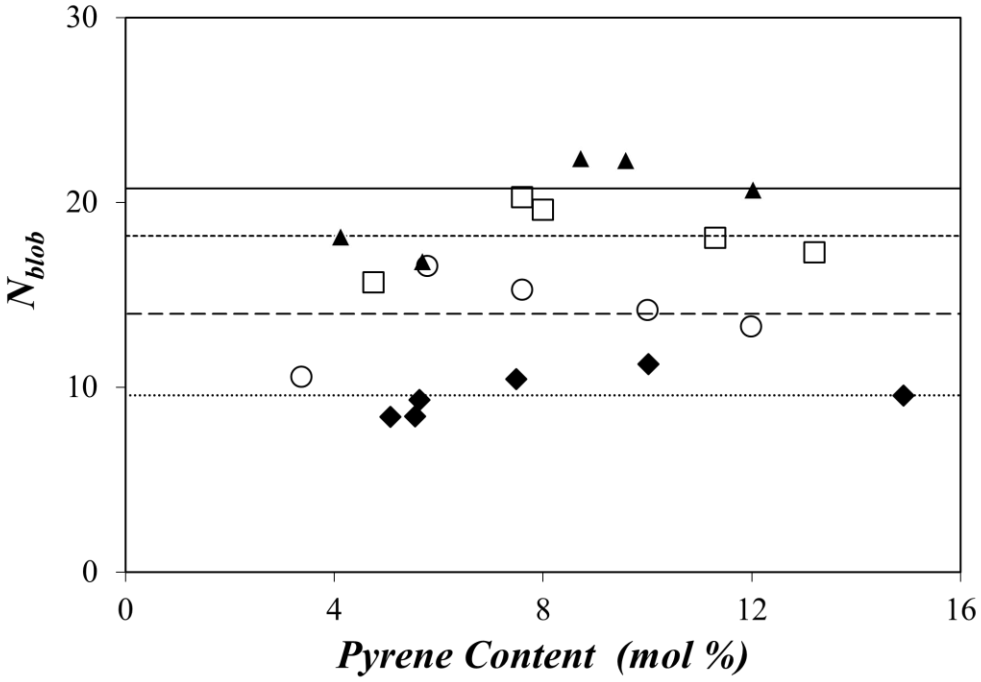

Figure 4.8. Plot of N_{blob} as a function of pyrene content for (▲, solid line) Py-Amylopectin, (□, line with short dashes) Py-NAF57, (○, line with long dashes) Py-NAF8.3, and (◆, dotted line) Py-Amylose.

Within experimental error, the N_{blob} values remained constant with pyrene content for a given pyrene-labeled polysaccharide. After averaging over all pyrene contents of a specific polysaccharide, $<N_{blob}>$ was found to equal 20 ± 3, 18 ± 2, 14 ± 2, and 10 ± 1 for Py-Amylopectin, Py-NAF57, Py-NAF8.3, and Py-Amylose, respectively. The $<N_{blob}>$ values obtained for Py-NAF8.3 and Py-NAF57 were substantially larger than for Py-Amylose, reflecting the branched nature of the NAFs interior as expected since they were produced from highly branched amylopectin. The $<N_{blob}>$ values obtained experimentally for Py-NAF8.3 and Py-NAF57 could then be related to the inter-axis distance ($d_{h\text{-}h}$) between the oligosaccharide helices arranged in a hexagonal manner inside a cluster as was shown in Chapter 3 where N_{blob}^{theo} obtained from MMOs

was plotted as a function of $d_{h\text{-}h}$ in Figure 3.11. This trend could be satisfyingly fitted with the logistic function shown in Equation 4.5 where the parameters A_1, A_2, x_o, and p were listed in Tables S3.6A-C along with their respective error.

$$N_{blob}^{theo} = A_2 + \frac{A_1 - A_2}{1 + (x / x_o)^p} \tag{4.5}$$

Based on Equation 4.5, an N_{blob} value of 18 obtained by fluorescence for Py-NAF57 would correspond to a $d_{h\text{-}h}$ value of 24.9 or 28.7 Å for a double or single helix, respectively. Similarly, an N_{blob} value of 14 for Py-NAF8.3 would correspond to a $d_{h\text{-}h}$ value of 25.8 and 29.8 Å for double and single helices, respectively. In turn, the interhelical distance $d_{h\text{-}h}$ can be used to determine with Equation 4.6 the density ρ_{fluo} of the oligosaccharide environment experienced by the pyrenyl labels inside a cluster of hexagonally packed oligosaccharide helices separated by an interhelical distance $d_{h\text{-}h}$. In Equation 4.6, M_o is the molar mass of an AGU (162 g/mol) and N_A is the Avogadro number (6.02×10^{23}). The parameter n_{AGU} is the number of AGUs per helix pitch (h) and n_{AGU} and h were deduced from the X-ray structures reported for single[19] and double[20] helices. For a single or double oligosaccharide helix, n_{AGU} equals 7 or 12 and h equals 8.8 or 21.5 Å, respectively.

$$\rho_{fluo} = \frac{n_{AGU} \times M_o}{\sin(60^o) \times h \times N_A} \times \left(\frac{1}{d_{h-h}} \right)^2 \tag{4.6}$$

The ρ_{fluo} values for Py-NAF8.3, Py-NAF57, and Py-Amylopectin were calculated based on the parameters listed above. They are listed in Table 4.1.

Table 4.1. N_{blob}, $d_{h\text{-}h}$, and ρ_{fluo} values obtained for a hexagonal array of single and double oligosaccharide helices.

	N_{blob}	$d_{h\text{-}h}$ (Single Helix) (Å)	$d_{h\text{-}h}$ (Double Helix) (Å)	ρ_{fluo} (Single Helix) (g/cm^3)	ρ_{fluo} (Double Helix) (g/cm^3)	ρ_{fluo} (Average) (g/cm^3)
Amylopectin	20	29.1	25.0	0.29	0.28	0.29 ± 0.01
NAF57	18	29.5	25.4	0.28	0.27	0.27 ± 0.01
NAF8.3	14	31.0	26.7	0.26	0.24	0.25 ± 0.01

The ρ_{fluo} values found for the NAFs were similar to that of 0.29 ± 0.01 g/mL found for amylopectin in Chapter 3. The ρ_{fluo} values were plotted as a function of D_h in Figure 4.6 along with the ρ values calculated with Equation 4.2. The ρ_{fluo} values were one-to-two orders of magnitude larger than the ρ values obtained from intrinsic viscosity measurements. This discrepancy could be rationalized by evoking the Sol-CL model introduced in Chapter 3 for amylopectin. As for amylopectin from which they were derived, NAF8.3 and NAF57 were constituted of dense clusters of oligosaccharide helices separated by a $d_{h\text{-}h}$ of 29.5 to 31.0 Å in the case of single helices. These clusters of helices were separated by excluded volumes which led to the much lower density determined from [η] measurements which probed the polysaccharides over distances of tens of nanometers. On the basis of the intrinsic viscosity measurements, smaller NAFs like NAF8.3, having less excluded volume due to their smaller size, were denser than larger NAFs like NAF57, which had more excluded volume. Yet NAF57 was smaller than amylopectin from waxy corn starch, which had a D_h of 200 nm as determined by introducing its [η] value of 122.5 mL/g into Equation 4.3. As a result, its density was lower than that of the NAFs. Yet over the less than 5 nm-length scale probed by PEF, excimer formation took place in the same manner

inside the clusters of oligosaccharide helices labeled with pyrene, yielding similar ρ_{fluo} values for NAF8.3, NAF57, and amylopectin. These concepts are illustrated in Figure 4.9. NAF8.3 and NAF57 are shown to be just fragments of the original amylopectin keeping its internal structural arrangements with the number of clusters of helices increasing with increasing NAF size.

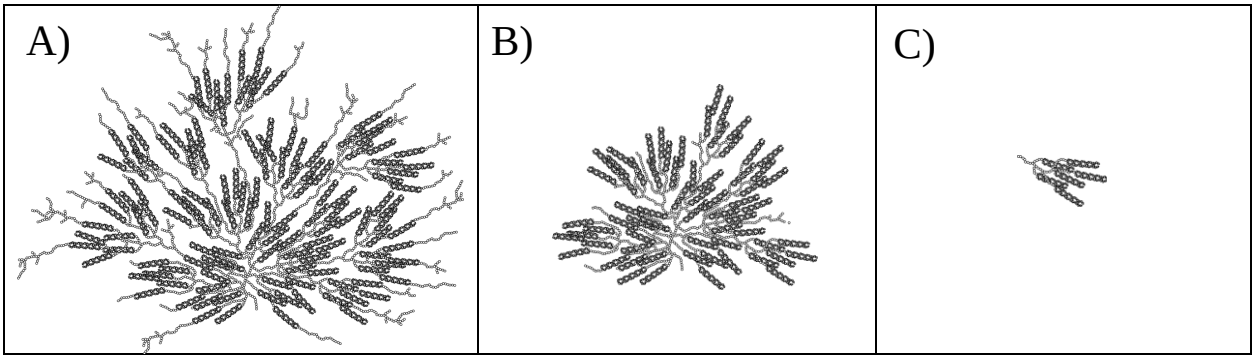

Figure 4.9. Depiction of the Sol-CL model describing the spatial arrangement of the clusters of helices for A) amylopectin, B) NAF57, and C) NAF8.3.

Osmotic pressure experiments: The data presented so far indicated that amylopectin and the NAFs derived from it exhibited excluded volume generated by the linear oligosaccharide segments separating the clusters of helices, whose number decreased with decreasing D_h. Consequently, smaller NAFs were expected to be less deformable than larger ones. To investigate this idea, four PEGs, namely PEG0.2, PEG0.4, PEG2.0, PEG5.0, and PEG10 with MW of, respectively, 0.2, 0.4, 2.0, 5.0, and 10 kg/mol were added to a dilute solution of Py(4.1)-Amylopectin, Py(4.8)-NAF8.3, and Py(5.8)-NAF57 labeled with 4.1, 4.8, and 5.8 mol% pyrene, respectively. The I_E/I_M ratio of the pyrene-labeled polysaccharide dispersions was monitored as a function of PEG concentration and the results are shown in Figure 4.10.

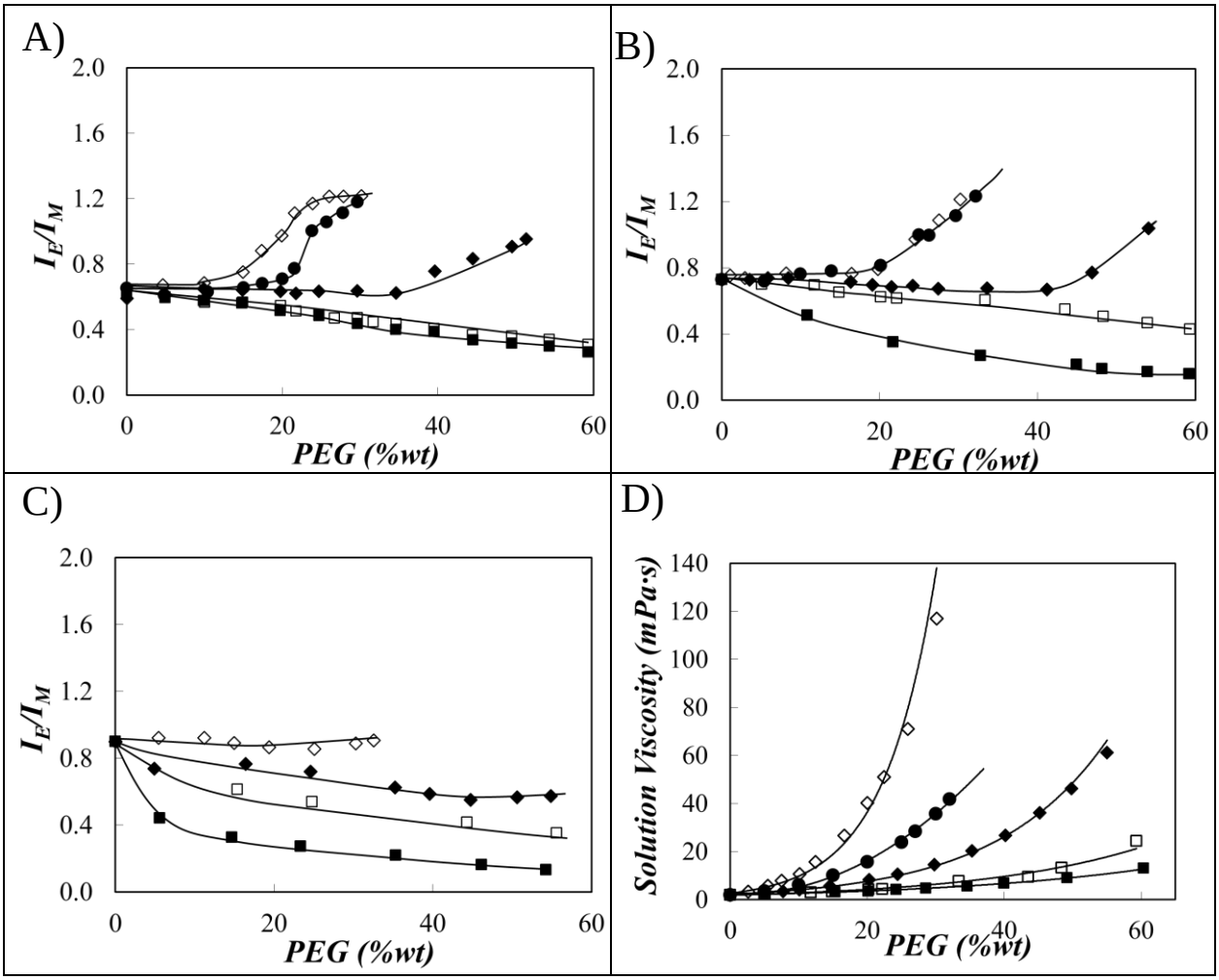

Figure 4.10. Plots of I_E/I_M as a function of PEG concentration for A) Py(4.1)-Amylopectin, B) Py(4.8)-NAF57, and C) Py(5.8)-NAF8.3. D) Plot of the solution viscosity as a function of PEG concentration. PEGs with M_n of (■) 0.2, (□) 0.4, (◆) 2.0, (●) 5.0, and (◇) 10 K. The experimental data for Py-Amylopectin in Figure 4.11A) were collected by undergraduate student Xiaofang Zhai under my direct supervision.

The trends obtained by plotting I_E/I_M as a function of PEG concentration in Figure 4.10A-C are best explained by evoking the relationship that exists between I_E/I_M and $k_{diff}\times[Py]_{loc}$. k_{diff} being the rate constant for PEF by diffusion is inversely proportional to the solution viscosity. To this end, the viscosity of the PEG solutions was measured as a function of PEG concentration and

it was plotted in Figure 4.10D. The viscosity of the PEG solutions increased dramatically with increasing PEG concentration. The increase in viscosity with PEG concentration was more pronounced for larger PEGs. The I_E/I_M ratio decreased with increasing PEG0.2 concentration for all three polysaccharides in Figure 4.10A-C. Surprisingly for a process that was diffusion controlled, the I_E/I_M ratio decreased less with the concentration of larger PEGs despite the fact that they yielded a larger solution viscosity (see Figure 4.10D). Since k_{diff} decreases with increasing PEG size at a given PEG concentration because it is inversely proportional to solution viscosity, the only explanation for the larger I_E/I_M ratios observed with increasing PEG size was that $[Py]_{loc}$ must have increased to offset the decrease in k_{diff}. The increase in $[Py]_{loc}$ with increasing PEG size suggested that the larger PEGs could not penetrate the crowded interior of the NAFs and amylopectin, thus applying osmotic pressure to the particles. Compression of the macromolecules concentrated the pyrene labels inside the particle interior, which yielded a larger I_E/I_M ratio. In fact, the deswelling of a swollen polymeric network can be induced by free polymers excluded from the network.[21-26]

The effect that the osmotic pressure generated by excluded PEG chains has on poly(*N*-isopropylacrylamide) (PNIPAM) microgels and macrogels has been investigated.[23-26] For a given PEG concentration, the deswelling ratio first increases with increasing molecular weight of the PEGs, before becoming independent from PEG MW when the free chains were fully excluded from the gel particles.[26] The results were actually in good agreement with the standard expression of the osmotic pressure derived by Flory and Huggins, whereby the osmotic pressure generated by the free chains depends on their volume fraction rather than their molecular weight.[27] It must be emphasized that this theory assumed that penetration of free chains into the particles could not occur. When the free chains in solution are small enough that they can diffuse into the gel particles,

the chemical potential difference between the interior and exterior of the particles is partially balanced, leading to a reduction in the deswelling ratio.

A similar effect was observed with Py-NAF57. The I_E/I_M ratio obtained for Py-NAF57 with PEG5 and PEG10 overlapped and displayed a more pronounced increase with increasing PEG concentration than that obtained with PEG2. The difference in behavior between PEG5 and PEG2 indicated that the mesh size of NAF57 corresponding to the distance separating the clusters of oligosaccharide helices was between the size of PEG2 and PEG5, since PEG5 was fully excluded from NAF57, whilst PEG2 partially penetrated it. Using the hydrodynamic diameter D_h ($D_h = 0.059 \times M_w^{0.5064}$ nm)[28] for PEG chains in aqueous solution, the D_h values of 2.8 and 4.4 nm for, respectively, PEG2 and PEG5 suggest that the mesh size of NAF57 would lay between these two values. We recall that our combination of MMOs and fluorescence experiments summarized in Figure 3.10 predicts that the clusters of helices must be separated by at least 3.2 nm, a length scale that agrees with the expected NAF mesh size.

Moreover, it is noteworthy that the compression induced by the osmotic pressure generated by the larger PEG chains would only occur for NAFs possessing sufficient excluded volume. As shown in Figure 4.10B, the larger Py-NAF57 sample had enough excluded volume to undergo a volume reduction in the presence of PEG10, while Py-NAF8.3 did not. In fact, for an interhelix distance ($d_{h\text{-}h}$) of ~3.0 nm predicted by fluorescence, a cluster of seven helices, as shown in Figure 4.9C, would have a diameter of ~7 nm and a thickness of 9 nm, equal to the thickness of crystalline lamellae found in dry amylopectin.[29] Consequently, Py-NAF8.3 would have a dimension comparable to that of a single cluster of helices, and as such would be very difficult to compress as was observed experimentally in Figure 4.10C.

4.5 Conclusions

This study has provided an in-depth characterization of research grade NAFs by using ^{1}H NMR, DLS, intrinsic viscosity, an iodine binding test, and a combination of experiments based on PEF, the FBM analysis, and MMOs. The experimental results suggest that the research grade starch nanoparticles displayed structural features that are similar to nanosized amylopectin fragments. Interestingly, the density (ρ) of the NAFs given by the ratio 2.5/[η] increased 3-fold as the NAF size decreased from 57 to 7 nm, approaching the ρ_{fluo} value obtained for amylopectin in Chapter 3 of this thesis for the smaller NAFs. To further probe the interior of the particles, NAF8.3 and NAF57 were labeled with 1-pyrenebutyric acid. Their ρ_{fluo} values were similar to the ρ_{fluo} value of amylopectin regardless of particle size. These results could be easily rationalized with the Sol-CL model. The larger NAFs having more linear oligosaccharide segments bridging the clusters of helices had more excluded volume which reduced their density ρ. The smaller NAFs however had fewer linear oligosaccharide segments and less excluded volume, resulting in higher density. The main consequence of this spatial arrangement of the clusters of helices was that only NAF57 could deform upon increasing the osmotic pressure of the dispersion while NAF8.3 remained unchanged.

As discussed above, the Sol-CL model depicted in Figure 4.9 provided a robust rational for all the experimental results presented in this and the previous chapters. As shown in Figure 4.10 B) and C), and confirmed by the fluorescence measurements, NAFs contain linear oligosaccharide segments that generate excluded volume whose extent varies with particle size. When dispersed in water, NAFs are expected to be swollen and the linear oligosaccharide segments inside the particles endow them with softness and deformability suitable for coating operations. On the other hand, macromolecules with an excess of linear segments, such as conventional cooked starch (dent corn), which is a mixture of amylose and amylopectin, would undergo much more shrinkage upon

drying, leading to a reduction in paper gloss.[30] It is clear that the Sol-CL model provides a clear answer to these observations, along with the results obtained from the osmotic pressure experiments described in this chapter.

Chapter 5:
Conclusions and Future Work

5.1 Summary of accomplished work

Starch, which consists of amylose and amylopectin, is the second most abundant biopolymer on earth after cellulose.[1,2] Besides its well-known role in the diet of many living beings, this renewable and biodegradable material has been widely used for encapsulation, as viscosifier or emulsifier, and as defoaming or sizing agent.[3] So far most of the starch used industrially must be chemically modified to improve its performance and endow it with additional properties.[3] This thesis has characterized the conformation and internal structure of amylose and amylopectin in solution. Such information is not only of great interest for researchers studying the physicochemical properties of starch, but is also relevant to expand the range of industrial applications for starch through specific physical or chemical modifications.

Traditional characterization methods, such as gel permeation chromatography (GPC), viscometry, or light scattering (LS) only provide averaged structures of polysaccharides in general and amylopectin in particular.[4] In order to obtain a detailed molecular level picture of amylose and amylopectin, this thesis has used pyrene excimer formation (PEF) as a new molecular ruler. PEF has been applied to multiple polymer systems to study their chain dynamics in solution since the 1980's.[5] However, its use was limited to characterize short monodispersed oligomers until the late 1990's, when the fluorescence *blob* model (FBM) was introduced.[6] The FBM operates by compartmentalizing the interior of macromolecules into *blobs*, where a *blob* represents the volume probed by an excited pyrene while it remains excited. Random labeling of a macromolecule with a pyrene derivative ensures that the pyrene labels are randomly distributed among the *blobs* according to a Poisson distribution described by the average number $\langle n \rangle$ of pyrenes per *blob*. Global analysis of the pyrene monomer and excimer fluorescence decays using the FBM yields $\langle n \rangle$, which can be combined with the pyrene content (λ_{Py}) to yield the maximum number (N_{blob})

of structural units that would allow two pyrenyl labels inside a *blob* to form excimer. As a result, N_{blob} provides structural information for a macromolecule in solution, since a large or small N_{blob} value reflects the internal density of the macromolecule, indicating whether it is structured or not, since a large density associated with a large N_{blob} would often indicate a structured macromolecule. Furthermore, FBM analysis of the monomer and excimer decays acquired with a pyrene-labeled macromolecule also yields the rate constant k_{blob} describing the diffusive motions of structural units and their side chains bearing a pyrenyl label located inside a *blob*. In turn, the product $k_{blob} \times N_{blob}$ has been shown to describe the internal dynamics of a macromolecule in solution.[5] Consequently, the FBM expands the application of PEF measurements from the characterization of end-labeled oligomers to that of polymers randomly labeled with pyrene. It is noteworthy that both N_{blob} and $k_{blob} \times N_{blob}$ provide a quantitative measure for the structure and internal dynamics of macromolecules in solution, respectively, so that these values can be compared with those for other polymer systems or those obtained using other methods. It is also obvious that polymers undergoing conformational or structural changes result in significant changes in N_{blob}, which can be related back to the original conformation of a polymer.

As described in this thesis, great effort was put into building an ensemble of N_{blob} values that could represent different conformations of amylose and describe the internal structure of amylopectin. This was accomplished by conducting molecular mechanics optimizations (MMOs) with HyperChem on pyrene-labeled constructs representing different conformations of a macromolecule. In effect, this approach enables one to extract quantitative structural information about a macromolecule in solution from its N_{blob} value. Consequently, this thesis not only brought new insights in the current understanding of the conformation of amylose and amylopectin in

solution, but even more importantly, it established a robust procedure based on a combination of PEF, FBM, and MMOs to reveal the internal structure of complex macromolecules in solution.

Starting with amylose whose chemical structure is relatively straightforward, the 2nd chapter of this thesis intended to resolve the long-standing debate in the scientific literature as to whether the conformation of this molecule is a helix or a random coil in dimethyl sulfoxide (DMSO).[7,8] This was accomplished by synthesizing a series of amylose constructs that were randomly labeled with pyrene (Py-Amylose). A flexible polymer randomly labeled with pyrene, namely poly(methyl acrylate) (Py-PMA), was used as a benchmark against which the results obtained with Py-Amylose could be compared. The FBM analysis revealed that the Py-Amylose constructs displayed significantly more aggregation of the pyrenyl labels as compared to the Py-PMA samples with a similar pyrene content. Furthermore, the $<k_{blob} \times N_{blob}>$ product was found to be comparable for amylose and PMA after adjusting N_{blob} for the number of chain atoms in the respective backbone. Both results indicated that the pyrene pendants attached onto amylose were probing a compact environment compatible with the notion that amylose adopted a helical conformation in DMSO. To further confirm that this was indeed the case, MMOs were conducted to determine the maximum number of structural units that could still enable PEF between two pyrenyl labels attached on an amylose backbone adopting a random coil or helical conformation. The more compact helical conformation of amylose resulted in an N_{blob}^{theo} value representing eleven glucose units, which was in excellent agreement with the results obtained by the FBM analysis of the fluorescence decays of the Py-Amylose solutions. This study represented the second example in the literature, after α–helical poly(*L*-glutamic acid), where PEF had been applied to confirm the helical conformation of a macromolecule in solution.[9,10] It also suggested that PEF constitutes a robust and novel analytical means for the characterization of polysaccharides.

Building on this first success in probing the conformation of polysaccharides in DMSO, the second study of this thesis described how PEF experiments conducted on pyrene-labeled amylopectin (Py-Amylopectin) provided spatial information about the distribution of the side chains of amylopectin in DMSO. The increase in N_{blob} from 11 for Py-Amylose to 20 for Py-Amylopectin indicated that PEF occurred more efficiently with the Py-Amylopectin constructs, which reflected the highly branched nature of amylopectin. MMOs were carried out to establish how N_{blob}^{theo} varied as a function of the spacing between single and double helices of oligosaccharides arranged in a hexagonal array used to mimic the side chains of amylopectin. Regardless of the nature of the helices, the side chains of amylopectin needed to be separated by an interhelical distance ($d_{h\text{-}h}$) between 25 and 29 Å for inter-helix PEF to result in an experimental N_{blob} value of 20. In turn, this interhelical spacing found by the PEF measurements led to an internal density for amylopectin in DMSO which was one order of magnitude larger than the density of amylopectin determined by intrinsic viscosity. This apparent contradiction led to the proposal of the Solution-Cluster (Sol-CL) model depicted in Figure 5.1. The Sol-CL model suggests that the interior of amylopectin is composed of dense clusters of helices held together by flexible oligosaccharide segments. Since pyrene labeling targets the denser clusters of helices, PEF occurs more effectively than predicted from the internal density of amylopectin determined by intrinsic viscosity measurements. The linear oligosaccharide segments connecting the clusters of helices induce excluded volume effects that lead to the smaller density determined by intrinsic viscosity.

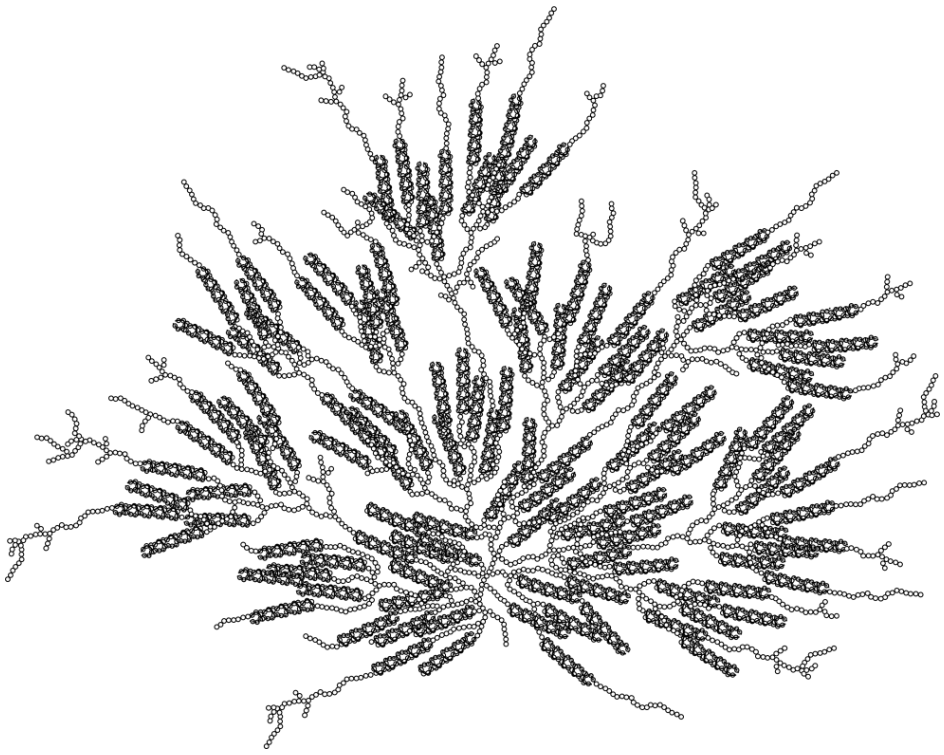

Figure 5.1. Depiction of the Solution-Cluster (Sol-CL) model, where dense clusters of double helices are connected to each other by flexible polysaccharide segments.

To expand the applicability of PEF to the characterization of polysaccharides used to prepare starch materials sold commercially and to further validate the Sol-CL model, the PEF-based procedure developed for the characterization of amylose in Chapter 2 and amylopectin in Chapter 3 was applied in the fourth chapter of this thesis to study starch nanoparticles (SNPs). These particles were prepared by extruding waxy corn starch at high temperature.[11] The chemical composition, amylose content, internal density, and hydrodynamic diameter of twenty-one research-grade SNPs were characterized by ^{1}H NMR, iodine binding test, viscometry, and dynamic light scattering (DLS), respectively. Analysis of the ^{1}H NMR spectra acquired with the SNPs indicated that the SNPs shared a same chemical composition as amylopectin. The iodine binding test confirmed that the SNPs were essentially amylose-free, a reasonable conclusion considering

that they were prepared from waxy corn starch which is >99% amylopectin. Indeed, the SNPs investigated in this thesis can be viewed as nanosized amylopectin fragments (NAFs). Intrinsic viscosity measurements indicated that their density increased from 0.04 to 0.12 g/mL in DMSO as their hydrodynamic diameter determined by DLS decreased from 57 to 8 nm.

While these preliminary experiments provided parameters describing the properties of NAFs averaged over their entire macromolecular volume, PEF measurements were conducted to probe the NAF interior at the molecular level. To this end, two NAFs, namely NAF8.3 and NAF57, where the number represents the NAF hydrodynamic diameter expressed in nanometers, were randomly labeled with pyrene. Comparison of the experimental N_{blob} value, determined by FBM analysis of the fluorescence decays of the Py-NAFs, with N_{blob}^{theo}, obtained from MMOs conducted on a hexagonal array of pyrene-labeled oligosaccharide helices, yielded a density close to that found for amylopectin in Chapter 3. In addition, the density of the NAFs, calculated from their intrinsic viscosity, approached the density of amylopectin determined from a combination of PEF, FBM, and MMOs as the size of the NAFs decreased from 57 nm to 8 nm. This result suggested that as the NAFs became smaller, the linear segments that bridged the clusters of helices and contributed to the excluded volume were cleaved off in a process that retained the densely packed clusters of double helices contributing to PEF. This hypothesis was tested by using PEF to probe changes in osmotic pressure experienced by the NAFs upon addition of poly(ethylene glycol)s (PEGs) of different lengths. The larger 10 kg/mol PEG was unable to penetrate the macromolecular interior of Py-Amylopectin and Py-NAF57. As a result, the osmotic pressure generated by the addition of 10 kg/mol PEG induced the compression of these polysaccharides with their deformation being enabled by the excluded volume due to the numerous linear oligosaccharide segments bridging the clusters of helices. In contrast, the smaller NAFs like Py-NAF8.7 could not

be compressed at the same 10 kg/mol PEG concentration, where deformation of the larger NAFs and amylopectin occurred, due to the lack of linear oligosaccharide segments, and thus the absence of excluded volume. These conclusions further supported the Sol-CL model which had been introduced in Chapter 3. This study provided an in-depth description of the spatial arrangement of the oligosaccharide side chains constituting amylopectin and the NAFs generated from amylopectin in solution. Such structural information about polysaccharides is valuable to better understand their behavior in solution.

5.2 Future Work

Chapter 4 introduced the use of PEF to probe the deformation of pyrene-labeled macromolecules upon addition of a polymer large enough to prevent it from penetrating the interior of the macromolecular volume. So far, Py-amylopectin, Py-NAF57 and Py-NAF8.3, which were labeled with 4.1, 4.8, and 5.8 mol% pyrene, respectively, have been tested by steady-state fluorescence only. The results of these experiments suggested that smaller NAFs were more rigid and deformed less compared to amylopectin and the larger NAFs. It would thus be interesting to apply the FBM analysis to the fluorescence decays with these pyrene-labeled polysaccharides to determine N_{blob} as a function of PEG concentration and see how N_{blob} changes upon compression of the Py-NAFs. In turn, comparison of the experimental N_{blob} values with N_{blob}^{theo} would yield the interhelical distance between clusters, and thus a measure of the density of the NAFs, as a function of compression. This experiment could be further expanded to study how NAFs deform as they form a film, as would be observed in industrial paper coating applications. In this case, naked NAFs would be added to dilute dispersions of Py-NAFs instead of PEGs and the fluorescence signal of the Py-NAFs would be followed as a function of the naked NAF concentration.

As mentioned above, this thesis has developed a robust procedure based on a combination of PEF, FBM analysis, and MMOs to characterize the spatial arrangement of structural motives of highly branched macromolecules in solution. This procedure was applied to characterize three different polysaccharides, namely amylose, amylopectin, and NAFs. However, the amylopectin sample studied in this thesis was extracted from waxy corn starch. Amylopectin from other sources, such as rice and barley, is known to behave differently based on an earlier iodine binding study.[12] Therefore, although amylopectin samples of different origins share a similar chemical composition, the spatial arrangement of their side chains might be different. Applying PEF to amylopectin samples extracted from different plants could provide an experimental means to trace their origin by comparing their internal density determined from their N_{blob} values.

It would also be interesting to apply this procedure to other polysaccharides. Glycogen, with a similar chemical composition and architecture as amylopectin but a much higher level of branching,[13] cellulose, which is a linear polysaccharide but composed of AGUs connected by β-(1-4) linkages,[14] pullulan, where the maltotriose structural units are connected by α-(1-6) linkages,[15] would be all worthy of investigation. Despite having different chemical and physical properties, these polysaccharides are composed of monosaccharides bound together through glyosidic linkages. As the *blob* size (N_{blob}) and PEF rate constant ($k_{blob} \times N_{blob}$) are quantitative measure of the internal structure and dynamics of polysaccharides, the preliminary studies conducted in this thesis suggest that comparison of these parameters across the large family of polysaccharides could shed some light on how minute changes at the molecular level in their chemical composition results in such a great diversity in their physical and chemical behaviours.

Letters of Copyright Permission

Copyright Clearance Center RightsLink®

Home | Help | Email Support | Lu Li

The molecular structures of starch components and their contribution to the architecture of starch granules: A comprehensive review

Author: Eric Bertoft, Serge Pérez
Publication: Starch
Publisher: John Wiley and Sons
Date: Jul 30, 2010

Order Completed

Thank you for your order.

This Agreement between Ms. Lu Li ("You") and John Wiley and Sons ("John Wiley and Sons") consists of your license details and the terms and conditions provided by John Wiley and Sons and Copyright Clearance Center.

Your confirmation email will contain your order number for future reference.

Printable Details

License Number	4870141365115
License date	Jul 15, 2020

Licensed Content

Licensed Content Publisher	John Wiley and Sons
Licensed Content Publication	Starch
Licensed Content Title	The molecular structures of starch components and their contribution to the architecture of starch granules: A comprehensive review
Licensed Content Author	Eric Bertoft, Serge Pérez
Licensed Content Date	Jul 30, 2010
Licensed Content Volume	62
Licensed Content Issue	8
Licensed Content Pages	32

Order Details

Type of use	Dissertation/Thesis
Requestor type	University/Academic
Format	Print and electronic
Portion	Figure/table
Number of figures/tables	3
Will you be translating?	No

About Your Work

Title	Characterization of Polysaccharides in Starch using Fluorescence Techniques
Institution name	University of Waterloo
Expected presentation date	Sep 2020

Additional Data

Portions	Figure 3, Figure 7, Figure 8

Chapter: CHAPTER VI MOLECULAR STRUCTURE OF STARCH
Book: Starch: Chemistry and Technology
Author: ROY L. WHISTLER,JAMES R. DANIEL
Publisher: Elsevier
Date: 1984

Order Completed

Thank you for your order.

This Agreement between Ms. Lu Li ("You") and Elsevier ("Elsevier") consists of your license details and the terms and conditions provided by Elsevier and Copyright Clearance Center.

Your confirmation email will contain your order number for future reference.

License Number	4870151129860
License date	Jul 15, 2020

Printable Details

Licensed Content

Licensed Content Publisher	Elsevier
Licensed Content Publication	Elsevier Books
Licensed Content Title	Starch: Chemistry and Technology
Licensed Content Author	ROY L. WHISTLER,JAMES R. DANIEL
Licensed Content Date	Jan 1, 1984
Licensed Content Pages	30
Journal Type	S&T

Order Details

Type of Use	reuse in a thesis/dissertation
Portion	figures/tables/illustrations
Number of figures/tables/illustrations	1
Format	both print and electronic
Are you the author of this Elsevier chapter?	No
Will you be translating?	No

About Your Work

Title	Characterization of Polysaccharides in Starch using Fluorescence Techniques
Institution name	University of Waterloo
Expected presentation date	Sep 2020

Additional Data

Portions	Figure 13

Chemical and Physical Properties of Starch

Author: French, Dexter
Publication: Journal of Animal Science
Publisher: Oxford University Press
Date: 1973-10-01

Order Completed

Thank you for your order.

This Agreement between Ms. Lu Li ("You") and Oxford University Press ("Oxford University Press") consists of your license details and the terms and conditions provided by Oxford University Press and Copyright Clearance Center.

Your confirmation email will contain your order number for future reference.

License Number	4870151282118
License date	Jul 15, 2020

Printable Details

Licensed Content

Licensed Content Publisher	Oxford University Press
Licensed Content Publication	Journal of Animal Science
Licensed Content Title	Chemical and Physical Properties of Starch
Licensed Content Author	French, Dexter
Licensed Content Date	Oct 1, 1973
Licensed Content Volume	37
Licensed Content Issue	4

Order Details

Type of Use	Thesis/Dissertation
Requestor type	Educational Institution/Non-commercial/ Not for-profit
Format	Print and electronic
Portion	Figure/table
Number of figures/tables	1
Will you be translating?	No

About Your Work

Title	Characterization of Polysaccharides in Starch using Fluorescence Techniques
Institution name	University of Waterloo
Expected presentation date	Sep 2020

Additional Data

Portions	Figure 4

Polymodal distribution of the chain lengths of amylopectins, and its significance

Author: Susumu Hizukuri
Publication: Carbohydrate Research
Publisher: Elsevier
Date: 15 March 1986

Order Completed

Thank you for your order.

This Agreement between Ms. Lu Li ("You") and Elsevier ("Elsevier") consists of your license details and the terms and conditions provided by Elsevier and Copyright Clearance Center.

Your confirmation email will contain your order number for future reference.

License Number	4870850819117
License date	Jul 16, 2020

Printable Details

Licensed Content

Licensed Content Publisher	Elsevier
Licensed Content Publication	Carbohydrate Research
Licensed Content Title	Polymodal distribution of the chain lengths of amylopectins, and its significance
Licensed Content Author	Susumu Hizukuri
Licensed Content Date	Mar 15, 1986
Licensed Content Volume	147
Licensed Content Issue	2
Licensed Content Pages	6
Journal Type	S&T

Order Details

Type of Use	reuse in a thesis/dissertation
Portion	figures/tables/illustrations
Number of figures/tables/illustrations	1
Format	both print and electronic
Are you the author of this Elsevier article?	No
Will you be translating?	No

About Your Work

Title	Characterization of Polysaccharides in Starch using Fluorescence Techniques
Institution name	University of Waterloo
Expected presentation date	Sep 2020

Additional Data

Portions	Figure 5

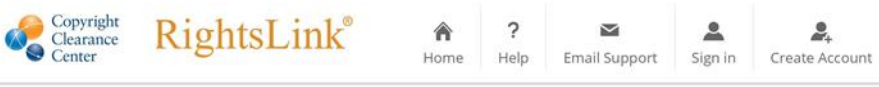

Conformation of Pyrene-Labeled Amylose in DMSO Characterized with the Fluorescence Blob Model

ACS Publications
Most Trusted. Most Cited. Most Read.

Author: Lu Li, Jean Duhamel
Publication: Macromolecules
Publisher: American Chemical Society
Date: Oct 1, 2016

Quick Price Estimate

This service provides permission for reuse only. If you do not have a copy of the portion you are using, you may copy and paste the content and reuse according to the terms of your agreement. Please be advised that obtaining the content you license is a separate transaction not involving RightsLink.

Permission for this particular request is granted for print and electronic formats, and translations, at no charge. Figures and tables may be modified. Appropriate credit should be given. Please print this page for your records and provide a copy to your publisher. Requests for up to 4 figures require only this record. Five or more figures will generate a printout of additional terms and conditions. Appropriate credit should read: "Reprinted with permission from {COMPLETE REFERENCE CITATION}. Copyright {YEAR} American Chemical Society." Insert appropriate information in place of the capitalized words.

I would like to...	reuse in a Thesis/Dissertatio	Format	Print
Requestor Type	Author (original work)	Select your currency	USD - $
Portion	50% or more of original artic	Quick Price	Click Quick Price

QUICK PRICE CONTINUE

To request permission for a type of use not listed, please contact the publisher directly.

Conformation of Pyrene-Labeled Amylose in DMSO Characterized with the Fluorescence Blob Model

ACS Publications
Most Trusted. Most Cited. Most Read.

Author: Lu Li, Jean Duhamel
Publication: Macromolecules
Publisher: American Chemical Society
Date: Oct 1, 2016

A Pyrene Excimer Fluorescence (PEF) Study of the Interior of Amylopectin in Dilute Solution

Author: Lu Li, Damin Kim, Xiaofang Zhai, et al
Publication: Macromolecules
Publisher: American Chemical Society
Date: Aug 1, 2020

Quick Price Estimate

This service provides permission for reuse only. If you do not have a copy of the portion you are using, you may copy and paste the content and reuse according to the terms of your agreement. Please be advised that obtaining the content you license is a separate transaction not involving RightsLink.

Permission for this particular request is granted for print and electronic formats, and translations, at no charge. Figures and tables may be modified. Appropriate credit should be given. Please print this page for your records and provide a copy to your publisher. Requests for up to 4 figures require only this record. Five or more figures will generate a printout of additional terms and conditions. Appropriate credit should read: "Reprinted with permission from {COMPLETE REFERENCE CITATION}. Copyright {YEAR} American Chemical Society." Insert appropriate information in place of the capitalized words.

I would like to...	reuse in a Thesis/Dissertatio	Format	Print
Requestor Type	Author (original work)	Select your currency	USD - $
Portion	50% or more of original artic	Quick Price	Click Quick Price

QUICK PRICE CONTINUE

To request permission for a type of use not listed, please contact the publisher directly.

A Pyrene Excimer Fluorescence (PEF) Study of the Interior of Amylopectin in Dilute Solution

Author: Lu Li, Damin Kim, Xiaofang Zhai, et al
Publication: Macromolecules
Publisher: American Chemical Society
Date: Aug 1, 2020

References

Chapter 1

1. Ashwar, B. A.; Gani, A.; Shah, A.; Masoodi, F. A. Physicochemical Properties, In-Vitro Digestibility and Structural Elucidation of RS4 from Rice Starch. *Int. J. Biol. Macromol.* **2017**, *105*, 471-477.

2. Ren, S. C. Comparative Analysis of Some Physicochemical Properties of 19 Kinds of Native Starches. *Starch/Stärke* **2017**, *69*, 1600367.

3. Bertoft, E.; Piyachomkwan, K.; Chatakanonda, P.; Sriroth, K. Internal Unit Chain Composition in Amylopectins. *Carbohydr. Polym.* **2008**, *74*, 527-543.

4. Bertoft, E. Understanding Starch Structure: Recent Progress. *Agronomy* **2017**, *7*, 56-74.

5. Buléon, A.; Colonna, P.; Planchot, V.; Ball, S. Starch Granules: Structure and Biosynthesis. *Int. J. Biol. Macromol.* **1998**, *23*, 85-112.

6. Jane, J., Chapter 6 - Structural Features of Starch Granules II. In *Starch (Third Edition)*, BeMiller, J.; Whistler, R., Eds. Academic Press: San Diego, 2009; pp 193-236.

7. Perez, S.; Bertoft, E. The Molecular Structures of Starch Components and Their Contribution to the Architecture of Starch Granules: A Comprehensive Review. *Starch/Stärke* **2010**, *62*, 389-420.

8. Whilstler, R. L.; Daniel, J. R., Molecular Structure of Starch. In *Starch: Chemistry and Technology*, Academic Press, Inc: Orlando, Florida, 1984; pp 153-182.

9. Bourne, E. J.; Peat, S. 2. The Amylose Component of Waxy Maize Starch. *J. Chem. Soc.* **1949**, 5-9.

10. Jane, J.; Chen, Y. Y.; Lee, L. F.; McPherson, A. E.; Wong, K. S.; Radosavljevic, M.; Kasemsuwan, T. Effects of Amylopectin Branch Chain Length and Amylose Content on the Gelatinization and Pasting Properties of Starch. *Cereal Chem.* **1999**, *76*, 629-637.

11. Yu, X.; Houtman, C.; Atalla, R. H. The Complex of Amylose and Iodine. *Carbohydr. Res.* **1996**, *292*, 129-141.

12. Schwartz, D.; Whistler, R. L., Chapter 1 - History and Future of Starch. In *Starch: Chemistry and Techonology*, BeMiller, J.; Whistler, R., Eds. Academic Press: San Diego, 2009; pp 1-10.

13. Carciofi, M.; Blennow, A.; Jensen, S. L.; Shaik, S. S.; Henriksen, A.; Buléon, A.; Holm, P. B.; Hebelstrup, K. H. Concerted Suppression of All Starch Branching Enzyme Genes in Barley Produces Amylose-Only Starch Granules. *BMC Plant Biol.* **2012**, *12*, 223-238.

14. Tan, Y.; Li, J.; Yu, S.; Xing, Y.; Xu, C.-J.; Zhang, Q. The Three Important Traits for Cooking and Eating Quality of Rice Grains are Controlled by a Single Locus in an Elite Rice Hybrid, Shanyou 63. *Theor. Appl. Genet* **1999**, *99*, 642-8.

15. Wu, X.; Zhao, R.; Wang, D.; Bean, S. R.; Seib, P. A.; Tuinstra, M. R.; Campbell, M.; O'Brien, A. Effects of Amylose, Corn Protein, and Corn Fiber Contents on Production of Ethanol from Starch-Rich Media. *Cereal Chem.* **2006**, *83*, 569-575.

16. Hassid, W. Z.; McCready, R. M. The Molecular Constitution of Amylose and Amylopectin of Potato Starch. *J. Am. Chem. Soc.* **1943**, *65*, 1157-1161.

17. McCready, R. M.; Hassid, W. Z. The Separation and Quantitative Estimation of Amylose and Amylopectin in Potato Starch. *J. Am. Chem. Soc.* **1943**, *65*, 1154-1157.

18. Tester, R. F.; Qi, X. β-Limit Dextrin - Properties and Applications. *Food Hydrocoll.* **2011**, *25*, 1899-1903.

19. Peat, S.; Whelan, W. J.; Pirt, S. J. The Amylolytic Enzymes of Soya Bean. *Nature* **1949**, *164*, 499.

20. Banks, W.; Greenwood, C. T. Physicochemical Studies on Starches Part XXXII. The Incomplete β-Amylolysis of Amylose: A Discussion of its Cause and Implications. *Starch/Stärke* **1967**, *19*, 197-206.

21. Baum, H.; Gilbert, G. A.; Scott, N. D. Oxidation as a Source of Anomalies in Amylose. *Nature* **1956**, *177*, 889.

22. Abdullah, M.; Catley, B. J.; Lee, E. Y. C.; Robyt, J.; Wallenfels, K.; Whelan, W. J. The Mechanism of Carbohydrase Action. XI. Pullulanase, an Enzyme Specific for the Hydrolysis of Alpha-1-6-Bonds in Amylaceous Oligo- and Polysaccharides. *Cereal Chem.* **1966**, *43*, 111-118.

23. Hizukuri, S.; Takeda, Y.; Yasuda, M.; Suzuki, A. Multi-Branched Nature of Amylose and the Action of Debranching Enzymes. *Carbohydr. Res.* **1981**, *94*, 205-213.

24. Takeda, Y.; Shirasaka, K.; Hizukuri, S. Examination of the Purity and Structure of Amylose by Gel Permeation Chromatography. *Carbohydr. Res.* **1984**, *132*, 83-92.

25. Greenwood, W. B. C. T., *Starch and Its Components*. Edinburgh University Press: Edinburgh, Scotland, 1975.

26. Everett, W. W.; Foster, J. F. The Conformation of Amylose in Solution. *J. Am. Chem. Soc.* **1959**, *81*, 3464-3469.

27. Banks, W.; Greenwood, C. T. Hydrodynamic Properties and Dimensions of Linear Potato Amylose Molecules in Dilute Aqueous Salt Solution. *Makromol. Chem.* **1963**, *67*, 49-63.

28. Banks, W.; Greenwood, C. T. Conformation of Amylose in Neutral Aqueous Salt Solution. *Carbohydr. Res.* **1968**, *7*, 349-357.

29. Banks, W.; Greenwood, C. T. The Hydrodynamic Behaviour of Native Amylose in Good Solvents. *Carbohydr. Res.* **1968**, *7*, 414-420.

30. Burchard, W. Das Viskositätsverhalten Von Amylose in Verschiedenen Lösungsmitteln. *Makromol. Chem.* **1963**, *64*, 110-125.

31. Cowie, J. M. G. Studies on Amylose and Its Derivatives. 1. Molecular Size and Configuration of Amylose Molecules in Various Solvents. *Makromol. Chem.* **1960**, *42*, 230-247.

32. Fujii, M.; Honda, K.; Fujita, H. Dilute-Solution of Amylose in Dimethylsulfoxide. *Biopolymers* **1973**, *12*, 1177-1195.

33. Nakanishi, Y.; Norisuye, T.; Teramoto, A.; Kitamura, S. Conformation of Amylose in Dimethyl Sulfoxide. *Macromolecules* **1993**, *26*, 4220-4225.

34. Norisuye, T. Conformation and Properties of Amylose in Dilute Solution. *Food Hydrocoll.* **1996**, *10*, 109-115.

35. Kodama, M.; Noda, H.; Kamata, T. Conformation of Amylose in Water. I. Light-Scattering and Sedimentation-Equilibrium Measurements. *Biopolymers* **1978**, *17*, 985-1002.

36. Yoshizaki, T.; Yamakawa, H. Dynamics of Helical Worm-Like Chains. 9. Dynamic Intrinsic Viscosity. *J. Chem. Phys.* **1988**, *88*, 1313-1325.

37. Rao, V. S. R.; Yathindra, N.; Sundararajan, P. R. Configurational Statistics of Polysaccharide Chains. Part I. Amylose. *Biopolymers* **1969**, *8*, 325-333.

38. Lewis, D. G.; Johnson, W. C. Optical Properties of Sugars. XI. Circular Dichroism of Amylose and Glucose Oligomers. *Biopolymers* **1978**, *17*, 1439-1449.

39. Erlander, S. R.; Purvinas, R. M.; Griffin, H. L. Transition from Helix to Coil at pH 12 for Amylose Amylopectin and Glycogen. *Cereal Chem.* **1968**, *45*, 140-148.

40. Rao, V. S. R.; Foster, J. F. Studies of Conformation of Carboxymethyl Amylose in Aqueous Solutions. *Biopolymers* **1965**, *3*, 185-193.

41. Rao, V. S. R.; Foster, J. F. Conformation of Pyranose Rings in Mono-, Di-, and Polysaccharides at High pH by Proton Magnetic Resonance Studies. *J. Phys. Chem.* **1965**, *69*, 636-645.

42. Stjacques, M.; Sundararajan, P. R.; Taylor, K. J.; Marchessault, R. H. Nuclear Magnetic-Resonance and Conformational Studies on Amylose and Model Compounds in Dimethyl-Sulfoxide Solution. *J. Am. Chem. Soc.* **1976**, *98*, 4386-4391.

43. Kitamura, S.; Tanahashi, H.; Kuge, T. Study of Polysaccharides by the Fluorescence Method. III. Chain Length Dependence of the Micro-Brownian Motion of Amylose in an Aqueous Solution. *Biopolymers* **1984**, *23*, 1043-1056.

44. Kitamura, S.; Matsumori, S.; Kuge, T. Study of Polysaccharides by the Fluorescence Method. V. Interaction of 2-*p*-Toluidinylnaphthalene-6-Sulfonate with Amylose and its Related Compounds in Aqueous Solution. *J. Incl. Phenom.* **1984**, *2*, 725-735.

45. Kitamura, S.; Yunokawa, H.; Kuge, T. Study on Polysaccharide by the Fluorescence Method. I. Fluorescence Depolarization of the Fluorescein Conjugates of Amylose and Dextran. *Polym. J.* **1982**, *14*, 85-91.

46. Kitamura, S.; Yunokawa, H.; Mitsuie, S.; Kuge, T. Study on Polysaccharide by the Fluorescence Method. II. Micro-Brownian Motion and Conformational Change of Amylose in Aqueous Solution. *Polym. J.* **1982**, *14*, 93-99.

47. Rees, D. A.; Scott, W. E. Polysaccharide Conformation. Part VI. Computer Model Building for Linear and Branched Pyranoglycans. Correlations with Biological Function. Preliminary Assessment of Inter-Residue Forces in Aqueous Solution. Further Interpretation of Optical Rotation in terms of Chain Conformation. *J. Chem. Soc. B* **1971**, 469-479.

48. Tvaroska, I.; Perez, S.; Marchessault, R. H. Conformational Analysis of (1 - 6)-α-D-Glucan. *Carbohydr. Res.* **1978**, *61*, 97-106.

49. Cowie, J. M. G. Studies on Amylose and Its Derivatives. III. The Effect of Temperature on the Intrinsic Viscosities of Amylose in Several Solvents. *Makromol. Chem.* **1962**, *53*, 13-20.

50. Dintzis, F. R.; Tobin, R. Optical Rotation of Some α-1,4-Linked Glucopyranosides in System H_2O-DMSO and Solution Conformation of Amylose. *Biopolymers* **1969**, *7*, 581-593.

51. Putseys, J.; Lamberts, L.; Delcour, J. Amylose-Inclusion Complexes: Formation, Identity and Physico-Chemical Properties. *J. Cereal Sci.* **2010**, *51*, 238-247.

52. Martinho, J. M. G.; Martinho, M. H.; Winnik, M. A.; Beinert, G. Cyclization Dynamics of Polymers, 26. End-to-End Cyclization of Polystyrene in Mixed Solvents. Effect of Chain Length. *Macromol. Chem. Phys.* **1989**, *15*, 113-125.

53. Cuniberti, C.; Perico, A. Intramolecular Excimers and Microbrownian Motion of Flexible Polymer Molecules in Solution. *Eur. Polym. J.* **1977**, *13*, 369-374.

54. Winnik, M. A.; Li, X. B.; Guillet, J. E. Cyclization Dynamics of Polymers. 13. Effects of Added Polymer on the Conformation and Dynamics of Polystyrene Containing Evenly Spaced Pyrene Groups. *Macromolecules* **1984**, *17*, 699-702.

55. Piçarra, S.; Duhamel, J.; Fedorov, A.; Martinho, J. M. G. Coil-Globule Transition of Pyrene-Labeled Polystyrene in Cyclohexane: Determination of Polymer Chain Radii by Fluorescence. *J. Phys. Chem. B* **2004**, *108*, 12009-12015.

56. Farhangi, S.; Duhamel, J. Long Range Polymer Chain Dynamics Studied by Fluorescence Quenching. *Macromolecules* **2016**, *49*, 6149-6162.

57. Duhamel, J. Polymer Chain Dynamics in Solution Probed with a Fluorescence Blob Model. *Acc. Chem. Res.* **2006**, *39*, 953-960.

58. Sjöö, M.; Nilsson, L., *Starch in Food: Structure, Function and Applications: Second Edition*. 2017; p 1-893.

59. Hanashiro, I.; Tagawa, M.; Shibahara, S.; Iwata, K.; Takeda, Y. Examination of Molar-based Distribution of A, B and C Chains of Amylopectin by Fluorescent Labeling with 2-Aminopyridine. *Carbohydr. Res.* **2002**, *337*, 1211-1215.

60. Li, H.; Lei, N.; Yan, S.; Yang, J.; Yu, T.; Wen, Y.; Wang, J.; Sun, B. The Importance of Amylopectin Molecular Size in Determining the Viscoelasticity of Rice Starch Gels. *Carbohydr. Polym.* **2019**, *212*, 112-118.

61. Hizukuri, S. Relationship Between the Distribution of the Chain Length of Amylopectin and the Crystalline Structure of Starch Granules. *Carbohydr. Res.* **1985**, *141*, 295-306.

62. Peat, S.; Whelan, W. J.; Thomas, G. J. Evidence of Multiple Branching in Waxy Maize Starch. *J. Chem. Soc.* **1952**, 4546-4548.

63. Haworth, W. N.; Hirst, E. L.; Isherwood, F. A. Polysaccharides. Part XIII. Determination of the Chain Length of Glycogen. *J. Chem. Soc.* **1937**, 577-581.

64. Staudinger, H.; Husemann, E. High Polymer Compounds-150th Announcement-The Composition of Starch. *Justus Liebigs Ann. Chem.* **1937**, *527*, 195-236.

65. Meyer, K. H.; Bernfeld, P. Research on Starch V-Amylopectin. *Helv. Chim. Acta* **1940**, *23*, 875-885.

66. Peat, S.; Whelan, W. J.; Thomas, G. J. The Enzymic Synthesis and Degradation of Starch. XXII. Evidence of Multiple Branching in Waxy-Maize Starch. A Correction. *J. Chem. Soc.* **1956**, 3025-3030.

67. Bathgate, G. N.; Manners, D. J. Multiple Branching in Glycogens. *Biochem. J.* **1966**, *101*, 3c-5c.

68. Bender, H.; Siebert, R.; Stadlerszoke, A. Can Cyclodextrin Glycosyltransferase Be Useful for the Investigation of the Fine Structure of Amylopectins?: Characterization of Highly Branched Clusters Isolated from Digests with Potato and Maize Starches. *Carbohydr. Res.* **1982**, *110*, 245-259.

69. French, D. Chemical and Physical Properties of Starch. *J. Anim. Sci*. **1973**, *37*, 1048-1061.

70. Manners, D. J. Recent Developments in Our Understanding of Amylopectin Structure. *Carbohydr. Polym.* **1989**, *11*, 87-112.

71. Lee, E. Y.; Mercier, C.; Whelan, W. J. A Method for the Investigation of the Fine Structure of Amylopectin. *Arch. Biochem. Biophys.* **1968**, *125*, 1028-1030.

72. Akai, H.; Yokobayashi, K.; Misaki, A.; Harada, T. Structural Analysis of Amylopectin Using Pseudomonas Isoamylase. *Biochim. Biophys. Acta*. **1971**, *252*, 427-431.

73. Hizukuri, S. Polymodal Distribution of the Chain Lengths of Amylopectins, and Its Significance. *Carbohydr. Res.* **1986**, *147*, 342-347.

74. Li, C.; Powell, P. Recent Progress toward Understanding the Role of Starch Biosynthetic Enzymes in the Cereal Endosperm. *Amylase* **2017**, *1*, *59-74*.

75. Robin, J. P.; Mercier, C.; Charbonniere, R.; Guilbot, A. Lintnerized Starches Gel-Filtration and Enzymatic Studies of Insoluble Residues from Prolonged Acid Treatment of Potato Starch. *Cereal Chem.* **1974**, *51*, 389-406.

76. Durrani, C. M.; Donald, A. Shape, Molecular Weight Distribution and Viscosity of Amylopectin in Dilute Solution. *Carbohydr. Polym.* **2000**, *41*, 207-217.

77. Bello-Perez, L. A.; Paredes-Lopez, O.; Roger, P.; Colona, P. Molecular Characterization of Amylopectins. *Cereal Chem.* **1996**, *73*, 12-17.

78. Tande, B. M.; Wagner, N. J.; Mackay, M. E.; Hawker, C. J.; Jeong, M. Viscosimetric, Hydrodynamic, and Conformational Properties of Dendrimers and Dendrons. *Macromolecules* **2001**, *34*, 8580-8585.

79. Yang, C.; Meng, B.; Chen, M.; Liu, X.; Hua, Y.; Ni, Z. Laser-light-scattering Study of Structure and Dynamics of Waxy Corn Amylopectin in Dilute Aqueous Solution. *Carbohydr. Polym.* **2006**, *64*, 190-196.

80. Sorensen, C. M. Light Scattering by Fractal Aggregates: A Review. *Aerosol Sci. Technol.* **2001**, *35*, 648-687.

81. Millard, M. M.; Wolf, W. J.; Dintzis, F. R.; Willett, J. L. The Hydrodynamic Characterization of Waxy Maize Amylopectin in 90% Dimethyl Sulfoxide - Water by Analytical Ultracentrifugation, Dynamic, and Static Light Scattering. *Carbohydr. Polym.* **1999**, *39*, 315-320.

82. Lee, J. H.; You, S.; Kweon, D. K.; Chung, H. J.; Lim, S. T. Dissolution Behaviors of Waxy Maize Amylopectin in Aqueous-DMSO Solutions Containing NaCl and $CaCl_2$. *Food Hydrocoll.* **2014**, *35*, 115-121.

83. Hanselmann, R.; Burchard, W.; Ehrat, M.; Widmer, H. M. Structural Properties of Fractionated Starch Polymers and Their Dependence on the Dissolution Process. *Macromolecules* **1996**, *29*, 3277-3282.

84. Han, J.-A.; Lim, H.; Lim, S.-T. Comparison between Size Exclusion Chromatography and Micro-Batch Analyses of Corn Starches in DMSO using Light Scattering Detector. *Starch/Stärke* **2005**, *57*, 262-267.

85. Roger, P.; Bello-Perez, L. A.; Colonna, P. Contribution of Amylose and Amylopectin to the Light Scattering Behaviour of Starches in Aqueous Solution. *Polymer* **1999**, *40*, 6897-6909.

86. Wu, C.; Zhou, S. Internal Motions of both Poly(N-isopropylacrylamide) Linear Chains and Spherical Microgel Particles in Water. *Macromolecules* **1996**, *29*, 1574-1578.

87. Schuler, B.; Eaton, W. A. Protein Folding Studied by Single-Molecule FRET. *Curr. Opin. Struc. Biol.* **2008**, *18*, 16-26.

88. Ha, T.; Ting, A. Y.; Liang, J.; Caldwell, W. B.; Deniz, A. A.; Chemla, D. S.; Schultz, P. G.; Weiss, S. Single-Molecule Fluorescence Spectroscopy of Enzyme Conformational Dynamics and Cleavage Mechanism. *Proc. Natl. Acad. Sci. U. S. A.* **1999**, *96*, 893-8.

89. Kim, H.-Y.; Park, S. S.; Lim, S.-T. Preparation, Characterization and Utilization of Starch Nanoparticles. *Colloids Surf. B* **2015**, *126*, 607-620.

90. Le Corre, D.; Bras, J.; Dufresne, A. Starch Nanoparticles: A Review. *Biomacromolecules* **2010**, *11*, 1139-1153.

91. Bel Haaj, S.; Thielemans, W.; Magnin, A.; Boufi, S. Starch Nanocrystals and Starch Nanoparticles from Waxy Maize as Nanoreinforcement: A Comparative Study. *Carbohydr. Polym.* **2016**, *143*, 310-317.

92. Dufresne, A.; Cavaille, J.-Y.; Helbert, W. New Nanocomposite Materials: Microcrystalline Starch Reinforced Thermoplastic. *Macromolecules* **1996**, *29*, 7624-7626.

93. Putaux, J. L.; Molina-Boisseau, S.; Momaur, T.; Dufresne, A. Platelet Nanocrystals Resulting from the Disruption of Waxy Maize Starch Granules by Acid Hydrolysis. *Biomacromolecules* **2003**, *4*, 1198-1202.

94. García, N. L.; Ribba, L.; Dufresne, A.; Aranguren, M.; Goyanes, S. Effect of Glycerol on the Morphology of Nanocomposites Made from Thermoplastic Starch and Starch Nanocrystals. *Carbohydr. Polym.* **2011**, *84*, 203-210.

95. Liu, D.; Wu, Q.; Chen, H.; Chang, P. R. Transitional Properties of Starch Colloid with Particle Size Reduction from Micro- to Nanometer. *J. Colloid Interf. Sci.* **2009**, *339*, 117-124.

96. LeCorre, D. S.; Bras, J.; Dufresne, A. Influence of the Botanic Origin of Starch Nanocrystals on the Morphological and Mechanical Properties of Natural Rubber Nanocomposites. *Macromol. Mater. Eng.* **2012**, *297*, 969-978.

97. Bel Haaj, S.; Magnin, A.; Pétrier, C.; Boufi, S. Starch Nanoparticles Formation via High Power Ultrasonication. *Carbohydr. Polym.* **2013**, *92*, 1625-1632.

98. Giezen Franciscus, E.; Jongboom Remigius Oene, J.; Feil, H.; Gotlieb Kornelis, F.; Boersma, A. Biopolymer Nanoparticles. US 6677386 B1, 2001/10/24, 2004.

99. Ma, X.; Jian, R.; Chang, P. R.; Yu, J. Fabrication and Characterization of Citric Acid-Modified Starch Nanoparticles/Plasticized-Starch Composites. *Biomacromolecules* **2008**, *9*, 3314-3320.

100. Chin, S. F.; Pang, S. C.; Tay, S. H. Size Controlled Synthesis of Starch Nanoparticles by a Simple Nanoprecipitation Method. *Carbohydr. Polym.* **2011**, *86*, 1817-1819.

101. Kim, J.-Y.; Lim, S.-T. Preparation of Nano-sized Starch Particles by Complex Formation with n-Butanol. *Carbohydr. Polym.* **2009**, *76*, 110-116.

102. Lamanna, M.; Morales, N. J.; García, N. L.; Goyanes, S. Development and Characterization of Starch Nanoparticles by Gamma Radiation: Potential Application as Starch Matrix Filler. *Carbohydr. Polym.* **2013**, *97*, 90-97.

103. Lee, D. J. B., S.; Leeuwen, J., Development of New Biobased Emulsion Binders. In *PaperCon*, Atlanta, 2010.

104. Kim, D.; Amos, R.; Gauthier, M.; Duhamel, J. Applications of Pyrene Fluorescence to the Characterization of Hydrophobically Modified Starch Nanoparticles. *Langmuir* **2018**, *34*, 8611-8621.

105. Patel, S.; Seet, J.; Li, L.; Duhamel, J. Detection of Nitroaromatics by Pyrene-Labeled Starch Nanoparticles. *Langmuir* **2019**, *35*, 13145-13156.

106. Zhang, Q.; Kim, D.; Li, L.; Patel, S.; Duhamel, J. Surfactant Structure-Dependent Interactions with Modified Starch Nanoparticles Probed by Fluorescence Spectroscopy. *Langmuir* **2019**, *35*, 3432-3444.

107. Lakowicz, J., *Principles of Fluorescence Spectroscopy*. Springer: 2006; Vol. 1.

108. Nishijima, Y. Fluorescence Methods in Polymer Science. *J. Polym. Sci. C Polym. Symp.* **1970**, *31*, 353-358.

109. Valeur, B.; Monnerie, L. Dynamics of Macromolecular Chains. 3. Time-Dependent Fluorescence Polarization Studies of Local Motions of Polystyrene in Solution. *J. Polym. Sci. B Polym. Phys.* **1976**, *14*, 11-27.

110. Valeur, B.; Monnerie, L. Dynamics of Macromolecular Chains. 4. Quenching and Fluorescence Polarization Studies of Polystyrene in Solution. *J. Polym. Sci. B Polym. Phys.* **1976**, *14*, 29-37.

111. Gradinaru, C.; Marushchak, D.; Samim, M.; Krull, U. Fluorescence Anisotropy: From Single Molecules to Live Cells. *Analyst* **2010**, *135*, 452-459.

112. Monnerie, L.; Gorin, S. Polarization of Fluorescence by Macromolecular Chains in Solution. *J. Polym. Sci. C Polym. Symp.* **1970**, *30*, 99-103.

113. Stryer, L.; Haugland, R. P. Energy Transfer: a Spectroscopic Ruler. *Proc. Natl. Acad. Sci. U. S. A.* **1967**, *58*, 719-26.

114. Moglich, A.; Joder, K.; Kiefhaber, T. End-to-End Distance Distributions and Intrachain Diffusion Constants in Unfolded Polypeptide Chains Indicate Intramolecular Hydrogen Bond Formation. *Proc. Natl. Acad. Sci. U. S. A.* **2006**, *103*, 12394-12399.

115. Duhamel, J. Global Analysis of Fluorescence Decays to Probe the Internal Dynamics of Fluorescently Labeled Macromolecules. *Langmuir* **2014**, *30*, 2307-2324.

116. Winnik, F. M. Photophysics of Preassociated Pyrenes in Aqueous Polymer Solutions and in Other Organized Media. *Chem. Rev.* **1993**, *93*, 587-614.

117. Bree, A.; Vilkos, V. V. B. A Study of Some Singlet Triplet Electronic States of Pyrene. *Spectrochim. Acta A Mol. Biomol. Spectrosc.* **1971**, *27*, 2333-2354.

118. Yao, C.; Kraatz, H.-B.; Steer, R. P. Photophysics of Pyrene-Labelled Compounds of Biophysical Interest. *Photoch. Photobio. Sci.* **2005**, *4*, 191-199.

119. Winnik, M. A.; Redpath, T.; Richards, D. H. The Dynamics of End-to-End Cyclization in Polystyrene Probed by Pyrene Excimer Formation. *Macromolecules* **1980**, *13*, 328-335.

120. Duhamel, J.; Kanagalingam, S.; O'Brie, T. J.; Ingratta, M. W. Side-Chain Dynamics of an α-Helical Polypeptide Monitored by Fluorescence. *J. Am. Chem. Soc.* **2003**, *125*, 12810-12822.

121. Mathew, A.; Siu, H.; Duhamel, J. A Blob Model To Study Chain Folding by Fluorescence. *Macromolecules* **1999**, *32*.

122. Ingratta, M.; Duhamel, J. Effect of Side-chain Length on the Side-chain Dynamics of α-Helical Poly(*L*-glutamic acid) as Probed by a Fluorescence Blob Model. *J. Phys. Chem. B* **2008**, *112*, 9209-9218.

123. Casier, R.; Duhamel, J. Pyrene Excimer Fluorescence as a Direct and Easy Experimental Means To Characterize the Length Scale and Internal Dynamics of Polypeptide Foldons. *Macromolecules* **2018**, *51*, 3450-3457.

124. Birks, J. B.; Dyson, D. J.; Munro, I. H.; Flowers, B. H. 'Excimer' Fluorescence II. Lifetime Studies of Pyrene Solutions. *P. Roy. Soc. Lond. A Math. Phys. Sci.* **1963**, *275*, 575-588.

125. Duhamel, J.; Winnik, M. A.; Baros, F.; Andre, J. C.; Martinho, J. M. G. Diffusion Effects on Pyrene Excimer Kinetics: Determination of the Excimer Formation Rate Coefficient Time Dependence. *J. Phys. Chem.* **1992**, *96*, 9805-9810.

126. Duhamel, J.; Yekta, A.; Winnik, M. A.; Jao, T. C.; Mishra, M. K.; Rubin, I. D. A Blob Model to Study Polymer Chain Dynamics in Solution. *J. Phys. Chem.* **1993**, *97*, 13708-13712.

127. Winnik, M. A. End-to-End Cyclization of Polymer Chains. *Acc. Chem. Res.* **1985**, *18*, 73-79.

128. Ingratta, M.; Mathew, M.; Duhamel, J. How Switching the Substituent of a Pyrene Derivative from a Methyl to a Butyl Affects the Fluorescence Response of Polystyrene Randomly Labeled with Pyrene. *Can. J. Chem.* **2010**, *88*, 217-227.

129. Pirouz, S. Quantitative Characterization of Polymeric Engine Oil Additives in Solution by Fluorescence. at the University of Waterloo, 2015.

130. Li, L.; Duhamel, J. Conformation of Pyrene-Labeled Amylose in DMSO Characterized with the Fluorescence Blob Model. *Macromolecules* **2016**, *49*, 7965-7974.

131. Hall, T.; Whitton, G.; Casier, R.; Gauthier, M.; Duhamel, J. Arborescent Poly(*L*-glutamic acid)s as Standards To Study the Dense Interior of Polypeptide Mesoglobules by Pyrene Excimer Fluorescence. *Macromolecules* **2018**, *51*, 7914-7923.

Chapter 2

1. Annable, T.; Buscall, R.; Ettelaie, R.; Whittlestone, D. The Rheology of Solutions of Associating Polymers: Comparison of Experimental Behavior with Transient Network Theory. *J. Rheol.* **1993**, 37, 695−726.

2. Krejtschi, C.; Hauser, K. Stability and Folding Dynamics of Polyglutamic Acid. *Eur. Biophys. J.* **2011**, 40, 673−685.

3. Costa, T.; Seixas de Melo, J. S. The Effect of γ-Cylcodextrin Addition in the Self-Assembly Behavior of Pyrene Labeled Poly(acrylic acid) with Difference Chain Sizes. *J. Polym. Sci., Part A: Polym. Chem.* 2008, 46, 1402−1415.

4. Banks, W.; Greenwood, C. T. The Hydrodyhamic Behaviour of Native Amylose in Good Solvents. *Carbohydr. Res.* **1968**, *7*, 414-420.

5. Banks, W.; Greenwood, C. T. Amylose: A Non-Helical biopolymer in Aqueous Solution. *Polymers* **1971**, *12*, 141-145.

6. Banks, W.; Greenwood, C. T. The Conformation of Amylose in Alkaline Salt Solution. *Carbohydr. Polym.* **1972**, *21*, 229-234.

7. Everett, W.; Foster, J. F. The Conformation of Amylose in Solution. *J. Am. Chem. Soc* **1959**, *81*, 3464-3469.

8. Cowie, J. M. G. Studies on Amylose and its Derivatives. Part I. Molecular Size and Configuration of Amylose Molecule in Various Solvents. *Makromol. Chem.* **1961**, *42*, 230-247.

9. Fujii, M.; Honda, J.; Fujita, H. Dilute Solution of Amylose in Dimethyl Sulfoxide. *Biopolymers* **1973**, *12*, 1177-1195.

10. Nakanishi, Y.; Norisuye, T.; Teramoto, A. Conformation of Amylose in Dimethyl Sulfoxide. *Macromolecules* **1993**, *1993*, 4220-4225.

11. Cheetham, N. W. H.; Tao, L. Amylose Conformational Transitions in Binary DMSO/Water Mixtures. *Carbohydr. Polym.* **1998**, *35*, 287-295.

12. St-Jacques, M.; Sundarajan, P.R.; Taylor, K.J.; Marchessault, R.H. Nuclear Magnetic Resonance and Conformational Studies on Amylose in Aqueous Solution. *Biopolymers* **1976**, *12*, 65-78.

13. Rees, D. A. Conformational Analysis of Polysaccharides. V. Characterization of Linkage Confirmations (Chain Conformations) by Optical Rotation at a Single Wavelength. Evidence for Distortion of Cyclohexa-amylose in Aqueous Solution. Optical Rotation and the Amylose Conformation. *J. Chem. Soc. B* **1970**, 877-884.

14. Tusch, M.; Krüger, J.; Fels, G. Structural Stability of V-Amylose Helices in Water-DMSO Mixtures Analyzed by Molecular Dynamics. *J. Chem. Theory Comput.* **2011**, 7, 2919−2928.

15. Cuniberti, C.; Perico, A. Intramolecular Excimers and Micro-Brownian Motion of Flexible Polymer Molecules in Solution. *Eur. Polym. J.* **1977**, *13*, 369-374.

16. Martinho, J. M. G.; Winnik, M. A. Excluded Volume Effects on the End-to-End Cyclization of Polystyrene in Mixed Solvents. *Macromolecules* **1986**, *19*, 2281-2284.

17. Kanagalingam, S.; Ngan, C.F.; Duhamel, J. Effect of Solvent Quality on the Level of Association and Encounter Kinetics of Hydrophobic Pendants Covalently Attached onto a Water-Soluble Polymer. *Macromolecules* **2002**, *35*, 8560-8570.

18. Zhang, M.; Duhamel, J. Effect of Solvent Quality toward the Association of Succinimide Pendants of a Modified Ethylene-Propylene Copolymer in Mixtures of Toluene and Hexane. *Macromolecules* **2006**, *38*, 4438-4446.

19. Gardinier, W. E.; Kane, M. A.; Bright, F. V. Effects of Added CO_2 on the Dynamics of Poly(dimethylsiloxane) Oligomers Dissolved in a Θ Solvent and a Poor Solvent. *J. Phys. Chem. B* **2004**, *108*, 18520-18529.

20. Kane, M. A.; Pandey, S.; Baker, G. A.; Perez, S. A.; Bukowski, E. J.; Hoth, D. C.; Bright, F. V. Effects of Density on the Intramolecular Hydrogen Bonding, Tail-Tail Cyclization, and Mean-Free Tail-to-Tail Distances of Pyrene End-Labeled Poly(dimethylsiloxane) Oligomers Dissolved in Supercritical CO_2. *Macromolecules* **2001**, *34*, 6831-6838.

21. Winnik, M. A.; Li, X.-B.; Guillet, J. E. Effects of Added Polymer on the Conformation and Dynamics of Polystyrene Containing Evenly Spaced Pyrene Groups. *Macromolecules* **1984**, *17*, 699-702.

22. Redpath, A. E. C.; Winnik, M. A. The Effect of Polymer Concentration on the Slowest Internal Relaxation Mode of a Labeled Polystyrene Chain. *Polymer* **1983**, *24*, 1286-1290.

23. Irondi, K.; Zhang, M.; Duhamel, J. Study of the Semidilute Solutions of Poly(*N*,*N*-dimethylacrylamide) by Fluorescence and Its Implications to the Kinetics of Coil-to-Globule Transitions. *J. Phys. Chem. B* **2006**, *110*, 2628-2637.

24. Redpath, A. E. C.; Winnik, M. A. Temperature d Dependence of Excimer Formation Between Pyrenes at the Ends of a Polymer in a Good Solvent. *J. Am. Chem. Soc* **1982**, *104*, 5604-5607.

25. Farinha, J. P. S.; Picarra, S.; Miesel, K. L.; Martinho, J. M. G. Fluorescence Study of the Coil-Globule Transition of a PEO Chain in Toluene. *J. Phys. Chem. B* **2001**, *105*, 10536-10545.

26. Picarra, S.; Duhamel, J.; Fedorov, A.; Martinho, J. M. G. Coil-Globule Transition of Pyrene-Labeled Polystyrene in Cyclohexane: Determination of Polymer Chain Radii by Fluorescence. *J. Phys. Chem. B* **2004**, *108*, 12009-12015.

27. Ingratta, M.; Duhamel, J. Effect of Side-Chain Length on the Side-Chain Dynamics of α–Helical Poly(*L*-glutamic acid) as Probed by a Fluorescence Blob Model. *J. Phys. Chem. B* **2008**, *112*, 9209-9218.

28. Farhangi, S.; Weiss, H.; Duhamel, J. Effect of Side-Chain Length on the Polymer Chain Dynamics of Poly(alkyl methacrylate)s in Solution. *Macromolecules* **2013**, *46*, 9738-9747.

29. Mathew, A.; Siu, H.; Duhamel, J. A Blob Model to Study Chain Folding by Fluorescence. *Macromolecules* **1999**, *32*, 7100−7108.

30. Duhamel, J. Polymer Chain Dynamics in Solution Probed with a Fluorescence Blob Model. *Acc. Chem. Res.* **2006**, *39*, 953-960.

31. Duhamel, J.; Kanagalingam, S.; O'Brien, T.; Ingratta, M. Side Chain Dynamics of an α-Helical Polypeptide Monitored by Fluorescence. *J. Am. Chem. Soc.* **2003**, *125*, 12810−12822.

32. Casier, R.; Duhamel, J. Pyrene Excimer Fluorescence as a Direct and Easy Experimental Means to Characterize the Length Scale and Dynamics of Polypeptide Foldons. *Macromolecules* **2018**, *51*, 3450-3457.

33. Birks, J. B. Photophysics of Aromatic Molecules; Wiley: New York, 1970; p 301.

34. Press, W. H.; Flannery, B. P.; Teukolsky, S. A.; Vetterling, W. T. Numerical Recipes. The Art of Scientific Computing (Fortran Version); Cambridge University Press: Cambridge, 1992.

35. Cuniberti, C.; Perico, A. Intramolecular Excimer Formation in Polymers. Pyrene Labelled Poly(vinyl acetate). *Eur. Polym. J.* **1980**, *16*, 887−893.

36. Boileau, S.; Mechin, F.; Martinho, J. M.; Winnik, M. A. End-to-End Cyclization of a Pyrene End-Capped Poly(bisphenol A-diethylene glycol carbonate). *Macromolecules* **1989**, *22*, 215−220.

37. Ingratta, M.; Hollinger, J.; Duhamel, J. A Case for Using Randomly Labeled Polymers to Study Long Range Polymer Chain Dynamics by Fluorescence. *J. Am. Chem. Soc* **2008**, *130*, 9420-9428.

38. Nishiyama, Y.; Mazeau, K.; Morin, M.; Cardoso, M.B.; Chanzy, H.; Purtaux, J. L. Molecular and Crystal Structure of 7-Fold V-Amylose Complexed with 2-Propanol. *Macromolecules* **2010**, *43*, 8628-9636.

Chapter 3

1. Manners, D. J. Recent Developments in our Understanding of Amylopectin Structure. *Carbohyd. Polym.* **1989**, *11*, 87-112.

2. Hancock, R. D.; Tarbet, B. J. The Other Double Helix – The Fascinating Chemistry of Starch. *J. Chem. Ed.* **2000**, *77*, 988-992.

3. Delcour, J. A.; Bruneel, C.; Derde, L. J.; Gomand, S. V.; Pareyt, B.; Putseys, J. A.; Wilderjans, E.; Lamberts, L. Fate of Starch in Food Processing: From Raw Materials to Final Food Products. *Annu. Rev. Food Sci. Technol.* **2010**, *1*, 87-111.

4. Nakamura, Y. Towards a Better Understanding of the Metabolic System for Amylopectin Biosynthesis in Plants: Rice Endosperm as a Model Tissue. *Plant Cell Phys.* **2002**, *43*, 718-725.

5. Beeren, S. R.; Hindsgaul, O. Nature's Dendrimer: Characterizing Amylopectin as a Multivalent Host. *Angew. Chem. Int. Ed.* **2013**, *52*, 11265-1168.

6. French, D. Organization of Starch Granules. In *Starch Chemistry and Technology*. 2nd Ed. Eds. Whistler, R. L.; BeMiller, J. N.; Paschall, E. F. Academic Press, Orlando, USA, 1984, 183.

7. Robin, J. P.; Mercier, C.; Charbonniere, Guilbot, A. Lintnerized Starches. Gel Filtration and Enzymatic Studies of Insoluble Residues from Prolonged Acid Treatment of Potato Starch. *Cereal Chem.* **1974**, *51*, 389-406.

8. Manners, D. J.; Matheson, N. K. The Fine Structure of Amylopectin. *Carbohydr. Res.* **1981**, *90*, 99-110.

9. Waigh, T. A.; Gidley, M. J.; Komanshek, B. U.; Donald, A. M. The Phase Transformations in Starch during Gelatinization: A Liquid Crystalline Approach. *Carbohydr. Res.* **2000**, *328*, 165-176.

10. Witt, T.; Gilbert, R. G. Causal Relations between Structural Features of Amylopectin, a Semicrystalline Hyperbranched Polymer. *Biomacromolecules* **2014**, *15*, 2501-2511.

11. Bloembergen, S.; Santos, M. P.; Greenall, P.; De Jong, R.; Shin, J. Y.; Jones, N.; Fleming, P. D.; Joyce, M. K.; Lee, I. The Effects of Bioloatex Binders on the Dynamic Water Retention Properties of Paper Coating Formulations. *O Papel* **2014**, *75*, 60-70.

12. Klass, C. P. New Nanoparticle Laytex Offers Natural Advantage. *Paper 360* **2007**, *2*, 30-31.

13. Hedin, J.; Östlund, Ä.; Nydén, M. UV Induced Cross-linking of Starch Modified with Glycidyl Methacrylate. *Carbohydr. Polym.* **2010**, *79*, 606-613.

14. Barikani, M.; Mohammadi, M. Synthesis and Characterization of Starch-Modified Polyurethane. *Carbohydr. Polym.* **2007**, *68*, 773-780.

15. Klavons, J. A.; Dintzis, F. R.; Millard, M. M. Hydrodynamic Chromatography of Waxy Maize Starch. *Carbohydrates* **1997**, *74*, 832-836.

16. You, S.; Fiedorowicz, M.; Lim, S.-T. Molecular Characterization of Wheat Amylopectins by Multiangle Laser Light Scattering Analysis. *Cereal Chem.* **1999**, *76*, 116-121.

17. Han, J.-A.; Lim, H.; Lim, S.-T. Comparison between Size Exclusion Chromatography and Micro-Batch Analyses of Corn Starches in DMSO Using Light Scattering Detector. *Starch* **2005**, *57*, 262-267.

18. Stryer, L.; Haugland, R. P. Energy Transfer: A Spectroscopic Ruler. *Proc. Natl. Acad. Sci.* **1967**, *58*, 719-726.

19. Drake, J. M.; Klafter, J.; Levitz, P. Chemical and Biological Microstructures as Probed by Dynamic Processes. *Science* **1991**, *251*, 1574-1579.

20. Farhangi, S.; Duhamel, J. Long Range Polymer Chain Dynamics Studied by Fluorescence Quenching. *Macromolecules* **2016**, *49*, 6149-6162.

21. Mathew, A.; Siu, H.; Duhamel, J. A *Blob* Model to Study Chain Folding by Fluorescence. *Macromolecules* **1999**, *32*, 7100-7108.

22. Duhamel, J. Polymer Chain Dynamics in Solution Probed with a Fluorescence Blob Model. *Acc. Chem. Res.* **2006**, *39*, 953-960.

23. Farhangi, S.; Duhamel, J. Long Range Polymer Chain Dynamics Studied by Fluorescence Quenching. *Macromolecules* **2016**, *49*, 6149-6162.

24. Li, L.; Duhamel, J. Conformation of Pyrene-Labeled Amylose in DMSO Characterized by the Fluorescence Blob Model. *Macromolecules* **2016**, *49*, 7965-7974.

25. Zhang, Q.; Kim, D.; Li, L.; Patel, S.; Duhamel, J. Surfactant-Structure Dependent Interactions with Modified Starch Nanoparticles Probed by Fluorescence Spectroscopy. *Langmuir* **2019**, *35*, 3432-3444.

26. Duhamel, J. New Insights in the Study of Pyrene Excimer Fluorescence to Characterize Macromolecules and their Supramolecular Assemblies in Solution. *Langmuir* **2012**, *28*, 6527-6538.

27. Duhamel, J. Global Analysis of Fluorescence Decays to Probe the Internal Dynamics of Fluorescently Labeled Macromolecules. *Langmuir* **2014**, *30*, 2307-2324.

28. Farhangi, S.; Weiss, H.; Duhamel, J. Effect of Side-Chain Length on the Polymer Chain Dynamics of Poly(alkyl methacrylate)s in Solution. *Macromolecules* **2013**, *46*, 9738-9747.

29. Farhangi, S.; Duhamel, J. Probing Side Chain Dynamics of Branched Macromolecules by Pyrene Excimer Fluorescence. *Macromolecules* **2016**, *49*, 353-361.

30. Duhamel, J.; Kanagalingam, S.; O'Brien, T.; Ingratta, M. Side-Chain Dynamics of an α–Helical Polypeptide Monitored by Fluorescence. *J. Am. Chem. Soc.* **2003**, *125*, 12810-12822.

31. Ingratta, M.; Duhamel, J. Effect of Side-chain Length on the Side-chain Dynamics of α–Helical Poly(*L*-glutamic acid) as Probed by a Fluorescence Blob Model. *J. Phys. Chem. B* **2008**, *112*, 9209-9218.

32. Seetharam, K.; Bertoft, E. Perspectives on the History of Research on Starch. Part V: On the Conceptualization of the Amylopectin Structure. *Starch* **2013**, *65*, 1-7.

33. Imberty, A.; Chanzy, H.; Pérez, S.; Bulèon, A.; Tran, V. The Double-Helical Nature of the Crystalline Part of A-starch. *J. Mol. Biol.* **1988**, 201, 365-378.

34. Casier, R.; Duhamel, J. Pyrene Excimer Fluorescence as a Direct and Easy Experimental Means to Characterize the Length Scale and Dynamics of Polypeptide Foldons. *Macromolecules* **2018**, *51*, 3450-3457.

35. Nishiyama, Y.; Mazeau, K.; Morin, M.; Cardoso, M. B.; Chanzy, H.; Putaux, J.-L. Molecular and Crystal Structure of 7-Fold V-Amylose Complexed with 2-Propanol. *Macromolecules* **2010**, 43, 8628-8636.

36. Pérez, S.; Bertoft, E. The Molecular Structures of Starch Components and their Contribution to the Architecture of Starch Granules: A Comprehensive Review. *Starch* **2010**, *62*, 389-420.

37. Callaghan, P. T.; Lelievre, J. The Size and Shape of Amylopectin: A Study Using Pulsed-Field Gradient Nuclear Magnetic Resonance. *Biopolymers* **1985**, *24*, 441-460.

38. Callaghan, P. T.; Lelievre, J. The Influence of Polymer Size and Shape on Self-Diffusion of Polysaccharides and Solvents. *Anal. Chim. Acta* **1986**, *189*, 145-166.

39. Durrani, C. M.; Donald, A. M. Shape, Molecular Weight Distribution and Viscosity of Amylopectin in Dilute Solution. *Carbohydr. Polym.* **2000**, *41*, 207-217.

40. Rojas, C. C.; Wahlund, K.-G.; Bergenstähl, B.; Nilsson, L. Macromolecular Geometries Determined with Field-Flow Fractionation and their Impact on the Overlap Concentration. *Biomacromolecules* **2008**, *9*, 1684-1690.

41. Dintzis, F. R.; Bagley, E. B.; Fekler, F. C. Shear-Thickening and Flow-Induced Structure in a System of DMSO Containing Waxy Maize Starch. *J. Rheol.* **1995**, *39*, 1399-1409.

42. Dintzis, F. R.; Berhow, M. A.; Bagley, E. B.; Wu, Y. V.; Felker, F. C. Shear-Thickening Behavior and Shear-Induced Structure in Gently Solubilized Starches. *Carbohydrates* **1996**, *73*, 638-643.

43. Chamberlain, E. K.; Rao, M. A. Rheological Properties of Acid Converted Waxy Maize Starches in Water and 90% DMSO/10% Water. *Carbohydr. Polym.* **1999**, *40*, 251-260.

44. Kapoor, B.; Bhattacharya, M. Dyanmic and Extensional Properties of Starch in Aqueous Dimethylsulfoxide. *Carbohydr. Polym.* **2000**, *42*, 323-335.

45. Kapoor, B.; Bhattacharya, M. Steady-Shear and Transient Properties of Starch in Dimethyl Sulfoxide. *Carbohydr. Polym.* **2001**, *44*, 217-231.

46. Ptaszek, A.; Ptaszek, P.; Dziubinski, M.; Grzesik, N. M.; Liszka-Skoczylas, M. The Effect of Structural Properties on Rheological Behavior of Starches in Binary Dimethyl Sulfoxide-Water Solutions. *PLoS One* **2017**, *12*, e0171109.

47. Millard, M. M.; Dintzis, F. R.; Willett, J. L.; Klavons, J. A. Light-Scattering Molecular Weights and Intrinsic Viscosities of Processed Waxy Maize Starch in 90% Dimethyl Sulfoxide and H_2O. *Carbohydrates* **1997**, *74*, 687-691.

48. Ma, Z.; Zhao, S.; Cheng, K.; Zhang, X.; Xu, X.; Zhang, L. Molecular Weight and Chain Conformation of Amylopectin from Rice Starch. *J. Appl. Polym. Sci.* **2007**, *104*, 3124-3128.

49. Flory, J. P. Principles of Polymer Chemistry. Cornell University Press, Ithaca, 1953.

Chapter 4

1. Le Corre, D.; Bras, J.; Dufresne, A. Starch Nanoparticles: A Review. *Biomacromolecules* **2010**, *11*, 1139-1153.

2. Giezen Franciscus, E.; Jongboom Remigius Oene, J.; Feil, H.; Gotlieb Kornelis, F.; Boersma, A. Biopolymer Nanoparticles. US 6677386 B1, 2001/10/24, 2004.

3. Pei, X.; Tan, Y.; Xu, K.; Liu, C.; Lu, C.; Wang, P. Pickering Polymerization of Styrene Stabilized by Starch-Based Nanospheres. *Polym. Chem.* **2016**, *7*, 3325-3333.

4. Ye, F.; Miao, M.; Lu, K.; Jiang, B.; Li, X.; Cui, S. W. Structure and Physicochemical Properties for Modified Starch-Based Nanoparticle from Different Maize Varieties. *Food Hydrocoll.* **2017**, *67*, 37-44.

5. Simi, C. K.; Emilia Abraham, T. Hydrophobic Grafted and Cross-Linked Starch Nanoparticles for Drug Delivery. *Bioproc. Biosyst. Eng.* **2007**, *30*, 173-180.

6. Pei, X.; Zhai, K.; Tan, Y.; Xu, K.; Lu, C.; Wang, P.; Wang, T.; Chen, C.; Tao, Y.; Dai, L.; Li, H. Synthesis of Monodisperse Starch-Polystyrene Core-Shell Nanoparticles via Seeded Emulsion Polymerization without Stabilizer. *Polymer* **2017**, *108*, 78-86.

7. Kim, D.; Amos, R.; Gauthier, M.; Duhamel, J. Applications of Pyrene Fluorescence to the Characterization of Hydrophobically Modified Starch Nanoparticles. *Langmuir* **2018**, *34*, 8611-8621.

8. Kim, D.; Amos, R.; Gauthier, M.; Duhamel, J. Assemblies of Hydrophobically Modified Starch Nanoparticles Probed by Surface Tension and Pyrene Fluorescence. In *Nanoparticle and Molecular Assemblies*, Nagarajan, R., Ed. ACS Book: 2020.

9. Kaufman, R. C.; Wilson, J. D.; Bean, S. R.; Herald, T. J.; Shi, Y. C. Development of a 96-well Plate Iodine Binding Assay for Amylose Content Determination. *Carbohydr. Polym.* **2015**, *115*, 444-447.

10. Zhu, T.; Jackson, D.; Wehling, R.; Geera, B. Comparison of Amylose Determination Methods and the Development of a Dual Wavelength Iodine Binding Technique *Cereal Chem.* **2008**, *85*, 51-58.

11. Mathew, A. K.; Siu, H.; Duhamel, J. A Blob Model to Study Chain Folding by Fluorescence. *Macromolecules* **1999**, *32*, 7100-7108.

12. Duhamel, J. Polymer Chain Dynamics in Solution Probed with a Fluorescence Blob Model. *Acc. Chem. Res.* **2006**, *39*, 953-960.

13. Li, L.; Duhamel, J. Conformation of Pyrene-Labeled Amylose in DMSO Characterized with the Fluorescence Blob Model. *Macromolecules* **2016**, *49*, 7965-7974.

14. Tizzotti, M. J.; Sweedman, M. C.; Tang, D.; Schaefer, C.; Gilbert, R. G. New 1H NMR Procedure for the Characterization of Native and Modified Food-Grade Starches. *J. Agric. Food. Chem.* **2011**, *59*, 6913-6919.

15. Ross, S. A.; Lowe, G. Downfield Displacement of the NMR Signal of Water in Deuterated Dimethylsulfoxide by the Addition of Deuterated Trifluoroacetic Acid. *Tetrahedron Lett.* **2000**, *41*, 3225-3227.

16. Tomasik, P.; Schilling, C. H., Complexes of Starch with Inorganic Guests. In *Adv. Carbohydr. Chem. Biochem.*, Horton, D., Ed. Academic Press: 1998; Vol. 53, pp 263-343.

17. Hirai, M.; Hirai, T.; Ueki, T. Effect of Branching of Amylopectin on Complexation with Iodine as Steric Hindrance. *Polymer* **1994**, *35*, 2222-2225.

18. Millard, M. M.; Dintzis, F. R.; Willett, J. L.; Klavons, J. A. Light-Scattering Molecular Weights and Intrinsic Viscosities of Processed Waxy Maize Starches in 90% Dimethyl Sulfoxide and H_2O. *Cereal Chem.* **1997**, *74*, 687-691.

19. Nishiyama, Y.; Mazeau, K.; Morin, M.; Cardoso, M. B.; Chanzy, H.; Putaux, J.-L. Molecular and Crystal Structure of 7-Fold V-Amylose Complexed with 2-Propanol. *Macromolecules* **2010**, *43*, 8628-8636.

20. Imberty, A.; Chanzy, H.; Pérez, S.; Bulèon, A.; Tran, V. The Double-Helical Nature of the Crystalline Part of A-Starch. *J. Mol. Biol.* **1988**, *201*, 365-378.

21. Bastide, J.; Candau, S.; Leibler, L. Osmotic Deswelling of Gels by Polymer Solutions. *Macromolecules* **1981**, *14*, 719-726.

22. Inomata, H.; Nagahama, K.; Saito, S. Measurement and Correlation of the Swelling Pressure of *N*-Isopropylacrylamide Gel. *Macromolecules* **1994**, *27*, 6459-6464.

23. Nagahama, K.; Inomata, H.; Saito, S. Measurement of Osmotic-Pressure in Aqueous-Solutions of Poly(Ethylene Glycol) and Poly(*N*-Isopropylacrylamide). *Fluid Phase Equilib.* **1994**, *96*, 203-214.

24. Ishidao, T.; Akagi, M.; Sugimoto, H.; Iwai, Y.; Arai, Y. Swelling Behaviors of Poly(*N*-Isopropylacrylamide) Gel in Poly(Ethylene Glycol) - Water Mixtures. *Macromolecules* **1993**, *26*, 7361-7362.

25. Ishidao, T.; Akagi, M.; Sugimoto, H.; Onoue, Y.; Iwai, Y.; Arai, Y. Swelling Equilibria of Poly(*N*-Isopropylacrylamide) Gel in Aqueous Polymer-Solutions. *Fluid Phase Equilib.* **1995**, *104*, 119-129.

26. Saunders, B. R.; Vincent, B. Thermal and Osmotic Deswelling of Poly(NIPAM) Microgel Particles. *J. Chem. Soc. Faraday T.* **1996**, *92*, 3385-3389.

27. Flory, P. J., *Principles of Polymer Chemistry*. Cornell University Press, Ithaca, 1953.

28. Ling, K.; Jiang, H.; Zhang, Q. A Colorimetric Method for the Molecular Weight Determination of Polyethylene Glyocol using Gold Nanoparticles. *Nanoscale Res. Lett.* **2013**, *8*, 538.

29. Perez, S.; Bertoft, E. The Molecular Structures of Starch Components and Their Contribution to the Architecture of Starch Granules: A Comprehensive Review. *Starch/Stärke* **2010**, *62*, 389-420.

30. Bloembergen, S.; Vanegdom, E.; Wildi, R.; McLennan, I. J.; Lee, D. I.; Klass, C. P.; Leeuwen, J. Biolatex Binders for Paper and Paperboard Applications. *J. Pulp Pap. Sci.* **2010**, *36*, 151-161.

Chapter 5

1. Sjöö, M.; Nilsson, L. *Starch in Food: Structure, Function and Applications: Second Edition*. 2017; p 1-893.

2. Hancock, R. D.; Tarbet, B. J. The Other Double Helix—The Fascinating Chemistry of Starch. *J. Chem. Educ.* **2000**, *77*, 988.

3. Ostrander, B. M., Maize Starch for Industrial Applications. In *Industrial Crops: Breeding for BioEnergy and Bioproducts*, Cruz, V. M. V.; Dierig, D. A., Eds. Springer New York: New York, 2015; pp 171-189.

4. Beeren, S. R.; Hindsgaul, O. Nature's Dendrimer: Characterizing Amylopectin as a Multivalent Host. *Angew. Chem. Int. Edit.* **2013**, *52*, 11265-11268.

5. Duhamel, J. New Insights in the Study of Pyrene Excimer Fluorescence to Characterize Macromolecules and their Supramolecular Assemblies in Solution. *Langmuir* **2012**, *28*, 6527-38.

6. Mathew, A.; Siu, H.; Duhamel, J. A Blob Model To Study Chain Folding by Fluorescence. *Macromolecules* **1999**, *32*.

7. Le Corre, D.; Bras, J.; Dufresne, A. Starch Nanoparticles: A Review. *Biomacromolecules* **2010**, *11*, 1139-1153.

8. Nakanishi, Y.; Norisuye, T.; Teramoto, A.; Kitamura, S. Conformation of Amylose in Dimethyl Sulfoxide. *Macromolecules* **1993**, *26*, 4220-4225.

9. Ingratta, M.; Duhamel, J. Effect of Side-Chain Length on the Side-Chain Dynamics of α–Helical Poly(*L*-glutamic acid) as Probed by a Fluorescence Blob Model. *J. Phys. Chem. B* **2008**, *112*, 9209-9218.

10. Duhamel, J.; Kanagalingam, S.; O'Brien, T. J.; Ingratta, M.W. Side-Chain Dynamics of an alpha-Helical Polypeptide Monitored by Fluorescence. *J. Am. Chem. Soc* **2003**, *125*, 12810-12822.

11. Giezen Franciscus, E.; Jongboom Remigius Oene, J.; Feil, H.; Gotlieb Kornelis, F.; Boersma, A. Biopolymer Nanoparticles. US 6677386 B1, 2001/10/24, 2004.

12. Zhu, T.; Jackson, D.; Wehling, R.; Geera, B. Comparison of Amylose Determination Methods and the Development of a Dual Wavelength Iodine Binding Technique 1. *Cereal Chem.* **2008**, *85*, 51-58.

13. Meléndez-Hevia, E.; Meléndez, R.; Canela, E. I., Glycogen Structure: an Evolutionary View. In *Technological and Medical Implications of Metabolic Control Analysis*, Cornish-Bowden, A.; Cárdenas, M. L., Eds. Springer Netherlands: Dordrecht, 2000; pp 319-326.

14. Bajpai, P., Chapter 3 - Structure and Properties of Cellulose and Nanocellulose. In *Pulp and Paper Industry*, Bajpai, P., Ed. Elsevier: 2017; pp 27-40.

15. Abhilash, M.; Thomas, D., 15 - Biopolymers for Biocomposites and Chemical Sensor Applications. In *Biopolymer Composites in Electronics*, Sadasivuni, K. K.; Ponnamma, D.; Kim, J.; Cabibihan, J. J.; AlMaadeed, M. A., Eds. Elsevier: 2017; pp 405-435.

Appendices

Chapter 2

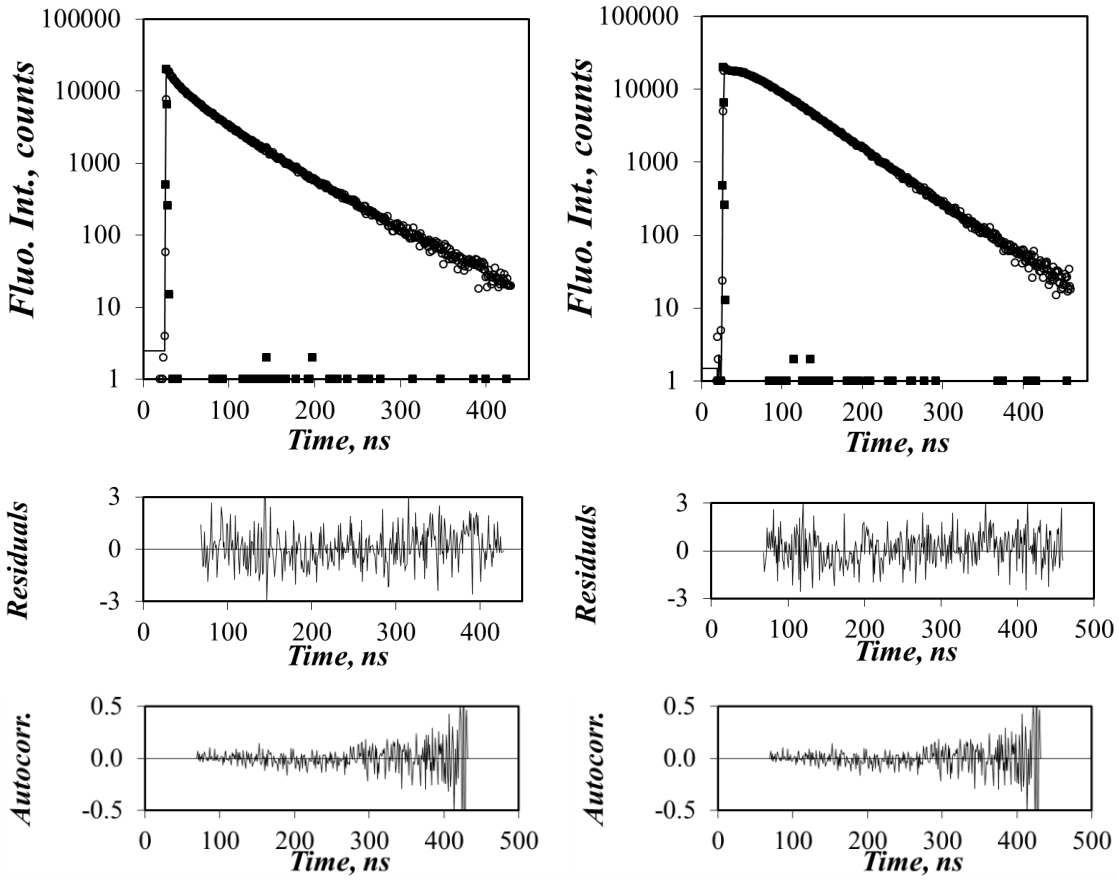

Figure S2.1. Monomer (left, λ_{em} = 375 nm) and excimer (right, λ_{em} = 510 nm) fluorescence decays of amylose labeled with 10 mol% pyrene in DMSO. The decays were analyzed globally using Equations 2.3 and 2.4; [Py] = 2.5×10^{-6} M, λ_{ex} = 346 nm, χ^2 = 1.15

Table S2.1. Parameters retrieved from the global FBM analysis of the monomer decays of Py-Amylose (aerated and degassed), and Py-PMA (aerated) in DMSO with Equation 2.3.

Sample	mol%	f_{Mdiff}	f_{Mfree}	k_{blob} ($10^7 s^{-1}$)	<n>	f_{k2}	$k_e[blob]$ ($10^7 s^{-1}$)	$\chi 2$
Amylose(aerated)	5.1	0.70	0.16	0.02	0.51	0.13	0.0080	1.13
	5.6	0.72	0.14	0.02	0.54	0.14	0.0072	1.18
	5.6	0.75	0.10	0.02	0.58	0.15	0.0071	1.12
	7.5	0.80	0.01	0.01	0.79	0.19	0.0063	1.17
	10.1	0.74	0.02	0.02	1.16	0.24	0.0071	1.15
	14.9	0.69	0.02	0.02	1.52	0.29	0.0087	1.23
Amylose(degassed)	5.1	0.74	0.12	0.02	0.54	0.14	0.0075	1.11
	5.6	0.72	0.12	0.02	0.59	0.16	0.0068	1.10
	5.6	0.76	0.07	0.01	0.72	0.17	0.0063	1.23
	7.5	0.73	0.06	0.01	0.93	0.21	0.0136	1.16
	10.1	0.70	0.02	0.01	1.43	0.28	0.0058	1.17
	14.9	0.61	0.03	0.01	1.74	0.36	0.0135	1.17
PMA (aerated)	1.7	0.74	0.15	0.01	0.77	0.10	0.0080	1.15
	2.6	0.79	0.06	0.01	1.16	0.15	0.0079	1.10
	2.6	0.81	0.02	0.01	1.26	0.17	0.0066	1.12
	6.2	0.68	0.00	0.01	2.57	0.32	0.0034	1.20
	6.7	0.62	0.00	0.01	2.87	0.38	0.0035	1.20
PMA (degassed)	1.7	0.75	0.13	0.01	0.82	0.11	0.0065	1.05
	2.6	0.78	0.05	0.01	1.28	0.14	0.0061	1.08
	2.6	0.77	0.04	0.01	1.40	0.19	0.0063	1.13
	6.2	0.61	0.01	0.01	2.73	0.38	0.0047	1.09
	6.7	0.57	0.01	0.01	3.17	0.43	0.0031	1.08

Table S2.2. Parameters retrieved from the global FBM analysis of the excimer decays of Py-Amylose (aerated and degassed), and Py-PMA (aerated) in DMSO with Equation 2.4.

Sample	mol%	τ_E	f_{Ediff}	f_{EES}	f_{Ek2}	f_{EE0}	χ^2
Amylose (aerated)	5.1	50	0.56	0.24	0.11	0.085	1.13
	5.6	50	0.53	0.27	0.11	0.088	1.18
	5.6	51	0.57	0.21	0.11	0.110	1.12
	7.5	47	0.53	0.23	0.13	0.106	1.17
	10.1	46	0.47	0.22	0.16	0.155	1.15
	14.9	44	0.47	0.13	0.20	0.197	1.23
Amylose (degassed)	5.1	58	0.53	0.27	0.10	0.095	1.11
	5.6	59	0.51	0.28	0.11	0.090	1.10
	5.6	57	0.51	0.27	0.11	0.104	1.23
	7.5	55	0.48	0.25	0.14	0.125	1.16
	10.1	54	0.43	0.24	0.17	0.159	1.17
	14.9	52	0.38	0.20	0.22	0.195	1.17
PMA (aerated)	1.7	44	0.86		0.12	0.020	1.15
	2.6	41	0.83		0.16	0.018	1.10
	2.6	41	0.81		0.17	0.017	1.12
	6.2	40	0.66		0.31	0.036	1.20
	6.7	40	0.58		0.35	0.064	1.20
PMA (degassed)	1.7	52	0.85		0.13	0.024	1.05
	2.6	49	0.80		0.18	0.022	1.08
	2.6	49	0.78		0.20	0.021	1.13
	6.2	47	0.59		0.37	0.040	1.09
	6.7	48	0.53		0.40	0.076	1.08

Table S2.3. Fractions of all pyrene species for Py-Amylose and Py-PMA, calculated from f_{Mdiff}, f_{Mfree}, f_{Ediff}, f_{Ek2}, and f_{EE0}.

Sample	mol%	f_{diff}	f_{free}	f_{E0}	f_{k2}
Amylose (aerated)	5.1	0.64	0.15	0.10	0.12
	5.6	0.64	0.12	0.11	0.13
	5.6	0.65	0.09	0.13	0.13
	7.5	0.69	0.01	0.14	0.17
	10.1	0.59	0.02	0.19	0.20
	14.9	0.53	0.02	0.22	0.23
Amylose (degassed)	5.1	0.65	0.10	0.12	0.13
	5.6	0.65	0.11	0.11	0.13
	5.6	0.66	0.06	0.13	0.15
	7.5	0.61	0.05	0.16	0.18
	10.1	0.55	0.02	0.20	0.22
	14.9	0.47	0.02	0.24	0.28
PMA (aerated)	1.7	0.73	0.15	0.02	0.10
	2.6	0.78	0.06	0.02	0.15
	2.6	0.80	0.02	0.02	0.16
	6.2	0.66	0.00	0.04	0.31
	6.7	0.58	0.00	0.06	0.35
PMA (degassed)	1.7	0.74	0.13	0.02	0.11
	2.6	0.76	0.05	0.02	0.17
	2.6	0.75	0.04	0.02	0.19
	6.2	0.59	0.01	0.04	0.36
	6.7	0.52	0.01	0.08	0.39

Chapter 3

Table S3.1. Parameters retrieved from the global FBM analysis of the monomer decays of Py-Amylopectin and Py-Amylose in DMSO.

Sample	mol%	f_{Mdiff}	f_{Mfree}	k_{blob} ($\times 10^7 s^{-1}$)	$<n>$	f_{k2}	$k_e[blob]$ ($\times 10^6 s^{-1}$)	$\chi 2$
Amylose τ_M = 89.5 ns $k_2 = 2.0\times10^8\ s^{-1}$	5.1	0.71	0.17	2.19	0.51	0.13	8.08	1.15
	5.6	0.73	0.13	1.89	0.53	0.14	6.93	1.19
	5.6	0.74	0.10	1.76	0.58	0.16	7.09	1.12
	7.5	0.78	0.04	1.53	0.81	0.19	6.88	1.16
	10.1	0.74	0.02	1.58	1.16	0.24	7.24	1.14
	14.9	0.70	0.02	1.66	1.45	0.28	9.43	1.21
Amylopectin τ_M =92 ns $k_2 = 2.7\times10^8\ s^{-1}$	4.1	0.84	0.03	1.63	0.77	0.13	10.07	1.12
	5.7	0.80	0.03	1.61	0.99	0.16	9.16	1.13
	8.7	0.74	0.01	1.25	1.96	0.26	8.73	1.01
	9.6	0.74	0.00	1.12	2.14	0.26	7.84	1.12
	12.0	0.68	0.01	1.22	2.49	0.31	8.79	1.16

Table S3.2. Parameters retrieved from the global FBM analysis of the excimer decays of aerated and degassed solutions of Py-Amylose and Py-Pmylopectin in DMSO with Equation 3.3. τ_{ES} is fixed to equal 3.5 ns in the analysis.

Sample	mol%	τ_E	f_{Ediff}	f_{EES}	f_{Ek2}	f_{EE0}	$\chi 2$
Amylose τ_M = 89.5 ns $k_2 = 2.0\times10^8\ s^{-1}$	5.1	50	0.56	0.24	0.11	0.090	1.15
	5.6	50	0.54	0.27	0.11	0.085	1.19
	5.6	51	0.57	0.22	0.12	0.100	1.12
	7.5	47	0.53	0.23	0.13	0.112	1.16
	10.1	46	0.47	0.26	0.16	0.154	1.14
	14.9	44	0.47	0.15	0.19	0.189	1.21
Amylopectin τ_M =92 ns $k_2 = 2.7\times10^8\ s^{-1}$	4.1	47	0.63	0.18	0.093	0.097	1.12
	5.7	46	0.58	0.19	0.11	0.11	1.13
	8.7	57	0.50	0.19	0.12	0.108	1.14
	9.6	55	0.50	0.26	0.13	0.108	1.13
	12.0	53	0.45	0.24	0.15	0.140	1.17

Table S3.3. Fractions of all pyrene species aerated solutions of Py-Amylopectin and Py-Amylose in DMSO calculated from f_{Mdiff}, f_{Mfree}, f_{Ediff}, f_{Ek2}, and f_{EE0}.

Sample	mol%	f_{diff}	f_{free}	f_{E0}	f_{k2}
Amylose (aerated) τ_M = 89.5 ns $k_2 = 2.0\times10^8\ s^{-1}$	5.1	0.64	0.15	0.10	0.12
	5.6	0.64	0.12	0.11	0.13
	5.6	0.65	0.09	0.13	0.13
	7.5	0.69	0.01	0.14	0.17
	10.1	0.59	0.02	0.19	0.20
	14.9	0.53	0.02	0.22	0.23
Py-Amylopectin (aerated) τ_M = 92 ns $k_2 = 2.7\times10^8\ s^{-1}$	4.1	0.743	0.031	0.116	0.111
	5.7	0.695	0.030	0.135	0.141
	8.7	0.619	0.001	0.164	0.216
	9.6	0.606	0.000	0.174	0.219
	12.0	0.552	0.001	0.194	0.254

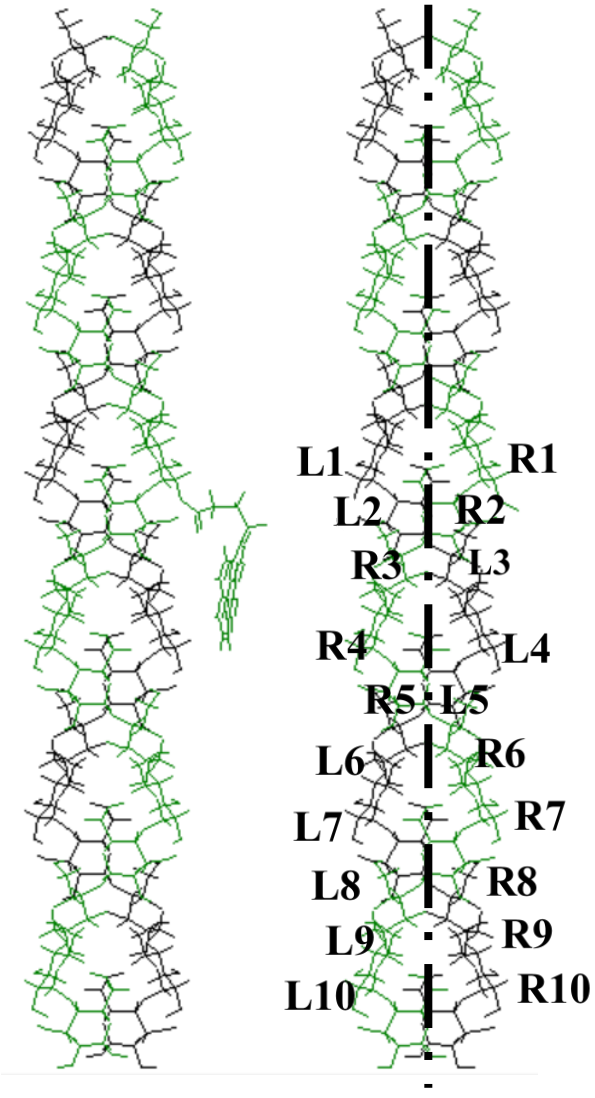

Figure S3.1. Assignment of the position of glucose residue along the double helix. The pyrene group is attached to the 7th glucose residue on the right strand of the double helix. This position is assigned as Position R1.

Table S3.4A. Number of overlapping carbons between the frame of the reference pyrene attached to double Helix #0 and that of a second pyrenyl label attached to double Helix #1 for $d_{h\text{-}h}$ values between 16 and 26 Å with the total number of residues ΔN_{blob} allowing a pyrene-pyrene overlap with 7 or more carbon atoms.

$d_{h\text{-}h}$ (Å)	16 Å		18 Å		20 Å		22 Å		24 Å		26 Å	
Position	(L)	(R)	(L)	(R)	(L)	(R)	(L)	(R)	(L)	(R)	(L)	(R)
1	0	8	0	9	0	8	0	9	0	8	0	8
2	5	6	6	9	0	10	1	9	0	8	0	6
3	8	2	7	2	9	4	8	3	7	2	6	2
4	9	0	8	0	8	0	8	0	8	0	7	0
5	6	4	6	5	4	2	3	2	2	1	2	1
6	4	2	3	3	3	2	2	1	1	0	1	0
7	0	0	0	0	0	0	0	0	0	0	0	0
8	0	0	0	0	0	0	0	0	0	0	0	0
9	0	0	0	0	0	0	0	0	0	0	0	0
10	0	0	0	0	0	0	0	0	0	0	0	0
ΔN_{blob}	**7**		**7**		**7**		**7**		**7**		**3**	

Table S3.3B. Number of overlapping carbons between the frame of the reference pyrene attached to double Helix #0 and that of a second pyrenyl label attached to double Helix #1 for $d_{h\text{-}h}$ values between 28 and 38 Å with the total number of residues ΔN_{blob} allowing a pyrene-pyrene overlap with 7 or more carbon atoms.

$d_{h\text{-}h}$ (Å)	28 Å		30 Å		32 Å		34 Å		36 Å		38 Å	
Position	(L)	(R)	(L)	(R)	(L)	(R)	(L)	(R)	(L)	(R)	(L)	(R)
1	0	8	0	6	0	5	0	3	0	1	0	0
2	0	6	0	2	0	0	0	0	0	0	0	0
3	3	0	1	0	0	0	0	0	0	0	0	0
4	6	0	6	0	5	4	2	0	0	0	0	0
5	2	1	2	1	1	0	0	0	0	0	0	0
6	0	0	0	0	0	0	0	0	0	0	0	0
7	0	0	0	0	0	0	0	0	0	0	0	0
8	0	0	0	0	0	0	0	0	0	0	0	0
9	0	0	0	0	0	0	0	0	0	0	0	0
10	0	0	0	0	0	0	0	0	0	0	0	0
ΔN_{blob}	**1**		**0**		**0**		**0**		**0**		**0**	

Table S3.4A. Number of overlapping carbons between the frame of the reference pyrene attached to double Helix #0 and that of a second pyrenyl label attached to double Helix #2 for $d_{h\text{-}h}$ values between 16 and 26 Å with the total number of residues ΔN_{blob} allowing a pyrene-pyrene overlap with 7 or more carbon atoms.

$d_{h\text{-}h}$ (Å)	16 Å		18 Å		20 Å		22 Å		24 Å		26 Å	
Position	(L)	(R)	(L)	(R)	(L)	(R)	(L)	(R)	(L)	(R)	(L)	(R)
1	0	9	0	9	0	9	0	9	0	8	0	8
2	8	5	6	6	4	6	3	5	2	5	0	3
3	8	0	7	0	8	0	8	0	6	0	5	0
4	7	0	8	0	8	0	8	0	7	0	5	0
5	0	3	0	0	0	0	0	0	0	0	0	0
6	0	0	0	0	0	0	0	0	0	0	0	0
7	0	0	0	0	0	0	0	0	0	0	0	0
8	0	0	0	0	0	0	0	0	0	0	0	0
9	0	0	0	0	0	0	0	0	0	0	0	0
10	0	0	0	0	0	0	0	0	0	0	0	0
ΔN_{blob}	**5**		**5**		**5**		**5**		**3**		**1**	

Table S3.4B. Number of overlapping carbons between the frame of the reference pyrene attached to double Helix #0 and that of a second pyrenyl label attached to double Helix #2 for $d_{h\text{-}h}$ values between 28 and 38 Å with the total number of residues ΔN_{blob} allowing a pyrene-pyrene overlap with 7 or more carbon atoms.

$d_{h\text{-}h}$ (Å)	28 Å		30 Å		32 Å		34 Å		36 Å		38 Å	
Position	(L)	(R)	(L)	(R)	(L)	(R)	(L)	(R)	(L)	(R)	(L)	(R)
1	0	6	0	5	0	4	0	2	0	0	0	0
2	0	1	0	1	0	0	0	0	0	0	0	0
3	3	0	1	0	0	0	0	0	0	0	0	0
4	4	0	3	0	1	0	0	0	0	0	0	0
5	0	0	0	0	0	0	0	0	0	0	0	0
6	0	0	0	0	0	0	0	0	0	0	0	0
7	0	0	0	0	0	0	0	0	0	0	0	0
8	0	0	0	0	0	0	0	0	0	0	0	0
9	0	0	0	0	0	0	0	0	0	0	0	0
10	0	0	0	0	0	0	0	0	0	0	0	0
ΔN_{blob}	**0**		**0**		**0**		**0**		**0**		**0**	

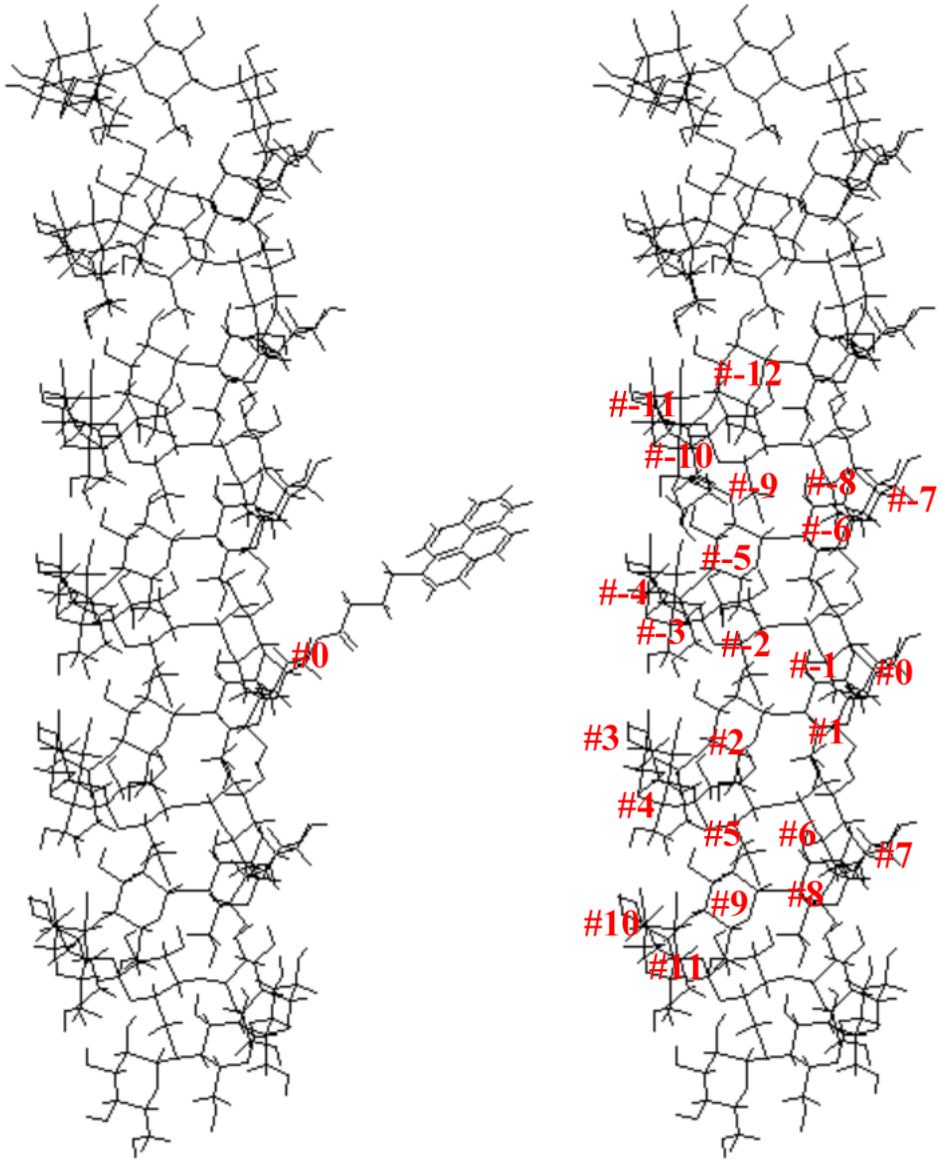

Figure S3.2. Assignment of the position of glucose residue along a single helix. The pyrene group is attached to the 26th glucose residue which referred as position #0.

Table S3.5A. Number of overlapping carbons between the frame of the reference pyrene attached to single Helix #0 and that of a second pyrenyl label attached to single Helix #1 for $d_{h\text{-}h}$ values between 16 and 38 Å with the total number of residues ΔN_{blob} allowing a pyrene-pyrene overlap with 7 or more carbon atoms.

$d_{h\text{-}h}$ (Å) / position	16 Å	18 Å	20 Å	22 Å	24 Å	26 Å	28 Å	30 Å	32 Å	34 Å	36 Å	38 Å
–11	6	5	5	4	3	3	0	0	0	0	0	0
–10	8	8	8	8	8	9	8	5	3	1	0	0
–9	8	8	7	8	7	8	5	3	1	0	0	0
–8	6	6	5	4	3	3	0	0	0	0	0	0
–7	4	2	2	1	1	0	0	0	0	0	0	0
–6	3	2	2	1	1	0	0	0	0	0	0	0
–5	5	5	4	3	3	3	3	2	1	0	0	0
–4	8	8	8	8	8	8	8	4	3	2	0	0
–3	9	8	9	8	9	8	9	9	7	4	2	0
–2	8	8	8	8	8	8	8	7	5	3	1	0
–1	6	5	6	4	4	3	3	0	0	0	0	0
0	2	2	2	1	1	0	0	0	0	0	0	0
1	3	2	2	1	1	0	0	0	0	0	0	0
2	5	5	4	4	3	3	2	0	0	0	0	0
3	8	8	8	8	8	8	8	3	1	0	0	0
4	9	9	8	9	9	9	9	9	8	6	4	0
5	8	8	8	8	8	8	8	8	6	4	2	0
6	6	6	6	5	5	5	5	5	4	2	0	0
7	2	2	2	1	1	1	0	0	0	0	0	0
8	3	2	2	1	1	0	0	0	0	0	0	0
9	5	5	4	2	2	1	0	0	0	0	0	0
10	5	5	5	5	5	3	1	1	0	0	0	0
11	8	8	8	8	8	8	8	6	4	2	1	0
12	5	8	8	8	8	7	6	4	2	0	0	0
ΔN_{blob}	*****	**10**	**10**	**10**	**10**	**10**	**8**	**4**	**2**	**0**	**0**	**0**

* Helices were too close

Table S3.5B. Number of overlapping carbons between the frame of the reference pyrene attached to single Helix #0 and that of a second pyrenyl label attached to single Helix #2 for $d_{h\text{-}h}$ values between 16 and 38 Å with the total number of residues ΔN_{blob} allowing a pyrene-pyrene overlap with 7 or more carbon atoms.

$d_{h\text{-}h}$ (Å) / position	16 Å	18 Å	20 Å	22 Å	24 Å	26 Å	28 Å	30 Å	32 Å	34 Å	36 Å	38 Å
–11	0	2	0	1	1	0	0	0	0	0	0	0
–10	0	7	7	8	7	5	3	3	0	0	0	0
–9	7	7	9	7	7	5	3	3	0	0	0	0
–8	6	6	5	4	4	4	2	1	0	0	0	0
–7	2	2	2	1	1	0	0	0	0	0	0	0
–6	3	2	2	1	1	0	0	0	0	0	0	0
–5	5	5	4	4	3	2	0	0	0	0	0	0
–4	0	5	4	5	6	5	3	0	0	0	0	0
–3	5	4	7	7	8	8	7	5	3	1	0	0
–2	6	8	9	9	8	9	7	6	3	0	0	0
–1	6	6	6	6	6	5	4	4	2	0	0	0
0	5	5	5	4	4	2	2	2	0	0	0	0
1	3	2	2	1	1	1	0	0	0	0	0	0
2	2	1	1	1	1	1	0	0	0	0	0	0
3	1	2	5	6	7	3	2	1	0	0	0	0
4	5	6	4	7	8	7	7	5	3	2	0	0
5	0	8	8	8	8	8	8	0	0	0	0	0
6	6	5	5	5	5	4	4	0	0	0	0	0
7	4	4	4	3	3	2	1	0	0	0	0	0
8	0	0	0	0	0	0	0	0	0	0	0	0
9	0	0	0	0	0	0	0	0	0	0	0	0
10	0	0	4	3	3	3	0	0	0	0	0	0
11	0	7	7	7	6	3	2	0	0	0	0	0
12	0	7	7	7	7	6	3	0	0	0	0	0
ΔN_{blob}	*****	**6**	**7**	**8**	**8**	**4**	**4**	**0**	**0**	**0**	**0**	**0**

* Helices were too close

Parameters retrieved from the fits of the N_{blob}-vs-$d_{h–h}$ profiles in Figure 3.10

Table S3.6A. Parameters retrieved from fitting the N_{blob}-*vs*-$d_{h–h}$ trend obtained with a hexagonal array of 7 double helices with Equation 3.3.

Parameter	Value	Error
A_1	28.7	0.3
A_2	10.9	0.3
x_o	25.0	0.1
p	24.3	2.6

Table S3.6B. Parameters retrieved from fitting the N_{blob}-*vs*-d_{h-h} trend obtained with a hexagonal array of 7 single helices with Equation 3.3.

Parameter	Value	Error
A_1	35.2	1.1
A_2	10.7	1.3
x_o	28.4	0.4
p	21.6	6.3

Table S3.6C. Parameters retrieved from fitting the N_{blob}-*vs*-d_{h-h} trend averaged for the hexagonal array of 7 single and 7 double helices with Equation 3.3.

Parameter	Value	Error
A_1	31.8	0.8
A_2	10.8	0.8
x_o	26.9	0.3
p	17.3	3.5

Chapter 4

Validation of the purification method: The objective of this experiment was to investigate whether precipitation was sufficient to purify the NAFs. DLS and intrinsic viscosity measurements were completed by Chengmeng Sun from the Duhamel group under my direct supervision. NAF14 was first purified by precipitation to yield pNAF14. DLS and intrinsic viscosity measurements were first conducted using pNAF14. The intrinsic viscosity measurements were repeated to obtain the error bars. This sample was dissolved in Milli-Q water at a concentration of 2% w/w. The dialysis membranes were immersed in Milli-Q water and dialysis was conducted for 5 days with stirring. The Milli-Q water was replaced twice a day. An aliquot (20 mL) of the solution was taken out of the tubing after 1, 2, 3 and 5 days, and precipitated in methanol dropwise. The product was then collected and dried in a vacuum oven overnight at 40 °C before measuring its [η] and D_h.

Table S4.1. D_h and [η] of unpurified NAF13 and NAF13 purified by precipitation followed by dialysis of 1, 2, 3 and 5 days.

	D_h (nm)	[η] (mL/g)
Unpurified NAF13	12.9 ± 0.7	
pNAF13	13.7 ± 0.9	25 ± 1
Day 1	11.5 ± 1.4	23
Day 2	12.3 ± 0.7	25
Day 3	11.3 ± 0.9	28
Day 5	12.3 ± 1.3	26

As shown in Table S4.1, additional dialysis ended up with products having similar [η] and D_h as pNAF13. This study confirmed that precipitation was sufficient to purify the NAFs.

Table S4.2. Summary of D_h, [η], and 2.5/[η] values for NAFs

	D_h (nm)	[η] (mL/g)	2.5/[η] (g/mL)
NAF57	56.8 ± 0.9	61	0.041
NAF47	47.4 ± 2.0	57	0.044
NAF28.7	28.7 ± 1.0	38	0.066
NAF28.8	28.8 ± 1.2	43	0.058
NAF24	24.3 ± 0.7	35	0.071
NAF23	22.9 ± 0.4	38	0.066
NAF20.6	20.6 ± 0.7	35	0.071
NAF20.3	20.3 ± 1.9	40	0.063
NAF18	18.1 ± 3.2	39	0.064
NAF17.3	17.3 ± 3.6	40	0.063
NAF17.2	17.2 ± 0.6	29	0.086
NAF17.1	17.1 ± 0.7	21	0.119
NAF15	14.8 ± 0.6	20	0.125
NAF14	13.9 ± 0.7	25	0.100
NAF12	12.1 ± 0.7	23	0.109
NAF11.8	11.7 ± 3.3	25	0.100
NAF11.7	11.8 ± 0.6	25	0.100
NAF11.5	11.5 ± 2.7	25	0.100
NAF8.3	8.3 ± 0.7	23	0.109
NAF7.0	7.0 ± 0.1	28	0.089
Degraded NAF57-37	37.4 ± 0.6	53	0.047
Degraded NAF57-22	21.5 ± 1.7	36	0.069
Degraded NAF57-16	16.0 ± 0.7	28	0.089

Table S4.3. Parameters retrieved from the FBM of the monomer decays of aerated and non-aerated solutions of Py-NAF8.3, Py-NAF20, and Py-NAF57 in DMSO.

Sample	mol%	f_{Mdiff}	f_{Mfree}	k_{blob} ($\times 10^7\ s^{-1}$)	$<n>$	f_{Mk2}	$k_e[blob]$ ($\times 10^6\ s^{-1}$)	χ^2
Py-NAF8.3	3.4	0.840	0.174	2.27	0.43	0.125	8.0	1.08
(aerated)	5.8	0.803	0.052	1.47	1.01	0.094	8.9	1.10
	7.6	0.740	0.019	1.43	1.18	0.217	7.0	1.19
τ_M = 92 ns	10.0	0.737	0.023	1.55	1.45	0.240	8.6	1.13
$k_2 = 2.5\times10^8\ s^{-1}$	12.0	0.684	0.008	1.38	1.60	0.262	7.4	1.10
Py-NAF20	8.8	0.75	0.01	1.27	1.63	0.24	8.3	1.27
(non-aerated)	10.4	0.76	0.01	1.36	1.75	0.24	9.9	1.23
	11.6	0.42	0.01	1.32	2.45	0.32	8.5	1.18
τ_M = 135 ns	12.4	0.67	0.01	1.42	2.59	0.32	9.3	1.32
$k_2 = 2.5\times10^8\ s^{-1}$	13.8	0.69	0.01	1.43	2.32	0.31	9.7	1.24
Py-NAF57	4.8	0.819	0.042	1.82	0.78	0.139	10.3	1.02
(aerated)	7.6	0.767	0.003	1.25	1.55	0.231	17.0	1.19
	8.0	0.760	0.000	1.25	1.57	0.240	6.8	1.24
τ_M = 92 ns	11.3	0.731	0.000	1.18	2.04	0.269	7.8	1.19
$k_2 = 2.1\times10^8\ s^{-1}$	13.2	0.676	0.002	1.30	2.29	0.322	10.5	1.14

Table S4.4. Parameters retrieved from the global FBM analysis of the excimer decays of aerated and non-aerated solutions of Py-NAF8.3, Py-NAF20, and Py-NAF57 in DMSO. τ_{ES} is fixed to 3.5 ns in the analysis.

Sample	mol%	τ_E (ns)	f_{Ediff}	f_{Ek2}	f_{EE0}	f_{EES}	χ^2
Py-NAF8.3 (aerated)	3.4	51.8	0.608	0.079	0.084	0.230	1.08
	5.8	46.3	0.526	0.156	0.095	0.222	1.10
τ_M = 92 ns	7.6	46.2	0.517	0.168	0.102	0.214	1.19
$k_2 = 2.5\times10^8\ s^{-1}$	10.0	45.9	0.466	0.170	0.141	0.223	1.13
	12.0	45.8	0.451	0.180	0.137	0.232	1.10
Py-NAF20	8.8	52	0.48	0.22	0.13	0.17	1.24
(non-aerated)	10.4	50	0.43	0.21	0.18	0.17	1.32
	11.6	52	0.43	0.21	0.15	0.20	1.18
τ_M = 135 ns	12.4	52	0.58	0.18	0.10	0.14	1.23
$k_2 = 2.5\times10^8\ s^{-1}$	13.8	54	0.55	0.17	0.11	0.17	1.27
Py-NAF57 (aerated)	4.8	47.5	0.594	0.101	0.097	0.209	1.02
	7.6	46.4	0.530	0.159	0.111	0.200	1.19
τ_M = 92 ns	8.0	45.6	0.528	0.167	0.112	0.194	1.24
$k_2 = 2.1\times10^8\ s^{-1}$	11.3	45.7	0.495	0.182	0.136	0.186	1.19
	13.2	44.3	0.429	0.205	0.148	0.218	1.14

Table S4.5. Fractions of all pyrene species in the aerated and non-aerated solutions of Py-Amylopectin, Py-NAF8.3, Py-NAF20, and Py-NAF57 in DMSO calculated from f_{Mdiff}, f_{Mfree}, f_{Ediff}, f_{Ek2}, and f_{EE0}.

Sample	mol%	f_{diff}	f_{free}	f_{E0}	f_{k2}
Py-NAF8.3 (aerated)	3.4	0.664	0.158	0.092	0.086
	5.8	0.645	0.046	0.117	0.192
	7.6	0.646	0.016	0.128	0.210
τ_M = 92 ns	10.0	0.588	0.019	0.178	0.215
$k_2 = 2.5\times10^8\ s^{-1}$	12.0	0.583	0.006	0.178	0.233
Py-NAF20	8.8	0.58	0.01	0.16	0.26
(non-aerated)	10.4	0.52	0.01	0.22	0.25
	11.6	0.47	0.01	0.16	0.36
τ_M = 135 ns	12.4	0.67	0.01	0.11	0.21
$k_2 = 2.5\times10^8\ s^{-1}$	13.8	0.65	0.01	0.13	0.21
Py-NAF57 (aerated)	4.8	0.723	0.037	0.118	0.122
	7.6	0.660	0.002	0.139	0.199
	8.0	0.655	0.000	0.139	0.207
τ_M = 92 ns	11.3	0.608	0.000	0.168	0.224
$k_2 = 2.1\times10^8\ s^{-1}$	13.2	0.548	0.001	0.189	0.262